Rab27a: Ligand and Interactome Discovery for a Secretory GTPase

A thesis submitted to Imperial College London in candidature for the degree of Doctor of Philosophy of Imperial College London

Wenye Zhao

Department of Chemistry
Imperial College London
London SW7 2AZ

September 2017

Declaration of Originality

I hereby declare that this thesis is my own work, generated as a result of my own original research.

Information derived from the published and unpublished work of others has been acknowledged in the text and references are given.

Wenye Zhao

September 2017

Acknowledgement of Collaboration

Mostafa Jamshidiha provided all forms of recombinant Rab27a, including Rab27a, biotin-Rab27a, Rab27a-Slp4 and Fusion-Rab27a. Details on their synthesis, purification and sequences may be found in his PhD thesis.

Charlotte Sutherell from the Tate group and Martin Rowlands from the Institute of Cancer Research performed all SPR assays.

Remi Serwa performed all proteomic searches on PEAKS.

Copyright Declaration

Abstract

Rab27a is a small GTPase belonging to the Ras superfamily. Normally involved in vesicle transport and docking, numerous studies from the past two decades have documented a positive correlation between its overexpression in tumour cells and the invasiveness of the cancer. These findings strongly suggest that Rab27a could be a novel cancer drug target, yet, the dearth of clinically successful drugs targeting other oncogenic members of the Ras superfamily reflects the difficulty of applying canonical medicinal chemistry techniques to this class of proteins, structurally flexible and have complex protein-protein interaction (PPI) networks.

The development of new biophysical methods in drug discovery holds promise in delivering where past methods have struggled. In this thesis, two top small molecular hits from a fragment assay against Rab27a were developed as part of structure-activity relationship (SAR) studies using a crystallised protein construct as guidance. Peptide binders were also sought, and a dipeptide was identified as the first positive control for Rab27a with a k_d of ~8 mM by SPR, and its affinity was improved by lactam bridging.

The PPIs of Rab27a were also investigated as part of the development of photocleavable crosslinkers for a novel chemical biology approach to interactome proteomics. A prototype lysine-targeting covalent crosslinker was designed, synthesised and validated with recombinant protein followed by Rab27a-spiked lysate. It was subsequently incorporated into a bespoke proteomic protocol and tested against HeLa lysate transfected with Twin-Step Tag (TST)-Rab27a. The results were analysed using label-free quantification (LFQ) in MaxQuant and peptide modifications inspected with PEAKS. The analysis workflow is discussed and critically analysed, offering many fruitful avenues for the future iterations of the protocol.

Acknowledgements

First of all, I would like to thank **Ed** for hosting me in his group and giving me the opportunity to pursue a PhD. I am grateful for our regular discussions his invaluable guidance. I am also grateful to Imperial College London for providing me with my scholarship.

I cannot tell you how happy I am for this opportunity to thank publicly all the wonderful people who have helped, stood by and put up with me during my PhD journey. Many thanks to **Mostafa** for the lively chats and advice. May your incorrigible enthusiasm for science last forever! Thank you also to everyone in the **Rab group** – you are some of the most dedicated people I have ever met. Good luck with everything!

I am very grateful to the Tate group, especially those who have taken the time to teach me about lab and research skills. Thank you to **Julia** for teaching me all about cell culture, SDS-PAGE and Western Blots, and thank you **Feny** and **Rhiannon** for helping me with peptide synthesis. Thank you, **Markus**, for all your help with plasmids, primers and transfecting bacteria. A ginormous thank you must go to **Remi** for helping me with all aspects of the proteomics - I learned so much in such a short space of time!

Huge thanks go to **Charlotte**, **Tom**, **Rhiannon** and **Remi** for proof-reading and discussing my thesis. Thank you **Yunyun, Rhiannon** and **Gee** for all the good times, and **Yunyun** for being a fantastic housemate over for over two years. We had a lot of fun in that tiny kitchen!

Outside of the lab, I must thank the Dirac Quartet (**Amalia**, **Ben** and **Jon**), **Alina** and **Siyao** for far too many fun and hilarious times to count - I stayed sane because of you! Thank you **ULSO** for the amazing music, to **Amy** and **Jon** for being the best committee members ever, to **John Crawford** for making me a better violinist than I'd ever been, and to **Sinfo** for the opportunity to lead and go on tour. Finally, I would like to thank my **parents** who have supported me unwaveringly throughout all my life, and **Ben**, for being you, for being there… and letting write up my thesis in your flat!

Contents

Abbreviations

AUC	area under the curve
CID	collision induced dissociation
DDA	Data dependent acquisition
DIA	Data independent acquisition
DIC	*N,N'*-diisopropylcarbodiimide
DIPEA	*N*,*N*-diisopropylethylamine
DSF	differential scanning fluorimetry
DSS	disuccinimidyl suberate
EDC	1-(3-dimethylaminopropyl)-3-ethylcarbodiimide
ESI	Electrospray ionisation
FBDD	fragment-based drug design
FP	fluorescence polarization
FRET	Förster resonance energy transfer
GAP	GTPase-activating protein
GDI	guanosine nucleotide dissociation inhibitor
GDP	guanosine diphosphate
GEF	guanine nucleotide exchange factor
GNP	5'-guanylyl imidodiphosphate
GTP	guanosine triphosphate
HBS	hydrogen bond surrogate
HOBt	Hydroxybenzotriazole
HPLC	high performance liquid chromatography
HRP	horseradish peroxidase
HTS	high throughput screen
ICAT-	isotope-coded affinity tags

iTRAQ	isobaric tags for relative and absolute quantitation
LAH	lithium aluminium hydride
LCMS	liquid chromatography mass spectrometry
LFQ	label-free quantification
m/z	mass to charge ratio
MS	mass spectrometry
MST	microscale thermophoresis
PAINS	pan-assay interference compounds
PDB	Protein Data Bank
POI	protein of interest
PSM	Peptide spectrum match
RBD	Rab binding domain
RP	Reverse phase
SAR	structure-activity relationship
SCX	Strong cation exchange
SEC	Size exclusion chromatography
SHD	Slp homology domain
SILAC	stable isotope labels with amino acids in cell culture
SOS	Son of sevenless
SPPS	solid phase peptide synthesis
SPR	surface plasmon resonance
SRM	Selective reaction monitoring
TFA	trifluoroacetic acid
TIC	total ion current
TIS	triisopropylsilane
TST	twin strep tag
waterLOGSY	water-Ligand Observed *via* Gradient SpectroscopY

1 Introduction

This thesis is concerned with two divergent approaches to investigate native and non-native ligands of the oncogenic GTPase Rab27a. The first section discusses the discovery of small molecule and peptide inhibitors for Rab27a, whilst the second part focuses on the development of a photocleavable crosslinker for use in proteomic mass spectrometry to pursue its endogenous effectors. The structure of the introductory chapter reflects this, starting with an overview of structure-guided attempts to find therapeutic inhibitors for the Ras superfamily, of which Rab27a is a member, alongside a discussion of the relevance and challenges faced when targeting Rab27a. It is followed by a short primer in quantitative proteomics, with particular focus on the use of crosslinkers to stabilise protein-protein interactions (PPIs) for mass spectrometry detection.

1.1 Clinical Relevance of Rab27a

Small monomeric GTPases are a class of guanosine-binding proteins (G-proteins), of which the Ras superfamily is the most well-studied. The five main subfamilies are Ras, Rab, Rho, Arf and Ran, and their roles span across the entire range of cellular processes. Over 60 Rab proteins exist in the human proteome and are involved in many aspects of vesicle trafficking.[1-2,3-4]

Rab27a and Rab27b are the two isoforms of Rab27. They are similar in structure and sequence with approximately 70% sequence homology.[5] Although they have been shown to bind to all the same effectors, there is evidence that they prefer to perform distinct roles within the same trafficking cascade.[5-7] This thesis will focus on Rab27a, in particular the nature of its dysregulation in cancer.

Rab27a is expressed in a variety of secretory cell types and is involved transporting and docking vesicles in various endocrine and exocrine exocytotic and endocytotic processes.[4, 8-12] The knockout mutation of Rab27a in humans causes a genetic disease called Griscelli syndrome type II that is characterised by albinism and severe immunodeficiency, invariably

resulting in a reduced lifespan.[13] These effects are due to impaired melanosome transport in melanosomes and defective secretion of lytic granules in T lymphocytes.[12, 14-15] The specific phenotype of this disease suggests a wide degree of redundancy in the functions of Rab GTPases. There is no current cure for Griscelli syndrome. Of more clinical interest is the dysregulation of Rab27a in chronic and progressive diseases like cancer, which is common to other members of the Ras superfamily.[16-22] This thesis will focus on targeting Rab27a in cancer.

1.1.1 Rab27a in Cancer

The large majority of drug discovery and chemical biology activity in the Ras superfamily field has focussed on inhibiting Ras, largely driven by the superabundance of hyperactive Ras subfamily members in cancer (over 20% of all cancers).[23-27] No clinically-approved drugs targeting the Ras oncogene have emerged since its discovery, and small GTPases have remained elusive drug targets due to their flexible, flat topologies and numerous PPIs.[28] Encouragingly, recent fragment-based drug design (FBDD) and improved biophysical methods have led to hits with promising selectivity and induced phenotypes, offering fresh hope to pursue these previously intractable proteins. On the contrary, other subfamilies have remained relatively unexplored; for example, only few inhibitory molecules have been reported for Rab proteins to date, despite being the largest subfamily.

Most publications of Rab27a's role in cancer show a positive correlation between the expression levels of Rab27a and several aspects of tumour progression that include tumour grade (a measure of cell differentiation), cell viability, invasiveness, proliferation and metastasis. Studies have also demonstrated the Rab27a-mediated secretion of pro-metastatic factors which modify the tumour environment to make it more amenable to invasion,[29] and its knockdown has decreased the activity and aggression of several cell lines and tumours both *in vitro* and *in vivo*. [30-43]

Conversely, the papers by Dong *et al.*[44] and Worst *et al.*[45] are of interest because they alone present a negative correlation between Rab27a levels and tumour progression, the opposite

of the prevalent trend. Although this seems paradoxical, these studies only demonstrated correlation and not causation, and suggests that competing mechanisms may be at play, depending on the cancer subtype.

Tumour-suppressing miRNAs operate by inhibiting the translation of oncogenic proteins. Several recent studies have reported the effect of tumour-suppressing microRNAs (miRNAs) on Rab27a expression.[35, 38, 43, 46-49] In all the studies, an increase in the intracellular levels of miRNAs correlated with the decrease of Rab27a and thus tumour-derived exosomes, as well as a reduction in tumour progression. Rab27a has also been found to be involved in exosomal secretion of tumour-suppressing miRNAs[35]. As Rab27a has a well-established role in exosome secretion, its inhibition may decrease the disposal of factors allowing the survival of cancerous cells.[5, 9, 50-51]

There is mounting evidence that Rab27a plays a significant contributive role in many cancer types. The studies above nominate Rab27a as a potential cancer biomarker and a target for therapeutic inhibition, and the evidence is enough to warrant further studies in its druggability and for further elucidation of its mechanisms in health and disease.

1.2 Structure-guided targeting small GTPases

Due to their related structures, Rab27a presents similar if not greater challenges than other members of the Ras superfamily. Given the structural similarities between the Ras GTPases, it is worth examining studies that have tackled other members of the family to give an idea of the scope and challenges facing the ligand discovery for Rab27a.

1.3 GTPase Structure and Function

Ras superfamily members share a highly conserved fold of six β-sheets, interconnected by loops, and five α-helices.[2, 52] Figure 1 shows the general structure of GTPases.[53] Two flexible switch regions (switch I and II) surrounding the nucleotide binding pocket are largely responsible for the differing conformations in the GDP and GTP-bound forms. The picture is complicated by further dynamic conformational states within each nucleotide-bound form,

particularly the GTP-bound form. The original idea that these proteins exist in rigid inactive and active states was thrown into question when ^{31}P NMR spectroscopy of H-Ras demonstrated the existence of two main conformational states (I and II) for the GTP form alone. State II is thought to be the effector-binding conformation, but the physiological role of state I is not clear.[54-57]

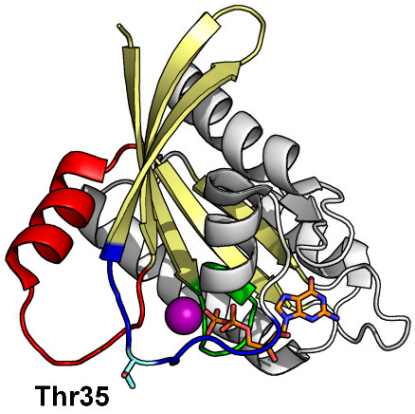

Figure 1 Structure of K-Ras-GDP with nucleotide-binding regions highlighted: P-loop (10-17, green), switch I (29-38, blue) and switch II (58-76, red), α-helices (white) and β-sheets (yellow), Mg2+ (purple), highly conserved threonine (T35 in K-Ras, cyan), and GDP (orange). [PDB code: 4LPK]

Importantly, the large majority of structural studies to date have been performed with truncated proteins without the C-terminal hypervariable region and its associated lipid modifications. In addition, the effect of membrane anchorage on these two states has not yet been explored. This raises the question of the physiological importance of the two conformational states *in vivo*, since active Ras is membrane-bound inside cells. Further investigation of protein dynamics in a membrane environment would be useful in illuminating this matter.

1.3.1 The GTPase Cycle

GTPases act as molecular switches in signalling cascades and their active and inactive states are toggled by the guanine nucleotide bound to them. The ‘on’ state is facilitated by loading with GTP, and its concomitant hydrolysis to GDP converts it to the ‘off’ state. It is the GTP-bound form that binds to effectors and facilitates downstream actions, whilst the GDP form does not usually bind to effectors. The presence and absence of the nucleotide’s

terminal γ-phosphate governs its temporal affinity to effectors by affecting conformational changes in the switch regions. This switch activity is regulated by numerous auxiliary proteins in the GTPase cycle (Figure 2).[3]

Ras superfamily proteins are singly or doubly prenylated at the C-terminus. These lipid groups are important for their localisation on relevant membranes when in their active state.[58] When inactive, the protein is stabilised in the cytosol by GDP dissociation inhibitors (GDIs) until the next round of activation. Guanine nucleotide exchange factors (GEFs) accelerate activation through the exchange of GDP for GTP *via* a nucleotide-free intermediate and GTPase-activating proteins (GAPs) catalyse the hydrolysis reaction.

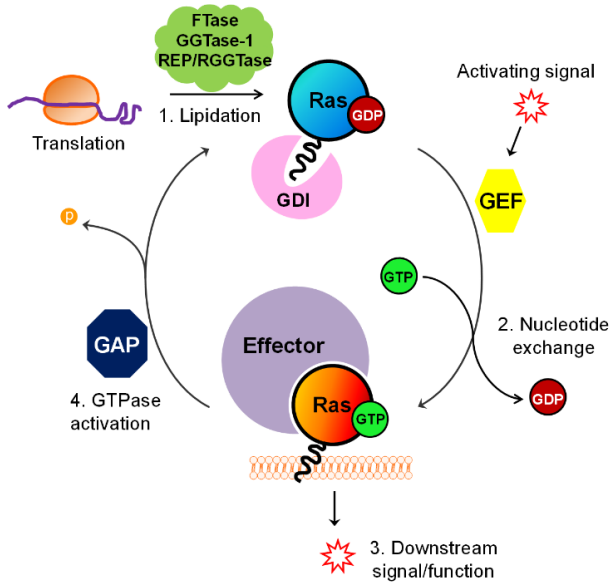

Figure 2 Generalised GTPase Cycle (1) Prenylation at the C-terminus. (2) GEF-mediated exchange of GDP to GTP via a nucleotide-free intermediate. (3) The active GTP-loaded Rab can bind to affectors and propagate downstream signals. (4) A GAP protein catalyses the hydrolysis of GTP to GDP, whereupon a GDI picks up the now inactive GTPase and stabilises it in the cytosol, facilitating intermembrane transport.

In principle, blockade at any stage of the GTPase cycle (Figure 2) could lead to inhibition. Direct approaches to target Ras proteins include targeting the nucleotide binding pocket, stabilisation of Ras complexes associated with the inactive state, or stabilising interactions at the PPI interface.[26] More indirect methods of disabling the GTPase cycle have the potential to circumvent some of the druggability challenges of the Ras proteins; however, they are beyond the scope of this thesis and the reader is directed to other reviews.[59-61]

1.4 Structure-Based Design of GTPase Inhibitors

Structure-based drug design (SBDD) requires detailed spatial information of the target protein(s). In this respect, x-ray crystallography offers the most immediate appreciation of protein topology and visual guidance to establish a structure-activity relationship (SAR) for a ligand series. It also facilitates the construction of virtual pharmacophores and docking models, paving the way for *in silico* screening.

Alongside the risk of artefactual binding to crystallographic constructs, a particularly important consideration for GTPases is the tendency for crystallisation to trap a protein in one specific low energy conformer. This is generally not an accurate representation of the equilibrium mixture of conformers in solution. Furthermore, the flexibility of Ras superfamily members is readily apparent in their NMR spectra where a full assignment is often not possible, limiting the quality and amount of information that is obtained.

In spite of these challenges, significant progress has been made towards discovery of novel Ras superfamily ligands through structure-guided approaches. Representative examples from each category are discussed below.

1.4.1 GTPase Active Site Inhibitors

Targeting the active site of any GTPase is intrinsically difficult due to the conserved nature of the nucleotide binding site and optimised affinity it has for guanine nucleotides. Even if a competitive molecule existed, it would be a pan-inhibitor and this would not be desirable as GTPases are involved in a broad range of functions and general toxicity would result.

A notable exception is the oncogenic K-Ras G12C mutant that has a mutated cysteine close to the nucleotide binding pocket and thus offers a disease-specific tethering site.[62] A few studies have exploited this G12C mutation, for example **1** (SML-8-73-1, Figure 3), a GDP analogue which acts as a conformational lock for the inactive GDP form.[63-64] In a similar vein, Wiegandt *et al.* produced conformationally locked GTPases by tethering **2a** (aGDP) and **2b** (aGTP, Figure 3) with cysteine-engineered Rab5.[65] Whilst this approach may

produce useful tools for probing Rab biology and druggability, inhibitors approaching the structure of nucleotides are likely to suffer from poor cell permeability.

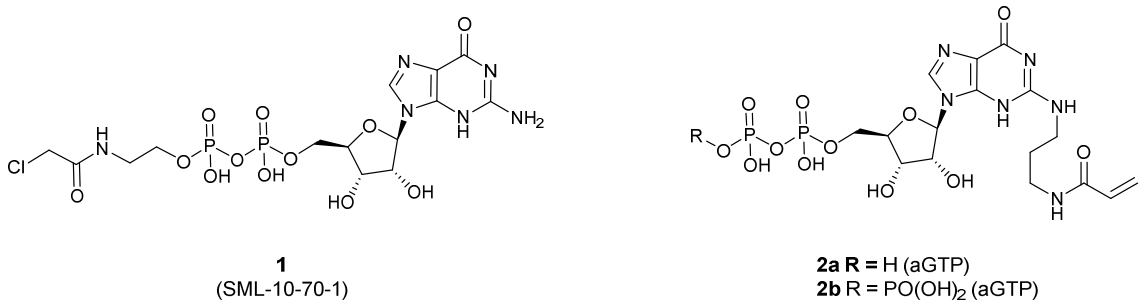

1
(SML-10-70-1)

2a R = H (aGTP)
2b R = $PO(OH)_2$ (aGTP)

Figure 3 Two examples of covalently reactive nucleotide analogues for conformationally locking cysteine-mutated GTPases.

1.4.2. In Silico Approaches

Virtual high-throughput screening (vHTS) can screen libraries of up to millions of compounds, comparable to the largest HTS but with significantly fewer resources in a much shorter time. In a typical example, a 3D representation of the protein binding site is built based on a crystal structure; molecules from a virtual library are computationally docked into the virtual pocket and ranked on the possession of (major) conformers with favourable complementary binding interactions. Nevertheless, this structure-based rationale suffers from the same caveats as conclusions based on crystal structures in general and is limited in predicting novel binding modes in flexible proteins.

Alternatively, a ligand-based screen may be performed against a virtual pharmacophore based on the predicted intermolecular interactions of a known ligand. The advantage of this is that it does not require knowledge of the crystal structure or a binding mode.[66]

Gao *et al.* docked a library of >140,000 into a surface groove of Rac1 (a Rho GTPase) in the Rac1-Tiam1 (a GEF) interface and obtained **3** (NSC23766, Figure 4) as a hit, which inhibited Rac1-GEF interactions *in vitro* with an IC_{50} of ~50 µM.[67-69] Montalvo-Ortiz *et al.* subsequently improved upon this structure with **4** (Ehop-016) which had an enhanced IC_{50} of 1.1 µM for Rac inhibition.[70] Adding to this work, the same group also identified **5** (Rhosin) as an inhibitor

of the interaction between RhoA and LARG (a GEF), which exploited the tryptophan residue in the LARG binding surface of RhoA.[71]

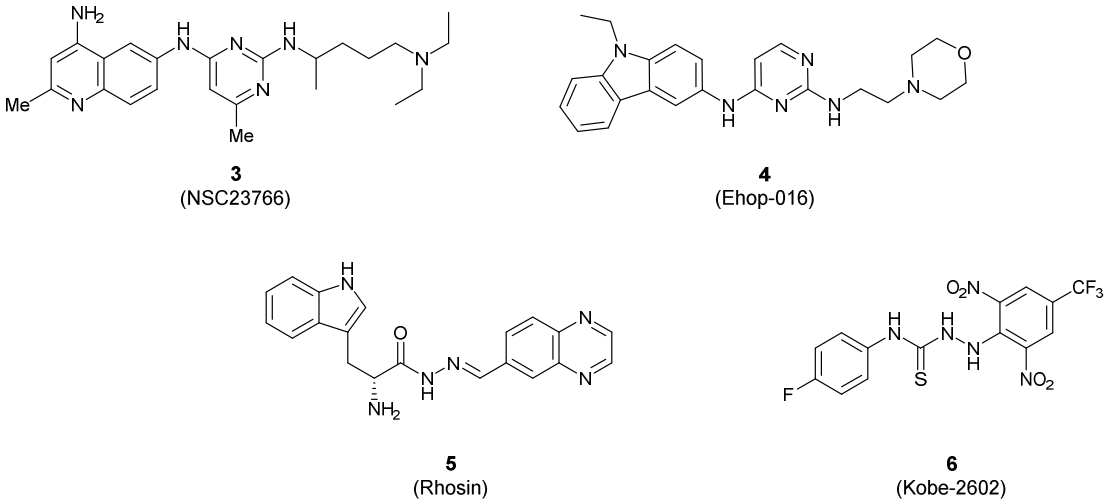

Figure 4 Structures of GTPase-targeting molecules derived from in silico screens.

Related approaches have targeted GTPase-effector interfaces. For example, Shima *et al.* undertook a computational docking screen of >40,000 compounds against M-RasP40D. Out of 97 virtual hits, only one competitive inhibitor was found (Kobe0075) with a K_i of ~50 µM to H-Ras-GTP by a radioactive pull-down assay. A subsequent virtual similarity search of ~160,000 compounds again yielded only one active hit **6** (Kobe2602), though this was less potent. Both compounds also inhibited the growth of human colon carcinoma xenografts *in vivo*. A more soluble analogue (Kobe2601) was shown to bind to the Ras-Raf interface by HSQC NMR.[72]

1.4.3 Fragment-based Approaches

Whilst a traditional HTS involves screening a library of 10^5-10^6 drug-like compounds, fragment-based drug design (FBDD) has emerged as a more ligand-efficient method for obtaining hit scaffolds. The size of a typical fragment has a molecular weight of less than 300 Da and allows for a much smaller compound library to cover the same breath of chemical space. Crystal structures greatly enables the growing and linking of initially weak-binding fragments (typically mM K_d) to increase affinity. In optimal cases, a well-designed

1,000-10,000 fragment library can offer 100-1,000 times higher validated hit rates than a traditional HTS, and the reader is referred to several recent reviews that describe in detail the rise and challenges of FBDD.[73-80]

Sun *et al.* performed a 11,000 fragment screen by NMR spectroscopy against ^{15}N labelled GDP-K-Ras, obtaining 140 hits with a variety of scaffolds. The top hits were successfully co-crystallised with GDP-K-Ras and all were found to occupy the same binding pocket. Following inspection of the crystal structure, the authors grew their chosen fragment into a neighbouring cleft by appending isoleucine and proline to an aniline moiety to obtain **7** and **8** respectively (Figure 5). This improved the binding affinity from ~1 mM for the fragment to ~200 μM with isoleucine.[81]

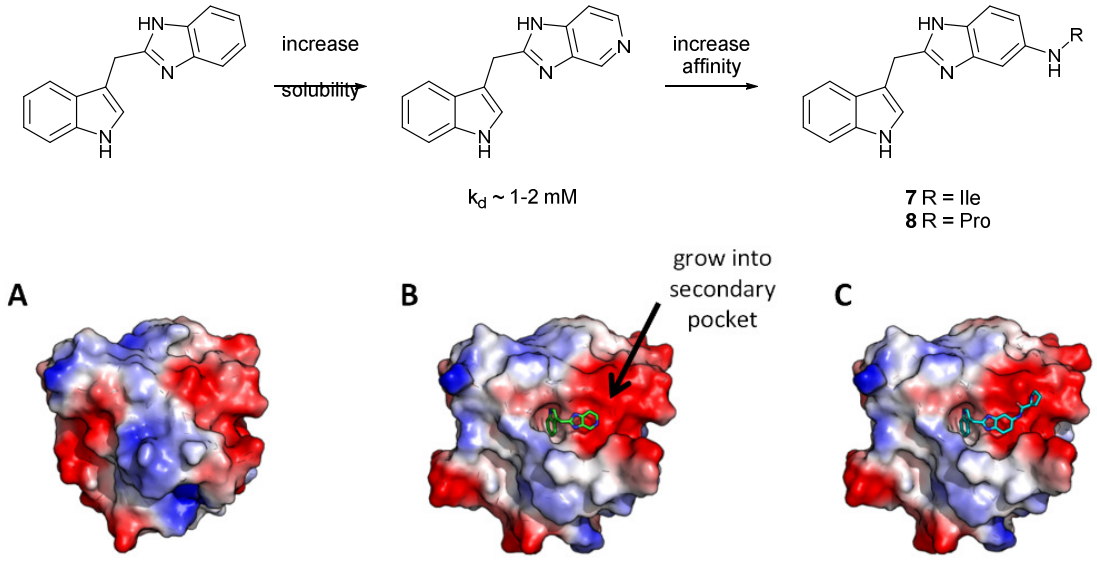

Figure 5 Progression of a ligand series by Sun et al. All fragments were found to induce a similar pocket on the surface of K-Ras-GDP. Panel A shows unliganded K-Ras-GDP with the absence of the pocket. A biaryl hit was selected for growth into an adjacent, positively charged pocket (B). The attachment of an isoleucine residue to obtain 11 gave the best results, but proline analogue 12 was crystallised (C).

Maurer *et al.* also published a fragment screen against GDP-K-Ras with NMR, using saturation transfer difference (STD) and HSQC experiments to obtain their top hit **9** (DCAI, Figure 6), which was co-crystallised with the target. However, no further fragment development was undertaken.[82] Gao *et al.* used NMR techniques to target the RhoA-LARG interaction, yielding fragment hit **10** (R1, Figure 6).[83]

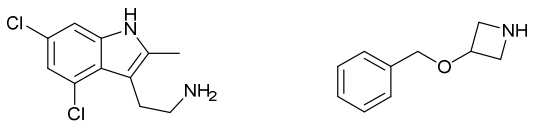

9
(DCAI)

10
(R1)

Figure 6 Examples of ligands obtained by NMR screens.

In contrast, fragment screening against the Rab GTPase-GEF complex could provide ligands that stabilise a non-productive complex that stalls exchange activity. Winter *et al.* screened against a heterodimeric structure of H-Ras-SOS (son of sevenless, a GEF that binds to Ras) using X-ray crystallography and obtained small molecules that formed ternary complexes by binding to the H-Ras-SOS interface. However, neither the fragment hits nor the optimised analogues inhibited SOS-induced nucleotide exchange.[84] This highlights the fact that it is important to establish biochemical activity in hit compounds as weakly-binding fragments obtained through FBDD may not be inherently biochemically active.

1.4.4 Tethering Approaches

The development of covalent inhibitors is becoming an increasingly accepted pathway for drug discovery.[85-89] The selectivity of the inhibitor is determined by the spatial positioning of the affinity component and the warhead; it does not require a very potent binder.

Ostrem *et al.* performed a disulfide tethering screen against the cysteine of the cancer-specific G12C K-Ras mutant and obtained allosteric ligands that stabilised the inactive GDP form: **11** is an example.[90] Similarly, Winter *et al.* identified maleimides such as **12** that inhibit SOS-mediated nucleotide exchange by targeting a mutated C118 residue in the nucleotide

pocket that only becomes accessible for reaction during SOS-mediated GDP-GTP exchange.[84]

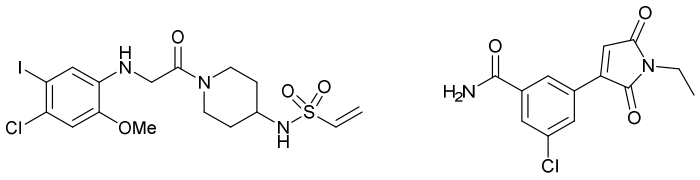

11 **12**

Figure 7 Examples of covalent ligands derived from tethering screens.

1.4.5 Peptidomimetic Approaches

The specificity of native PPIs arises from binding partner complementarity between two protein surfaces. Synthetic peptides have a high intrinsic potential for inhibiting PPIs as they are made of the same combinatorial building blocks. Binding hotspot sequences are often coiled into a relatively rigid α-helical structure; however, in isolation as a peptide they often become linear and have much lower affinity due to the increased entropic penalty upon binding. Further, peptides often suffer from poor membrane permeability which makes them unsuitable for intracellular targets. There have been many studies on improving the physical properties of potentially therapeutic peptide inhibitors, but universally-applicable solutions have so far been elusive.[91-93]

The conformation dynamics of peptides can by controlled by introducing an alkyl linker, appropriately positioned to induce helicity. This can be achieved in a variety of methods, but two that been extensively studied are hydrogen bond surrogates (HBS)[94-98] and peptide stapling.[95, 99-101]

For HBS, a single turn of the α-helix is fixed at the N-terminus by replacing a hydrogen bond with an alkyl chain to induce helicity through the rest of the peptide. The group of Arora synthesised HBS peptides derived from an α-helical region of SOS. Their optimised structure **13** (HBS 3, Figure 8), was found to reduce SOS-induced activation of Ras.[102]

In contrast, peptide stapling fixes two turns of the α-helix using an alkyl chain formed by ruthenium-catalysed metathesis of two unnatural amino acids with terminal alkenes - usually at positions *i* and *i* + 3. In some cases, this can also increase cell permeability of the peptide.[99] Leschiner *et al.* adopted this approach to make stapled peptides based on an α-helix of SOS. Ensuring that the peptide staple would lie on the opposite side from the PPI, the authors obtained **14** (SAH-SOS1, Figure 8) and achieved binding affinities of 100-175 nM by fluorescence polarisation (FP).[103]

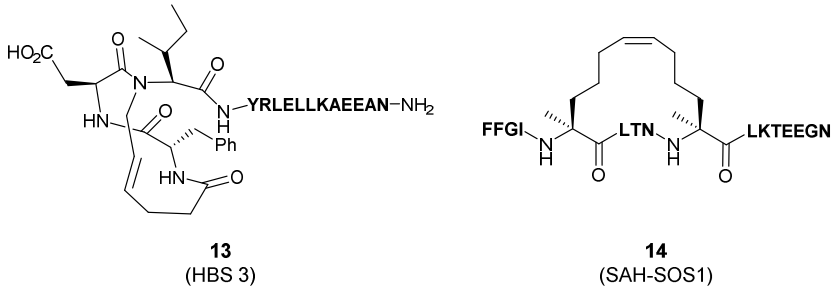

13 (HBS 3) **14** (SAH-SOS1)

Figure 8 Structures of HBS and hydrocarbon stapled peptides.

Spiegel *et al.* synthesised short fluorescein-conjugated peptides taken from binding motifs of Rab effectors and screened them by FP against several Rab proteins. Only the singly stapled structure, **15** (StRIP3), was found to bind Rab8a loaded with 5'-guanylyl imidodiphosphate (GNP or GppNHp), the non-hydrolysable analogue of GTP, and to compete with Rab8a-effector binding *in vitro*.[101] Later, in 2016, the authors created a doubly stapled version that improved its affinity, resistance to protease hydrolysis and bioavailability.[100]

1.5 Small Molecule Inhibitors of Rab27a

Small inhibitory molecules of Rab27a are few, with only four papers claiming to have found positive hits. Figure 9 displays the structures of the ligands reported to target Rab27a. They vary widely in the depth and breadth of their validation, but so far none of them have been explicitly structure-validated by x-ray crystallography or NMR. As such, the actual target and mode of action of these compounds is unknown.

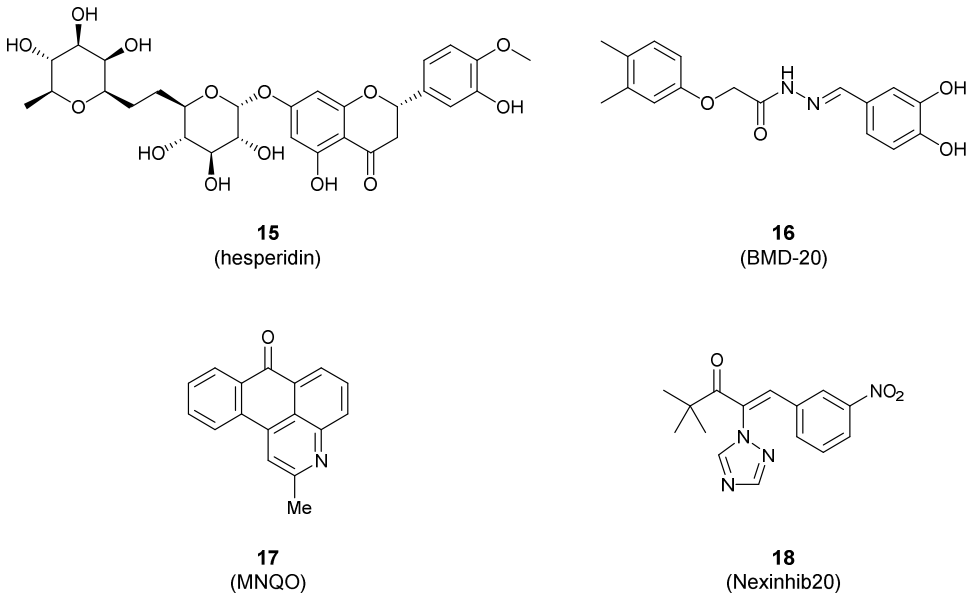

Figure 9 Structures of the putative small molecule inhibitors of Rab27a in the literature.

During 2013-16, three papers were published by Hwang Jae Sung's group. As a group working in a Molecular Skin Biotechnology laboratory, the authors conducted the studies with a view to produce new skin-lightening agents by disabling Rab27a's role in melanosome transport as opposed its regulation in pathological states.

In 2013, Kim *et al.* performed a docking study of 273 natural products from the Korea Food and Drug Administration (KFDA) against the Rab27a-Slac2a (melanophilin) interface. From the ten top-scoring compounds, the authors chose to focus on **15** (hesperidin) as it was already approved for cosmetic use.[104] **15** was tested in cell-based and phenotypic assays where it was positive for melanosome aggregation, suggestive of Rab27a-Slp2 inhibition, and was found to inhibit three tyrosinases that are involved in synthesising melanin pigment, but did not have any effect on melanin secretion. Finally, the authors claimed that **15** caused increased brightness in a cultured human skin model.

In 2015, Joung *et al.* published a hit from a pharmacophore-based *in silico* screen. Superimposing the crystal structures of Rab27a-Slp2 [PDB: 3BC1] and Rab27b-Slac2a [PDB: 2ZET], they constructed a virtual pharmacophore based around Arg29 in Slac2a which was judged to be a strongly interacting residue in the putative Rab27a-Slac2a

interface. This model was used to screen against a virtual compound library of 190,000 compounds. After filtering for drug-likeness, a total of 25 compounds progressed to a melanosome transport cell assay, in which **16** (BMD-20) performed the best. This was the only non-virtual validation that the authors performed; there were no attempts to prove binding to Rab27a.[105] Follow-up work by Kang *et al.* included the development of a series of sulfonamide analogues based on **16**, but once again relied only on phenotypic tests with cells.[106]

In 2016, Park *et al.* claimed that 2-methyl-naphtho[1,2,3-de]quinolin-8-one **17** (MNQO) decreases the RNA expression levels of Rab27a, Slac2a and myosin Va in melanocytes. The authors did not state how they obtained their candidate compound, but tested it for melanosome localisation, melanin content and melanin production in a reconstructed human skin model, and was further shown to decrease UVB-induced skin pigmentation in brown guinea pigs.[107]

None of the above studies performed any biophysical assays to demonstrate binding to Rab27a or any of its related proteins, but relied purely on phenotypic tests to verify their hypothesised mechanisms. It remains to be seen whether inhibition of Rab27a can be exploited for skin lightening. A topical application is envisaged, as an endemic distribution would likely incur side effects and may even compromise the immune system as for Griscelli syndrome. However, there is not enough evidence to suggest that those molecules are acting on target.

In late 2016, Johnson *et al.* published a class of inhibitors called Neutrophil Exocytosis Inhibitors (Nexinhibs) that block the Rab27a-Slp1 interaction. 32,000 compounds from two Maybridge libraries were screened against an in-house time-resolved FRET (TR-FRET) assay. Twenty hit compounds were tested in cell assays and for ROS scavenger activity, after which **18** (Nexinhib20) was obtained as the best performing compound. It was validated for Rab27a-Slp1 binding by co-precipitation, pull-down and ELISA assays and underwent TR-FRET counterscreens against the Rab11-Munc13-4 and Rab27a-Munc13-4 interactions.

In an *in vivo* mouse model, pre-treatment with Nexinhib20 before insult with lipopolysaccharide (LPS) endotoxin decreased plasma levels of neutrophil secretory proteins, suggesting anti-inflammatory properties.[108]

18 (Nexinhib20) appears to be the best in its class. However, inspection of the chemical structures of the Nexinhibs reveals a concerning number of function groups that are known to cause problems: α,β-unsaturated ketones are susceptible to addition by nucleophiles, while nitro groups cause toxicity after metabolic conversion.[109] Further, there is insufficient evidence of on-target binding from the limited TR-FRET counterscreens and the lack of biophysical assays to characterise binding, such as by NMR.

Significantly, members and collaborators of the Tate group have conducted in-house tests on **16** and **18** by waterLOGSY and surface plasmon resonance (SPR) assays and found no binding to Rab27a. This corroborates the fact that none of the above studies had credible validation of target-specific activity and leaves open to question the origin of their observed effects.

1.6 Rab27a Effectors

An effector is a molecule that binds to a specific protein and modulates its biochemical activity. For GTPases, this usually means a protein that binds to its active state to propagate a signalling cascade. As the second part of this thesis seeks to investigates unknown endogenous interactions for Rab27a, it is worth inspecting the identities of its known effectors.

There are currently thirteen known effectors of Rab27a: eleven that bind to GTP-Rab27a and two that bind to GDP-Rab27a, excluding proteins solely involved in regulating the GTP-GDP cycle (GDIs, GAPs, GEFs). Rab27a's effectors are not as widely expressed as Rab27a itself. Typically, only 2 or 3 types of effector are found in one cell type, thus possibly controlling cell-type-specific roles for Rab27a. It may explain how Rab27a can have such a

wide range of roles in a wide range of cell types. Note that all effectors of Rab27a also bind to Rab27b, but they prefer to participate in distinct stages of exocytosis.[5-7, 110]

The effectors of GTP-Rab27a can be grouped in into three classes according to the nature of their binding domains. Slp1-5 and rabphilin contain the N-terminal Slp homology domain (SHD) as well as the C-terminal phospholipid-binding domains C2A and C2B. Slac2-a, Slac2-c and Noc2 have only the SHD, whereas Munc13-4 only has the C2 domains (Figure 10).[7, 50, 111-114]

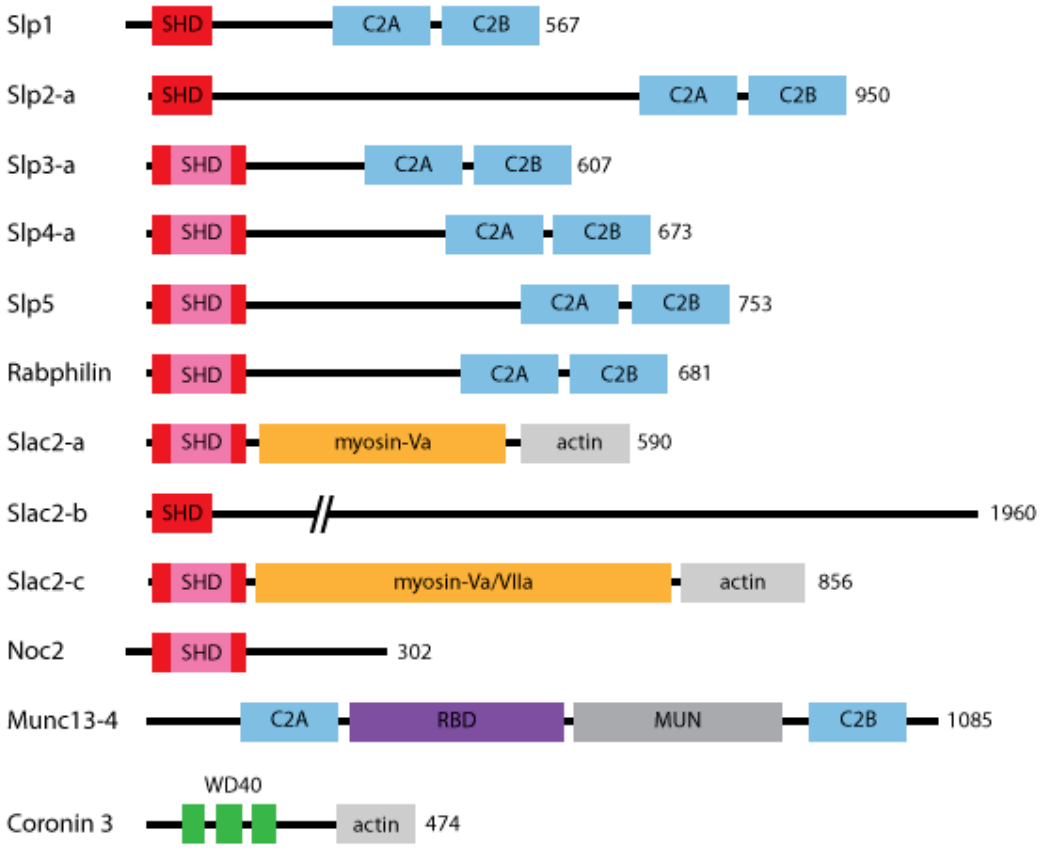

Figure 10 Binding regions of the GTP-Rab27a effectors. Amino acid lengths are shown on the right hand side. Image adapted from M. Fukuda.[50]

Booth *et al.*'s recently proposed new interactor ATP1a1 lack both the SHD and C2 domains[115] and binds independent of the nucleotide states. Coronin-3 and IQGAP1 have been proposed as effectors of GDP-Rab27a.[8, 116-117] The Slp and Slac2 effectors have

several alternative names in common circulation. Table 1 lists the effectors, their pseudonyms and references.

Name	Alternatives	Gene	Domains	Ref
Slp1	JFC1 Exophilin-7	SYTL1	SHD, C2A, C2B	118-120
Slp2	Slp2a Exophilin-4	SYTL2	SHD, C2A, C2B	112, 121
Slp3	Slp3a Exophilin-6	SYTL3	SHD, C2A, C2B	122-123
Slp4	Granuphilin Exophilin-2	SYTL4	SHD, C2A, C2B	124-126
Slp5	Exophilin-9	SYTL5	SHD, C2A, C2B	127-128
Rabphilin	Rabphilin 3A	RPH3A	SHD, C2A, C2B	129-132
Slac2-a	Melanophilin Exophilin-3	MLPH	SHD	133 112, 132
Slac2-b	Exophilin-5	EXPH5	SHD	5, 50
Slac2-c	MYRIP Exophilin-8	MYRIP	SHD	134
Noc2	Rab effector Noc2	RPH3AL	SHD	129-130, 135
Munc13-4		UNC13D	C2A, C2B	6, 118, 136-138
Coronin-3	Coronin-1C	CORO1C	“	8, 117
IQGAP1		IQGAP1		116
ATP1a1		ATP1A1		115

Table 1 Known protein binders to Rab27a. Most are effectors which recognize only the GTP-loaded protein. Coronin-3 binds only to GDP-Rab27a and there is limited evidence that Slp4 has affinity for both nucleotide states. SHD = Slp homology domain, RBD = Rab-binding domain.

Conversely, little is known about Rab27a-specific GAPs and GEFs. While GAPs tend to have a relatively broad spectrum, GEFs are often specific to a particular family of proteins or even a single subfamily member, though there is limited structural information to explain their binding selectivity.[139-141] Rab3GEP is the only known GEF for Rab27a, and EPI64 and EPI64B are proposed to be GAPs (Table 2).

Name	Alternative	Gene	Role	Ref
EPI64	TBC1D10	TBC1D10A	GAP	51, 142-144
EPI64B	FLJ13130	TBC1D10B	Broad spectrum GAP	145
Rab3GEP	DENN MADD	MADD	GEF	146

Table 2 Known GAPs, GEFs and GDIs of Rab27a.

1.7 Introduction to Quantitative Proteomics and Crosslinking Mass Spectrometry for Interactomics

1.7.1 The Use of Mass Spectrometry in Studying Protein-Protein Interactions

PPIs and their spatiotemporal changes facilitate nearly all biochemical processes in living organisms. They are of enormous interest to the scientific community as the knowledge of interaction networks in normal and pathological states are key for the elucidation of signalling pathways and the discovery new targets for disease treatment.

The plethora of techniques that have been employed to survey PPIs reflect their relative difficulty to study. This is likely due to their enormous heterogeneity: their varying degrees of transiency and diverse topologies along with promiscuity and redundancy means that the goal of finding a single comprehensive strategy has been elusive.

Most traditional methods require the synthesis of a recombinant bait protein that requires immobilization *e.g.* protein microarrays,[147] affinity-purification,[148] tagged fluorophores (to enable study by FP or FRET), affinity tags[149] or with NMR-active isotopes.[150] Several *in vivo* techniques also exist, such as yeast-2-hybrid (Y2H), protein-fragment complementation assay (PCA), mammalian protein–protein interaction trap (MAPPIT). Furthermore, *in silico* text mining and analyses based on phylogenetics can predict which PPIs may be fruitful to study. More detailed discussion on the classical methods of discovering PPIs and their advantages and disadvantages may be found in several reviews.[151-156]

Mass spectrometry (MS) is the technical basis on which the field of proteomics, the global protein profiling of cells, tissues or organisms, is based. By extension, it is also becoming the relied-upon technique for the study of interactomes.[157-159] Its rise and spreading adoption rides upon advances in technology as well as the improvement of search algorithms and bioinformatic software. The two together offer an incredibly powerful, efficient and versatile platform for scientists, empowering them to answer questions of wider scope in fewer

experiments. Both discovery and targeted approaches are possible, and different ionisation, fragmentation and detection regimes can be tailored to suit the experiments' needs.[160-161]

Many factors can determine the quality and reproducibility of MS data. Mass spectrometers themselves differ in their sensitivity, mechanisms of ionisation, fragmentation and data collection, and many software packages can be used to process and analyse the data output. These factors can considerably influence the conclusions drawn and it is important for the researcher to have insight in all processes to interpret the data. This is a growing field that is still building momentum, so we will no doubt see many improvements in all fronts in the years to come.[162]

The following introductory minireview is intended for non-experts and provides an overview of the techniques and practical aspects of quantitative proteomics before covering the use of covalent crosslinkers to study interactomes.

1.7.2 Bottom-up, Top-down and Shotgun Proteomics

MS involves measuring the mass to charge ratio (m/z) of gas-phase ions. The many iterations of improvements since the 19th century have rendered modern machines capable of detecting a wide range of masses with extremely high precision and sensitivity. With today's ionisation capabilities, molecules as large as intact proteins and even macromolecules can be detected. Tandem mass spectrometry (MS^n, n = 2, 3) involves two or more consecutive rounds of mass detection, and fragmentation by collision induced dissociation (CID) or electron transfer dissociation (ETD) ahead of MS^2 and MS^3 enables *de novo* sequencing of peptides. After data collection, bioinformatic software assembles the MS output into tables of identified proteins and quantities.

Top-down proteomics is where MS^1 detects the mass of the intact protein and MS^2 detects fragments of the protein. This method detects proteoforms and is better for low MW proteins. However, there are advantages to be had from digesting into peptides before sample injection. This is called bottom-up proteomics and it remains the more prevalent technique,

especially as it is generally more sensitive despite more limited sequence coverage and the possible loss of labile PTMs. Figure 11 depicts the difference between the two. The bottom-up strategy will be assumed in the rest of this thesis.[163]

In bottom-up, the first mass spectrometer (MS^1) detects the m/z of peptides, which are sent for fragmentation. The products of the fragmentation process are then detected by the second MS (MS^2). The fragmentation pattern elucidates its amino acid sequence, which can be sequenced *de novo* or matched to sequence databases or peptide spectral libraries. Most proteins can be identified by a unique sequence of only seven amino acids.[164] Post-translational modifications (PTMs) can be detected by modifying the search parameters, though without enrichment they may be difficult to detect because of their low abundance amongst a large dynamic range.

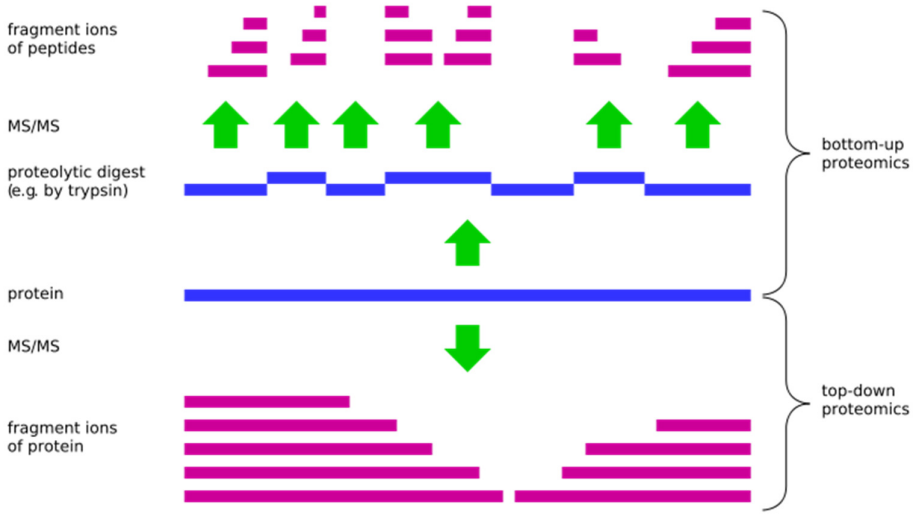

Figure 11 Diagram depicting top-down and bottom-up proteomics. In the bottom-up approach, proteins are digested into peptides before mass detection. In top-down proteomics, no pre-digestion occurs and the full mass of the protein is detected before fragmentation. Image by Magnus Palmblad.

Shotgun proteomics refers to the method of analysing highly complex samples (such as lysates) by combining high performance liquid chromatographical (HPLC) separation before partitioning to the mass spectrometry stage (LC-MS/MS).

1.7.3 Data-dependent and Data-independent acquisition

Discovery proteomics is performed with samples of high complexity with the intention of monitoring global changes in the proteome, and deliberately allows for detecting unforeseen changes or new proteins. Associated with the shotgun method, it is HTP and generally uses data-dependent acquisition (DDA) where only the most abundant ions are analysed in each detection cycle.; this occurs continuously until the end of the elution run.

Consequently, shotgun proteomics with DDA offers large coverage of the proteome but will be affected most by issues of dynamic range and reproducibility. DDA precludes absolute quantification because ion selection is biased towards the most abundant ions, and the cut-off for the number of ions allowed through to detection is arbitrary, many ions are missed, and this cannot be controlled or predicted. However, relative quantification may be achieved by means of isotope labelling and label-free quantification.[165]

At the other extreme, selected reaction monitoring (SRM) is a sensitive and quantitative method where the mass spectrometer is programmed to select only precursor ions for targeted studies, such as for biomarkers[166-169]. Data-independent acquisition (DIA) is a newer intermediary technique that scans every ion within a window of m/z range per cycle, and then iterates with the next range until the entire range is covered.[167, 170-173]

A table summarising the attributes of DDA, DIA and SRM can be found in a review by Hu *et al.*[171]. At the time of writing, DDA is the most common method of ion selection due to its simplicity, flexibility and cost. However, the advantages of DIA's higher reproducibility and precision of quantification means we may see an increase in its adoption in discovery proteomics, particularly if its ease of analysis is improved. Better data acquisition techniques along with more powerful instrumentation will reduce the need for enrichment and pre-fractionation steps, leading to less sample loss and more biologically representative data.

1.7.4 Enrichment Strategies

Modern mass spectrometers are now very sensitive, enabling the detection of minute quantities of proteins in complex mixtures. However, in discovery proteomics where ideally every protein in a sample is identified and quantified, it is not so much the complexity of the mixture but the dynamic range that is the problem: the concentration of the most abundant proteins can be 10^7–10^{12} times higher than the least;[174] conversely, it is often the rarer proteins that are of interest. Without enrichment, this can be problematic with DDA: the high background prevalence of common proteins such as actin or haemoglobin can suppress the detection of other proteins, even if the latter on its own is above the detection threshold.

Enrichment and fractionation methods reduce the dynamic range by removing proteins that are not of interest, or by separating out samples based on physical properties. The simplest example is the LC component of LC-MSMS; this technique is routine for shotgun proteomics.

Alternatively, enrichment can occur on the protein or peptide level. The solubility of proteins differs wildly. If complete coverage is important, then cellular fractionation can be performed, though this is more often used for investigating the localisation of proteins, and each fraction must be carefully solubilised. Proteins can also be fractionated based on size by running on an SDS-PAGE gel and cutting out the bands in a lane (1D) or a spot (2D). In-gel digestion is then performed to release the peptides.[175-177]

Fractionation of peptides is also possible using parameters such as charge, polarity, hydrophobicity and size for separation. This can be done with ion exchange chromatography (IEX), RP-LC with high or low pH eluents, and isoelectric focusing (IEF). The most common combination is strong cation exchange (SCX) chromatography followed by neutral RP-LC. More than one can be used in combination, allowing multi-dimensional fractionation.[175 177]

Affinity pull-down (PD) involves a solid support coated with a moiety that strongly attracts a chemical label affixed on a protein, which can be endogenous (*e.g.* biotin) or introduced (*e.g.* His-tag). The main advantage of this approach is that, with a suitable affinity handle it is

possible to enrich proteins of very low abundance. Various forms of affinity handles include: (i) peptide-tagged proteins (spiked-in or transfected),[178-179] (ii) PTMs[180-186] and (iii) activity- and affinity-based probes.[187-192]

1.8 Techniques for Quantitative Proteomics

The ability to quantify changes within a proteome under different conditions provides crucial information on the dynamic behaviours of protein networks. Both label-free and isotope-labelled methods are in common use today with the premise of achieving accurate, precise, HTP and reproducible quantification. Each method has its own distinct merits and are elaborated below.

1.8.1 Stable Isotope Labelling

Peptides labelled with heavy isotopes such as ^{2}H (deuterium), ^{15}N, ^{13}C or ^{18}O behave chemically in a near identical manner but are seen as separate peaks by MS. This makes them invaluable as standards, where experimental samples can be mixed with the heavy-labelled standard in a fixed ratio. This method tolerates technical inconsistencies between samples and experiments because a verifiable control is present in every sample, distinguished by a predetermined mass shift for each peptide. There is also scope for multiplexing by mixing samples labelled with different isotopes combinations, which gives more data per run and reduces sample preparation time.[193-196]

Stable isotope labelling with amino acids in cell culture (SILAC) involves feeding cells with isotopically enriched media. Here, heavy (^{15}N and ^{13}C) lysine and arginine are commonly used for metabolic incorporation into the proteomes of cell cultures. Only a few passages are required for near full integration, though this method only works for cell lines and excludes any that can synthesise their own amino acids which would result in substoichiometric labelling.[193, 197-200]

Peptide labelling methods, usually at N-termini and lysine side-chains, are more universally applicable and include dimethyl labelling (reductive methylation of amine groups with heavy

and light methyl groups),[194, 201] isotope-coded affinity tags (ICAT)[196, 202] and isobaric labelling such as isobaric tags for relative and absolute quantitation (iTRAQ)[203-205] and tandem mass tags (TMT).[206-207]

1.8.2 Label-free quantification

Label-free quantification (LFQ) does not use any form of chemical or metabolic labelling and samples are run individually, Figure 12 shows the mixing regimes of label-free, SILAC and isobaric labelling strategies.[195] Relative quantification is achieved by matching peptide identifies across different samples based on retention time and comparing either ion intensities (area under the curve (AUC) or maximum peak height) or spectral counts (number of identified MS/MS hits).

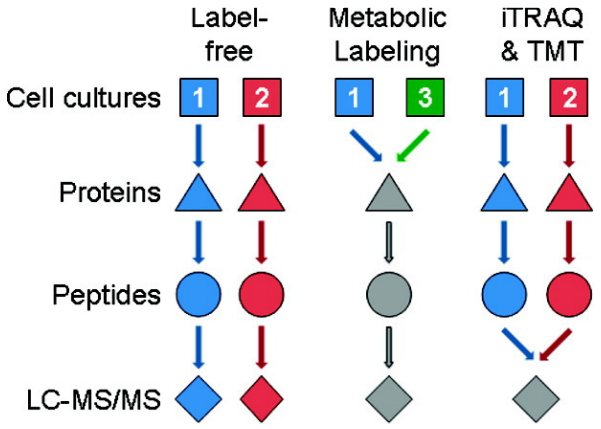

Figure 12 Mixing regimes in label-free and isotope-labelled quantification methods. LFQ samples are run individually and require no mixing. Metabolically labelled samples are mixed at the protein stage so that both experiment and standard are treated identically during sample preparation. Conversely, isobaric labelling is performed on peptides after digestion so they can by mixed at the last stage, which has a risk of increased sample variation. Image by Zhou et al.[195]

LFQ boasts shorter workflows, lack of expensive labelling reagents and a higher throughput than the above-mentioned isotope-labelling methods. However, the latter have traditionally been preferred over LFQ for their superior reproducibility and more accurate quantification. In the past, lower quality mass spectrometers in combination with less sophisticated bioinformatic algorithms meant that run-to-run variability and the stochastic nature of DDA hampered the alignment and consistent identification of the same peptide across multiple samples.[195, 208-214]

However, major improvements in MS technology and processing software has made LFQ an increasingly attractive option, and it is seeing increased adoption in research groups worldwide.

1.9 Crosslinking Mass Spectrometry

Crosslinking mass spectrometry (CLMS or XLMS) is a technique that uses covalent crosslinkers to stabilise PPIs so that binder partners can be identified by MS. Unlike immunoprecipitation, XLMS potentially allows for HTP identification of both transient and stable interactions either on a targeted or proteome-wide scale. Further, it is possible to identify modified residues, providing topographical information on the interface.[158, 215-225]

Three modes of crosslinks are possible. Figure 13 shows the nomenclature that will be used in this thesis – there currently is no standardised terminology.[215] Type 0 are monoreacted crosslinkers that have failed to react to a partner protein and become either hydrolysed or quenched at the unreacted end. Type 1 crosslinks occur when both ends of one crosslinker reacts on the self-same protein, essentially stabilising its own 3D structure. This may be useful for protein structure elucidation, but for interactomics it could block the chance of inter-crosslinking.

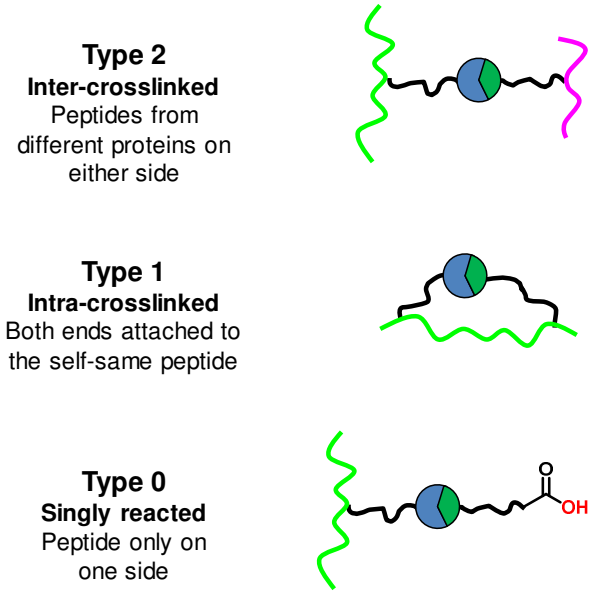

Figure 13 Types of crosslinks formed with peptides.

Type 2 inter-crosslinks are the typically the most sought-after - if both peptides on either side of the crosslink are unique, the interacting pair of proteins may be identified. The choice of spacer arm length and warhead reactivity is pivotal as each combination is optimal only for a subset of PPIs.

1.9.1 XLMS Workflows

A typical XLMS workflow is illustrated in Figure 14. If the crosslinking is to take place in a prepared lysate, the lysis buffer must have a low surfactant concentration that preserves PPIs, but is able to solubilise a significant proportion of the proteome and must be free of any basic amines; Tris buffers are not suitable. The crosslinker is then added, and the reaction is quenched. Enrichment steps may occur before or after enzymatic digestion, after which the samples are run and processed.

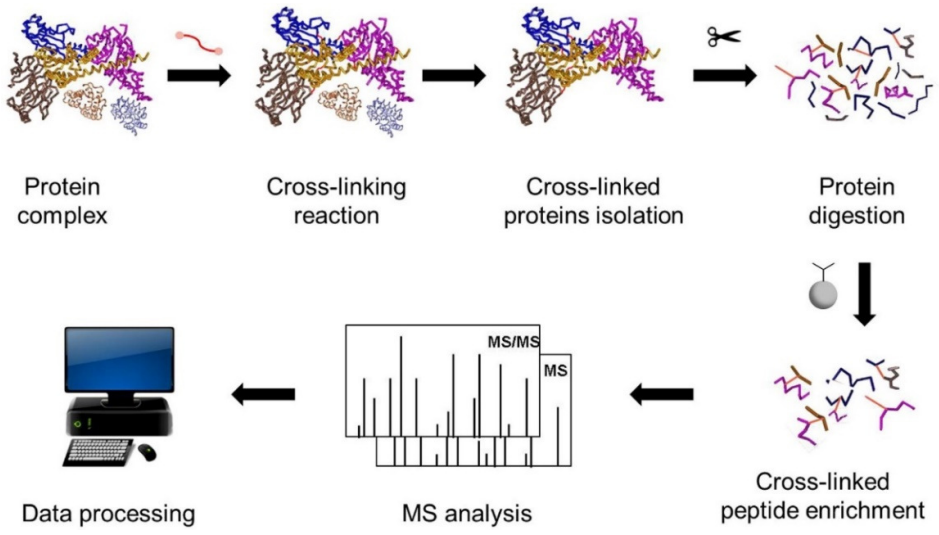

Figure 14 Example of a XL-MS workflow featuring pull-down of type 2 interlinks. Image by Tran et al. [217]

1.9.2 Crosslinker Considerations in XLMS

1.8.2.1 *Reactivity and Specificity*

Targeting lysines gives statistically the best chance of forming crosslinks across the proteome. The lysine composition of proteins is about 7%, making it a fairly common amino acid. Serine, leucine, valine and glycine occur at similar percentages, whilst alanine is the most common at 9%.[226]. However, the majority of lysines will be found on the surface of proteins as the solvation of its charged side chain is favourable, whereas more lipophilic residues have a higher propensity of residing in internal folds (the lipophilic effect). As such, lysine is the most common surface residue,[226] so targeting them gives a statistically favourable chance of forming side-chain crosslinks across the proteome.

For Rab27a at 221 residues and an average of 6% of lysines, we would predict it to contain (0.06 x 221) 13 lysine residues, close to the real figure at 12. It is anticipated that most are surface-accessible and thus able to react with crosslinkers (section 5.4.3).

Crosslinking molecules for XLMS should be specifically reactive towards the chosen residue sidechain and resistant to hydrolysis. The use of homobifunctional *N*-hydroxysuccinimide (NHS) esters to target lysines is widespread. NHS esters are largely specific towards lysines, though reaction against serine, tyrosine and threonine have been observed.[227-228] Maleimide and disulfide compounds are used to target cysteines, the advantage of which is that it pairs the most reactive sidechain, the sulfhydryl moiety, with one of the most stable (and thus specific) warheads.[229] However, as cysteine residues occur less commonly than lysines, this method may not be suited to PPIs with few nearby cysteines. Two studies to date have targeted acidic residues aspartic and glutamic acids with hydrazides *e.g.* **23** (DHSO) in Figure 16).[230-231]

The main drawback to crosslinking residue side-chains is the inability to target hydrophobic surfaces. Photocrosslinking, either in the form of photoreactive probes[232] or in engineered proteins with photoreactive side-chains[233], is a crosslinking strategy that can overcome this, but is beyond the scope of this thesis.

1.8.2.2 Length

Crosslinkers come in a wide range of length and complexity. Zero-length crosslinkers leave no trace of themselves once crosslinked to a target protein *e.g.* 1-ethyl-3-(3-dimethylaminopropyl)carbodiimide (EDC); alternatively, formaldehyde forms very short and reversible crosslinks between lysines.[234-235] However, zero-length and short linkers may fail to capture weaker interactions as they require the reacting side-chains to be very close, and the reagents may suffer from non-specificity due to their high chemical reactivity. Longer crosslinkers will be able to cover a wider range of lysine distances.

Studies have shown that DSS, which has a length of 11.4 Å when fully extended, is capable of bridging two lysine C_αs (C-alphas) of a distance up to 30 Å. [236] Clearly, the maximum distance will increase as the end-to-end length of the crosslinker. However, specificity will need to be balanced with versatility when it comes to deciding the size of a linker. Short crosslinkers are more likely to capture true interactions; longer ones may give rise to intra-

protein loops (type 2, Figure 13)[237]. The physical properties of the crosslinker must also be considered; they would ideally operate at physiological conditions.

1.9.3 MS-Cleavable Crosslinkers

Identifying type 2 inter-crosslinks (Figure 13) is key in many studies of XLMS but there are many challenges to overcome to achieve this goal, particularly in a large-scale proteome level. The number of possible peptide combinations scales quadratically with the number of peptides in a mixture. As such, the computational search space becomes prohibitively large at a proteome level and puts the onus on accurate and precise mass detection in order to assign correct matches.[216, 238]

This problem is circumvented if peptides on either side of the crosslinker can be fragmented separately. Unfortunately, crosslinked peptides do not fragment as predictably as linear ones and it may not be possible to identify the peptide source if the linkers themselves do not easily fragment such as **19** (DSS) and **20** (BS3) in Figure 15.

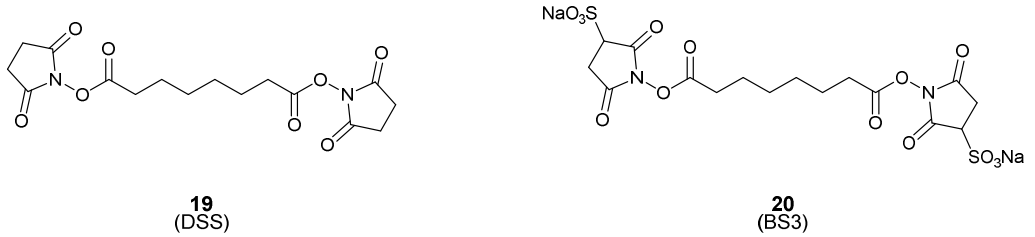

19 (DSS) **20** (BS3)

Figure 15 Examples of non-cleavable crosslinkers.

To combat this, a wide variety of MS-cleavable crosslinkers have been developed with the inclusion of a labile bond, which is cleaved at a much lower energy than the peptide backbone. The MS-cleavable bond fragments first, separating the two peptides. Strategies using MS^2, MS^3 and reporter ions have been employed. In an MS^2 instrument, the peptides also fragment in the same round and sequencing is finally possible by deconvoluting characteristic patterns of fragmentation. In MS^3, the masses of the cleaved peptides are measured before a second round of fragmentation and third mass detection. Data gathered

with MS^3 is easier to analyse, but MS^3 is time-consuming, can give low-resolution results and the machines are expensive and not as widespread.[216]

Figure 16 shows examples of MS-cleavable crosslinkers aimed to discover PPIs and structural studies. The symmetrical nature of the crosslinkers ensures that the same adducts will result on every peptide, thereby simplifying analysis. Crosslinker **21** (BuUrBu) is cleaved on either side of a central urea group, forming characteristic doublets for every modified peptide.[239-241] However, sulfoxides are now the most widely used cleavage moieties, whereupon the C-S bonds are labile under collision induced dissociation (CID). Liu *et al.* demonstrated the utility of this approach in discovery interactomics by applying **22** (DSSO) for proteome-wide protein network discovery.[219]

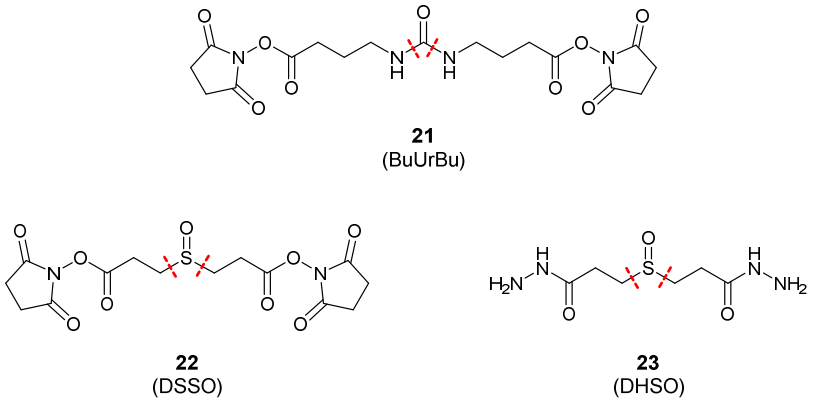

Figure 16 Examples of MS-cleavable crosslinkers that have been used to study PPIs. Their MS-cleavage sites are marked by red dashed lines.

1.9.4 Enrichment of Crosslinked Peptides

Crosslinked proteins, and thus peptides, occur in low abundance, exacerbating the pre-existing issue of dynamic range. This is because not every reactive residue will be successfully crosslinked due to factors such as steric hindrance, the local chemical environment and competing hydrolysis reactions at physiological pH. The issue is particularly acute for interlinks between already low-abundant proteins, so an effective enrichment strategy is critical if type 2 linked peptides are to be found (Figure 13).

The enrichment techniques employed for crosslinked peptides overlap with many of the strategies described earlier in the chapter, like gel excision and fractionation. Several methods that take advantage of the physically distinct nature of type 2 interlinks.

Size-exclusion chromatography (SEC) can be used to concentrate cross-linked molecules of interest since they have twice the molecular weight on average of single peptide. Crosslinked peptides have more N-termini and arginines and are more highly charged under acidic conditions, and thus elute later in strong cation exchange chromatography (SCX). For the same reasons, they have higher charge states once ionised that can be subsequently selected for fragmentation and acquisition by MS. Further, crosslinked peptides usually are more hydrophobic than non-crosslinked peptides and elute later in RP-HPLC.[216]

Pull-down enrichment of the crosslinker incorporates an affinity handle such as biotin, for example in **24** (BDP-PIR)[242-246], **25** (CBDPS)[247] and **26** (Leiker)[248-249] (Figure 17), though there is a risk of the added bulk hindering PPIs. Alternatively, the crosslinker may incorporate an azide or alkyne group to facilitate click-tagging of the affinity handle, for example click-enabled linker for interacting proteins **27** (CLIP)[250], as well as **28a** and **28b** (azide- and alkyne-A-DSBSO), which also has an acid-labile acetal group which releases the intercrosslinked peptide after pull-down. However, the added steps will inevitably entail some sample loss, which may put some low-abundant species below detection thresholds.[251]

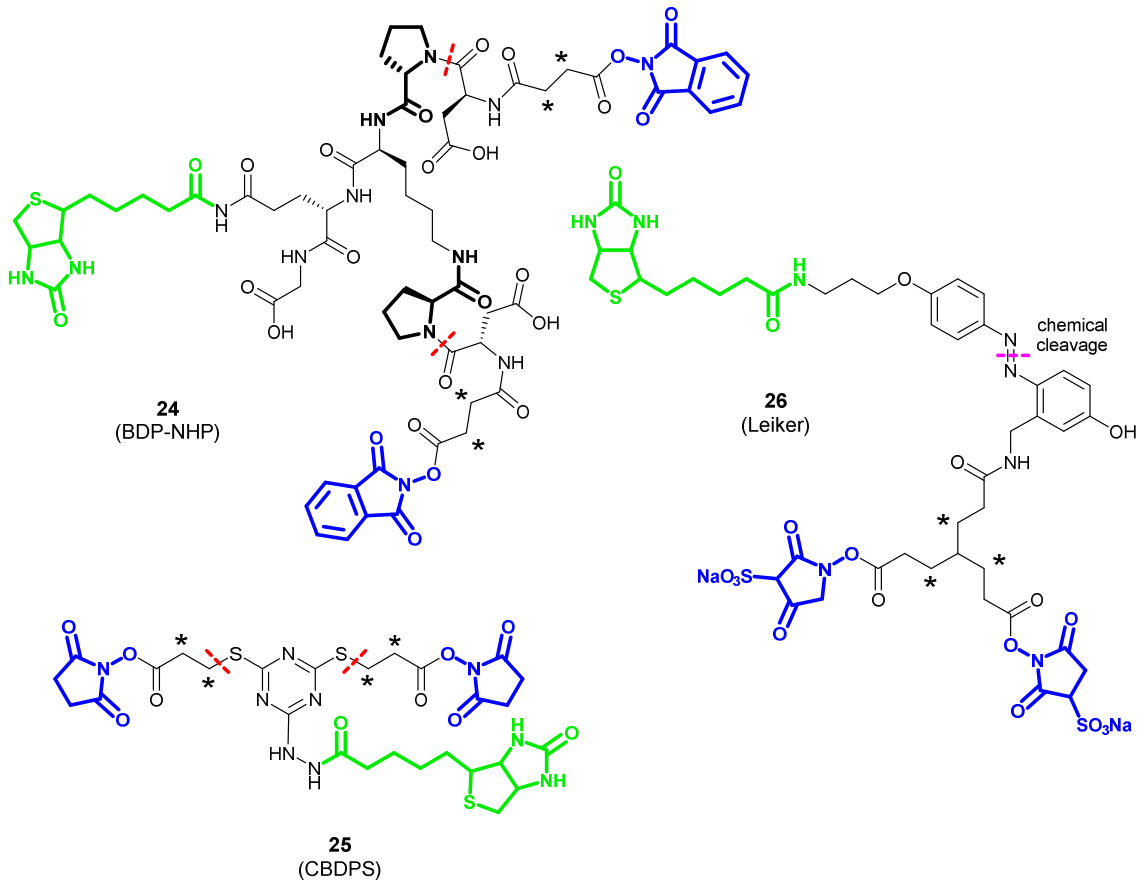

Figure 17 Examples of crosslinkers containing a biotin group that facilitates pull-down without further modification of the linker. Asterisks indicate where CH_2 is replaced with CD_2 in their heavy isotopic forms and red dotted lines indicate MS-cleavable bonds.

Finally, the ability to produce a reporter ion during MS fragmentation can supplant some of the need for offline purification. A reporter ion is an ion of a characteristic mass that is produced reliably from the crosslinker during fragmentation. Detection of this reporter ion can allow the MS to choose whether to send ions for detection, resulting in a lower background signal. Examples include the middle component of **24** (BDP-PIR, Figure 16) and the NO_2 moiety in **27** (CLIP) (Figure 18). However, not all MS instruments are capable of selecting ions for detection based on the presence of a reporter.

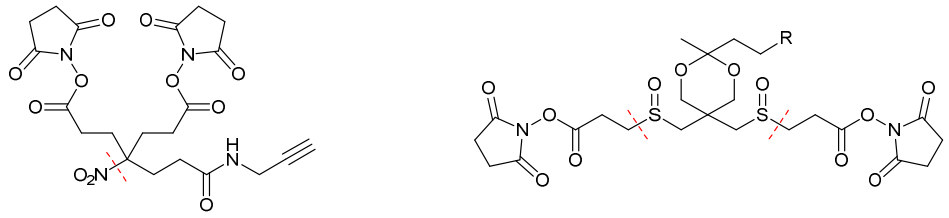

Figure 18 Examples of crosslinkers, with either an alkyne or azide group to allow post-crosslink click-labelling with an affinity group.

1.9.5 Photocleavable Crosslinkers

Various photocleavable crosslinkers have been made for structural studies, including MALDI-cleavable **29** (BiPs) by Petrotchenko *et al.*, cysteine-targeting linkers **30** by Milanesi *et al.*[252] and **31** by Omran *et al.*[253] (Figure 19). However, photocleavable crosslinkers that have been designed for PPI discovery are in their infancy. The Bruce group have extended their range of PIR crosslinkers to include a photocleavable form called pcPIR, where the two mass-cleavable regions have been replaced by photocleavable 2-nitrobenzyl group (Figure 20).[254-255]

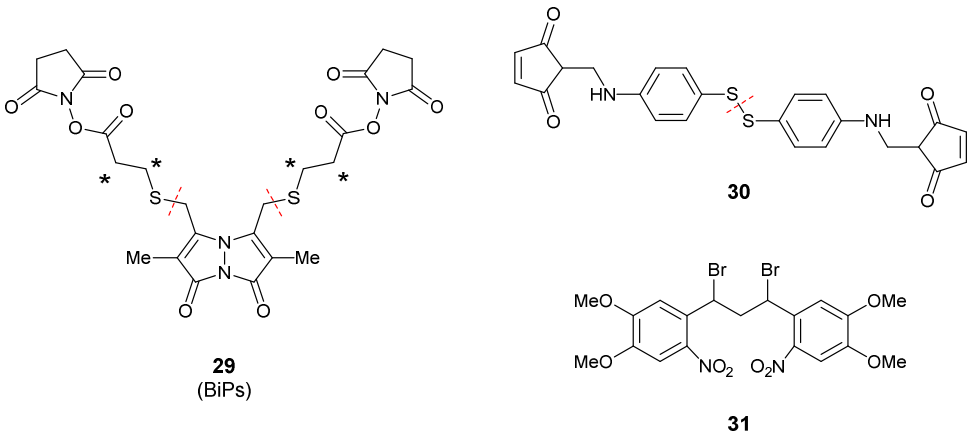

Figure 19 Photocleavable crosslinkers used to study protein structure

As with other PIR crosslinkers, pcPIR contains a biotin affinity tag for pull-down enrichment of intercrosslinked peptides and releases a characteristic reporter ion. Inline photocleavage, where UV light is directed at the ESI spray tip, cleaves both sites after LC separation but before ionisation. The virtue of this method is that peptides are cleaved after LC separation

whilst still in aqueous solution which can produce ions in higher charged states, leading to better fragmentation and identification of crosslinked peptides.

Although MS-cleavage is a powerful and enabling technique to the identification of type 2 crosslinks, gas phase dissociation of the crosslinker can produce ions of low charge states which do not fragment as efficiently and are less amenable for detection. This also means that pairs of peptides can be analysed together, which would not be the case if photocleavage had occurred prior to sample injection.[254-255]

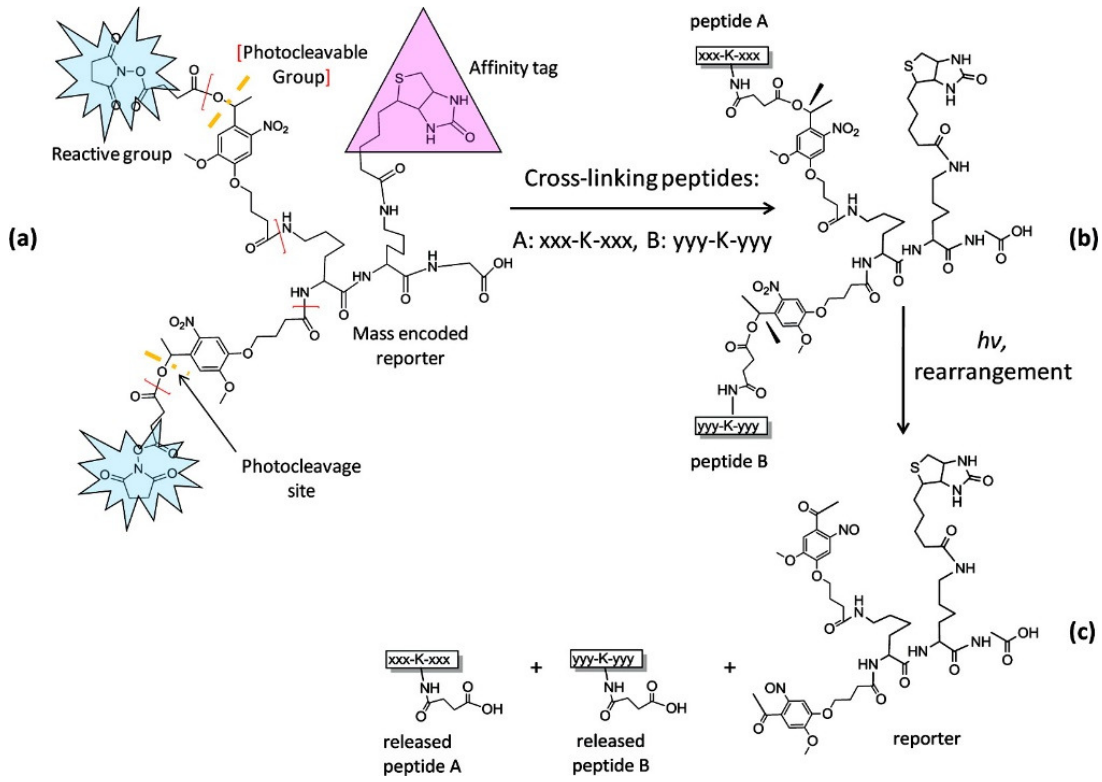

Figure 20 Scheme showing the structure, reaction and photoinduced rearrangement of photocleavable PIR (pcPIR) from the paper by Yang et al.[254] The crosslinker contains two NHS ester warheads, two photocleavage sites, a biotin affinity tag for pull-down enrichment and a reporter group for MS selection. An in-line UV laser photocleaves the linker just before ionisation, releasing both peptides and the reporter on.

pcPIR, as with its predecessors, remains a long molecule of considerable bulk, and it is questionable as to whether this hinders the formation of PPIs. In an *in vivo* application in *E. coli* cells, more than 1600 modified peptides were discovered and only 53 intercrosslinked peptides were validated. This does not compare favourably with the group's latest isotope-labelled reincarnation of PIR linkers (**24**, BDP-NHP), with which they quantified 941

nonredundant cross-linked pairs from a total of 1213 identified ones, though it should be noted that search algorithms and data analysis software have had major improvements in the intervening seven years.[242]

As the technological capabilities of MS increases, so too will bioinformatic algorithms that make use of the increased data output. Sensitivity will increase, preparation times will become shorter and processing speed faster. The growth of these two areas in combination with the development of more sophisticated chemical tools looks set increase the PPI space that is detectable by XLMS. It will be exciting to see the progression of this field in the next decade.

2 Project Aims

This thesis is centred around finding molecules that interact with Rab27a. It has two distinct threads: one that is in search for man-made chemical entities that inhibit its interactions with effectors, and the other develops a chemical biology approach in conjunction with crosslinking mass spectrometry (XLMS) in order to probe its endogenous intracellular protein-protein interactions (PPIs).

The aims and objectives of each thread are laid out in turn.

2.1 Towards an Inhibitory Ligand for Rab27a

Chapter 3 describes the design and synthesis of small molecule analogues which build upon two top hits from a fragment screen using a thermal shift assay. It then discusses constraining a downsized helical section of the effector Slp2a to achieve a short peptidic inhibitor that fits into a putative druggable pocket in Rab27a

Aims:

- Discover a specific ligand for Rab27a that can be developed either into a tool molecule for probing the druggability of Rab27a.
- Find a Rab27a-binding peptide that inhibits Rab27a-effector interactions using the Rab27a-Slp2-a co-crystal structure as a starting point. It was envisaged that the peptide would block effectors sharing the same interface.

2.2 Rab27a Interactomics – Photocleavable Crosslinkers with Proteomics

Chapter 4 discusses the design, synthesis and gel-based validation of a prototype UV-cleavable crosslinker, NitroXL, and Chapter 5 explores its integration into a proteomic workflow for discovering the endogenous effectors of Rab27a.

Aims:

- Develop a homobifunctional crosslinker that can be cleaved in two with UV light.
- The crosslinker itself would be non-specific but sample complexity will be reduced by pulling down affinity-tagged Rab27a from a lysate.
- Establish a proteomic workflow incorporating NitroXL that is quantifies binding partners pulled down by Rab27a in the presence and absence of crosslinker.

3 Inhibitory Ligands for Rab27a

3.1 Introduction

Rab27a has been shown to play an active role in numerous cancers and is an attractive novel target for anti-metastatic therapies. Existing inhibitors claimed in the literature have lacked evidence of target engagement and furthermore have failed to show binding in the Tate group's hands (Chapter 1). As no structurally validated and biologically efficacious inhibitor of Rab27a has yet been found. It was the aim of this project to identify one.

It was of interest to inhibit Rab27a directly rather through its regulatory proteins. This includes targeting its GTP-bound form to block interaction with effectors, or targeting the GDP-bound protein to slow its activation by nucleotide exchange. As well as high selectivity and potency, it would be desirable for the inhibitor to possess drug-like properties,[256] which would be important for sufficient uptake and bioavailability in cellular and *in vivo* testing at a later stage. However, it would not be realistic to expect early analogues to possess the qualities of a final oral drug, but aqueous solubility was considered at every stage as it affected the usability of the analogues in binding tests.

Structure-guided ligand development offers an efficient method of improving ligand hits as x-ray structures offer an intuitive visual guide for structure-activity relationship (SAR) studies. Unfortunately, unlike K-Ras and even other Rabs, wild type Rab27a does not crystallise on its own.

NMR would be a reasonable alternative to study its binding interactions, but this is made more difficult by the fact that Rab27a undergoes conformational changes in solution at a rate comparable with NMR acquisition. This means that may of its peaks are not present in its NMR structure, posing a significant challenge to assigning them (PhD thesis by M. Jamshidiha).

Fortunately, one heterodimeric crystal structure exists in the Protein Data Band (PDB), by Chavas *et al.* It is formed of Rab27a and a truncated version Slp2-a, which is one it its effectors. (Figure 21; PDB: 3BC1). The presence of Slp2-a appears to stabilise Rab27a and provide key crystal contacts to enable crystallisation.[121]

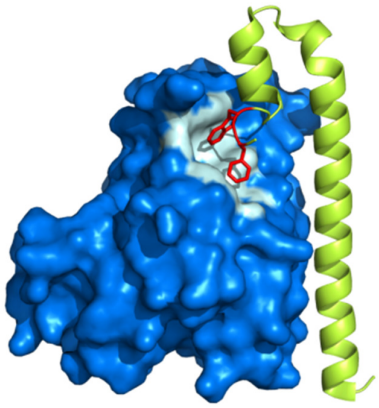

Figure 21 PyMol-rendered image of the Rab27a-Slp2-a co-crystal by Chavas et al (3BC1). Rab27a is in dark blue and Slp2-a is in lime green. The SF4 pocket in Rab27a highlighted in pale blue.

It should be noted that the Rab27a sequence in 3BC1 deviates from its endogenous structure in several ways. It is missing its C-terminal section (and hence all of its PTMs) and has several substitutions: C123S and C188S, which replace two surface cysteines with serine to avoid complications with oxidation, and Q78L which greatly reduces the hydrolytic activity of the GTPase. This, alongside with using of GNP as the loaded nucleotide (Figure 22, effectively locks Rab27a in approximately its active conformation.

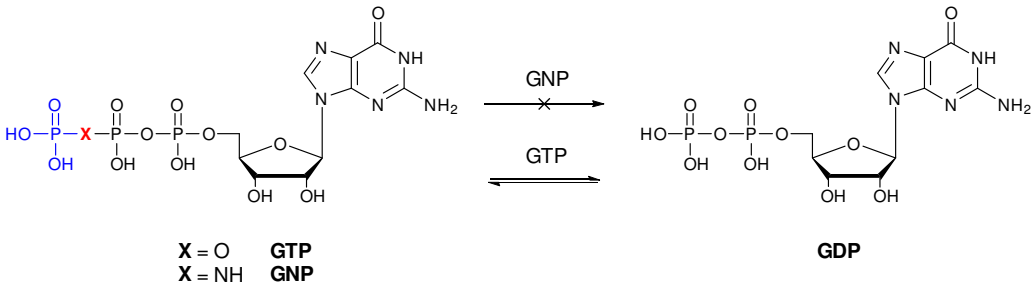

Figure 22 Structures of GTP, GNP and GDP. GNP is a non-hydrolysable analogue of GTP and cannot be converted to GDP. It locks whatever GTPase it inhabits into a locked form.

Despite these limitations, and the fact that the Slp2-a helix obscures the very interface that we wished to explore, this crystal structure was an important starting point for the group's efforts both to create crystallisable forms of Rab27a as well as to investigate ways to block Rab27a-effector interactions.

3.1.1 Previous Work

3.1.1.1 Fusion-Rab27a

In revealing the nature of Rab27a's interactions with Slp2-a, the structure of 3BC1 began to suggest ways in which the Rab-effector interface could be targeted.

Firstly, it was noticed that a couple of residues in Slp2-a appeared to reside in a pocket in Rab27a in an area in the SF4 region of the protein (highlighted in cyan in Figure 21). This region is variable amongst small GTPases, and alignment studies in Mostafa Jamshidiha's PhD thesis showed that the local sequence is specific to Rab27a. Conversely, many other regions, especially surrounding the nucleotide pocket, are conserved. It was hypothesised that this SF4 pocket could be druggable in the classical sense *i.e.* that a small molecule designed to fit or induce the pocket could be an inhibitor against the Rab27a-Slp2-a interaction, and any other effectors that share the same interface.

Mostafa Jamshidiha, a co-worker in the Tate group, developed and optimised a protocol for synthesising recombinant GNP-Rab27a from bacteria and made all recombinant protein mentioned in this thesis. Further, all recombinant forms of Rab27a and its variants (Fusion-Rab27a, biotin-Rab27a, Rab27a-Slp4) used in subsequent experiments were loaded with GNP (see Figure 22) and shared the same omissions and mutations as the Rab27a protein in 3BC1, with the exception of Q87L.

Taking inspiration from Chavas's heterodimer, Jamshidiha also modified the sequence of 3BC1 to generate a crystallisable fusion protein that covalently linked the *N*-terminus of Rab27a to the lower portion of the Slp2-a helix in a manner that left the SF4 pocket empty (Figure 23). This protein was named Fusion-Rab27a.

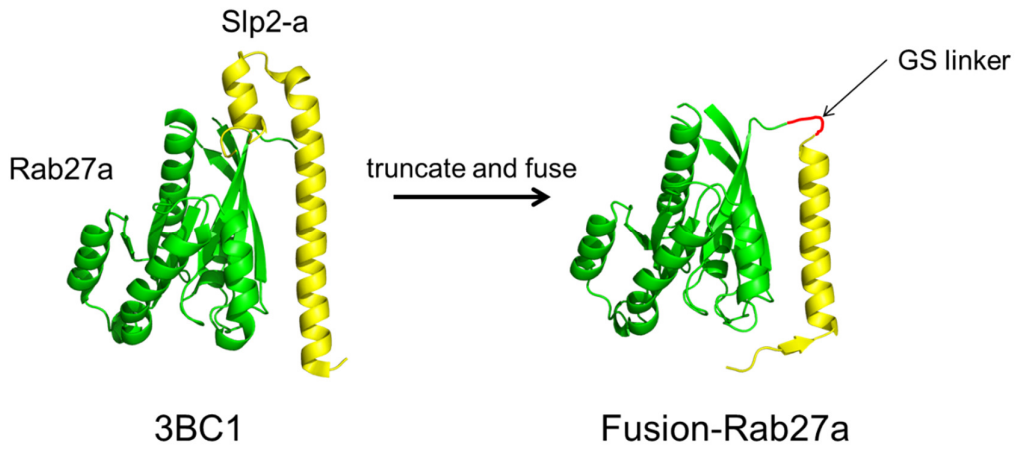

Figure 23 Crystal structure of Fusion-Rab27a in relation to 3BC1. The Rab27a-Slp2-a heterodimer (3BC1) was modified to create a single crystallisable protein named Fusion-Rab27a by removing the top part of the Slp2-a helix and joining the remainder to the N-terminus of Rab27a with a glycine/serine linker. The resulting construct was able to be crystallised, as shown by the PyMol visualisation on the right hand side. Fusion-Rab27a crystal structure by M. Jamshidiha.

The conformation of Fusion-Rab27a as revealed by x-ray crystallography was similar to that of 3BC1, including that of the SF4 pocket. Thus, it was hypothesised that the empty pocket may favour the binding of inhibitors that mimicked the Slp2-a helix.

3.1.1.2 Fragment Screen by Differential Scanning Fluorimetry

A well-designed fragment library can explore the same or greater variation of protein interfaces as a traditional HTS library, whilst being orders of magnitude smaller in size. Individual compounds in fragment libraries are also comparatively smaller and look very much like building blocks of existing drugs. The downside is that the intrinsic affinities of hit fragments are low, so detection methods must be very sensitive. Even if this is the case, it is advised to cross-validate the results with as many biophysical tests as is feasible to minimise the number of false positives, as each test has its idiosyncratic biases.

Prior to the work described in this thesis below, the Tate group performed a fragment screen using Differential Scanning Fluorimetry (DSF)[257-258] against recombinant GNP-Rab27a with a fragment library from Maybridge that contained 2500 fragments. Also called thermal shift, this assay detects the change in the melting temperature of a protein in the presence of a ligand. Any ligand can be accommodated as long as they do not interact with the fluorescent

dye or contribute their own fluorescence. The melting temperature, T_m, is the midpoint value of the thermal unfolding transition.[259] A molecule that binds to the protein will usually stabilise its conformation and thus raise its melting temperature (ΔT_m).

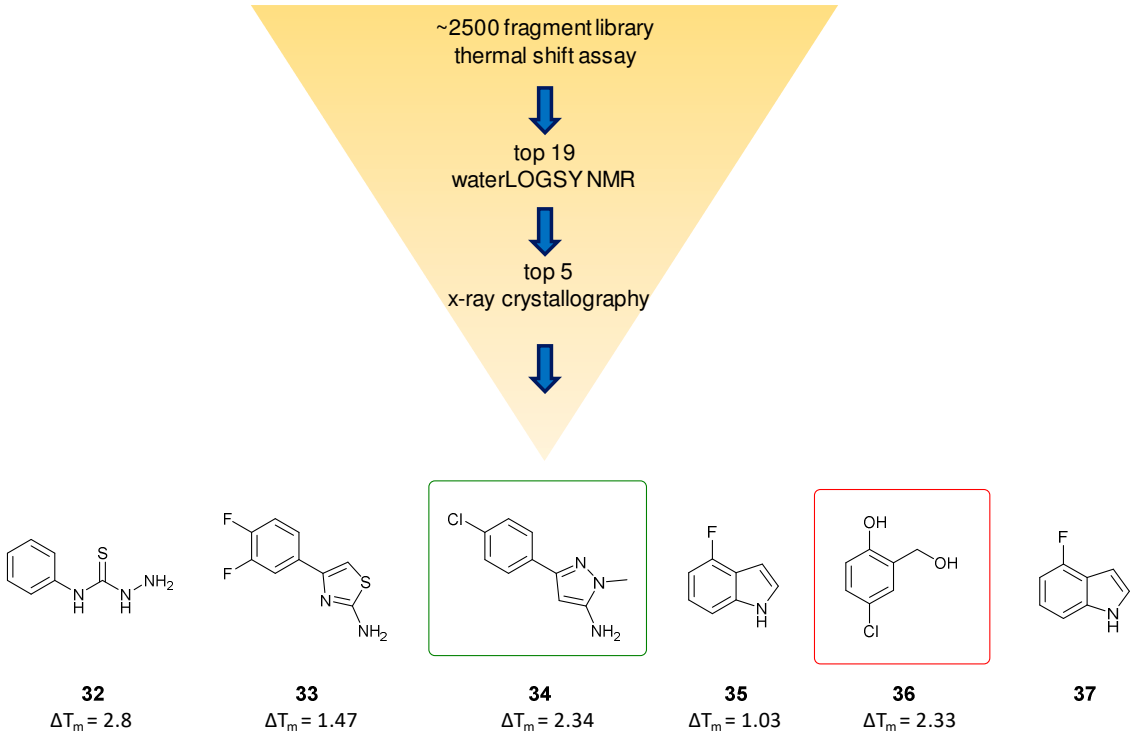

Figure 24 Schematic of the DSF fragment screen. 19 initial hits were obtained from 2500 fragments. Cross-validation by waterLOGSY gave six top fragments, which were crystallised within Fusion-Rab27a. Their averaged changes in melting temperatures (in Celsius) are given in the figure and the highlighted structures were progressed for SAR studies. Full details may be found in M. Jamshidiha's PhD thesis.

3.1.1.3 WaterLOGSY Validation of Initial Hits

The nineteen compounds with the largest increase in T_m were tested using an NMR experiment called waterLOGSY. Six compounds (**32**-**37**, Figure 24) out of 19 were determined to be active with this technique.

WaterLOGSY, which stands for "water-Ligand Observed *via* Gradient SpectroscopY, is a 1D ligand-observed NMR experiment that tests if a small molecule, preferably one containing some aromatic protons, is a weak to moderate binder of a macromolecule (it will not work for very strong binders).

The waterLOGSY pulse sequence involves selectively saturating the water signal. Through the nuclear Overhauser effect (NOE), it discriminates bound ligands from free ligands based on their different relaxation pathways due to the large difference in tumbling rates when in close proximity to a protein or free in solution.

WaterLOGSY was the chosen technique in part because it is sensitive enough to detect binders with millimolar $k_{d..}$ A key advantage for its use for Rab27a is that no structural information is required for the protein, which is too dilute to show up in the spectrum, and no modifications or tags are required for the protein or ligand.

Its drawbacks include being resource-heavy and low through-put. It requires large amounts of protein and it takes 40-50 minutes to acquire a full set of experiments for one ligand. Furthermore, the binding information obtained is qualitative with no indication of binding modes or locations.[258, 260-261]

3.1.1.4 Inspection of the Crystallised Hits

Each of the six compounds were successfully crystallised in the Fusion-Rab27a crystal structure and occupied in one out of two unique locations. **34** and **36** were selected as the representative analogues for each location as their scaffolds offered the widest scope for future customisation (Figure 25**A**).

Figure 25 shows cartoon structures and schematic diagrams with a superposition fragments **34** and **36**. The two Fusion-Rab27a units face one another in a manner similar to that of Rab27a-Slp2-a by Chavas *et al.* [PDB: 3BC1].[121] Both fragments appeared to reside in a narrow channel formed by the proximity of the two Slp2 helices along with the sides of Rab27a. It is unclear from the crystal structure if the fragments interacted more with the helix or with Rab27a. For the purposes of analogue development, we will talk about the fragments in relation to one protein unit only, under the hypothesis that the fragments were interacting more with Rab27a than the Slp2-a helix.

The top binding spot occupied by **36** was close to the SF4 pocket, and it was conjectured that upward growth towards the pocket might increase its affinity against effectors. **34** was positioned near to the N-terminal end of the Slp2a, though quite close to the pair of short β-sheets that are residual sequences from the protein construct and do not occur in the endogenous protein.

Larissa See, a Masters student in the group, pursued the benzyl alcohol **36**, whilst I developed mainly the aminopyrazole fragment **34**. The following section details the synthesis and the rationale behind the analogues synthesised for structure-guided SAR studies.

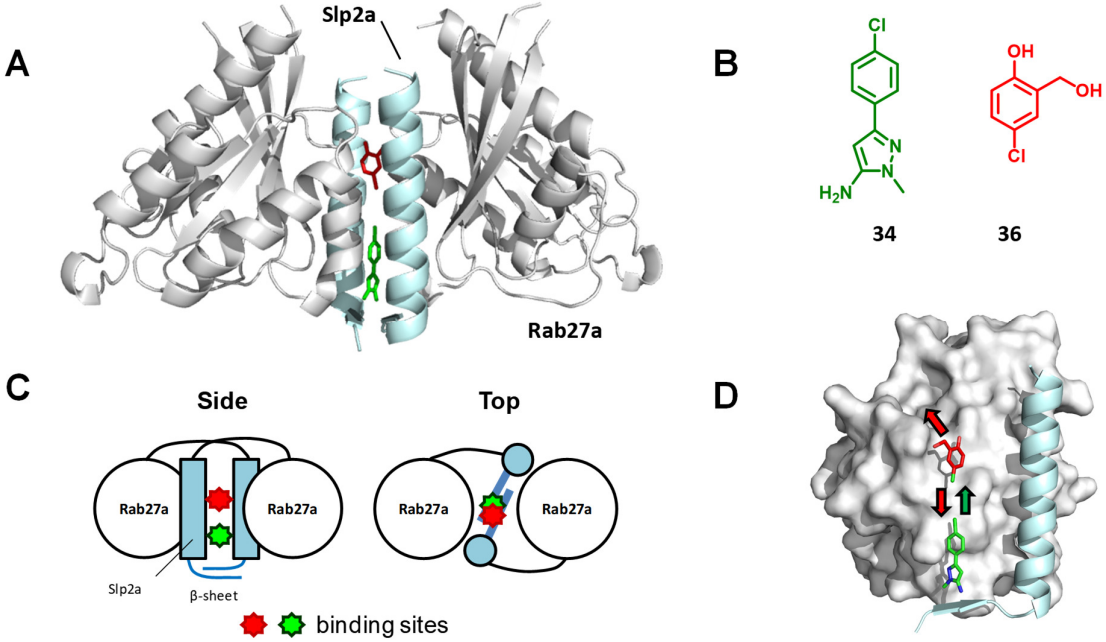

Figure 25 (**A**) Crystal structure of Fusion-Rab27a with the two distinct positions occupied by the top 5 fragments illustrated by the benzyl alcohol (**34**) and aminopyrazole fragments (**36**). The two Rab27a structures are white, the covalently linked Slp2-a segments are pale blue. (**B**) Structures of the two top hits advanced through to SAR studies. (**C**) A schematic of the binding positions in the Fusion-Rab27a crystal structure. (**D**) Cutaway of the crystal structure of Fusion-Rab27a and the same two fragments. The arrows represent proposed directions of fragment growth.

3.2 Structure-Guided Fragment Development

3.2.1 Inspection of the Crystallised Fragments

The residues of Fusion-Rab27a surrounding fragments **34** and **36** were inspected more closely (Figure 26).

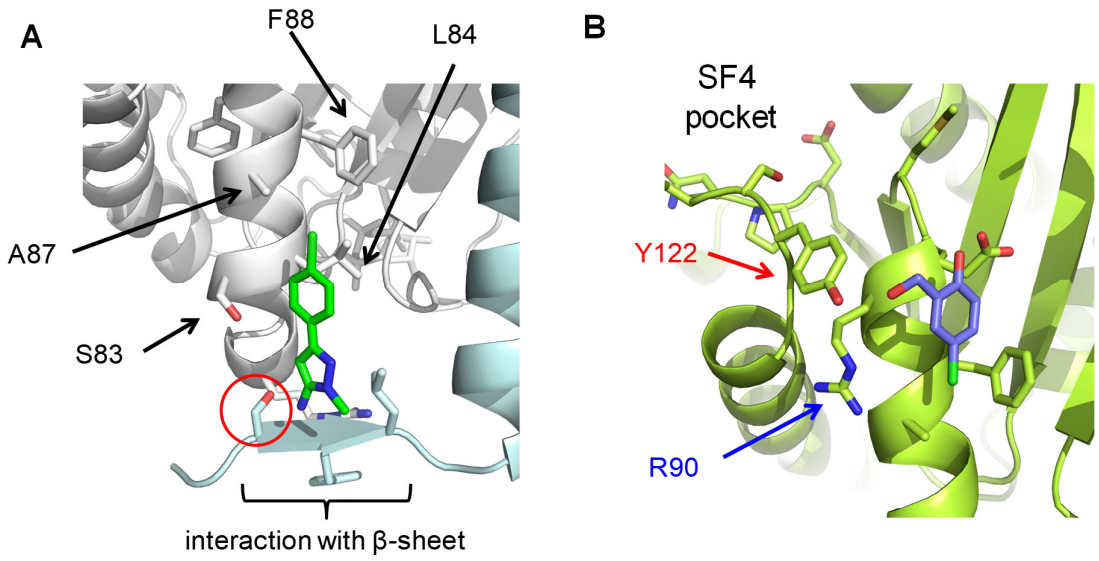

Figure 26 Close-up of the structures of the fragment 34 (A) and the fragment 36 (B) crystallised in Fusion-Rab27a. The exogenous serine residue thought to be interacting with **34** at the N-terminus of Fusion-Rab27a is circled.

The aminopyrazole **34** appears to interact with a short β-sheet at the N-terminal end of the Slp2-a structure, though this is not part of the endogenous protein. The serine residue at the end of the small β-sheet (circled in Figure 26) may be hydrogen-bonding to the free amine from pyrazole ring. Additionally, S83 from Rab27a could be hydrogen-bonding *via* a water molecule to the sp^2 nitrogen atom from the pyrazole ring if it faced the other way (the middle bond joining the two rings may be rotatable). The rest of the nearby amino acid side chains are hydrophobic in nature – L84, A87, F88, and could be interacting *via* van der Waals forces and π-stacking of aromatic rings.

The benzyl alcohol **36** resides further up the channel and approaches the SF4 pocket. A hydrophobic region with F, A and L from Rab27a sit below it, the same one that sits above the **34**. R90 and Y122 from Rab27a lie close to the proposed position of the benzyl alcohol moiety (Figure 26**B**). Y122 is particularly important, as Chavas *et al.* found that its substitution with alanine prevented its crystallisation with Slp2-a.[121] It was envisaged that If this fragment could be developed to block the interaction between Y122 and Slp2-a, it could become a potent inhibitor of the Rab27a-Slp2-a interaction.

3.2.2 Analogue Development for Fragment SAR

Figure 27 **A** and **B** show the analogues developed for the aminopyrazole and benzyl alcohol fragments. **38** - **42** were synthesised in an effort to bind to the lower hydrophobic pocket, with polar substituents to try to form H-bonding interactions to R90. **43** – **54** were molecules synthesised by Larissa See to grow fragment **35** into the SF4 pocket and to interact with Y122. They sought to explore the hydrogen-bonding of the fragment by methylating benzylic and phenolic alcohols in turn to establish key SARs. Details of these analogue series can be found in Larissa See's MRes thesis.

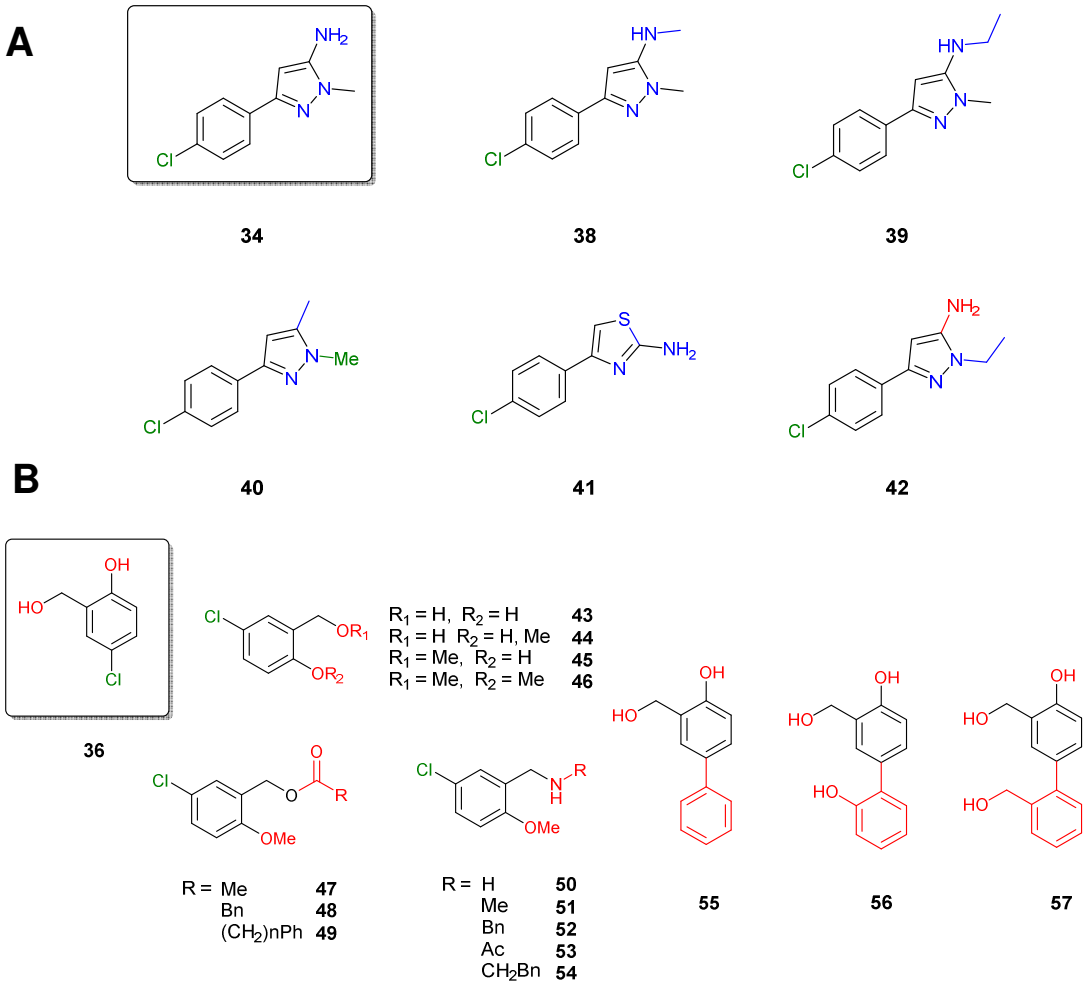

Figure 27 *S*ummaries of the fragment analogues synthesised for SAR studies.

3.2.3 Synthetic Routes

The following section discusses the synthesis of the fragment analogues synthesised to explore their SARs.

58 and **59** were synthesised from the aminopyrazole **34** (Figure 28). Due to the difficulty of controlled alkylation of primary amines, a reductive amination strategy was employed to put a methyl and an ethyl onto the sole amine substituent. The amine was first acylated by conventional means and then reduced with lithium aluminium hydride (LAH). Unfortunately, the crude mixture for **39** could not be purified, but **38** was obtained with 15% yield.

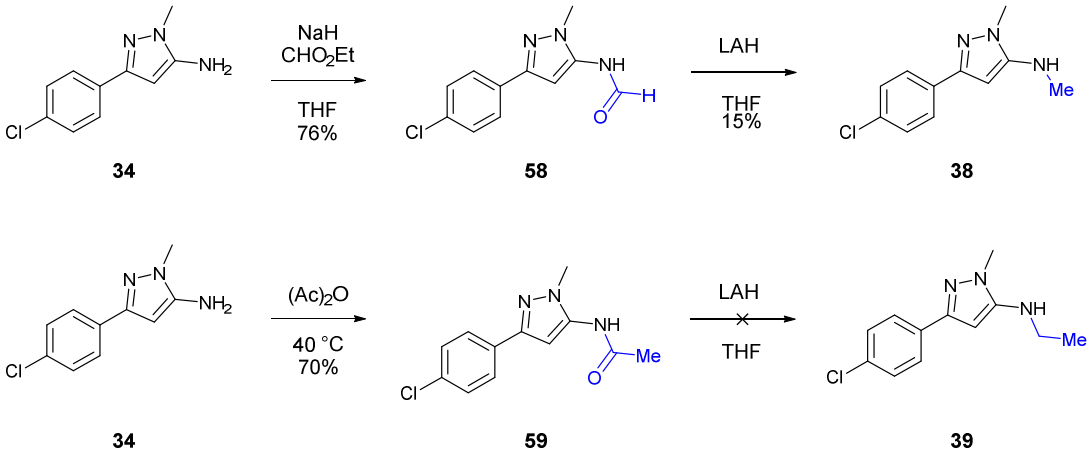

Figure 28 Synthesis of analogues obtained by reductive alkylation of primary amine.

For **40**, a new 5-membered heterocyle was synthesised *ab initio*. Following a Claisen condensation between the aromatic ester **60** and acetone, the 1,3-diketone **61** was condensed with hydrazine to give pyrazole **62** and then methylated with methyl iodide (Figure 29).

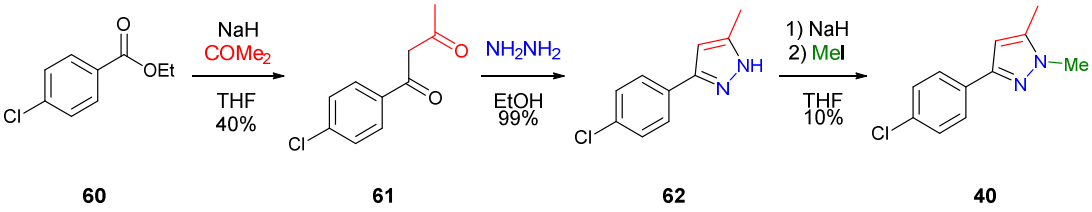

Figure 29 Synthetic route for the doubly methylated pyrazole analogue.

Aminothiazole **41** was made to test the effect of a different heterocyclic core. Although the reaction was expedient, the physical properties of the analogue were less than desirable. **41** was not very soluble, and there is evidence of these groups being pan-assay interference compounds (PAINS), which prevented further development.[262] **42** was synthesised by condensing a 1,3-keto-nitrile **64** with ethyl hydrazine.

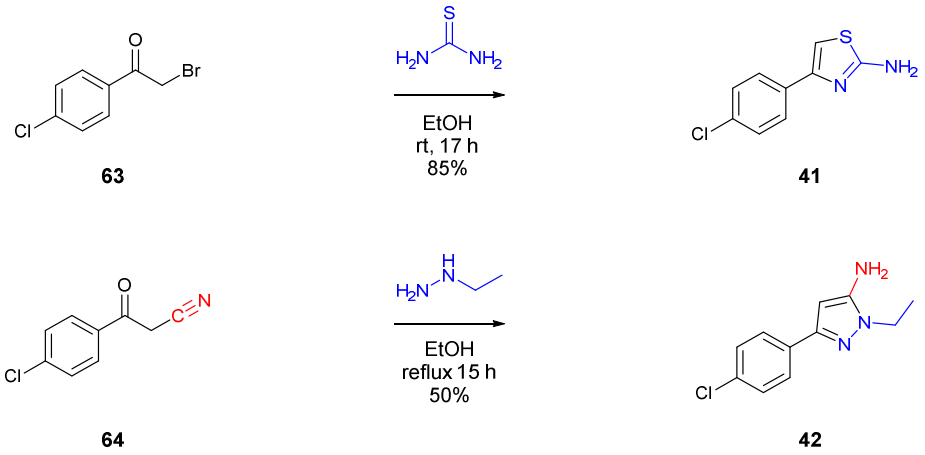

Figure 30 Synthesis of aminothiazole and ethylpyrazole analogues.

Finally, I synthesised **55**, **56** and **57** from **65** *via* acetal protection followed by Suzuki coupling, finished with acetal deprotection, though yields were only enough for NMR analysis for **56** and **57** (Figure 31).

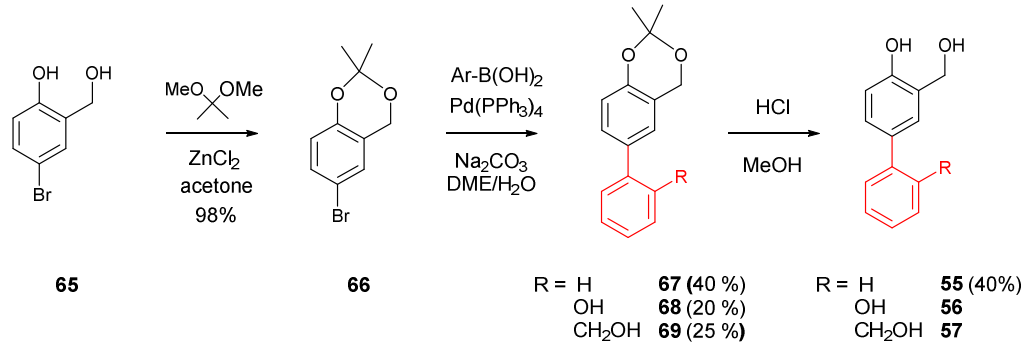

Figure 31 Acetal protection, Suzuki coupling and deprotection for benzyl alcohol analogues.

3.2.4 DSF Validation of Analogues

The top fragment hits and synthesised analogues were tested for binding to recombinant Rab27a by DSF. Table 3 shows the melting temperatures of Rab27a when tested with the original fragment hits **32**, **34** - **37** and synthesised analogues **41**, **42**, **58**, **59** and **62**. ΔT_m was defined as the average melting temperature, T_m, minus the T_m of Rab27a with 2% DMSO. Fluorescence traces and replicate values can be found in Appendix A.

Compound	T_m	ΔT_m*
Buffer only	60.5	**-0.2**
2% DMSO	60.7	**0.0**
32	60.3	**-0.4**
34	60.4	**-0.2**
35	60.4	**-0.3**
36	60.4	**-0.3**
37	60.3	**-0.4**
41	N/A	**N/A**
42	60.4	**-0.3**
58	61.1	**0.4**
59	60.4	**-0.3**
62	N/A	**N/A**

Table 3 Results of a DSF assay showing melting temperatures of recombinant Rab27a in the absence and presence of top hits from the fragment screen and synthesised analogues for SAR studies. The values shown are averages of quadruplicate data. *$\Delta T_m = T_m - T_m$ (2% DMSO).

Melting temperatures could not be calculated for **41** or **62** due to the non-sigmoidal shape of their fluorescence traces. Interestingly, the shape of the curve for **41** appeared to have two turning points, suggestive of the compound being able to stabilise two different conformations of the protein. However, the majority of compounds tested had negative ΔT_m, including the top fragment hits from the screen. This contradicts the results of the screen, but these esults were consistent even after multiple rounds of testing.

Because of these major inconsistencies, the DSF assay was not used for further investigations of Rab27a ligands. Following from this, an SPR screen was developed by other members of the group in conjunction with the Institute of Cancer Research at the

latter's facility in Sutton, and the technique was used to test the compounds in the next section of this chapter.

3.3 Peptide Binders

Peptides offer an alternative to small molecules as inhibitory binders. As they are composed of the same building blocks as proteins, the potential for binding complementarity is intrinsic. Intuitively, it should merely require the right sequence, possibly requiring additional stabilisation, to have selected affinity for an interface. An advantage of using peptides is their relative ease of construction. Being combinatorial, they do not require bespoke synthetic routes like small molecules do and numerous automated procedures exist for their synthesis, the most prominent being solid phase peptide synthesis (SPPS) with *N*-Fmoc-protected amino acids. However, creating small peptides to emulate the binding properties of large proteins is challenging, and many peptides have physical properties that make them unsuitable for drug use.

As with the fragment screen, the goal was to create a peptide that would inhibit Slp binding by targeting the Rab27a-specific region in the SF4 pocket. The binding interactions of Slp2-a in 3BC1 were inspected. At 59 residues (although only a small fraction of the total protein of 936 residues), it is too long to count as a small molecule inhibitor. A short peptide would be more suitable as this would likely have fewer issues of synthesis, solubility and cell permeability. The downside to short peptides is their conformational freedom; they almost always require chemical stabilisation to maintain secondary structures such as α-helices.[99, 263]

3.3.1 Dipeptide WF

It was proposed that a short peptide could be obtained by downsizing the helix whilst maintaining its binding affinity to the proposed SF4 hotspot. Figure 32 illustrates this thought process.

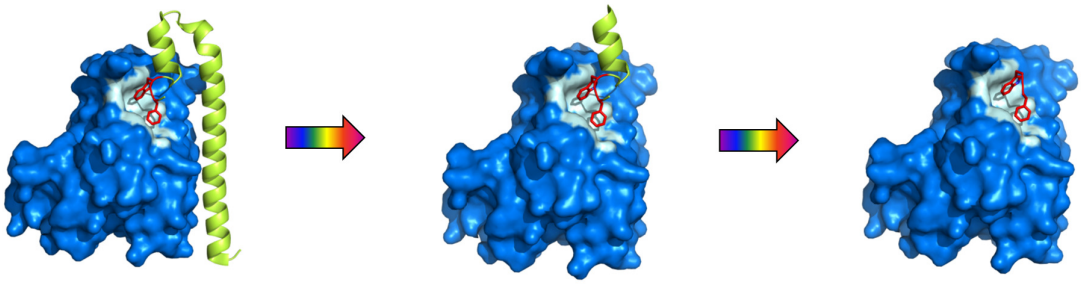

Figure 32 Downsizing the structure of Slp2-a to obtain a smaller, more ligand-efficient binder of the SF4 pocket (highlighted in light blue), capable of inhibiting effector interactions.

The regions of Rab27a that bind to the lower helix of Slp2-a are more conserved and less useful for finding a Rab27a-specific inhibitor. When the crystal structure of 3BC1 was inspected, it appeared that the side chains of adjacent tryptophan (W) and phenylalanine (F) residues were most strongly interacting with Rab27a in the SF4 pocket, based on the depth of the pocket that surrounded them (Figure 33). It was hypothesised that the dipeptide WF could be a weak binder for Rab27a.

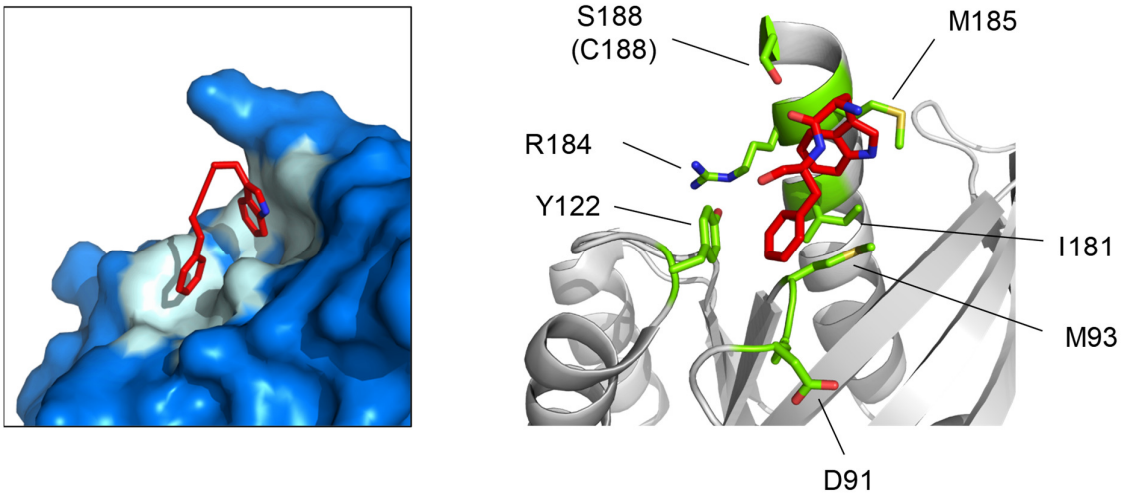

Figure 33 A closer look at how the side chains of W and F lie in the SF4 pocket of Rab27a (3BC1).

Doubly capped Ac-WF-NH_2 was synthesised by SPPS. Uncapped variants were considered unsuitable as they would introduce charged groups in solution that are not present in the native structure. Hence, WF was used for all subsequent experiments, and all references to "WF" now refer to the acylated and amidated dipeptide.

3.3.2 WaterLOGSY of WF

When WF was tested for binding by DSF, it showed no increase in the melting temperature of Rab27a (Appendix A). However, it tested positive for binging by waterLOGSY. Figure 34 shows the results. The images show overlays three NMR experiments in the aromatic region of the dipeptide (the alkyl region is largely obscured by the suppressed water signal). The green trace is a scaled down 1D HMR spectrum of 1 mM WF in 10% D_2O in 50 mM HEPES, 150 mM NaCl and 5 mM $MgCl_2$. The blue trace is the waterLOGSY spectrum of 1 mM WF alone, and the red trace is of 1 mM WF plus 10 µM of protein. The protein signal is too weak to see in the spectrum. An inversion, or partial inversion, of the red trace is observed for molecules that bind to the protein.

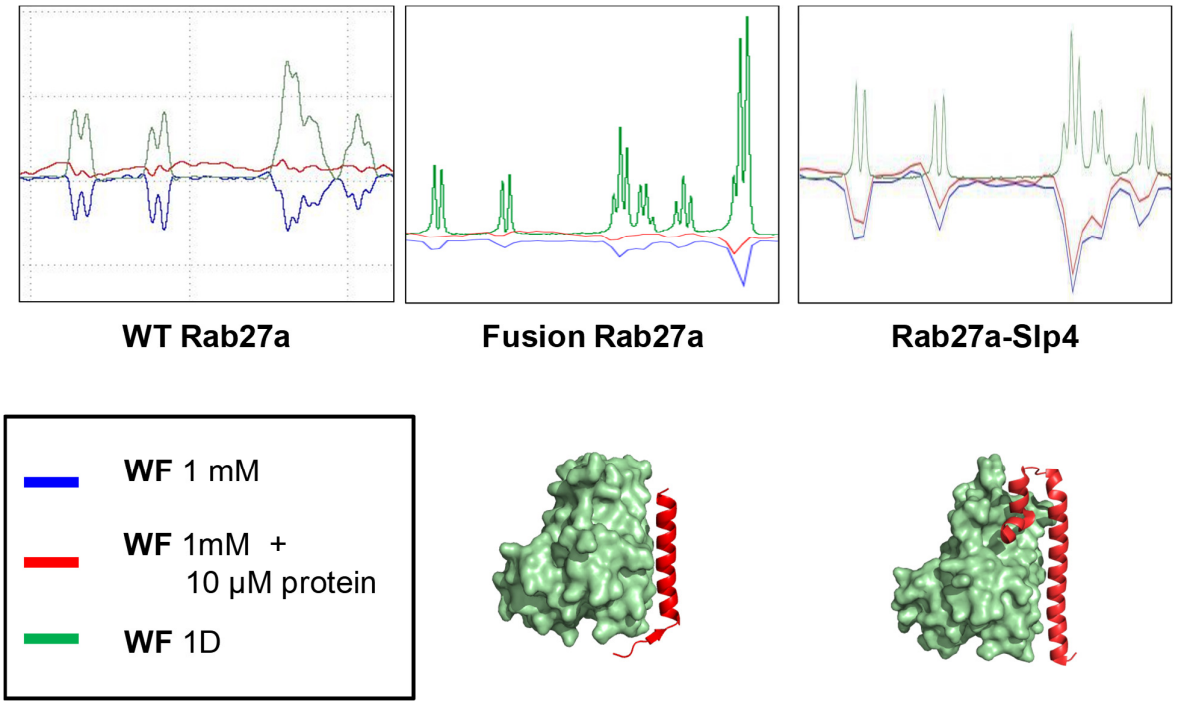

Figure 34 WaterLOGSY results for the dipeptide WF. The NMR spectra show a portion of the aromatic region and are superpositions of the 1D proton spectrum, the waterLOGSY spectra of the ligand alone and of both protein and ligand. The 1D spectrum has been scaled down by 0.1; it is for reference only. Binding is positive if the presence of protein causes the waterLOGSY signal to become less negative or to invert. Inversion occurs for WT Rab27a. It occurs to a lesser extent for Rab27a and even less so for Rab27a-Slp4, which has its SF4 pocket occupied. The crystal structures above are of Fusion-Rab28 and of 3BC1, but the structure Rab27a-Slp4 is thought to be similar to the latter.

As shown in Figure 34, WF binds to both wt-Rab27a and Fusion-Rab27a, proteins which have the SF4 pocket open, but not to the Rab27a-Slp4 complex, in which the SF4 pocket is

occupied. This was a promising indication that the dipeptide binds in or close to the SF4 pocket.

SPPS is an expensive way to make a large quantity of a dipeptide, largely due to the high ratio of resin to peptide output even if the yield is high. Thus, to synthesise a large batch for further validation and as positive controls in future experiments, a solution-phase synthesis was devised and performed (Figure 35). Acylated tryptophan and amidated phenylalanine were coupled in solution with DIC and HOBt. After filtering the by-product and purification by column chromatography, the dipeptide was obtained with a yield of 8%.

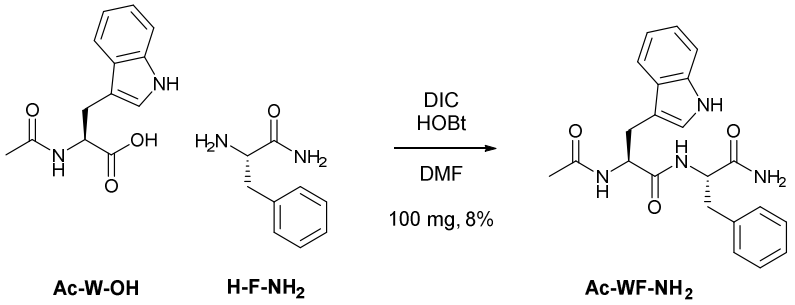

Figure 35 A one step solution-phase synthesis of doubly capped WF.

3.3.3 Surface Plasmon Resonance (SPR) Assay

In the absence of structural information on endogenous Rab27a and the need to obtain quantitative data on binding molecules, the technique of surface plasmon resonance (SPR) was chosen to overcome the drawbacks of waterLOGSY.

SPR is a high-throughput and sensitive technique that gives a high quantity of information in a single run. It tracks the change in absorption of a laser directed at the interface of a prism and a thin gold chip onto which the target protein adsorbed. When molecules bind to the protein on the chip, the absorbed wavelength changes. SPR assays have many advantages. It can be fully quantitative with the use of titrations, it gives kinetic data on the on/off binding of molecules and it is capable of real-time observation of binding. Further, it does not require structural data of the protein of interest and neither does the protein nor the binders require fluorescent, isotopic or radioactive labels. The chip can also be reused.[264-265]

However, SPR is not a trivial assay to set up and run. It requires a significant amount of preparation and optimisation and bears significant overhead costs. It is very sensitive to variations in the conditions (*e.g.* DMSO percentage), and poorly solubilised compounds may aggregate and give spurious results. This is a key issue for fragment screens as weak binders require higher test concentrations. Solubility tests can be run beforehand, but this would add to the workload.

Charlotte Sutherell and Mostafa Jamshidiha from the Tate group, alongside Martin Rowlands from the Institute of Cancer Research (ICR), developed an SPR assay with recombinant biotin-Rab27a and Fusion-Rab27a adsorbed on Neutravidin-coated chips. WF was tested in this set-up and was found to bind consistently to Rab27a with a sensogram shape indicating specific binding to Rab27a. Extrapolation of the binding titration gave a rough k_d of 8 mM. Although this classifies WF as a very weak binder, it demonstrates the sensitivity of SPR and corroborates the positive binding results from waterLOGSY. WF also bound to Fusion-Rab27a, though more weakly. The dose-response graphs and sensograms are shown in Figure 36.

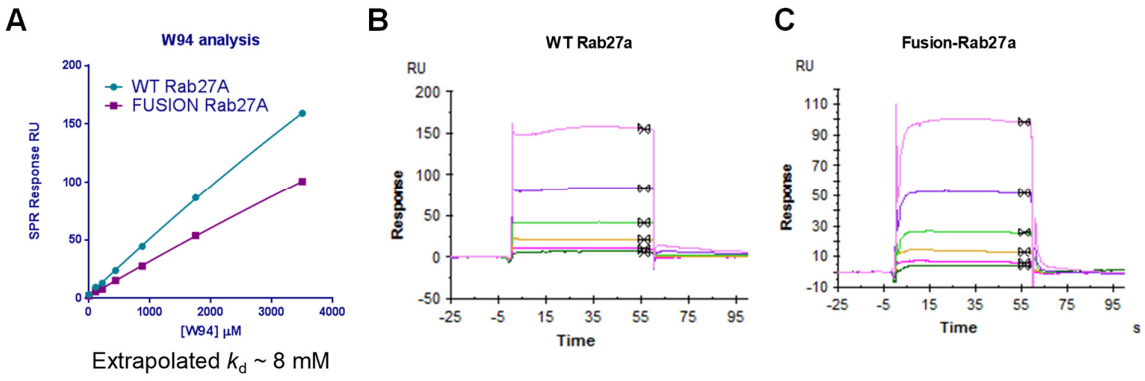

Figure 36 SPR results for WF. WF was tested by SPR for binding against wild type Rab27a and against Fusion-Rab27a. It was a specific binder of both, as evidenced from the sensogram shape (clean binding and dissociation), albeit weakly. The maximum response was higher for wt Rab27a than for Fusion-Rab27a. The extrapolated k_d of WF against wt Rab27a was 8 mM. Images by Martin Rowlands (ICR).

Unfortunately, WF could not be crystallised with Fusion-Rab27a, likely due to its weak binding. However, the results for WF were nevertheless a major breakthrough as it now provided us with a positive control. Jamshidiha, along with Nathan Brown from ICR,

subsequently used the dipeptide as the ligand model in an *in silico* screen; further details may be found in Jamshidiha's PhD thesis. In this chapter, the next task was to increase WF's binding affinity.

3.3.4 Extending WF - Short Linear Peptides

Figure 37 shows the structure of the truncated Slp2-a of 3BC1. Examining the structure on either side of WF (circled), we chose to investigate whether including amino acids on either side would improve affinity and/or solubility. Other modifications trialled also included reversing the WF to FW, and using D-tryptophan instead of the native L-tryptophan.

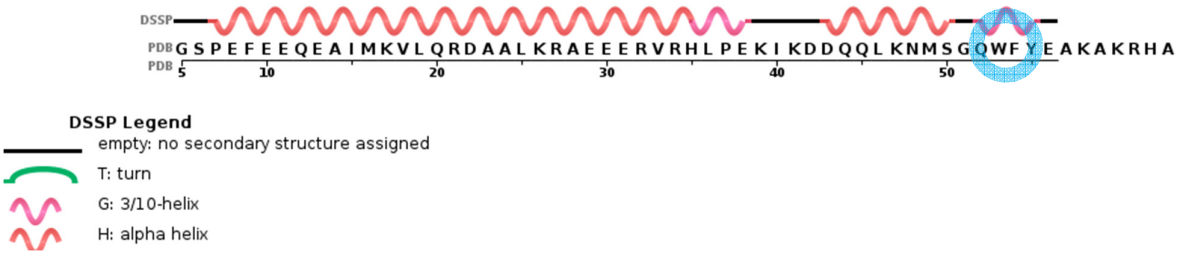

Figure 37 Sequence of the Slp2-a protein fragment in the heterodimer crystal 3BC1. The WF residues are circled. Beyond E56, the residues are not visible in the crystal structure, more likely due to flexibility.

Table 4 displays the short linear peptides (**70**-**85**) synthesised by SPPS and the qualitative result from waterLOGSY tests. Images of the NMR spectra can be found in Appendix B.

Ref	Peptide	Binds to wt-Rab27a?
-	WF	Yes
70	FW	No
71	wF*	Yes (insoluble)
72	fluorescein-WF	Yes
73	QWF	No
74	GWF	No
75	H-WAF	Yes

76	H-WFY	Inconclusive
77	WFYE	Inconclusive
78	WFYK	Inconclusive
79	QWFYE	No
80	GQWFYE	No
81	WFYEAK	No
82	WFYQAK	No
83	WFYQHK	No
84	WFYEAKA	No
85	YY (negative control)	No

Table 4 Short linear peptides synthesised by SPPS and tested by waterLOGSY. All peptides are acetyl and amide capped unless specified. Please see Appendix B for NMR traces. *with D-tryptophan

It became much more difficult to interpret waterLOGSY spectra once the sequence exceeded four amino acids. Not only did the aromatic region become crowded with peaks, the increased number of very intense and relatively broad NH signals started to overlap with many peaks in the region.

Aside from WF itself, only **71** (wF, with D- instead of L-tryptophan), *N*-terminally labelled **72** (fluorescein-WF) and **75** (WAF) appeared to show binding by waterLOGSY. However, **71** suffered from poor solubility and the result for **72** was questionable as the fluorescent tag is half as large as the proposed binding epitope and was synthesised at low yield. The addition of fluorescein essentially appends a highly non-polar group to WF and may have induced non-specific binding to hydrophobic regions of the protein surface.

The main conclusion of this work was that peptides of greater than three amino acids in length have a decreased chance of being a binder to Rab27a. This may be because the additional amino acids do not interact with the surface of Rab27a but rather are integral to

maintaining the secondary and tertiary structure of the Slp2-a helix. Thus, including them alongside WF will not increase the binding affinity because the additional loss in entropy will not be made up for by an increase in binding enthalpy.

3.3.5 Stapled Slp2-a Peptides

When the WF motif is part of the Slp2-a helix, its conformation is constrained by the rest of the protein. If it is assumed that WF binds in the SF4 pocket, then it is possible that the weakness of the dipeptide's interaction is because of its conformational flexibility. Because there is more entropic loss upon binding for a flexible molecule, binding becomes thermodynamically less favourable. Ways were sought with which to constrain the peptide to adopt the favoured conformation.

Peptides have been successfully constrained through a variety of stapling methods (see Chapter 1). Previously, Tiffany Chan, a Masters student in the Tate group, attempted to staple the top portions of the Slp2-a helix by replacing K47 and Q52 (numbering from 3BC1) with (*S)*-pentenylglycines or with cysteines, to be cyclised *via* ring closing metathesis and with para-dibromoxylene respectively. Unfortunately, both methods of cyclisation gave very low yields and the cyclised peptides did not show binding by DSF, waterLOGSY or protein-observed HSQC.

3.5.5 Lactam-bridged peptides

Alkene-stapling methods are often expensive, not least because of the cost of ruthenium catalysts and in either obtaining or synthesising enantiomerically pure pentenylglycines and alanines. Using a microwave adds potential complications and increases the need for optimisation, further adding to expenses. A peptide-stapling method that avoids some of these issues is lactam bridging, which describes a technique where an amide bond is formed between the side chains of a lysine and an acidic residue (aspartic or glutamic acid) spaced in an *i*, *i* + 3 fashion.[266-267]

Here, no unnatural amino acids are involved and the synthetic method incorporates a simple intervention at the last stage of an automated solid phase peptide synthesis (SPPS) run.

The Fmoc-protected K and D/E amino acid reagents must have highly acid-labile protecting groups that can be cleaved under orthogonal conditions. Instead of the usual Boc, the amine in K is protected with methoxymethyltrityl (Mmt) or methyltrityl (Mtt). D and E are protected by 2-phenylisopropyl ester instead of the more usual *t*-butyl, which needs more strongly acidic conditions to remove. Thus, deprotection by 3% TFA in DCM reveals the free amine and carboxylic acid groups whilst leaving all standard protecting groups intact. These specifically deprotected reactive groups are then joined by usual peptide coupling methods such as DIC/HOBt or PyBOP (Figure 38), before cleavage from the resin by conventional methods.

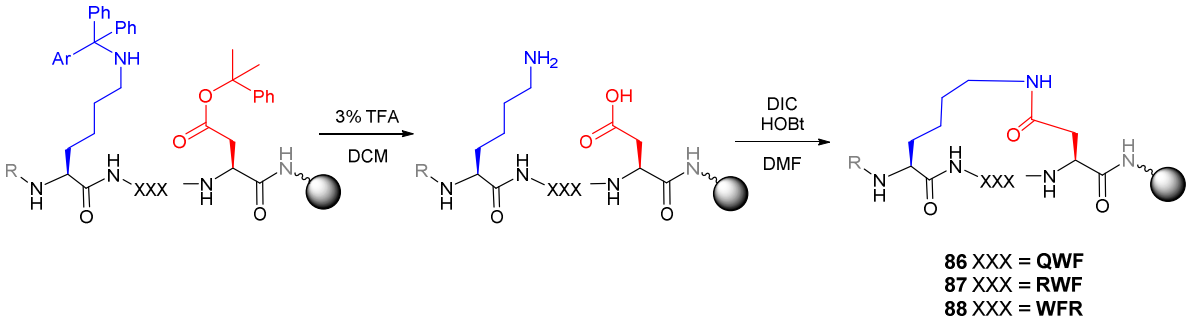

Figure 38 Deprotection and cyclisation steps for lactam-stapled α-helical peptides.

The 3_{10} helical backbone surrounding WF in Slp2-a has close to a 90° bend in it (**Error! Reference source not found.**). Thus, it would not make sense to extend the sequence much beyond either side of WF as a straight helix would not be favoured, certainly not past the Q towards the N-terminus. For this reason, the lactam bridge was introduced predominately as a conformational constraint rather than as a means to induce secondary structure. Harrison *et al.* showed that the highest helicity is obtained with the sequence **K**XXX**D**. Here, we chose to prioritise helicity over length of the amino acid sequence.[267] Hence, this template was adopted for all lactams synthesised for this project.

The minimum length of amino acids required for an *i*, *i*+3 lactam helix was 5 amino acids long. K and D at either end were fixed, and of the three inside, W and F were also fixed. The remaining amino acid was a free choice and this was at first exploited in an attempt to increase the solubility.

Three short lactams-bridged peptides were successfully synthesised (Figure 38). Longer lactams were also attempted, including of other portions of the Slp2 helix (**89**-**92**). However, these suffered either from solubility, yield or conversion issues solubility issues (**Table 5**). Further, when the lactam-cyclisation reaction was analysed by LCMS, most samples appeared to be only partially reacted even after multiple additions of fresh coupling agent. It was difficult to achieve greater than 50% conversion even for the smallest lactams.

	Sequence	Purified
86	**K** Q W F **D**	Yes
87	**K** R W F **D**	Yes
88	**K** W F R **D**	Yes
89	E E Q **K** A I M **D** V L Q R A A L K	
90	E E Q **E** A I M **K** V L Q R	
91	**K** E E Q **D** A I M K V L Q R	
92	A E Q **K** H I R **D** V L Q R	

Table 5 List of lactam-bridged peptides synthesised. The majority suffered from poor conversion or solubility. Amino acids in bold indicate the lactam-bridged residues.

The three WF-containing lactams **86**-**88** were tested by SPR (by Charlotte Sutherell and Martin Rowlands), first for non-specific binding and then titrated to obtain a binding affinity in the form of a dissociation constant, k_d.

Binding titrations to **86** (QWF) and **88** (WFR) were obtained (Figure 39). Unfortunately, **87** was a non-specific binder and was not tested further. Their relatively low solubility prevented them from being tested at higher concentrations so their rough k_d values were obtained by extrapolation of the curve. However, they did appear to bind more strongly than WF.

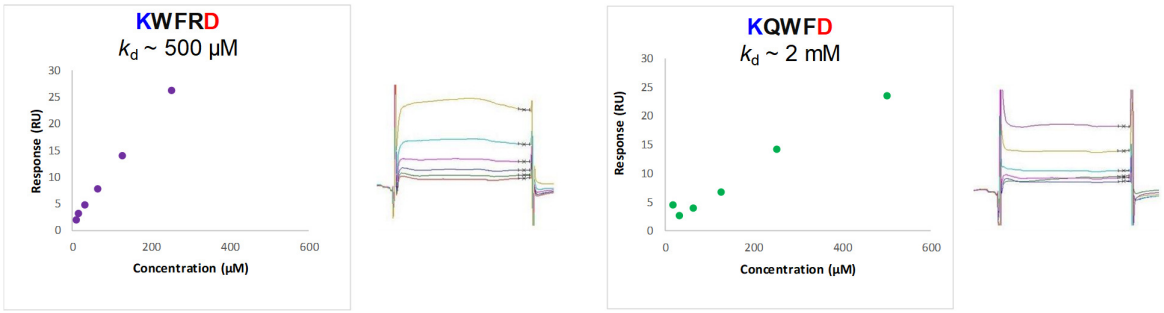

Figure 39 SPR results from two lactam-bridged peptides

This result suggests that other amino acid combinations within the lactam bridge could be improve the binding of WF. The third amino acid could be placed in any combination of XWF, WXF and WFX, and so a wide range of permutations is possible. Given the prevailing issues of low solubility and binding affinity, future work should start by focusing on ones that increase solubility or otherwise modify the bond angles in the restricted helix to cover more conformational space, for example Lys, Asp, Glu, Pro, or even unnatural amino acids.[268] The lactams would need testing by SPR, ideally at higher concentrations, and against a control protein to show that binding is specific. Other assays would also be required for cross-validation.

3.4 Conclusions

In this chapter, attempts were made to develop a small molecule inhibitor and a short peptide inhibitor of Rab27a.

Following from a DSF fragment screen and validation against recombinant Rab27a by Mostafa Jamshidiha and other members of the Tate group, analogues were synthesised for the fragment hits **34** and **36** for SAR studies. When tested using DSF, most analogues gave no shift in the melting temperature. However, the original hit fragments also failed to reproduce their behaviour in the screen.

It was concluded that the results from the DSF screen could not be reproduced, and as a result thus the group turned towards developing an SPR assay in collaboration with ICR to obtain high-throughput and quantitative results.

In hindsight, DSF was likely a suboptimal choice of an assay for a fragment screen against a protein like Rab27a. Rab27a is a flexible protein that interchange between different conformers in solution. It is possible that different binders stabilise different conformations, which could cause the T_m to fluctuate or even decrease from control conditions. Further, it was possible that the fragment's binding to the crystal structure was entirely artefactual, caused by the narrow water channel in the middle where the two protein units met. If this was the case, then it nullifies the rationale behind the SAR studies.

A fragment screen requires higher concentrations of test molecules to see binding. Insolubility and aggregation may become an issue at these higher concentrations (>1 mM). If the screen were to be repeated, it may be pertinent to screen the library compounds for solubility and auto-fluorescence under the assay conditions in order to rule out those types of false-positives. A lower ligand concentration may also be considered.

Like many small GTPases, development of inhibitors for Rab27a presents significant challenges. To succeed with Rab27a, not only will new technology be required, but also new ways of approaching drug design. Techniques like SPR, *in silico* and fragment screening are relatively modern and have not yet enjoyed decades of active use. These and the advent of other new, highly sensitive biophysical detection methods such as NMR, fluorescent polarisation (FP) and microscale thermophoresis (MST) are methods that are enjoying more use in the scientific community.

As for the peptide side, much remains to be explored. The dipeptide WF gave a surprising positive initial result; despite being a weak binder with a k_d of ~8 mM, it has shown consistent binding to Rab27a and to Fusion-Rab27a by waterLOGSY and SPR. Work by other members of the group is currently ongoing to mine its potential, for example by

attaching an acrylamide warhead to turn it into a covalent binder to Rab27a's surface cysteines which reside along the rim of the SF4 pocket.

There is scope to be explored on the lactam-bridged peptides, with many other permutations that could be synthesised with W, F and an amino acid of choice. A variety of properties may be achieved with different combinations. It is unknown as of yet whether the lactam approach will be successful, so this idea remains for a future project.

4 Development and Synthesis of Photocleavable Crosslinkers

4.1 Introduction

The subject of this chapter is the design, synthesis and validation of a photocleavable crosslinker intended for use in a proteomics workflow that can identify and quantify the both transient and stable interaction partners to Rab27a.

Co-immunoprecipitation (co-IP) is traditionally used for pulling down protein complexes with solid-supported antibodies. The immobilised complexes are washed carefully to minimise disruption of PPIs. However, this technique is unable to capture transient interactions. Even stronger interaction may easily be lost; every binding equilibrium comprises rates of and this equilibrium (comprised of k_{on} and k_{off}) will always favour dissociation after pull-down. Therefore, only stable interactions remain even with mild wash buffers. Further, the surface of the protein-antibody interface may exclude some interactions.

The chemical biology approach of XLMS (Chapter 1) has been developed in part with a purpose to rectify these drawbacks, and crosslinkers have been used for both protein structure studies and for mapping protein interaction networks. With the correct attuning of the warhead reactivity, they are able to crosslink only proteins that come into close proximity.

The introduction of a photocleavable moiety to a crosslinker for use in XLMS enables the possibility of releasing the binding partners cleanly from the immobilised POI or from one another, depending on the set-up. It essentially adds an orthogonal purification step for simplifying the analysed mixture.

The ultimate aim of this project is to develop an expedient means of elucidating Rab27a's binding partners to investigate further its roles in health and disease. Once the methodology is established, it could be applicable to any protein of interest (POI).

4.2 Proposed Workflow

The initial concept is presented in Figure 40, which formed the basis for the rationalisation of our early designs. For reasons that will be discussed later, the proteomic experiments described in Chapter 5 used a slightly different set-up.

A biotin affinity tag for Rab27a was originally envisioned to be pulled down by NeutrAvidin coated agarose beads as in many other workflows within the Tate group. This was first used as a spike-in bait protein, before later being replaced by transfected Twin Strep Tagged (TST-)Rab27a.

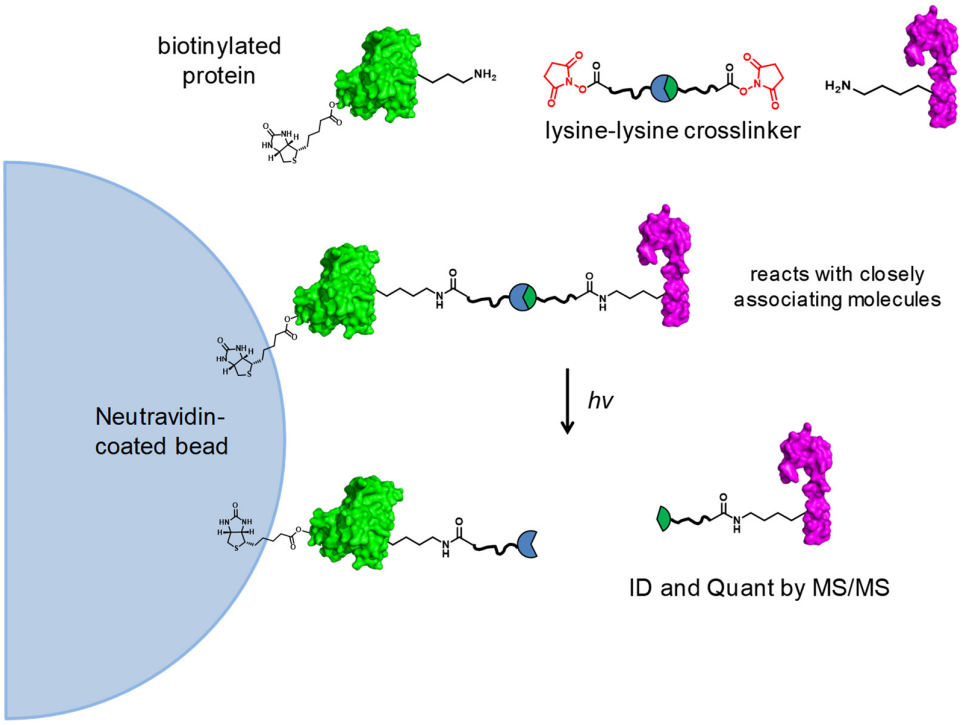

Figure 40 An illustration of the concept behind photocleavable crosslinkers. For this method to work, the POI must have an affinity tag, e.g. biotin, for enrichment purposes. Addition of a crosslinker covalently stabilises PPIs occurring in the mixture. Solid-supported NeutrAvidin pulls down the POI along with its linked partners. Application of UV light releases the effectors into solution, giving a clean mixture that is then digested and analysed.

4.3 Crosslinker Design Considerations

The putative photocleavable crosslinker requires careful consideration a number of factors including warhead reactivity, length, photocleavage properties, water solubility, stability in water, facile synthesis and ease of introducing further functionalities. These properties are discussed in turn below. Figure 41 summarises the ideal properties the proposed crosslinker (XL).

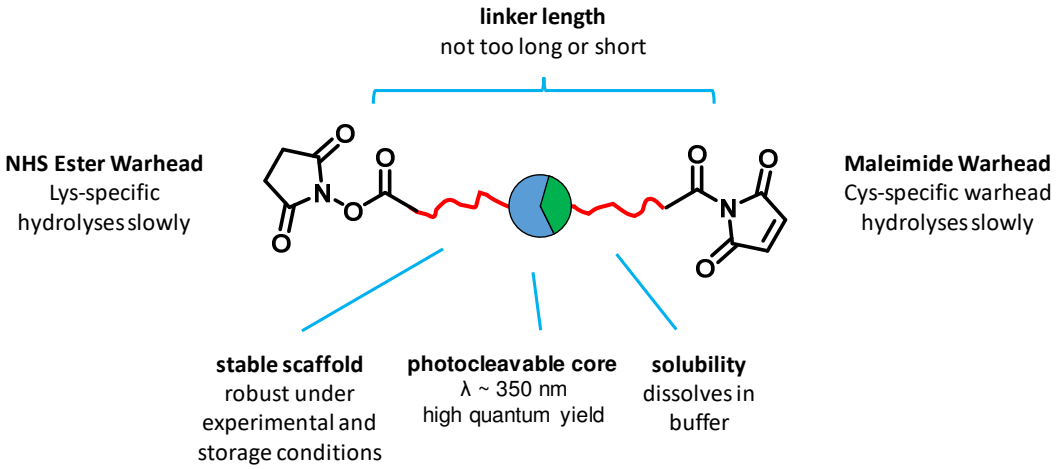

Figure 41 Summary of the considerations for the design of bifunctional crosslinker. The NHS ester and maleimide warheads represent the two most common electrophilic groups for targeting lysines and cysteines respectively. They are both shown here to illustrate the choice.

The warhead is an electrophilic moiety that forms the covalent bond to a nucleophilic residue. It must be selectively reactive for its target residue but be insensitive to variations in that residue's reactivity caused by different protein environments. As water is the most numerous albeit weak nucleophile, warhead reactivity must be balanced against hydrolysis. The latter cannot be prevented, but it would suffice if the rate of hydrolysis was significantly slower than the rate of residue conjugation.

The scaffold of the molecule needs to be stable enough that it does not lose its integrity in storage as a DMSO stock, nor in aqueous solution for the duration of the experiment. The full workflow would include crosslinking, quench, UV irradiation, proteomic sample preparation and sample running, which span a period of time approaching 72 h in aqueous solution at physiological pH.

Once the crosslinker is attached at one end, the other must also react before it is hydrolysed. The efficiency of crosslinking will depend on how well matched the length of the crosslinker is to the distance between reactive residues on the PPI. Very short linkers give higher resolution data but may miss many interactions. This suggests that long and flexible crosslinkers could be more versatile because they can span a greater range of distances. However, long linkers might increase the likelihood of self-reacting (type 1 crosslinks), and may have undesirable physical properties, and the bulk might prevent PPIs from forming.

The photocleavable core should be cleaved with high quantum yield upon application of a strong source of UV of a wavelength of around 350 nm. However, it needs to be relatively stable under ambient light such that it survives sample handling. In the laboratory, samples can be covered with foil or put into cupboards wherever possible, but this does not eliminate exposure to light.

The choice of photocleavable core and its synthetic route should leave ample scope for further functionalisation; this will become relevant during further development and optimisation of the initial prototype. Changes could include: potential addition of useable groups *e.g.* fluorophores, affinity labels, clickable moieties, ease of changing linker lengths and warheads.

Rab27a contains five cysteines, one of which is internal and two are prenylated at the C-terminus leaving only two free for labelling. In contrast, Rab27a has twelve lysines distributed across its sequence (Figure 42; additionally Figure 71 from Chapter 5). Therefore, it was decided that the crosslinker was to target lysines exclusively using N-hydroxysuccinimide (NHS) esters as both warheads

A commonly used and commercially available non-cleavable crosslinker is disuccinimidyl suberate (DSS) with MW 368.34 and a length of 11.4 Å. This will be considered the control molecule, and our initial designs were based on the idea of inserting a photocleavable core into the middle of the structure.

Figure 42 shows an example of a pair of lysines, K11 from Rab27a (green) and K26 Slp2-a (yellow) that we would expect to be crosslinked. The bond distance measurement in PyMOL comes to 6.6 Å, so it was envisaged that a mid-length linker like DSS should have no problem linking them together.

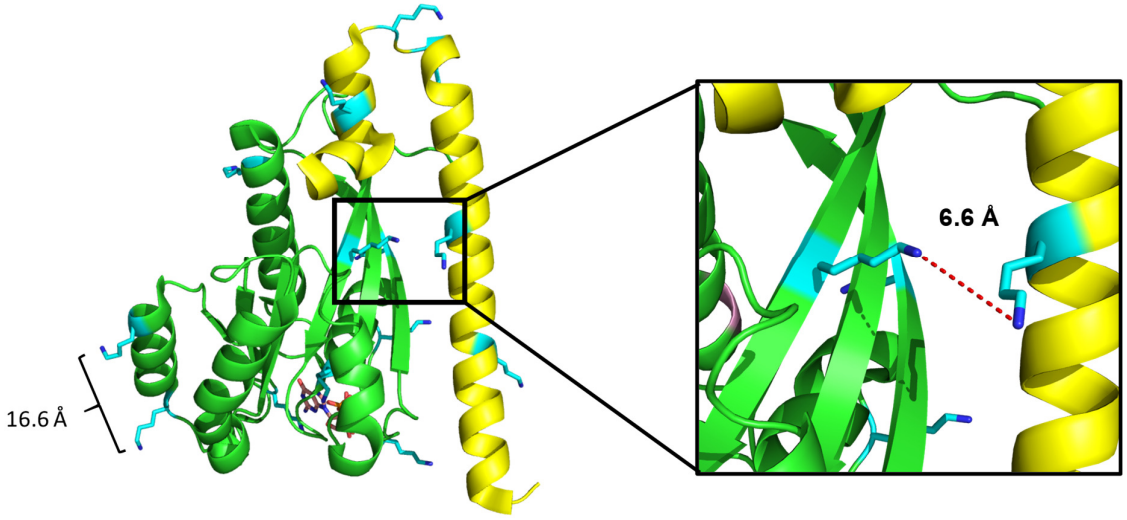

Figure 42 PyMOL-rendered image of 3BC1 showing the lysines on Rab27a and a closeup lysines K11 in Rab27a and K26 from Slp2-a. The distance between the nitrogen atoms in the structure is 6.6 Å and would be suitable for crosslinking by a mid-length linker such as DSS (11.4 Å).

4.4 Synthetic Routes

Many choices of photocleavable groups that have been investigated in the literature.[253, 269-270] Figure 43 displays the some commonly used structures that cleave when exposed to radiation at 350 nm.

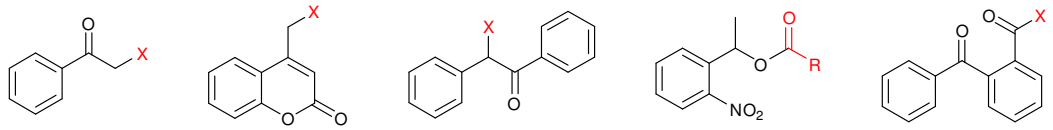

Figure 43 Common photocleavable groups with X showing the leaving group after UV irradiation.

Synthetic routes for coumarin, benzoin and 2-nitrobenzyl, crosslinkers were designed and executed as far as time allowed. There was no specific reason for choosing these scaffolds

over others. Indeed, future studies should consider other well-established moieties. Figure 44 shows their photocleavage mechanisms.[269-270]

2-Nitrobenzyl

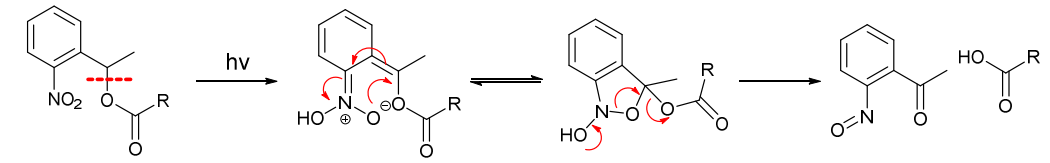

Coumarin

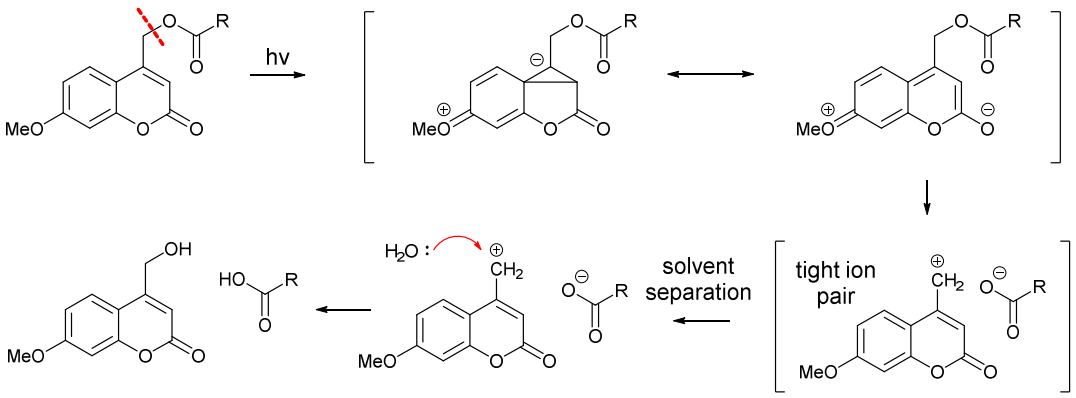

Benzoin

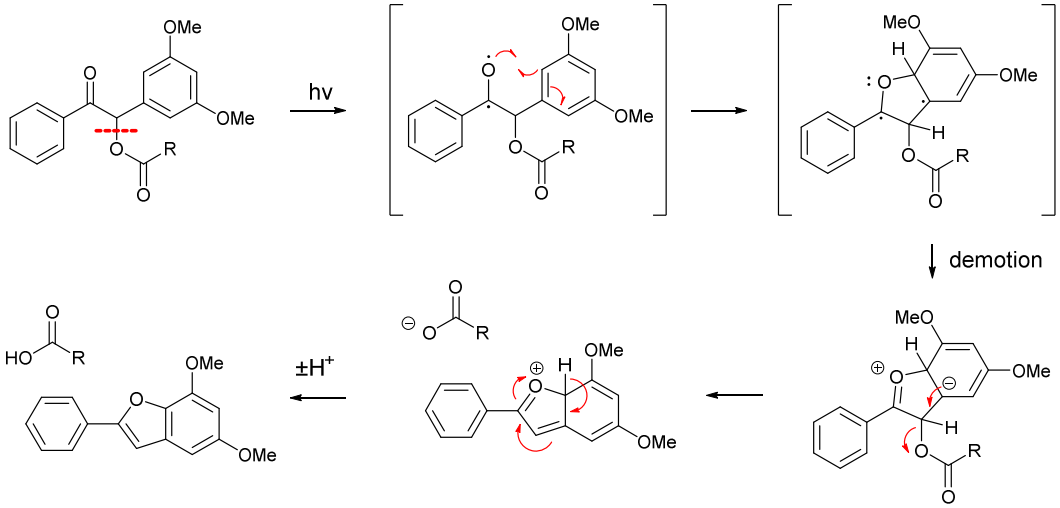

Figure 44 Cleavage sites and mechanisms for the 2nitrobenzyl, coumarin and benzoin cores.

The routes for nitrobenzyl and coumarin were designed by Thomas Lanyon-Hogg (Figure 45 and Figure 46). Each synthesis presented unique problems, but time constraints meant that not all roadblocks could be cleared in time.

In the coumarin route, 3-ethylaminophenol **93** was condensed with neat ethyl acetoacetate to form the coumarin species **94**. The nucleophilic substitution reaction of *t*-butyl bromoacetate to form the coumarin intermediate **95** took a long time, likely due to the weakly nucleophilic nature of the amine. The allylic oxidation of **95** using selenium dioxide was successful but only produced analytical quantities of the alcohol **96**.

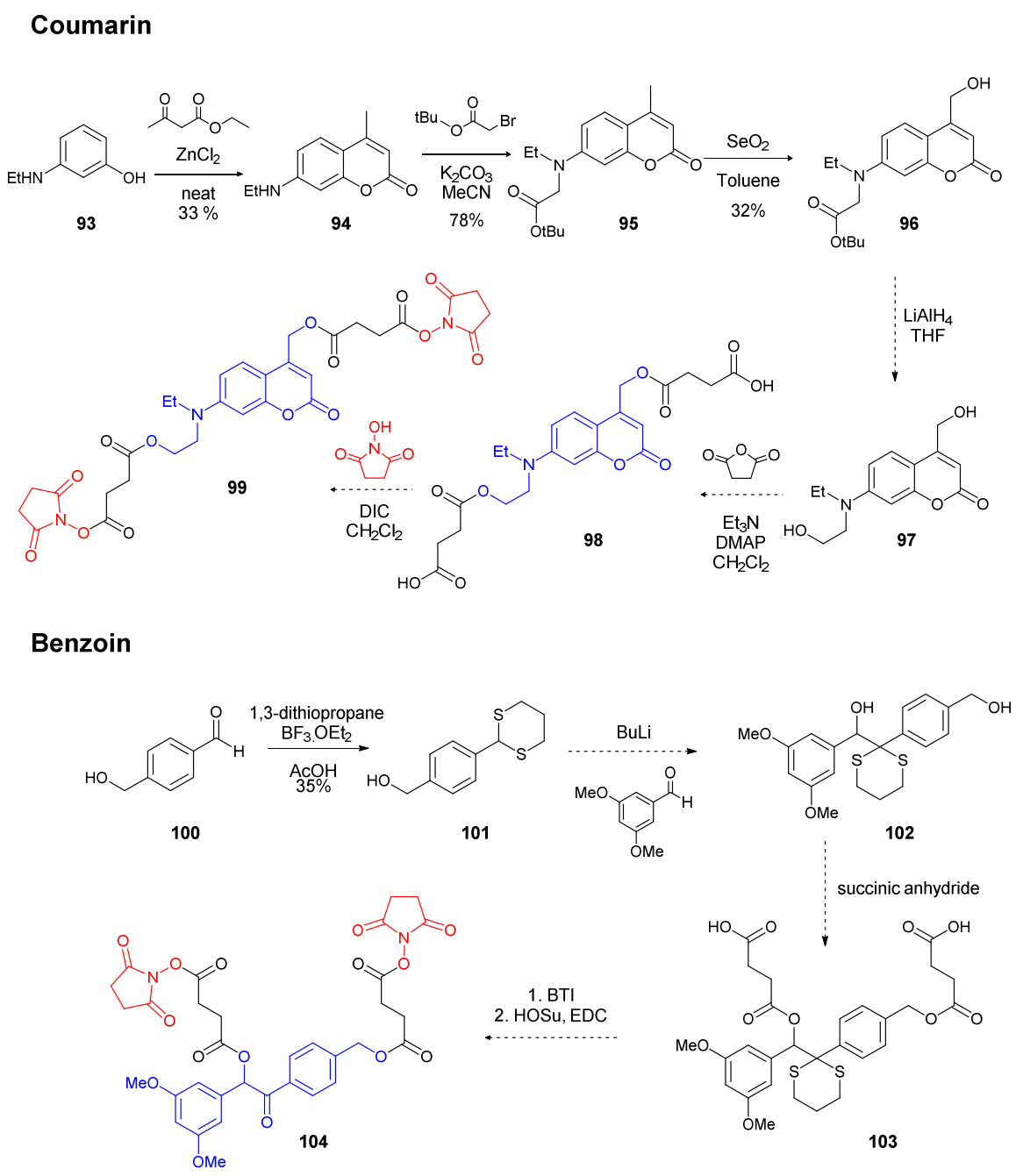

Figure 45 Synthetic routes for the proposed coumarin and benzoin crosslinkers. The solid arrows indicate successful reactions; dotted arrows refer to reactions that were not performed or were unsuccessful.
BTI = [bis(trifluoroacetoxy)iodo]benzene

The proposed benzoin route offered the most scope for functionalisation at either or both aromatic rings. The only requirement was that the benzyl alcohol aryl ring be more electron-rich than the carbonyl side for more efficient photoreaction.[271] The benzaldehyde starting material was successfully protected with thiol with a protocol adapted from DeMartino *et*

al.[272] However, the deprotonation and subsequent addition to the dimethoxybenzaldehyde was unsuccessful, likely due to the difficulty in achieving double deprotonation. More optimisation will be required for the addition of the deprotonated dithiane to the benzaldehyde, and would likely involve protecting the benzyl alcohol beforehand.

Because of time constrains, efforts became focussed on the *2*-nitrobenzyl core, which had the shortest synthetic route. The resulting crosslinker was successfully synthesised and was dubbed NitroXL.

4.4.1 Synthesis of *NitroXL*

Figure 46 displays the synthetic scheme for NitroXL. Starting from nitroterephthalic acid, diol **106** was synthesised according to literature procedures.[273] However, the titanium-mediated addition of methyl groups to dialdehyde **107** was not trivial. Although methods for Grignard-type additions to benzaldehydes is routine, few references exist for double alkylation of aromatic dialdehydes. Nearly all examples in the literature involved titanium, suggesting that only titanium organometallic complexes are reactive against this system.

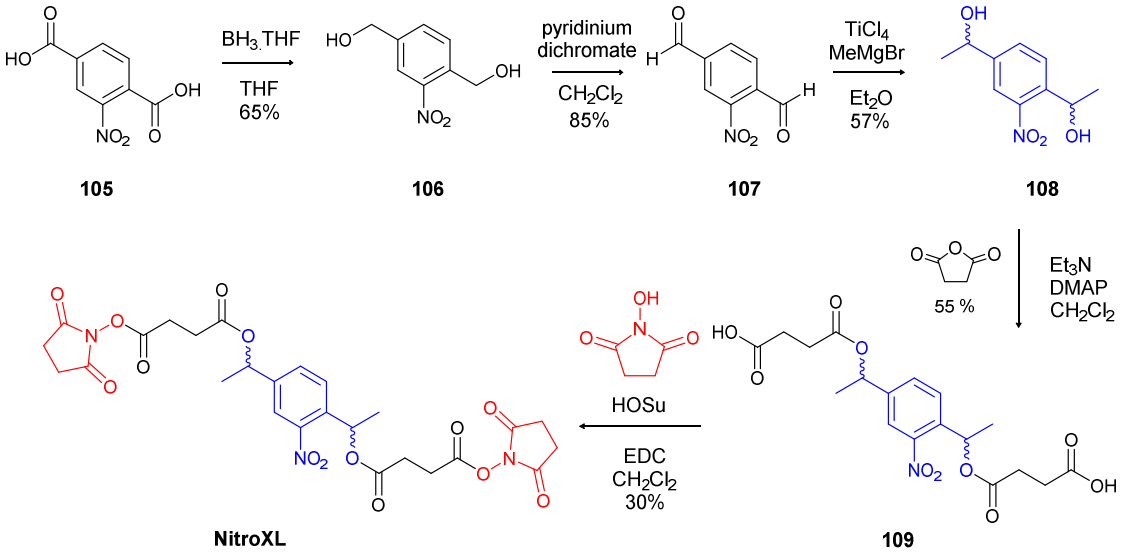

Figure 46 Synthetic route for the nitrobenzyl-based crosslinker *NitroXL*.

It was found that the age and quality of the $TiCl_4$ reagent strongly influenced the outcome of this reaction. Initial attempts with an old and insufficiently sealed bottle gave no reaction, but

a fresh bottle gave the product at a modest yield. This in turn started to give decreasingly poor yields after a couple of months. Scaling up the reaction from 50 to 200 mg of starting material made little if any improvement on the yield. First-time use of ultra-pure $TiCl_4$ gave the most successful reaction but the yields decreased thereafter. This suggests that the integrity of $TiCl_4$ is paramount for this reaction and that everything would ideally be performed in a glovebox. As such, the reaction was performed multiple times to accumulate the di-alcohol intermediate.

The subsequent addition steps with succinic anhydride and then *N*-hydroxyl succinimide (NHS), to give **109** and NitroXL respectively, were straight-forward. Both sample handling and yields greatly improved with larger scale (20 mg vs 100 mg). These molecules were difficult to purify to a satisfactory purity by silica column; hence they were purified by reverse-phase (RP) LCMS. The final double NHS-ester product NitroXL survives the aqueous nature of the LCMS purification if the solvent is removed immediately after the preparative runs.

4.5 Validation of NitroXL

NitroXL was synthesised and purified by LCMS. It was dissolved at 100 mM in DMSO, aliquoted and stored at -20 °C during the time that the experiments were performed. For long-term storage, the aliquots were transferred to -80 °C.

Before trialling NitroXL in proteomics, it was necessary to validate its capability of the tasks it was designed for. In light of the desired properties discussed above, the questions that needed answering were:

1. Can NitroXL be cleaved by UV into its expected products?
2. Can it crosslink a recombinant heterodimer?
3. Can it crosslink proteins in lysate?

The following experiments were designed to address these questions.

4.5.1 Cleavage Under UV by LCMS

NitroXL was first tested for UV cleavage by LCMS. For the control sample, 1 mM of NitroXL was dissolved in 10% DMSO in water and analysed immediately. This is the concentration that will be used for crosslinking, following various examples in the literature. Although this the concentration was too low to produce a meaningful UV absorption spectrum, mass spectrometry is a much more sensitive technique as seen by evidence of the intact crosslinker in the mass spectrum (Figure 47).

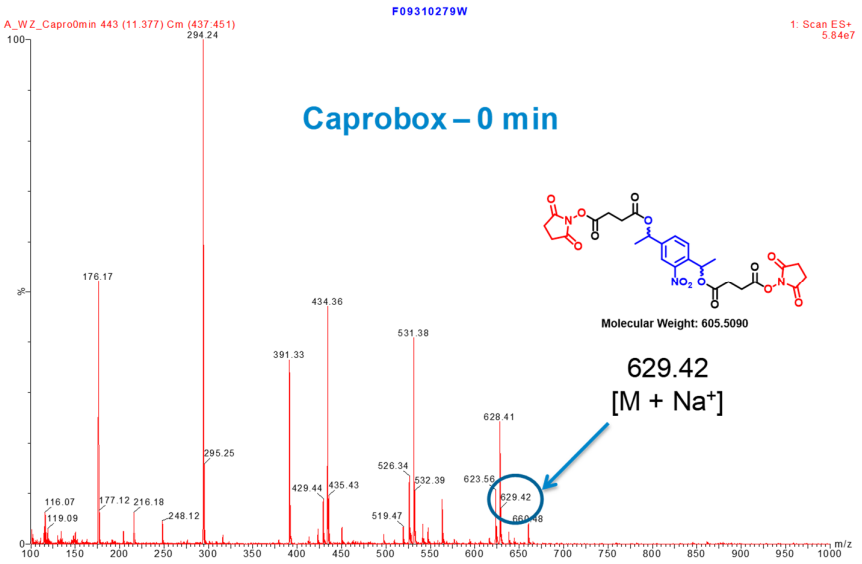

Figure 47 LCMS mass spectrum of a sample of *NitroXL* without UV irradiation. Circled is the molecular ion corresponding to the intact *NitroXL* crosslinker.

Another sample of 1 mM NitroXL in 10% DMSO and HEPES buffer was irradiated for 30 minutes under UV in a specially designed UV device called a Caprobox by caprotec bioanalytics GmbH. This was a cooled rack for PCR tubes below a small bank of UV lamps; unfortunately, this machine is no longer manufactured. The two expected cleavage products, the nitroso aryl and succinic acid, (refer to Figure 44 for the mechanism) were present in the mass spectrum (Figure 48); conversely, no evidence of the parent compound was detected. This shows that NitroXL photocleaves as expected.

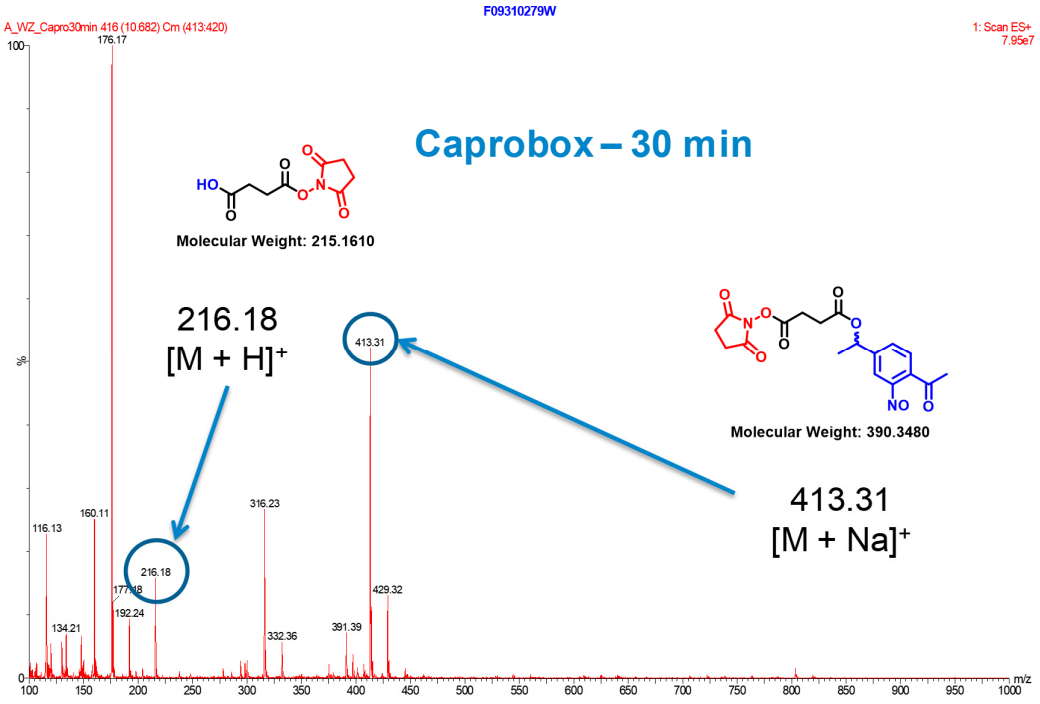

Figure 48 LCMS mass spectrum of a sample of NitroXL with 30 minutes of UV irradiation in the Caprobox. Circled are the masses of the two proposed cleavage products found in the spectrum.

4.5.2 NitroXL and Recombinant Protein

4.5.2.1 Self-Crosslinking of Recombinant Rab27a by DSS

It was originally intended to spike-in *N*-terminally biotinylated Rab27a into cell lysates and to exploit the biotin handle to purify the covalently linked complexes. To establish the ballpark concentration of protein, a range of concentrations of pure Rab27a (without biotin) was tested with 1 mM of DSS to see at what concentrations we would see significant quantities of covalent dimerization.

Figure 49 shows the silver stain of crosslinked Rab27a at a range of concentrations. Silver stain was used because of its higher sensitivity compared with Coomassie Blue. It was reacted with 1 mM of DSS in every sample except the control and quenched with 50 mM Tris. 1 µM of Rab27a without DSS gave one band in the gel. A mysterious lower band appeared upon addition of DSS, and a higher MW one appears at 10 µM, which likely corresponds to dimerised Rab27a due to increased proximity between each protein. Lanes D and E suggests that 0.1 µM of Rab27a is around the detection limit of the silver stain.

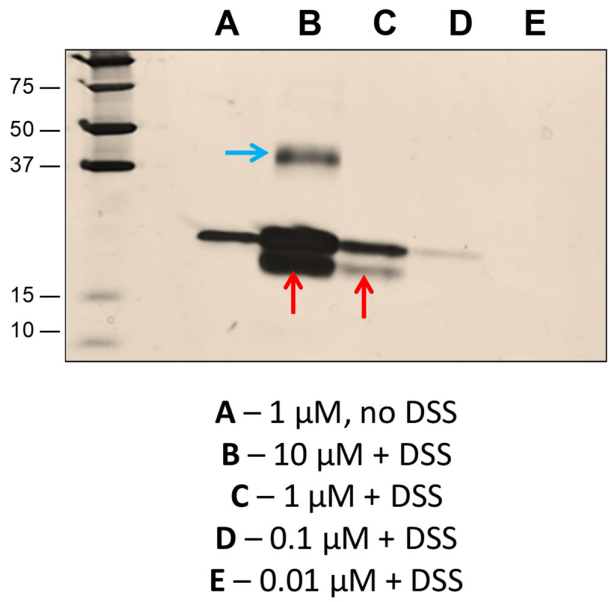

Figure 49 Silver stain of varying concentrations of recombinant Rab27a with and without 1 mM of DSS. The blue arrow points to a band thought to be a dimer of Rab27a, whereas the red arrows point to a new lower MW band, conjectured to be Rab27a reacted with crosslinker. The change in band position may be to do with its change in isoelectric point.

4.5.2.2 NitroXL vs DSS – Silver stain

Recombinant Rab27a-Slp4 (a truncated version of Slp4 at 17 kDa, similar to the Slp2-a in 3BC1) was reacted with NitroXL and irradiated for 1 h 30 min under the UV lamp in a TLC-visualisation box. Although the Caprobox worked well previously, it could only process very small sample sizes in PCR tubes, and so alternative methods of UV reaction were sought. The non-cleavable crosslinker DSS was used as a control. Because both DSS and NitroXL are apolar molecules, they required an additional 10% DMSO to increase their solubility.

Figure 50 shows the silver-stained SDS-PAGE gels of the Rab27a-Slp4 complex crosslinked with DSS and NitroXL. A new band is seen upon the addition of either crosslinker at around 40 kDa, which fits with the sum of the masses of Rab27a and Slp4 fragment (23 + 17 kDa).

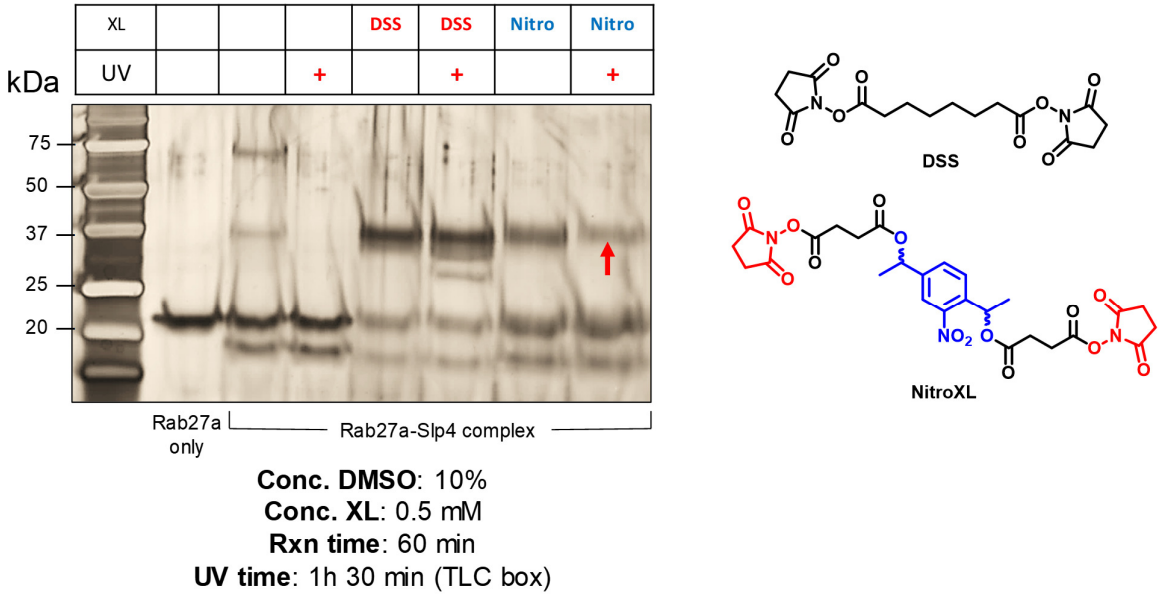

Figure 50 Silver stained polyacrylamide gel showing the effects of DSS and NitroXL with and without UV irradiation. The red arrow points at the crosslinked Rab27a-Slp4 complex appearing to be fainter in the sample crosslinked with NitroXL after UV irradiation. This may be an indication that photocleavage is occurring.

A Western blot was not possible because there was no reliable Slp4 antibody, and the recombinant Rab27a lacked the C-terminal segment that is the recognition site of all Rab27a- antibodies. One could argue that the top band in lane 7 with NitroXL and UV irradiation is fainter than the one without UV. This could indicate a relative loss of the crosslinked species, suggesting the separation of the complex's constituent proteins.

4.5.2.3 Time Course - Irradiation of NitroXL-Crosslinked Rab27a-Slp4

With evidence to suggest the photocleavage of NitroXL-crosslinked Rab27a-Slp4, it was thought pertinent to investigate the length of UV irradiation required for complete cleavage.

Figure 51 shows the SDS-PAGE gel of a time course experiment with Rab27a-Slp4 crosslinked NitroXL undergoing a range of UV exposure times. All lanes contained Rab27a-Slp4 at 1 µM, and lanes 2-5 were reacted with 1 mM NitroXL and quenched with 50 mM glycine (final concentration).100 µL of the resulting solution was pipetted into a well in a clear 96-well plate that was positioned on crushed ice and placed 1- 3 cm under a 352 nm UV lamp in a Spectrolinker™ XL-1500 UV Crosslinker (Spectroline) for the specified time, or left on the bench at room temperature in the dark.

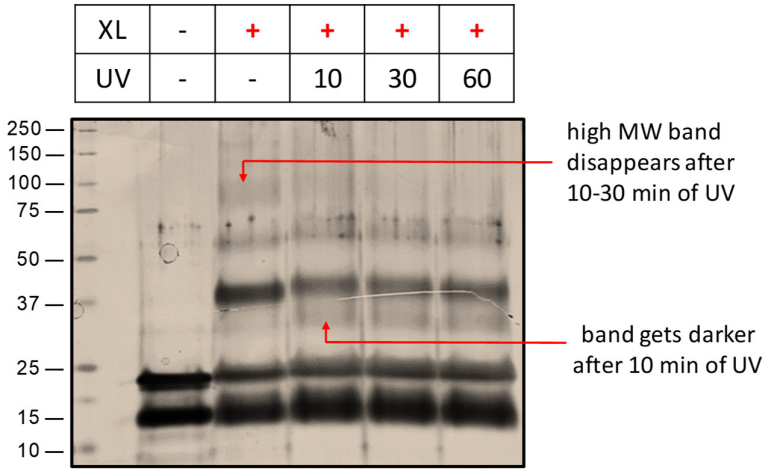

Figure 51 A silver-stained polyacrylamide gel of 1 µM Rab27a-Slp4 crosslinked with 1 mM of NitroXL and exposed to UV for 0, 10, 30 and 60 minutes Spectrolinker XL-1500.

There is a clear decrease in intensity of the band at 40 kDa after 10 min, after which there is no change. Of the even higher molecular weight bands, the one at 70 kDa, did not fade until after 30 min.

It is not known why we do not see a time-dependent decrease in band intensity of the new bands. It could be aggregates forming, or perhaps the proteins become photo-crosslinked.

4.5.3 NitroXL Crosslinking in Lysates

4.5.3.1. Western Blot analysis of crosslinked loading controls

Antibodies raised against Rab27a are typically raised against its C-terminal region. Bacterially-produced recombinant Rab27a and biotin-Rab27a lack this region, and therefore cannot be detected using such antibodies. Nor were there reliable antibodies against any of its known effectors at the time of writing.

Rather than blotting against the biotin moiety of biotin-Rab27a, which was time-consuming to synthesise, it was thought that crosslinking in lysates could first be detected by Western Blot against loading controls. The benefit of using loading control proteins is that they are ubiquitous and abundant so their results should not be particularly sample or cell-line dependent. If one or more were found to work, then they could be used as a crosslinking control for later experiments.

shows Western Blots against the common loading controls: GAPDH, HSP90, tubulin and VDAC2. MDA-MB-231 lysate was crosslinked with 1 mM DSS only (1 h, quench with 50 mM glycine for 20 min).

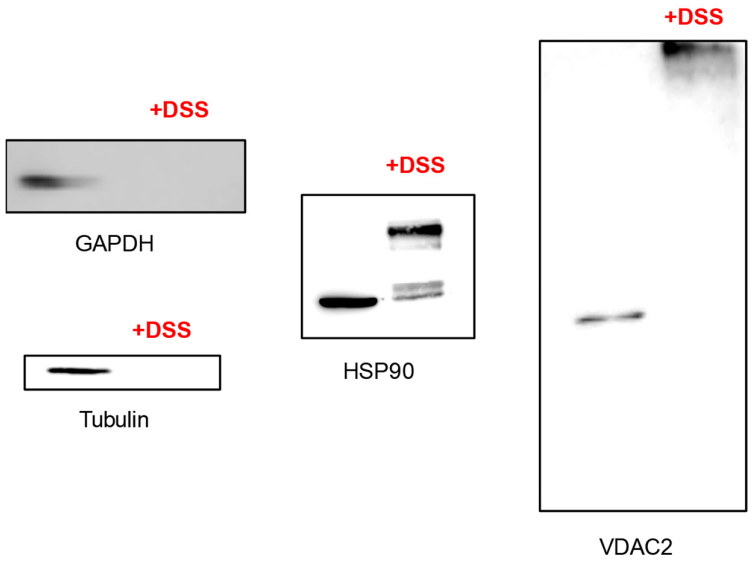

Figure 52 Western Blots of MDA-MB-231 lysate with and without 1 mM DSS blotted against five loading controls. All parts of the blots that are not shown were entirely blank.

There was a significant change in the bands for all the proteins tested. This by itself already shows that the presence of DSS is modifying the proteins to a large extent. For HSP90 and VDAC2, and the lower molecular weight (WB) band for monomeric protein disappeared, and higher MW bands appeared. However, there were no bands to be seen at all for GAPDH and tubulin.

This could be due to efficient coverage of the protein's lysines enough to disrupt protein-antibody binding, or because multiple proteins become crosslinked together and are no longer recognised, or they have such a high molecular weight that they travelled negligibly in the 12% gel and were excised from the WB membrane. It is also possible that the crosslinked proteins had aggregated and never entered the gel.

4.5.3.2 UV Time course of NitroXL-linked lysate, Western Blot against HSP90 and tubulin

The next step was to perform a UV time course to establish crosslinking and photocleavage of NitroXL for proteins in a lysate. Considering the results from the precious section, HSP90 and tubulin were selected as for WB analysis. MDA-MB-231 lysate (1 mg/mL) was crosslinked with 1 mM NitroXL and quenched with 50 mM glycine. Both control and crosslinked samples were irradiated for 0, 10, 20 and 30 minutes in the Spectrolinker. The samples were run on a 12% SDS-PAGE gel, transferred to a WB membrane and blotted against HSP90 and tubulin. Figure 53 shows the visualised WB.

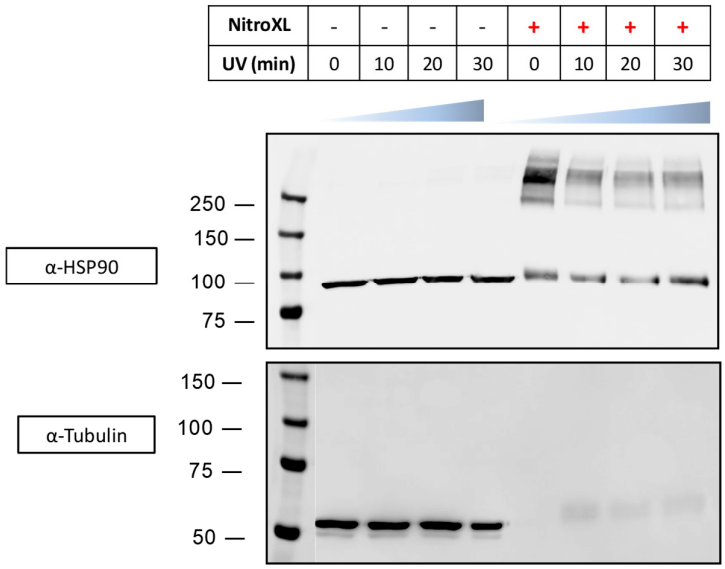

Figure 53 Western Blots of MDA-MB-231 lysate crosslinked with NitroXL subjected to varying exposures of UV. The top blot shows bands recognised by α-HSP90, the bottom by α-tubulin.

Without any crosslinker, neither the bands for HSP90 nor tubulin change appreciably with the application of UV. For HSP90, higher MW bands appear strongly after reacting with NitroXL. Like for the NitroXL-crosslinked Rab27a-Slp4 complex, an exposure time of 10 min produced the most dramatic reduction in band intensity of the crosslinked proteins, and changed little after that. The bottommost band corresponding to monomeric HSP90 appears to increase in intensity, especially at 30 minutes. The fact that it is slightly higher than the control band is likely due to the added mass of the crosslinker, at ~400 Da per linker.

For tubulin, no bands appear at all after NitroXL is added, but faint bands appeared with UV irradiation. Again, these are higher than the control bands, likely for the same reasons as above. Taken together, this result is indicative of NitroXL cleavage.

4.5.3.3 Against NeutrAvidin (biotin-Rab27a spiked MDA-MB-231 lysate)

The time-course experiment was subsequently performed on MDA-MB-231 lysate spiked with biotin-Rab27a and blotted against NeutrAvidin-HRP, which recognises the biotin moiety. The resulting blot is shown in Figure 54. The appearance of higher MW bands is suggestive of crosslinking, but UV-dependent decrease in intensity of those bands is still not seen. Nor is it clear if the bands are increasing in intensity. A repeat of the experiment (Figure 55) gave similar inconclusive results.

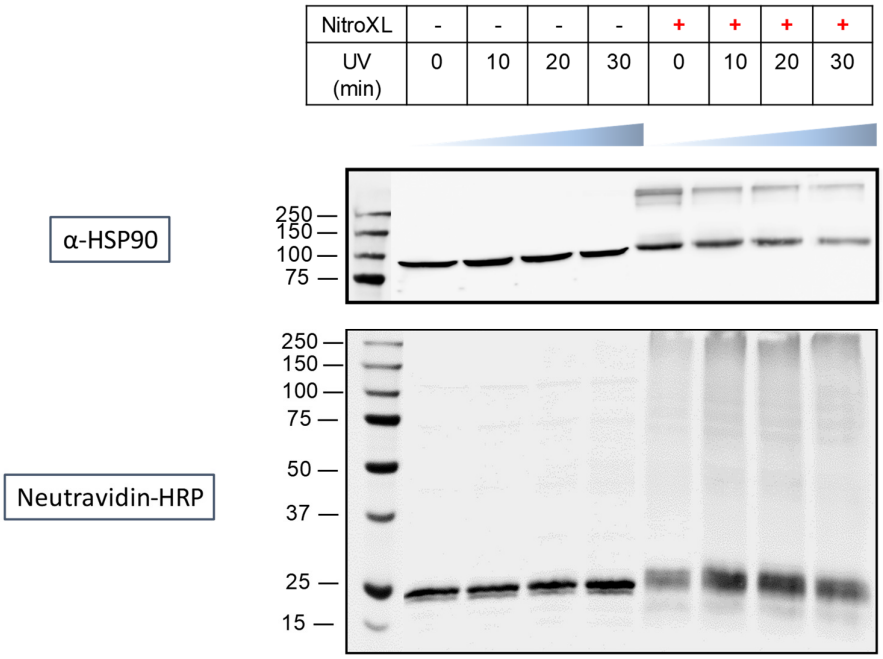

Figure 54 Western Blots of MDA-MB-231 lysates crosslinked with NitroXL, subjected to varying exposures of UV. The top blot shows bands recognised by α-HSP90 (control) and the bottom blot by NeutrAvidin-HRP which detects the spiked in biotin-Rab27a.

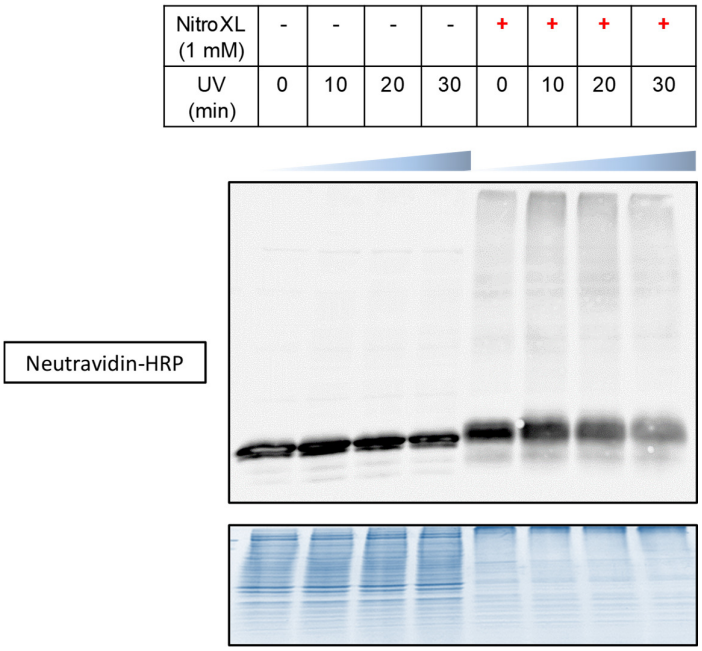

Figure 55 A repeat of the experiment in Figure 54.

A number of factors could be at play. The biotin-Rab27a is a recombinant protein that is biotinylated on an extension of the N-terminus. It also lacks the C-terminal section which normally include the lipidation sites that anchors active Rab27a to membranes, where the effector interactions occur. All the recombinant Rab27a used for this thesis are loaded with GppNHp, which is a non-hydrolysable GTP mimic. However, any limitations in its mimicry would result in the disruption of GAP, GEF and effector interactions.

Further, the higher MW bands caused by the presence of NitroXL had a grey background rather than discrete bands. This suggests that although biotin-Rab27a is being modified by NitroXL, the majority are not picking up binding partners and a significant portion was crosslinking indiscriminately.

4.5.3.4 Conclusions from Western Blots

The Western Blot results show NitroXL is capable of crosslinking proteins in lysates. Some proteins like HSP90 show UV-dependent cleavage, but it is less clear with the biotin-Rab27a, and others are not detected at all once crosslinked. Since the results of these Western Blots are very much dependent on the recognition of epitopes by antibodies and the

crosslinker can change or affect these epitopes, they are only able to give qualitative indications of how some band intensities change with UV irradiation. This does not preclude detection by MS, which does not rely on epitope structures.

Despite Western Blots not giving comprehensive results, they have shown that NitroXL is capable of crosslinking proteins and that UV irradiate decreases the intensity of some higher MW bands and paves the way towards the use of NitroXL in proteomics. As MS is a much more sensitive technique that also inherently lends itself to quantitation, it will give us more a comprehensive appraisal on the development of this methodology.

4.6 Transfection of TST-tagged proteins

The requirement of the protein of interest to have an affinity handle is central to this methodology, as enrichment would not be possible without it. However, it then follows necessarily that the protein of interest will not be in the endogenous form. How, then, can it be ensured that the modified version will behave like the native one, and associate with all the right proteins? This is an important question, but not a trivial one to answer. It might also be possible that this approach will work with some proteins but not others, depending on how the tag interferes with its PPIs and localisation.

The main limitation with the spike-in method was that, not only did the Rab27a have an extra biotinylated sequence at the N-terminus, the recombinant protein was missing its prenylated C-terminal section, which is important for its affinity to membranes and GDIs. This is because bacterially produced proteins cannot be lipidated *in situ*. Conversely, if an N-terminally tagged Rab27a is expressed in a mammalian cell, it would emerge with the correct PTMs. This would likely approximate the native protein better. Furthermore, it could be already pre-associated with its interaction partners after lysis, so that crosslinking may become more efficient. Ectopic expression of the native sequence would also result in a more representative distribution of nucleotide loading state, whereas the recombinant proteins were loaded with GNP.

4.6.1 The Twin Step Tag

Of the numerous options of peptide affinity tags that are available, the Twin Strep tag (TST) was chosen because it has been reported to give a very clean pull-down with Streptactin, an engineered form of streptavidin that binds TST more much more strongly than lone Strep tags, but bound proteins can also be eluted with high concentrations of biotin.[274-276] Plasmids of TST-KRas and TST-PDE6δ (synthesised by Dr. Antonios Konitsiotis) were available in the group. A mammalian expression vector containing a sequence of N-terminally tagged TST-Rab27a, with the TST sequence and linker was taken from the TST-KRas plasmid, was purchased from InVitrogen (Appendix D).

Biotin was a strong contender for the affinity tag, but this would have involved additionally transfecting cells with BirA, an enzyme that is necessary for the transfer of biotin onto the appropriate peptide motif. It was decided that the complications of double transfection outweighed the disadvantages of the TST tag, which was mainly its large size - approximately 30 residues.

4.6.2 Validation of Transfections by Western Blot

Both MDA-MB-231 and HeLa cells were tested for transfection efficiency using Lipofectamine 2000 and OptiMEM. The transfection efficiency was found to much higher for HeLa cells, so HeLa cells were used for the remainder of this thesis.

HeLa cells were transfected with TST-Rab27a, TST-PDE6δ and TST-K-Ras plasmids to test for successful expression and antibody recognition of the tagged proteins. Crosslinking behaviour was also checked by reacting samples with DSS as with previous validation experiments. The proteins were blotted against Streptactin-HRP, which recognises TST, and against α-Rab27a and α-PDE6δ, α-HSP90 as a control. No reliable α-KRas antibody was available, so its transfection efficiency was observed with Streptactin-HRP alone.

Figure 56 shows the Western blot of transfected HeLa lysates with and without DSS, blotted with Streptactin-HRP and with α-HSP90. There is a clean and dark band in every lysate that has not been crosslinked with DSS, indicating successful expression of TST-tagged protein.

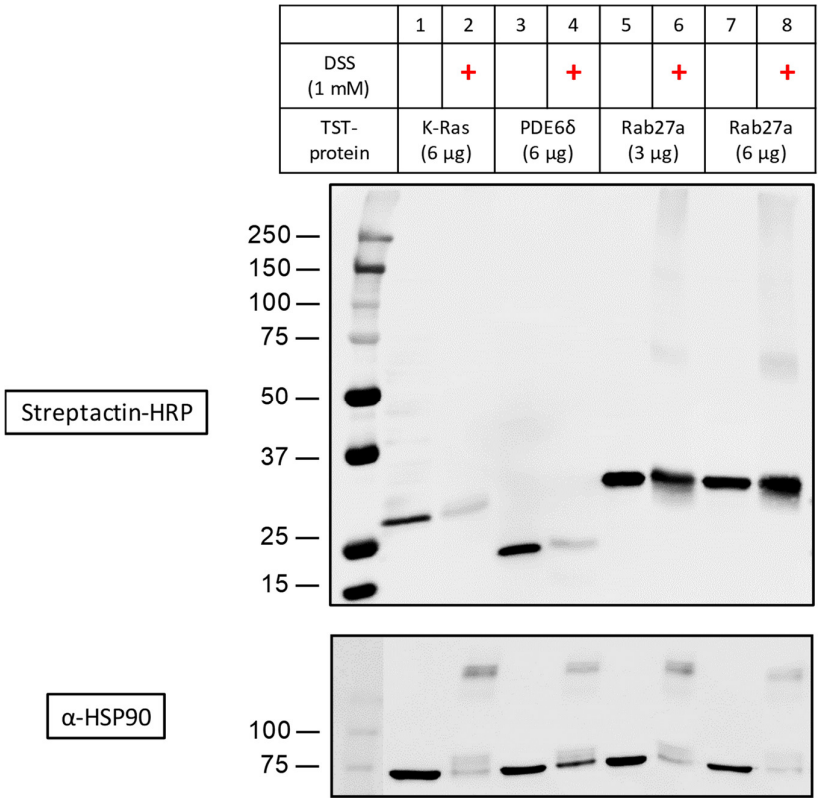

Figure 56 Western Blots showing the successful transfection of HeLa cells with TST-KRas, TST-PDE6δ and TST-Rab27a plasmids blotted with StrepTactin-HRP and anti-HSP90. The plasmid amounts were for each 10 cm circular plate. Each lysate was tested with and without DSS. Streptactin-HRP was used to visualise the bands. Every band or smear correlates to the presence of the TST, which does not occur endogenously. The lysates were also blotted against HSP90 as a control.

Figure 58 displays blots of the lysates successfully blotted with α-Rab27a, α-PDE6δ, and α-HSP90 and shows that the transfected protein is present as well as the TST tag. All the crosslinked lysates show distinct bands or smears at higher MWs except for K-Ras and PDE6δ where their bands become fainter. This is a promising indication of crosslinked proteins, and in the case of the Streptactin-HRP blot, also an indication of what can be pulled down by the Streptactin-coated beads that will be used later for pull-downs. In this particular blot, there was still a lot of TST-Rab27a that did not seemed to become

crosslinked. This suggests that under these particular conditions, the vast majority of protein that gets pulled down will be modified but not crosslinked TST-Rab27a proteins.

The amount of TST protein was not quantified in any of these samples; however, there appeared to be a significantly higher concentration of TST-Rab27a in the lysate when using 6 µg of plasmid DNA per 10 cm plate, compared to 3 µg. In the experiments occurring after Figure 57, the amount of TST-Rab27a plasmid added was reduced to 1 µg per 10 cm plate, which gave more than adequate quantities of TST protein; further, less cell death had occurred at the point of lysis.

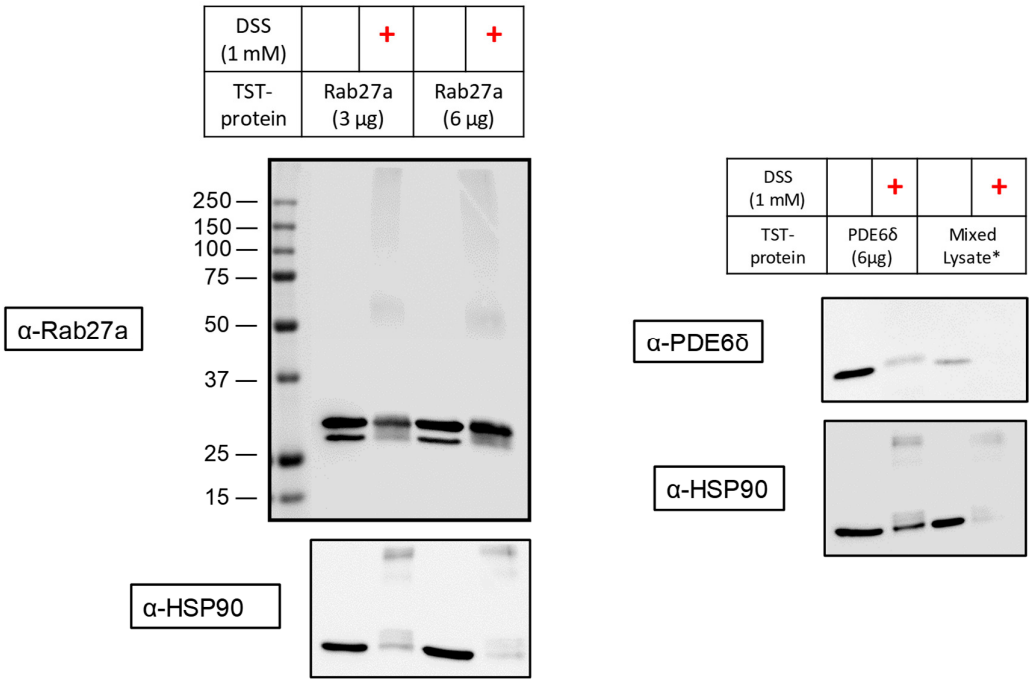

Figure 58 Western Blots showing the successful transfection of HeLa cells with TST-K-Ras, TST-PDE6δ and TST-Rab27a plasmids blotted with anti-HSP90, - Rab27a and -PDE6δ. Again, the plasmid quantities were for each 10 cm circular plate. Each lysate was tested with and without DSS. The lysates were blotted with α-Rab27a and α-PDE6δ as there was no good α-KRas antibody available at the time. The lysates were also blotted against HSP90 as a control. The bands coincided with the ones show with Streptactin-HRP, though a new band appeared for Rab27a. This may be the endogenous Rab27a or a non-specific interaction.

It is not certain why Rab27a appears as two bands – it may be possible that the small band with the smaller MW corresponds to endogenous Rab27a, whereas the main band is TST-Rab27a; alternatively, it was a non-specific interaction.

These Western Blots indicate that the transfection protocols were successful and that the lysates produced were adequate for use as the basis for subsequent proteomic experiments.

4.7 Pull-down Experiments with MagStrep Beads

4.7.1 Bead Volume Optimisation

Commercially available Streptactin-coated magnetic beads were chosen for enriching TST proteins. Called MagStrep, these beads are fine magnetic particles coated with Streptactin protein. A key advantage of MagStrep beads is that, by being magnetic, they are easily pelleted from suspension using a magnetic Eppendorf rack. There is no need to centrifuge, and smaller bead volumes can be accommodated compared with non-magnetic beads like agarose. However, they are expensive and not reusable, so an experiment was performed to gauge the appropriate bead volume, which here refers to the volume of a 50% bead suspension, for 100 µL of lysate at 1 mg/mL.

Figure 59 shows the Western Blots HeLa lysate transfected with TST-Rab27a, with and without crosslinking by DSS and pulled down with a range of MagStrep bead volumes. The beads were incubated with the lysates at 4 °C for 2 h and released by boiling the beads at 95 °C for 10 min into a 1:4 mixture of loading buffer to lysis buffer.

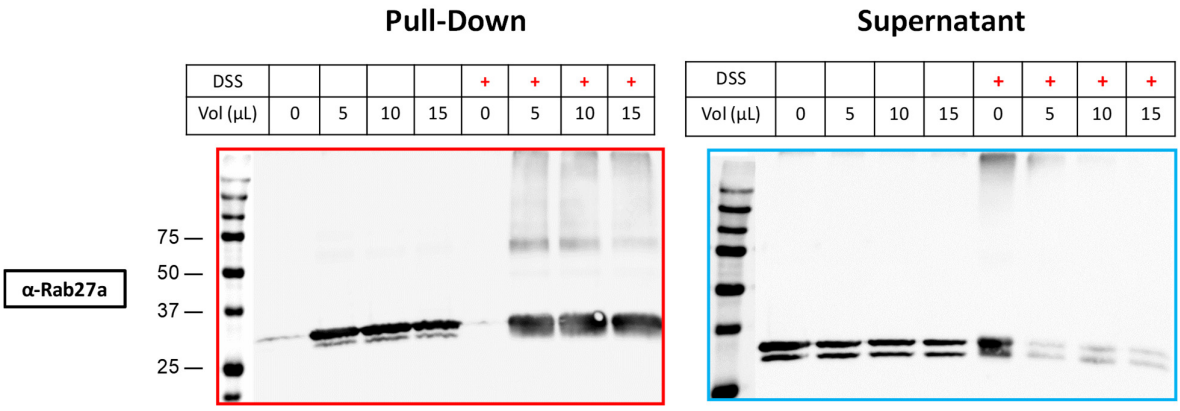

Figure 59 Western Blots showing how much Rab27a protein is pulled down by 0, 5, 10 and 15 µL bead suspensions of MagStrep beads, which are magnetic particles coated with Streptactin. PD refers to the pulled down proteins; SN refers to the supernatant left over after pull-down. All were blotted with α-Rab27a.

The result show that all of 5, 10 and 15 µL of beads per 100 µL pulled down a similar amount of protein by Western Blot, and only in the remaining supernatants were there any

difference between the lanes, with the samples with no beads at all having slightly thicker bands.

In light of this, it was decided that 5 µL per 100 µL was sufficient for further experiments as the most efficient and cost-effective bead volume.

4.7.2 Pull-Down with Crosslinked Protein – DSS v NitroXL

An experiment was set up this time with NitroXL as the crosslinker to investigate the pull-down efficiency of crosslinked and photocleaved TST-Rab27a. Lysate from HeLa cells transfected with TST-Rab27a was crosslinked with DSS or NitroXL, quenched with 50 mM glycine and then subjected to UV irradiation as before. Subsequently, 5 µL of MagStrep beads were added to 100 µL of crosslinked lysate. Western Blotting with α-Rab27a was performed for the whole lysate (not pulled down), the pull-down fraction and the supernatant.

In Figure 60, the bands in the blots were darker with DSS than with NitroXL in all the crosslinked samples. It may be possible that NitroXL obscures the binding epitope of Rab27a. However, some higher MW bands were pulled down even in the NitroXL-crosslinked lysates, though they are fainter than the DSS-crosslinked samples. The application of UV (30 min) did not affect the band intensities with DSS samples, but with NitroXL the band for Rab27a appears to be larger in the photocleaved PD lane.

The lack of bands in the samples with NitroXL relative to DSS might be because the greater bulk of NitroXL obscures epitope recognition by the antibody. It may even be that some NitroXL was degraded by the loading buffer or by the boiling process. Again, the use of mass spectrometry would resolve this issue because no loading buffer will be used and the proteins will be released by in-gel digestion.

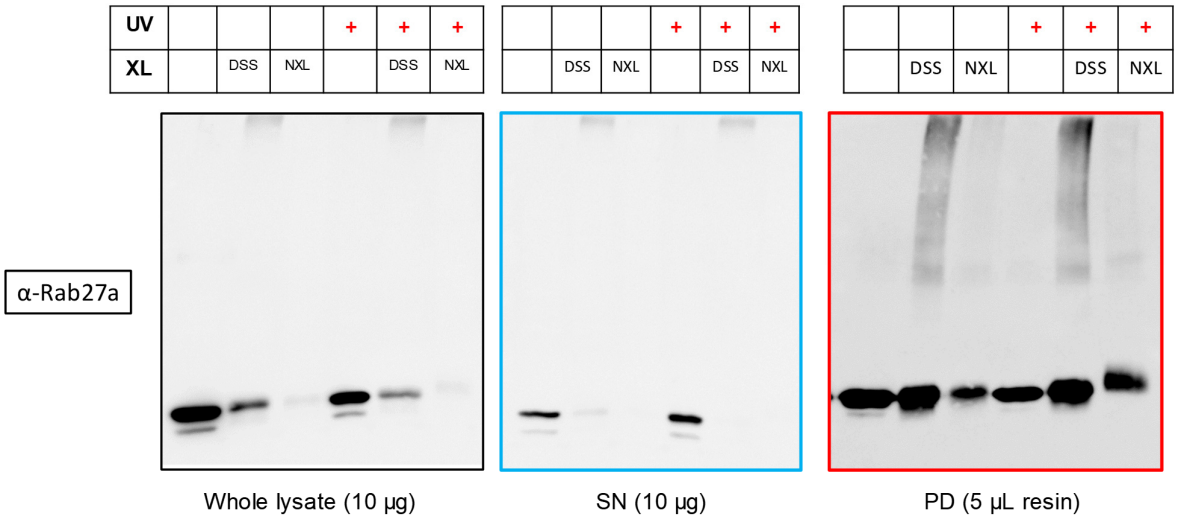

Figure 60 Western Blots showing how much *NitroXL*-crosslinked protein is pulled down by 5 µL suspension of MagStrep bead before and after UV irradiation.

4.8 Conclusions

A prototype photocleavable crosslinker called NitroXL was designed and successfully synthesised and its crosslinking abilities were tested with pure Rab27a, Rab27a-Slp4 complex using silver-stained SDS-PAGE gels, against loading controls, biotin-Rab27a spiked into MDA-MB-231 lysates and in TST-Rab27a transfected HeLa lysate by Western Blotting.

In almost all cases, crosslinking by NitroXL behaved similarly to DSS, and upon UV irradiation the higher MW bands decreased in intensity, particularly after 10 min, and the monomeric band often increased in intensity. Thus, NitroXL fulfils most of the desired requirements that were set out in the design brief in being a mid-length linker that incorporates well-known NHS ester warheads to selectively target lysines and a commonly used photocleavable core that cleaves after exposure to UV at around 350 nm.

On the other hand, it lacks water-solubility and requires 10% DMSO for dissolution, on par with DSS. Also, the synthetic route leaves little flexibility for later functionalisation. However, it has a relatively straight-forward synthetic route that was simple to synthesis in large quantities.

In total, NitroXL satisfied the brief enough to be used as a test crosslinker in proteomics. After obtaining feedback from the full proteomic workflow, it is projected that further iterations of the crosslinker design and crosslinking protocols will resolve the outstanding issues.

5 Incorporation of NitroXL in a Proteomics Workflow

This chapter reports on the proteomic experiments performed with the prototype photocleavable crosslinker NitroXL, the development and validation of which are detailed in the previous chapter. It focuses on the establishment of a proteomic workflow involving crosslinking and photocleavage of NitroXL with TST-Rab27a-transfected HeLa cell lysates. The experimental set-up and expected results are described, and the resulting data is discussed in detail. This chapter uses single-letter abbreviations of amino acids.

5.1. Experimental Set-up

In the previous chapter, the prototype photocleavable crosslinker NitroXL was demonstrated to crosslink TST-Rab27a in lysate that could be pulled down, and for the crosslinked proteins to exhibit photocleavage under UV irradiation as shown by silver stained SDS-PAGE gels and Western Blotting. Thus, in fulfilling the majority of its design brief, NitroXL was progressed to being tested by proteomics.

NitroXL was envisaged to be used in the same conditions as its validation experiments: 1 mM for 1 h, followed by a glycine quench. All proteomic experiments in this chapter uses TST-Rab27a-transfected HeLa lysate at 1 mg/mL, and all crosslinking reactions required 10% DMSO for NitroXL and DSS to have acceptable solubility.

A protocol was developed with a view to crosslink ectopically expressed TST-Rab27a to its interaction partners in cell lysate, pull down its crosslinked complexes and identify and quantify the partner proteins. HeLa cells were transfected with TST-Rab27a and were lysed in a buffer containing 1% Triton, 10% glycerol, 50 mM HEPES, 100 mM NaCl and 5 mM $MgCl_2$ (“Lysis Buffer”) after 24 h. The lysate was adjusted to 1 mg/mL and aliquoted into nine identical samples of 100 µL with added 10 µL DMSO. The samples were grouped into three triplicate sets that were to undergo the following treatments:

Set A (samples 1-3) - No NitroXL, no UV

Set B (samples 4-6) - NitroXL, no UV

Set C: (samples 7-9) – NitroXL, 1 h UV

Figure 61 depicts the experimental set-up.

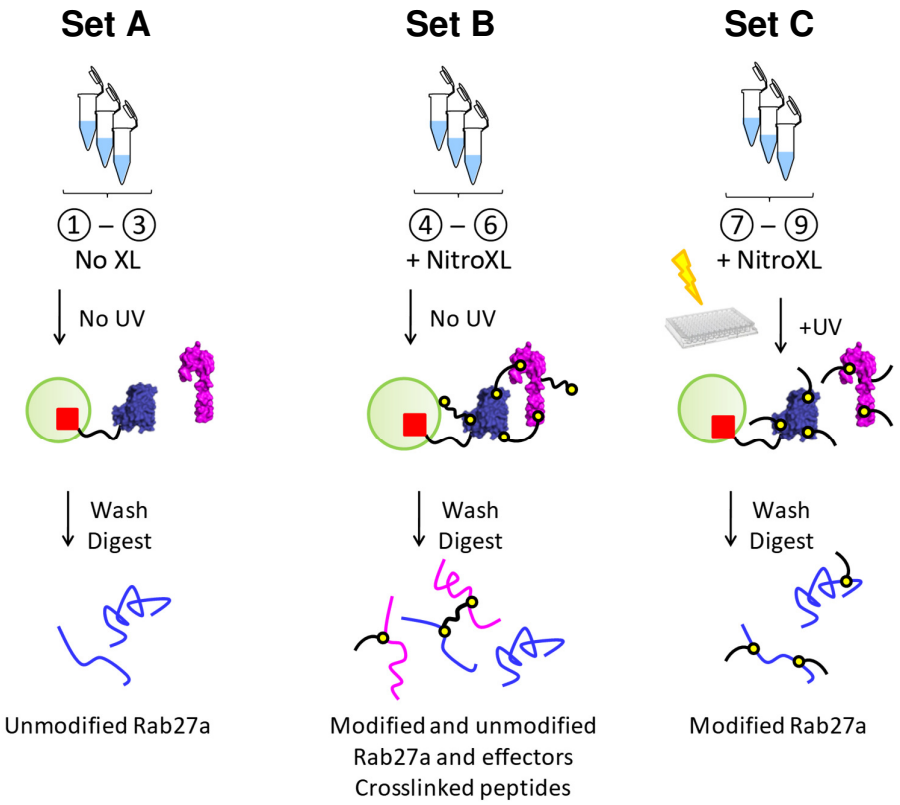

Figure 61 Diagram of the set-up for the proteomic analysis of crosslinked TST-Rab27a-transfected lysates. The three experimental conditions are tested in triplicate.

1 mM NitroXL was added to sets **B** and **C** (1 µL from 100 mM stock in DMSO) and the samples were rotated in the dark at room temperature for 1 h. Glycine was added to a final concentration of 50 mM. Samples in set **C** were irradiated with 365 nm of UV light for 1 h. The pull-down was performed with MagStrep beads and on-bead tryptic digestion was performed overnight. Due to the light-sensitive nature of NitroXL, samples were covered in foil wherever possible. A detailed protocol may be found in Chapter 7.

Because the affinity handle was on the target protein and not on the crosslinker, it was envisaged at this stage quantification would be performed with unmodified and type 0 (attached to hydrolysed crosslinker) peptides, which was assumed to be in the majority, and

would be obtained from the enrichment of proteins in set **B** *vs* set **C**. Type 2 inter-crosslinked peptides would not be identified or quantified. LFQ would be performed in MaxQuant, and PEAKS Studio 8.5 will be used to identify the presence and qualitative abundance of NitroXL-related modifications.

5.2 Experiments Performed

Three sets of experiments will be analysed in this chapter. They consist of the following pairs of crosslinkers and digestion enzymes:

1. **NitroXL-trypsin** (Sets A, B and C)
2. **NitroXL-chymotrypsin** (Sets A1, B1 and C1)
3. **DSS-trypsin** (Sets D and E, but with the same conditions as A and B respectively)

Trypsin is the most commonly used digestion enzymes. It cleaves specifically after arginine and lysine, which are two common amino acids which together occur often enough to produce peptides of a suitable length and charge for ionisation and fragmentation in MS. Though normally effective, these advantages are lessened when lysine-targeting crosslinkers are in use. Once linked to a crosslinker (type 0), the lysine is no longer recognised or cleaved by trypsin. This has the effect of a missed cleavage, and modified digested peptides are on average twice as long, increasing the difficulty of its ionisation and fragmentation in the standard instrumentation used for bottom-up MS, and therefore the difficulty in detecting the modifications.

Proteases with alternative cleavage sites have been used to mitigate this issue. [277] Thus, chymotrypsin was used as the digestion enzyme for otherwise the same experimental set-up, which cuts peptides specifically after F, W, Y and less specifically to L. Neutrophil elastase was also attempted – cleaving after V and A – but the digestion process was unsuccessful. In the future, more proteases can also be tested to optimise the coverage of different proteins.

A small control experiment was also performed with DSS, non-cleavable and more flexible crosslinker, to investigate differences in modification sites between NitroXL and DSS. but without samples undergoing UV irradiation**.**

5.2.1 Expected Results

In set **A**, because the lysis buffer is relatively mild, the method for this set is essentially the same as a co-immunoprecipitation experiment. Thus, we would expect to see unmodified peptides of predominantly TST-Rab27a, followed by strong non-covalent binders to TST-Rab27a and finally nonspecific proteins that bind to the beads alone. As the TST does not occur endogenously and StrepTactin has been specifically engineered for TST affinity, the background level of non-specific binders to Rab27a is expected to be low.

In set **B**, NitroXL is added but the samples are not subjected to UV irradiation. This means that the photocleavable core should stay intact throughout the entire experiment. Figure 62 shows the expected adducts arising from NitroXL; the only adducts expected to appear are MonoOH and MonoGly, the hydrolysis and glycine adducts of singly reacted NitroXL respectively. With no application of UV, TST-Rab27a should be pulled down along with its covalently attached partners. Proteolytic digestion will cleave both TST-Rab27a and its partners into peptides. Thus, set **B** is the only set that should contain peptides of Rab27a effectors, and the set with the highest expected number of proteins.

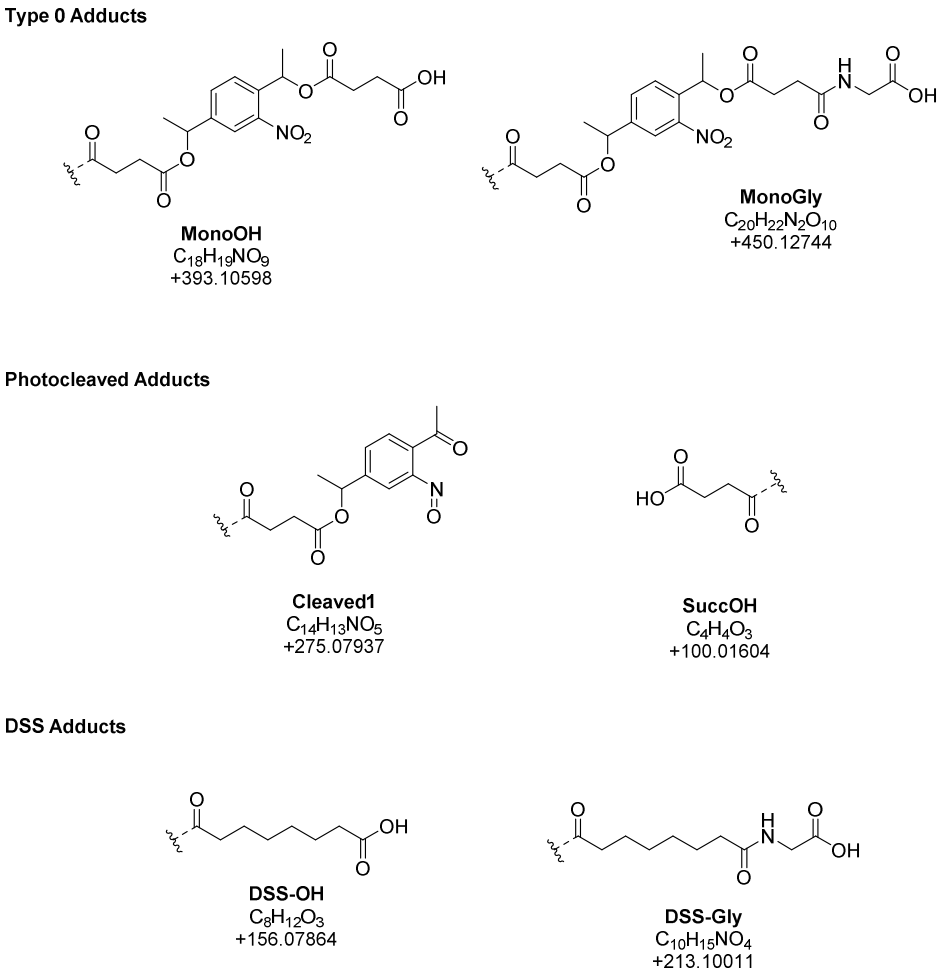

Figure 62 Expected adducts arising from NitroXL and DSS, their chemical compositions and their monoisotopic adduct masses.

Set **C** was treated with NitroXL and then irradiated with 365 nm UV light for 1 h before pull-down. The photocleavable core of NitroXL is expected to cleave and release the crosslinked partners before TST-Rab27a is separated out by the beads. It is expected that the dataset will be much like Set A, but the peptides would be modified in similar quantities to SuccOH and Cleaved1. Generally, we would expect to see similar protein profile to set **A**, but the peptides will be modified with SuccOH and Cleaved1. The comparison between sets **A** and **C** may give an indication to effect of NitroXL on the overall detection and identification of peptides as the presence of crosslinker could cause aggregation, reduce the ionisation of peptides and affect their fragmentation.

Sets **A1**, **B1** and **C1** are analogous to **A**, **B** and **C** and the expected results are the same; the use of chymotrypsin instead of trypsin may give better coverage or identification. Sets **D** and **E** are analogous to **A** and **B** respectively, but with DSS-OH and DSS-Gly as the expected adducts in set **E**.

Summary

The objective was to see what interaction partners are covalently pulled down with TST-Rab27a. These are expected to occur mainly in sample set **B**. Thus, in the analysis, the following comparisons were proposed:

- Sets **A** against **C** compares the effect of treating the lysate with NitroXL and UV irradiation. Past tests (data not shown) have demonstrated that the radiative conditions employed make negligible difference to the protein samples.
- Sets **A** and **B** compares the effect of NitroXL only.
- Sets **B** against **C** compares what effectors have been cleaved off by UV irradiation of the NitroXL crosslinker.
- Sets **B** against **D** compares the difference between pulled-down crosslinked proteins between NitroXL and DSS respectively, but the comparison would only be pertinent if the same digestion enzyme was used.

5.3 Label-Free Quantification of Unmodified Peptides

The experiments described above were performed and the samples analysed by a Q Exactive™ Hybrid Quadrupole-Orbitrap™ Mass Spectrometer at Imperial College London's departmental facility. MaxQuant was used to search the raw MS data and LFQ was performed using the software's in-built algorithm.[208] Briefly, the algorithm outputs the parent protein's LFQ intensity as a composite of its constituent peptides' AUC ion intensities. Search parameters may be found in the Experimental, Chapter 7. Perseus 1.6.0.7 was used to visualise the data. Known contaminants, reverse sequences and peptides only identified by site were immediately excluded. All LFQ intensity values were

transformed with a $\log_2(x)$ function. For each group of sets analysed, the results were filtered such that proteins appeared in at least two out of three samples in at least one set.

5.3.1 Number of identified proteins – Venn diagrams

Venn diagrams were constructed sets of samples to show the extent of overlap of identified proteins. This was intended to give an overview of the crude differences between sample sets in each experiment and between experiments. Figure 64 shows the Venn diagrams for the three experiments; each circle represents a set.

5.4.1.1 By Set

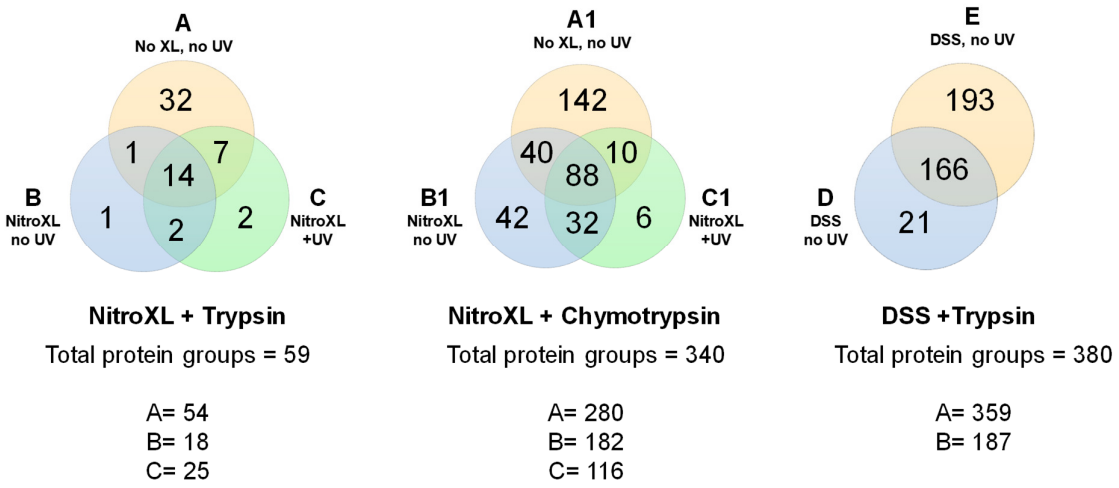

Figure 63 Venn diagrams of the number of protein groups found in each experiment, group by set. The results were filtered such that in each experiment there were at least two valid measurements in at least one set.

For the NitroXL + trypsin experiment, only 59 proteins were found in total. This either indicates a very clean pull-down or a low quality experiment. Either way, it is not desirable because having a measurably stable level of background protein is required for the normalisation step of LFQ. It is clear from the Venn diagram that the control samples in set **A** contain the most unique proteins. Set **C** was expected to have the same composition as set **A**, but it in fact contained only a subset of proteins found in set **A**. This could be because the pulldown efficiency of proteins may be reduced after reaction with NitroXL, or because a

significant portion have been modified by crosslinker adducts and were not included in the quantification.

The experiments with chymotrypsin and DSS identified many more proteins, 340 and 380 respectively. For the DSS + trypsin experiment, the total number of proteins found was comparable to the chymotrypsin experiment. Only 21 proteins were found only in DSS sample set, with a fair degree of overlap, but again set **E** has the most proteins by far. This suggests that the presence of the crosslinker hinders the pull-down other proteins.

5.4.1.2 By Experiment

Sets **A**, **A1** and **D** have exactly the same experimental conditions and should in theory have very similar compositions. However, the Venn diagram in Figure 64 shows 84 proteins identified exclusively in set **A1** and 162 in set **D**. This either signifies major differences in the lysate used for the three experiments or human error in executing the protocol and requires investigation.

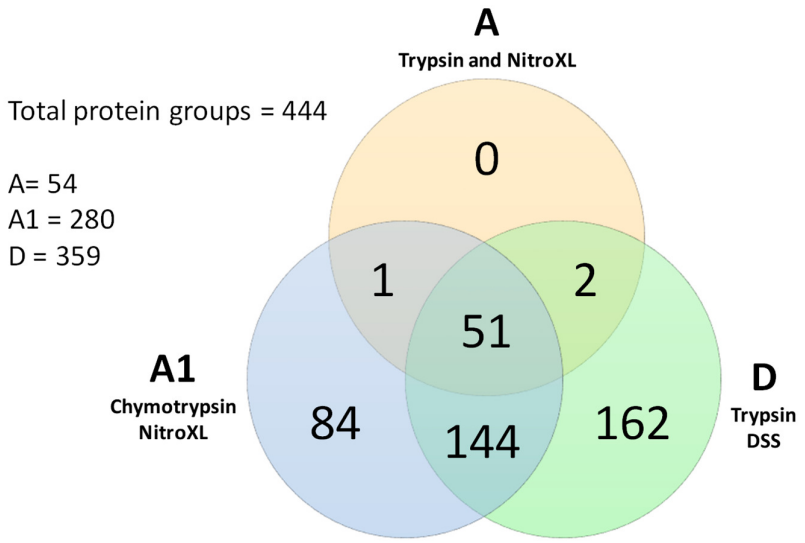

Figure 64 Venn diagram showing the overlaps in protein IDs found in the non-crosslinked sets of samples: A, A1 and D.

5.3.2 Statistical Analysis – Volcano Plots

Because of the poor quality and few hits obtained from the NitroXL-trypsin dataset, only the chymotrypsin-NitroXL experiment was chosen for statistical analysis. The Perseus software

was used to compute two-sample Student's T-tests with sets **A1** vs **C1** and with **B1** vs **C1** and **A1** vs **B1** from the chymotrypsin experiment, and also sets **D** and **E** from the DSS experiment.

This statistical analysis requires valid values for every replicate. However, this would mean that proteins that are reliable found in one set but not the other cannot be included in statistical tests. The Venn diagrams above revealed many such proteins. To be able to include them, the missing values were imputed. This means replacing the invalid values with a narrow distribution of numbers close to the intensities of peptides identified close to the detection limit of the instrument. This is akin to treating the invalid values as ones that are at the very left-most side of a normal distribution curve.

Once the values were imputed, volcano plots were generated by plotting the difference between the averaged $\log_2$ (LFQ intensities) in the two sets on the x-axis and the significance expressed as $-\log_2$(p-value) calculated from the t-test on the y-axis. The following section examines the volcano plots generated by Perseus. Proteins that passed the significance threshold value (p-value = 0.05) are highlighted in blue; proteins that were enriched in set **B1** are highlighted in red. TST-Rab27a is always labelled in green and all known effectors of Rab27a are highlighted in black.

5.4.2.1 Set A1 vs C1

Proteins on the right-hand side (RHS) with a positive difference are enriched in set **A1** (no XL, no UV) over set **C1** (NitroXL, UV). As in the Venn diagram in Figure 63, the volcano plot in Figure 65 shows a skew towards more protein being found in set **A1**. Two putative Rab27a effectors were identified, ATP1a1 and Iqgap1, but neither their quantities did not differ significantly in the sets.

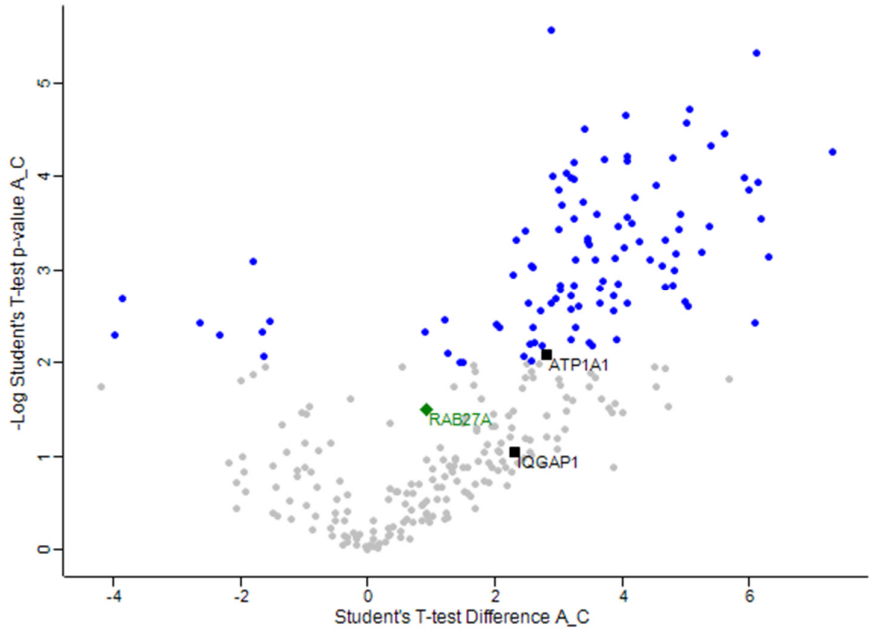

Figure 65 Volcano plot showing the results of a T-test between set 1A (no XL, no UV) and set C1 (NitroXL, UV).

The presence of crosslinker adducts on binding partners could result in decreased affinity for Rab27a, especially if the modified residue is in or very close to the interface. It could also destabilise the secondary structure of the protein, or crosslink multiple proteins together, either of which can cause aggregation of precipitation which could preclude it from pull-down and analysis. Also, because the MaxQuant search only identified unmodified peptides, the quantity of peptides will decrease in set **C1**.

5.4.2.1 Set B1 vs C1

Figure 66 compares sets **B1** and **C1** in a volcano plot. Both sets were treated with NitroXL^{AP1} but **C1** was exposed to UV, thus cleaving all crosslinks. Set **B1** was expected to retain more protein and the skew of data points towards the RHS of the volcano plot appears to support this. However, few proteins were found to be above the significance threshold. Pleasingly, Iqgap1 had the highest significance value and was found to be 2^4-fold enriched in set **B1**, suggesting that crosslinking between Rab27a and one of its putative effectors could have

been successful. However, although the interaction between Iqgap1 with Rab27a is supposed to require Cdc42,[116] no Cdc42 was found in any of the samples.

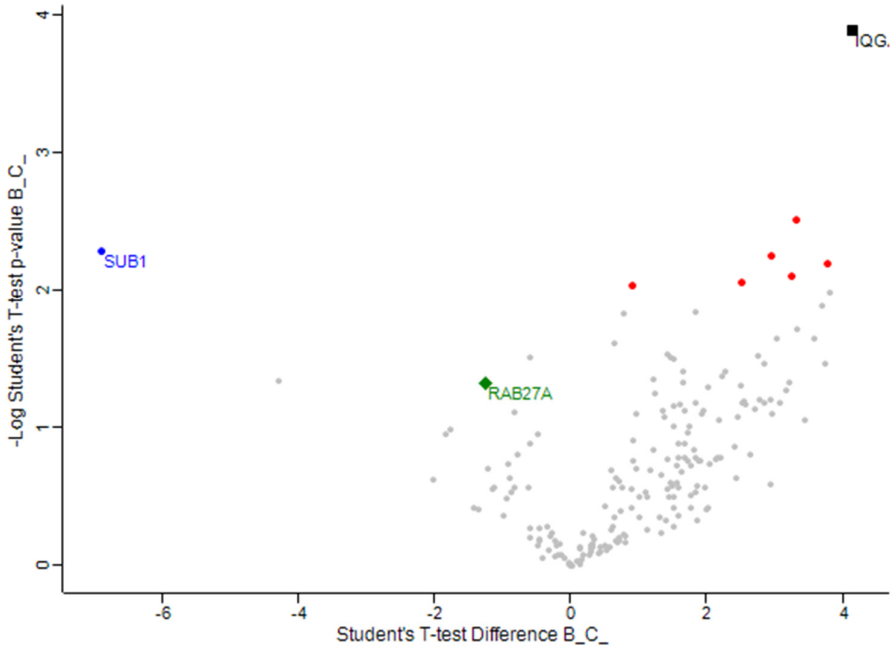

Figure 66 Volcano plot showing the results of a T-test between set B1 (NitroXL, no UV) and set C1 (NitroXL, UV).

5.4.2.1 Set A1 vs B1 and D vs E

Figure 67 shows volcano plots for sets **A1** vs **B1** compared with sets **D** and **E** respectively, which had the same experimental conditions but **E** was crosslinked with DSS instead of NitroXL. This was intended to give a qualitative view of the differences caused by changing the crosslinker. Both experiments show more proteins identified in the sets without crosslinker. The reasons may be similar to those described for sets **A1** *vs* **C1** above.

Iqgap1 was not identified in the DSS experiment, whereas Slp4 (SYLT4) was not identified any of the NitroXL experiments. ATP1a1 was more abundant in sets **A1** and **D** than in **B1** and **E** but not be a large amount. The insignificance of change in Slp4 quantity is contrary to the crosslinker validation experiments with recombinant Rab27a-Slp4 described in Chapter 4.

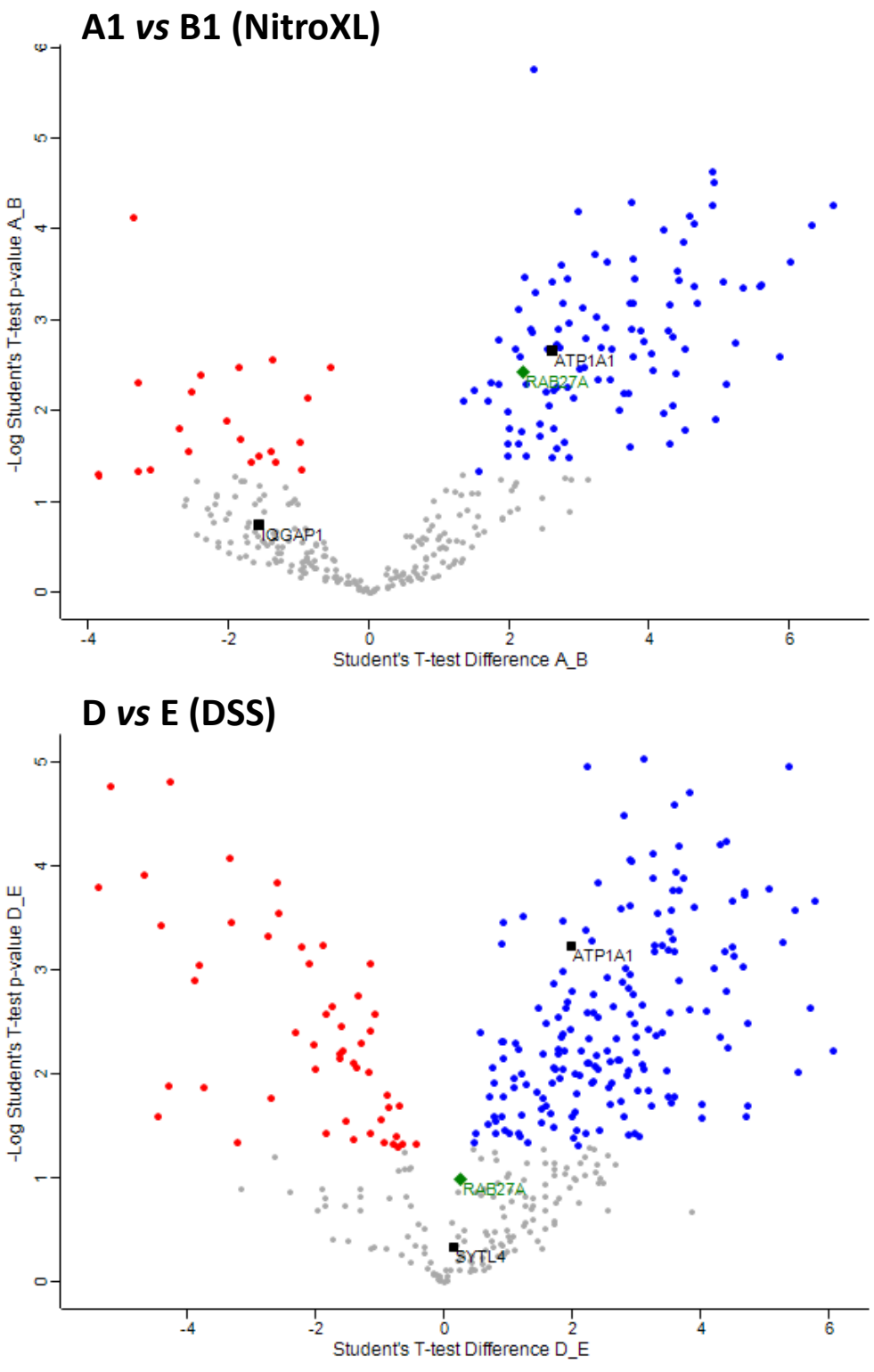

Figure 67 Volcano plot showing the results of t-test between sets A1 (no XL, no UV) and B1 (NitroXL, no UV), and between sets D (no XL, no UV) and E (DSS, no UV).

5.3.3 Summary

- Samples that were not treated with either DSS or NitroXL had higher quantities of proteins identified than those treated with crosslinker. This decrease in the LFQ intensities could be due to the exclusion of modified peptides, which were not counted in this search.
- The differences between the proteins enriched in sets **B1** and **E** over **A1** and **D** respectively either reflect the difference between the selectivities of DSS and NitroXL or were simply fluctuations in the background.
- A significant result was of Iqgap1, a known GDP-Rab27a effector, that was significantly enriched in set **B1** over **C1** and is suggestive of the successful pull-down of a crosslinked binder.

The volcano plots described above have helped to visualise the data obtained from the newly designed workflow described at the beginning of this chapter. The next section will continue to explore the modified peptides in these experiments and examine the differences in residue selectivity between NitroXL and DSS.

5.4 Analysis of modified peptides (PEAKS)

5.4.1 Peptide Modifications

PEAKS Studio 8.5. was used to search for modifications and PTMs using the same raw data that was used for MaxQuant. All crosslinker modifications (Figure 62) searched for on K and also on C, S, T,Y and N-termini to check for the extent of cross-reactivity. Table 6 shows the protein groups for which modified peptides were found by PEAKS for the trypsin (sets **A**, **B** and **C**) and chymotrypsin (sets **A1**, **B1** and **C1**) experiments. Only modifications with an A-score of over 20 were included, giving a total of 42 proteins that were found with NitroXL-derived modifications.

	Gene	Description	Coverage (%)	#Pep	#Mono OH	#Mono Gly	#Clea-ved1	#Succ OH
1	RL27	60S ribosomal protein L27	32	3	0	0	0	1
2	GRP78	78 kDa glucose-regulated protein	40	21	0	0	0	1
3	TCP4	Activated RNA polymerase II transcriptional coactivator p15	77	15	0	0	0	1
4	ADT2	ADP/ATP translocase 2	69	29	0	0	0	1
5	ARF5	ADP-ribosylation factor 5	44	10	0	0	0	1
6	ANXA2	Annexin A2	38	12	0	0	0	2
7	ATPB	ATP synthase subunit beta mitochondrial	25	11	0	0	0	1
8	DX39A	ATP-dependent RNA helicase DDX39A	37	23	0	0	0	1
9	COF1	Cofilin-1	48	9	0	0	0	2
10	QCR2	Cytochrome b-c1 complex subunit 2 mitochondrial	38	17	0	0	0	1
11	DEST	Destrin	9	2	0	0	0	2
12	RPN2	Dolichyl-diphosphooligosaccharide--protein glycosyltransferase subunit 2	36	18	3	0	0	3
13	ALDOA	Fructose-bisphosphate aldolase A	36	12	1	0	0	4
14	G3P	Glyceraldehyde-3-phosphate dehydrogenase	81	36	0	0	0	5
15	RAN	GTP-binding nuclear protein Ran	54	15	1	0	0	0
16	HSP7C	Heat shock cognate 71 kDa protein	41	25	0	0	0	1
17	HSPB1	Heat shock protein beta-1	91	24	0	0	0	2
18	HS90B	Heat shock protein HSP 90-beta	50	35	0	0	0	1
19	HNRH1	Heterogeneous nuclear ribonucleoprotein H	14	6	0	0	0	2
20	LDHB	L-lactate dehydrogenase B chain	45	12	0	0	0	1
21	NDKB	Nucleoside diphosphate kinase B	26	4	1	0	0	2
22	PPIA	Peptidyl-prolyl cis-trans isomerase A	59	14	1	0	0	1
23	MPCP	Phosphate carrier protein mitochondrial	25	14	0	0	0	3

24	PROF1	Profilin-1	61	15	0	0	0	5
25	KPYM	Pyruvate kinase PKM	53	33	0	0	0	1
26	**TSTRB27A**	**Ras-related protein Rab-27A**	**98**	**75**	**28**	**8**	**3**	**164**
27	RB27B	Ras-related protein Rab-27B	32	16	4	0	0	1
28	RACK1	Receptor of activated protein C kinase 1	24	7	0	0	0	1
29	SRSF3	Serine/arginine-rich splicing factor 3	40	14	1	0	0	10
30	SRSF7	Serine/arginine-rich splicing factor 7	18	4	0	0	0	1
31	SRP14	Signal recognition particle 14 kDa protein	32	2	0	0	0	1
32	DX39B	Spliceosome RNA helicase DDX39B	24	12	0	0	0	1
33	SFPQ	Splicing factor proline- and glutamine-rich	11	6	0	0	0	1
34	TBA1C	Tubulin alpha-1C chain	77	60	4	0	0	18
35	TBA4A	Tubulin alpha-4A chain	67	54	4	0	0	10
36	TBB5	Tubulin beta chain	86	59	0	0	0	5
37	TBB3	Tubulin beta-3 chain	59	36	0	0	0	5
38	TBB4B	Tubulin beta-4B chain	86	62	0	0	0	5
39	TBB6	Tubulin beta-6 chain	69	43	0	0	0	5
40	RS27A	Ubiquitin-40S ribosomal protein S27a	26	4	0	0	0	1
41	VDAC1	Voltage-dependent anion-selective channel protein 1	30	6	0	1	0	2
42	VDAC2	Voltage-dependent anion-selective channel protein 2	39	9	0	0	0	1

Table 6 List of protein groups found by PEAKS to have NitroXL-derived modifications from combined sets A, B and C (trypsin) and A1, B1 and C1 (chymotrypsin). The number of peptides includes unmodified counterparts. Modification counts are no. of different peptides found with the modification.

Table 7 shows the list of proteins found with DSS-derived modifications from experimental sets D and E, which has a total of 18 proteins. However, four of them forms of keratin which is more than likely a contaminant, and six are forms of tubulin, which is a highly abundant protein in cells. This suggests that the level of non-specific background proteins is higher for the DSS samples.

	Gene	Description	Coverage (%)	#Peptides	#DSS-OH	#DSS-Gly
1	ACACA	Acetyl-CoA carboxylase 1	28	46	2	2
2	ALDOA	Fructose-bisphosphate aldolase A	41	10	1	0
3	CDK1	Cyclin-dependent kinase 1	60	16	2	0
4	COPE	Coatomer subunit epsilon	19	4	0	3
5	GRP78	78 kDa glucose-regulated protein	41	27	1	0
6	RB27B	Ras-related protein Rab-27B	49	13	1	7
7	SRSF2	Serine/arginine-rich splicing factor 2	59	13	1	0
8	SRSF3	Serine/arginine-rich splicing factor 3	43	11	11	2
9	TBA1C	Tubulin alpha-1C chain	65	28	3	0
10	TBA4A	Tubulin alpha-4A chain	59	25	3	0
11	TBB2B	Tubulin beta-2B chain	24	24	1	0
12	TBB3	Tubulin beta-3 chain	53	22	1	0
13	TBB5	Tubulin beta chain	71	26	1	0
14	TBB6	Tubulin beta-6 chain	57	21	1	0
15	**TSTRB27A**	**Ras-related protein Rab-27A**	**100**	**44**	**217**	**79**

Table 7 List of protein groups found by PEAKS to have DSS-derived modifications from sets D and E. Number of peptides include unmodified counterparts. Modification counts are no. of different peptides found with the modification.

5.4.1.1 Modified Peptide Spectra

The mass spectra of well-fragmented modified peptides are given below. The spectrum, along with the assigned b and y ions, are generated by PEAKS. Capital letters refer to the unmodified amino acids; uncapitalized letters correspond to those found with a modification.

Figure 68 shows the spectrum of a chymotrypsin-digested peptide from TST-Rab27 modified with Cleave1 on S13 (A-score was 25.70). This is part of the twin Strep tag which comes after Rab27a's N-terminus. The peptide was fragmented at all but one of the possible sites. Mostly b ions were detected, that is, where the N-terminal end of the peptide fragment was detected. The number specifies how many amino acids from the N-terminus comprises the fragment. Similarly, the y ions refer to C-terminal fragments in the same way.

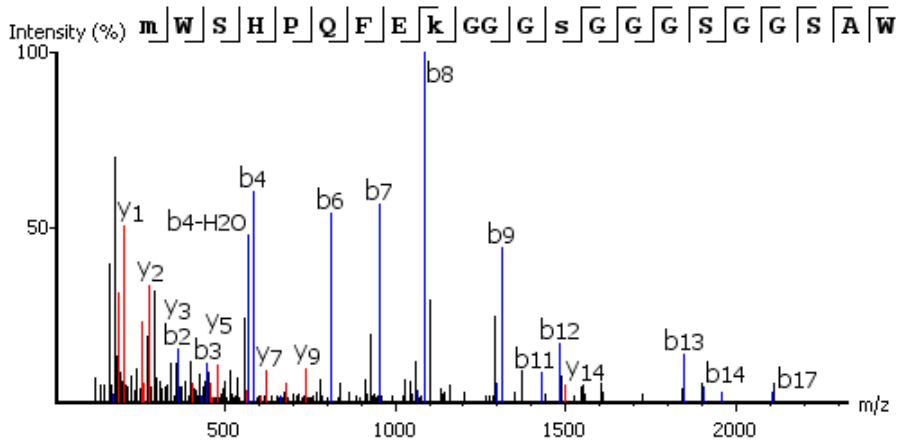

Figure 68 PEAKS-generated mass spectrum of a chymotrypsin-digested peptide on TST portion of Rab27a with S13 (marked by an arrow) modified by Cleaved1.

Figure 69 shows the spectrum this time of a trypsin-digested fragment with a K47 modified with DSS-Gly (A-score = 101.94). This time, more y ions were detected. Nearly all bonds along the peptide had fragmented. Note that the enzyme cleaved at the C-terminal end of an unmodified lysine.

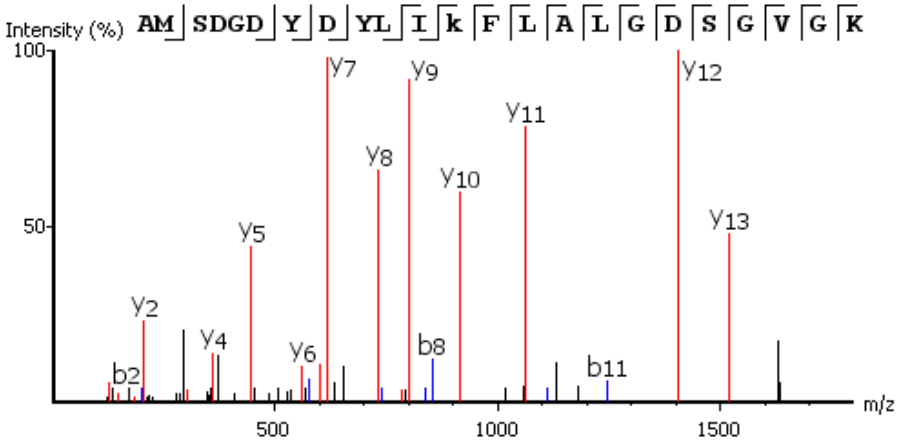

Figure 69 Mass spectrum of a trypsin-digested peptide from TST-Rab27a, where K47 (marked by an arrow is modified by DSS-Gly) modified by Cleaved1.

5.4.2 Overview of Coverage and Adducts on Rab27a

PEAKS identified the most peptides for TST-Rab27a. This is not surprising as not only was it the target of the pull-down, but it was highly abundant in the lysate to begin with, and much more so than its binders expressed at native levels. In this section, we will examine the crosslinker coverage on TST-Rab27a to view the behaviour of NitroXL on a peptide level.

Figure **70** shows the peptide coverage, enzyme cleavage points and modifications for TST-Rab27a in the three experiments.

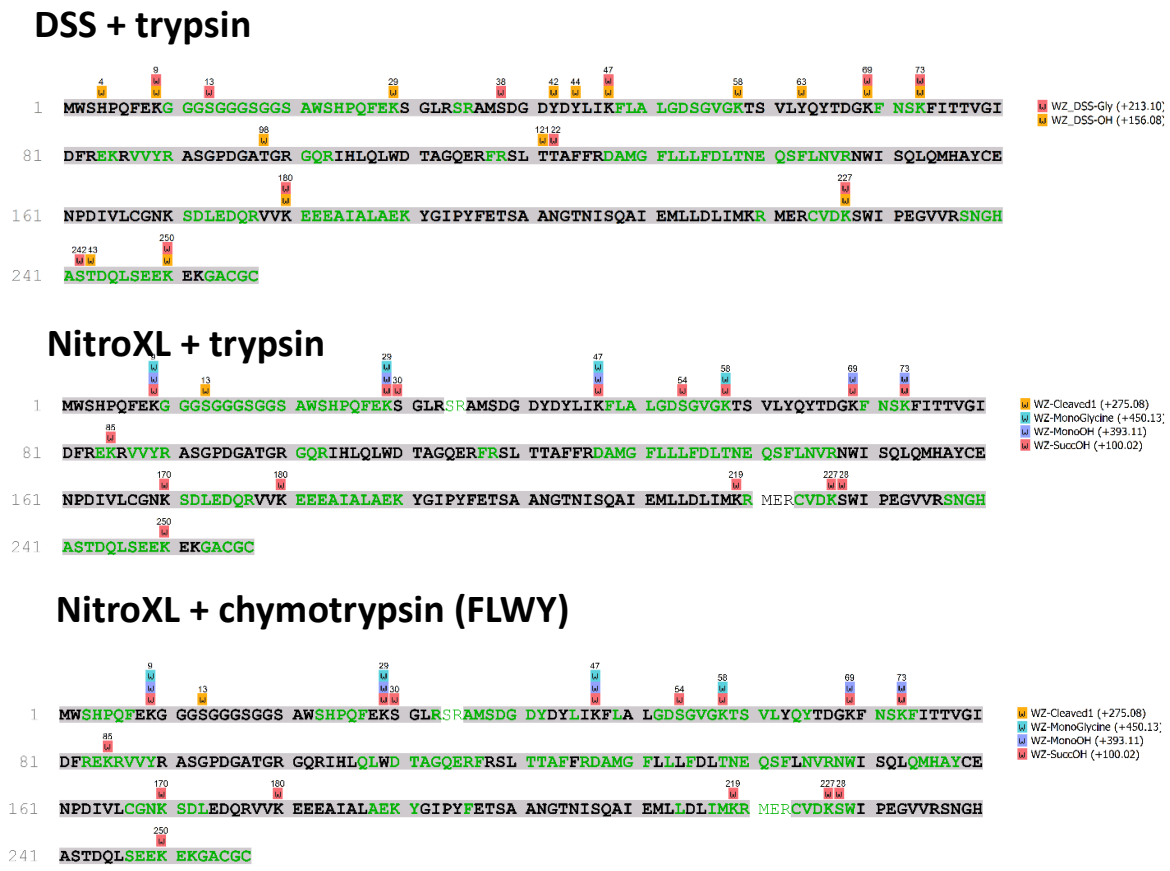

Figure 70 Peptide coverage and modifications of TST-Rab27a. The boundaries between the black and green text signify the enzyme cleavage sites. The trypsin and chymotrypsin experiments were analysed together so their modifications appear identical in this summary view.

Coverage of TST-Rab27a is complete in three experiments. Interestingly, NitroXL appeared to label only lysine and some serines, whereas DSS was found to be less residue-specific and reacted with similar numbers of the S, T and Y. This result is in spite of the two crosslinkers having the same warhead. Table 8 compares the residues of TST-Rab27a found to be modified by NitroXL and DSS. NB the native sequence of Rab27a starts at M37, so K9, S13, K29 and S30 are all on the TST tag.

NitroXL adduct residues	DSS adduct residues
K9	K9
S13	S13
K29	K29
S30	
	Y42
	Y44
K47	K47
	S38
S54	
K58	K58
	Y63
K69	K69
K73	K73
K85	
	T98
	T121
	T122
K170	
K180	K180
K219	
K227	K227
S228	
	S242
	T243
K250	K250
K: 12	K: 9
S: 4	S: 3
T: 0	T: 4
Y: 0	Y: 3
Total: 16	Total: 19

Table 8 Summary of the residues of TST-Rab27a that had crosslinker modifications. No cysteine modifications were found in any of the samples; however, because of a lack of a reducing agent such as DTT or TCEP in the solution, that a significant proportion of sulfhydryl moieties were either oxidised or bound up in a non-native disulfide bridge at the time of crosslinking.

5.4.3 Visualisation of Modified Lysines from the Crystal Structure of Rab27a

Figure 71 displays the lysine sidechains visible in the structure of Rab27a as part of the Rab27a-Slp2-a heterodimeric crystal structure by Chavas *et al.* [PDB: 3BC1]. The residue numbering corresponds to that of TST-Rab27a, and residues found in the C-terminal region and in the TST itself are not shown.

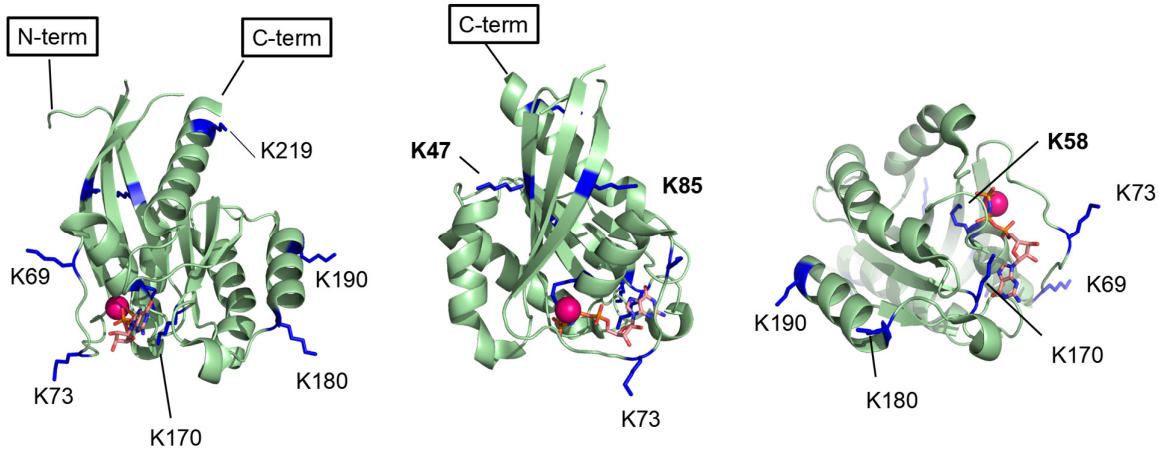

Figure 71 PyMOL-rendered images of a single Rab27a molecule from the crystal structure by Chavas et al [PDB: 3BC1], displaying all lysine residues. The residue numbering is for TST-Rab27a; the C-terminal region and the TST are not visible. Numbering is for TST-Rab27a.

K58 and K170 are situated close to the nucleotide. If these are important for the protein's interaction with the nucleotide, then they may be expected to be unreactive or at least labelled less frequently. Nevertheless, crosslinker adducts were seen on both of those lysines, but Rab27a is a flexible protein and lysines have relatively long and flexible side-chains. How the crosslinker at these sites would affect the stability and conformation of the protein is unknown; it is feasible that a reaction at certain residues would render the protein unsuitable for effector interaction.

No crosslinking was detected on K190 or K252 (not visible in 3BC1). Upon inspection of the neighbouring amino acid sequence, they may be speculated to be unreactive due to a salt bridge interaction with a glutamic acid residue (E) on an adjacent turn of the helix in an *i*, *i* + 3 relationship) *i.e.* ExxxK.

5.4.4 Crosslinker-derived adducts for tryptic digests with NitroXL and DSS

PEAKS has an in-built function that visualises the percentage of modified vs unmodified residues for all residues found with modifications. The quantification is based the AUC of ion intensities of modified and unmodified peptides that contain the residue.

Because every peptide identity differs in detection efficiency in MS, the values of ion intensities cannot be directly compared – only relative changes of the same peptide/protein between different samples are valid. However, these profiles may give a qualitive overview that may be useful in justifying or falsifying later conclusions.

The following section looks at the profiles of NitroXL-derived modifications in the trypsin and chymotrypsin sample sets.

5.2.4.1 MonoOH

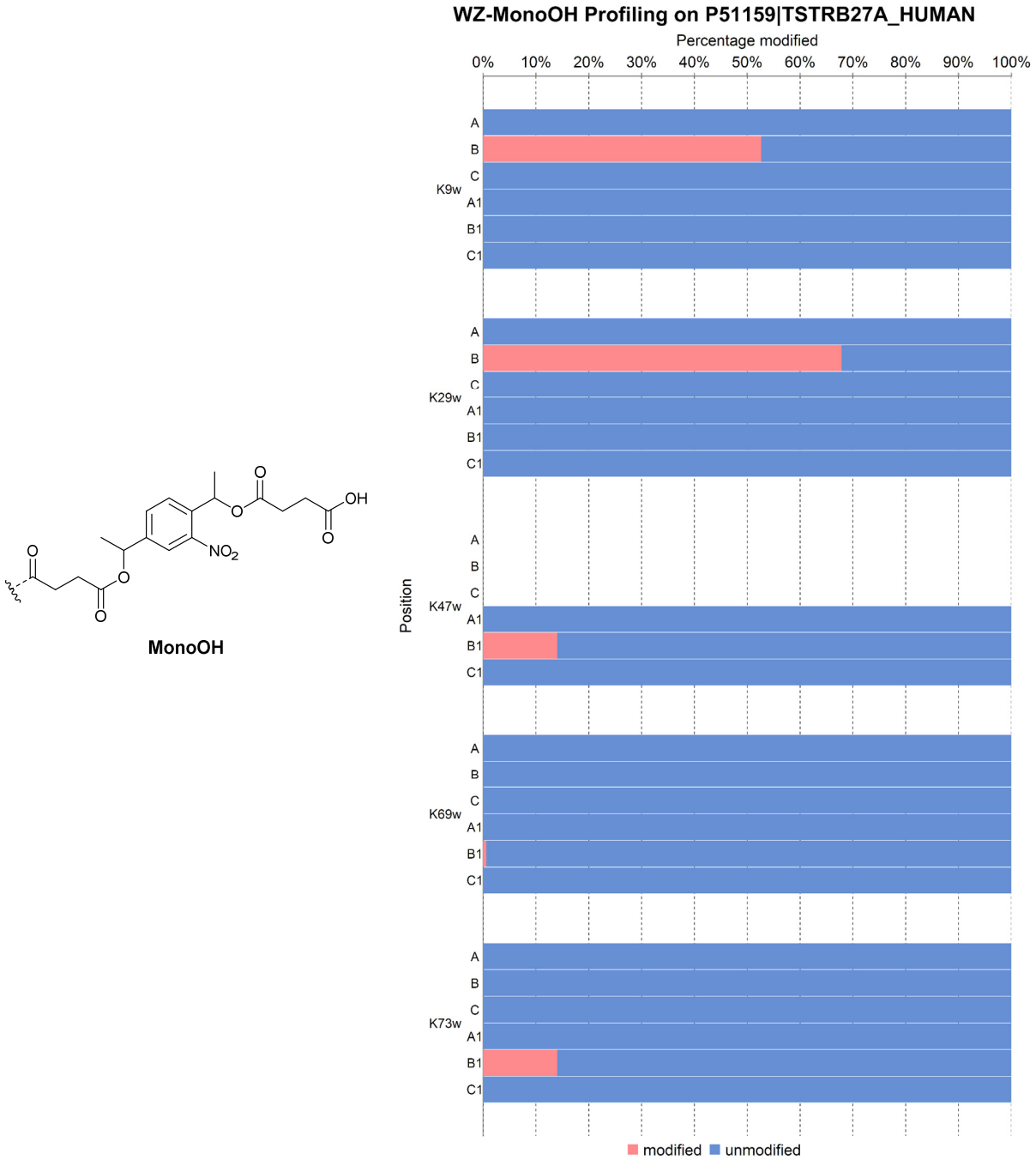

Figure 72 Profile of MonoOH adducts in trypsin (A, B, C) and chymotrypsin (A1, B1 and C1) sample sets generated by PEAKS along with the structure of MonoOH.

MonoOH is the hydrolysed type 0 NitroXL adduct (Figure 62). The profile in Figure 72 shows that it only appears in either **B** (trypsin) or **B1** (chymotrypsin) sets, though never both. It is not clear why this is. What is striking is the percentage of modified peptides can have such a

large range, ranging from ~1% to 70%, though these numbers cannot be taken to mean the real percentage. Otherwise, it is in line with its expected behaviour, in that it does not appear in set **C**/**C1**, where the photocleaved adducts would be expected instead, nor in **A**/**A1** which were not treated with crosslinker.

5.2.4.2 MonoGly

MonoGly is the type 0 adduct of NitroXL where the terminal NHS ester has been reacted with glycine from the reaction quench. A much smaller number of residues were found to be modified by MonoGly than by MonoOH, and the modified peptides were also found at lower percentages (Figure 73). This suggests that most exposed NHS esters are quenched by water within 1 hour, and indicates that the time required for crosslinking can be reduced in future experiments.

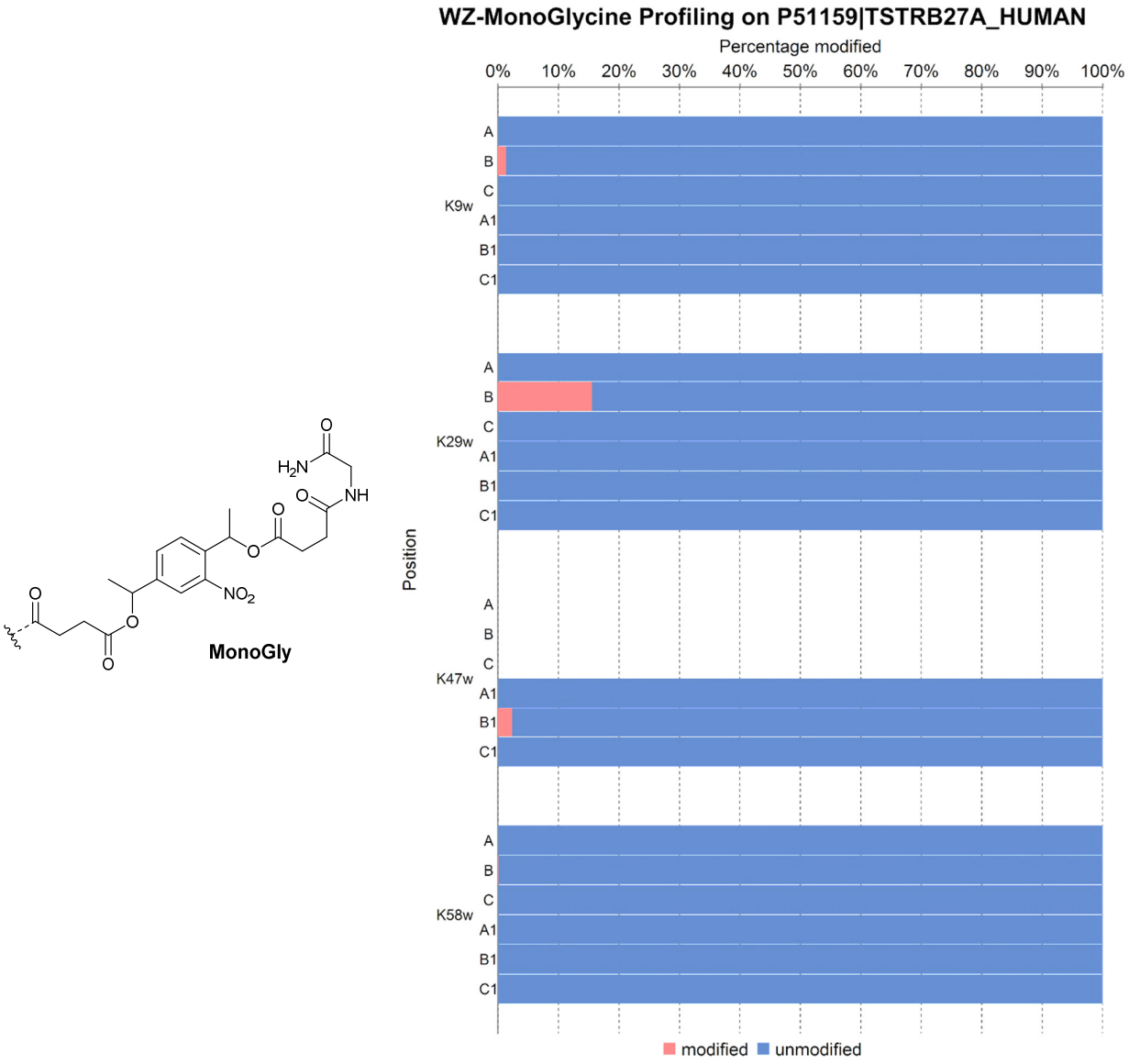

Figure 73 Profile of MonoGly adducts in trypsin (A, B, C) and chymotrypsin (A1, B1 and C1) sample sets generated by PEAKS, along with the structure of MonoGly.

5.2.4.4 SuccOH (succinylation)

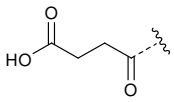

SuccOH

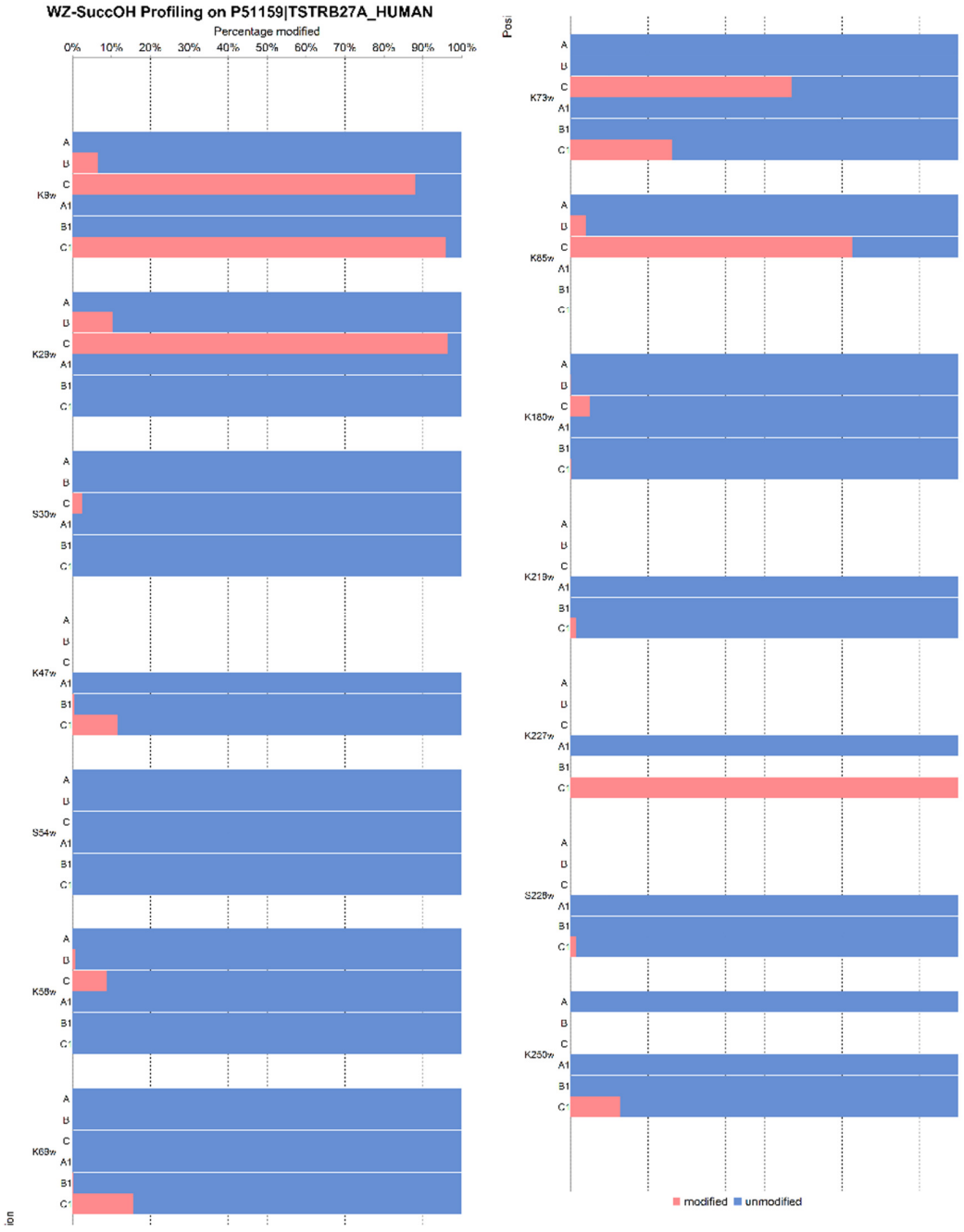

Figure 74 Profile of SuccOH adducts in trypsin (A, B, C) and chymotrypsin (A1, B1 and C1) sample sets generated by PEAKS along with the structure of SuccOH.

SuccOH is succinylation. This is a modification may originate from photocleavage of NitroXL or from hydrolysis of both the NHS ester and the internal ester groups from NitroXL (

Figure 75), but it also occurs as an endogenous PTM. As there was no succinylation found in sets **A**/**A1**, it was concluded that levels of endogenous succinylation was negligible in all samples. Therefore, we would expect most succinylated proteins to be found in sets **C**/**C1**, and indeed this was the case. Again, there was a large range of the percentage of modified residues versus their non-modified counterparts - between 10-100%. This implies that some residues are more reactive than others.

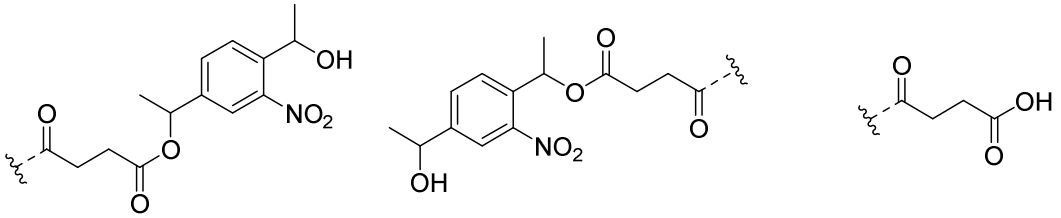

AroHydro
$C_{14}H_{15}NO_6$
+293.08994

SuccOH
$C_4H_4O_3$
+100.01604

Figure 75 NitroXL-derived adducts formed as a product of internal ester hydrolysis.

Succinylation was also observed in sets B and B1. This may have been caused by photodegradation as the samples were exposed to light during preparation, or from ester and hydrolysis. Either way, they occurred in smaller ratios. A search was set up in PEAKS to look for AroHydro (Figure 75), but no partially hydrolysed adducts were found (data not shown).

5.2.4.3 Cleaved1

Cleaved1 is the aromatic nitroso species that is expected when the 2-nitrobenzyl group is cleaved by UV irradiation. As the results from PEAKS show, this species was rarely found, with only one modified residue found in TST-Rab27a found (Figure 76).

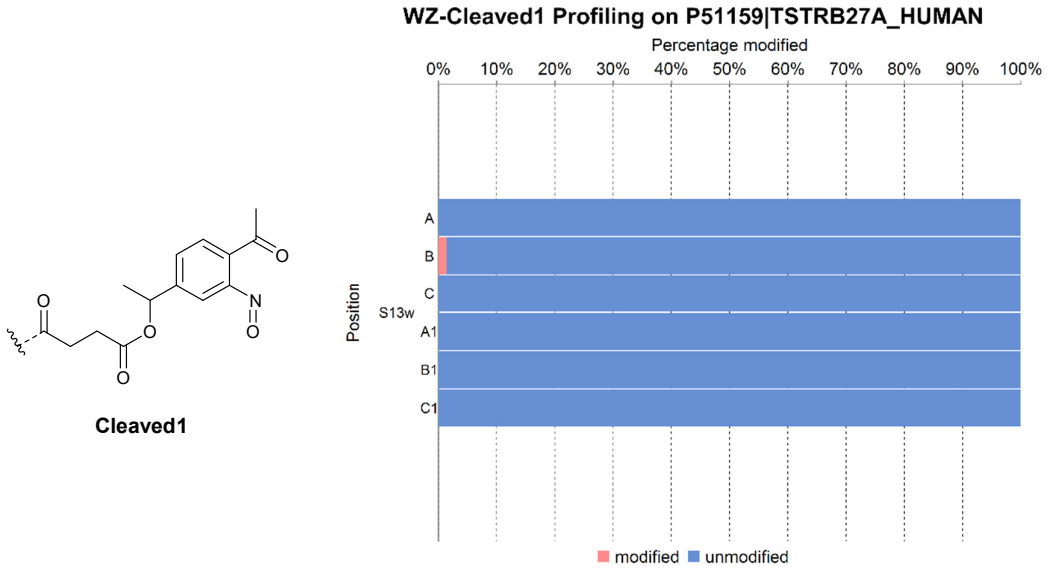

Figure 76 Profile of Cleaved1 adducts in trypsin (A, B, C) and chymotrypsin (A1, B1 and C1) sample sets along with the structure of Cleaved1.

The photocleavage of NitroXL results in a nitroso aromatic species (Cleaved1) and succinic acid (SuccOH). Therefore, we might reasonably expect similar quantities of SuccOH to Cleaved1. However, it is clear that SuccOH far outnumbered Cleaved1 in the number of modified residues and PSMs.

This could be because the nitroso group had reacted further or has undergone further photoreaction from prolonged UV exposure to give unknown adducts which no longer corresponded to the searched mass. It may be possible that the one residue where it was found was in a chemical environment that slows this process. Further investigation is necessary, or the photocleavable core could be changed into one that cleaves into more chemically stable fragments.

5.5 Refinements for LFQ – Consideration of the Discrete Behaviours of Peptides

The LFQ method used in MaxQuant earlier in this chapter assumed that the total percentage of modified peptides was low enough such that the overall protein quantification will not be affected.

MaxQuant's inbuilt LFQ algorithm quantifies proteins by creating a composite of its AUC peptide quantities. At this point, it is worth examining the different categories of peptides that can contribute to this composite. In theory, there are several types of peptides that exist in the samples which are predicted to have discrete quantification behaviours under each experimental conditon:

1. Unmodifiable peptides (no reactive residues)
2. Modified peptides
3. Unmodified counterparts of the modified peptides

The search method used in this chapter had put every unmodified peptide through to LFQ (type A and C). The validity of this rests on the assumption that the overall proportion of modified peptides is low, such that their behaviour will not affect the overall quantification behaviour of the protein.

However, the PEAKS data in section 5.4.4 suggests that some residues are significantly modified. In this case, the contribution of modified peptides towards protein quantification could potentially change the conclusions drawn about certain proteins.

With these considerations, a new search in MaxQuant was set up to identify all four NitroXL adducts from the chymotrypsin experiment. Modified peptides (type B) and their unmodified counterparts (type C) would be identified as part of the search, but their intensities would not be counted for protein quantification. This means that the quantification behaviour of proteins would be dependent only on their pulled-down quantities. Furthermore, inspection of the quantification behaviour of the peptides categories may reveal if their parent protein is a covalent or non-covalent binder (Figure 77).

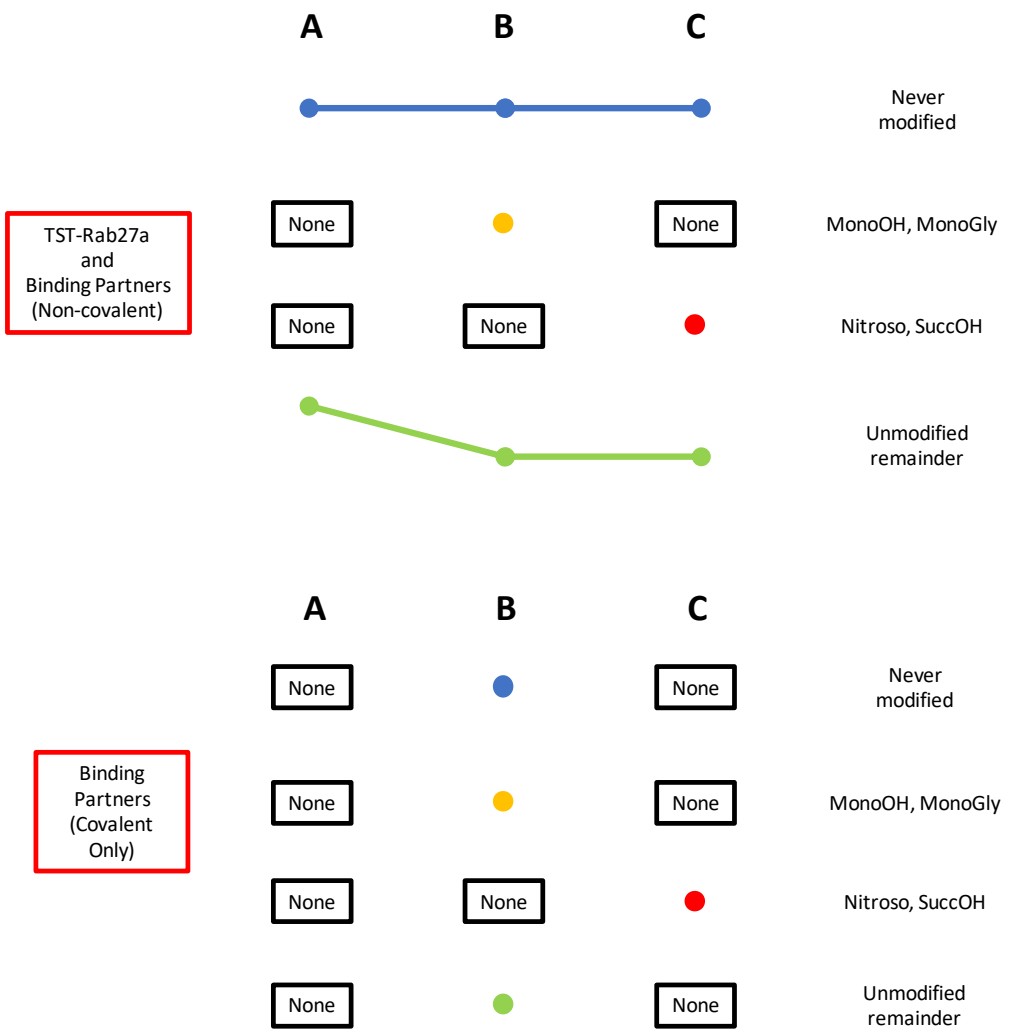

Figure 77 Predicted ideal behaviour of different types of peptides in each experimental set. In the previous search, the behaviours of never-modified and unmodified counterpart peptides would have been summed together, ignoring all modified peptides. This summation is not useful if there is both significant and variable proportions of modified peptides.

No XL is added in set A, so there are no modified peptides in any set A sample. Assuming that the same amount of TST-Rab27a is pulled down in each sample, the proportion of its never-modified peptides should stay constant in all sets. Because peptides are modified by the same proportion in sets **B** and **C**, the relative amount of unmodified counterparts will decrease from **A**. MonoOH and MonoGly adducts are expected only to occur in in set **B** with no UV treatment, and Cleaved1 and SuccOH are only expected in set **C** where samples were UV-irradiated.

If it is assumed that crosslinker cleavage is complete in set **C**, it is relatively simple to predict the behaviours of peptides belonging to covalent-only binders of Rab27a. These proteins should only appear in set **B**. In a real experiment, it is envisaged that “none” means at a lower intensity.

However, the nature of this more complex search was problematic when performed with our standard software and hardware platforms. Even after several days of run time, the searches had not undergone significant progress. Improved hardware and possibly alternative software should be considered for the next phase of the project. It is important for this alternative search method to be considered as far as practically possible as it would directly impact the nature of the conclusions drawn from the analysis.

5.6 Future Experiments

In this section, a novel proteomic protocol was involving the prototype photocleavable crosslinker NitroXL was established and tested using lysed HeLa lysate with ectopically expressed TST-Rab27a. The first iteration of MS data was obtained with initial best-guess parameters, and LFQ was performed using MaxQuant taking into account all unmodified peptides. However, the results from t-tests and modification data from PEAKS showing that some residues are very efficiently labelled suggest that precluding modified peptides from LFQ may invalidate the enrichment data. A new search scheme was proposed wherein LFQ only quantifies never-modified peptides, but this could not be completed in time. It is envisaged that future efforts using more powerful processors may yield more representative results.

Nevertheless, these initial experiments were instrumental in revealing the non-triviality of interpreting the MS results and in elucidating the improvements required to contribute to the success of this methodology.

5.6.1 Sample Preparation

To remove non-covalently bound proteins from the analysis. a precipitation step may be added before the pull-down After re-dissolving, the proteins will have lost much of their tertiary structure and will have reduced affinities for their binding partners. However, covalent crosslinks will be intact.

It may also be prudent to try a different lysis buffer. The Triton, magnesium and glycerol content may all have adverse effects on protein stabilities and interactions and their inclusion in the lysis buffer needs to be scrutinised. The fact that high-throughput screens for the extraction medium for affinity-based capture have been published as recently as 2015[278] suggests that it could make a big difference, but also that optimisation may be required depending on the target protein. This would be prevented if crosslinking was done *in vivo.* Alternatively, or in addition, a milder wash buffer could be used after the pull-down step.

A successful crosslink requires a ratio of two proteins two on one crosslinker. If the crosslinker is both too abundant and efficiently reactive, then there is a chance that the lysines on both the target protein and the effector both have singly-reacted crosslinkers, in which case they will not be crosslinked. It would be of use to perform a screen of crosslinker concentrations to minimise this.

5.6.2 Proteomics

Repeats of the initial experiments are necessary to establish the variation and reliability of the protocol. Aside from this, it would be beneficial to conduct a proteomic analysis of the entire HeLa lysate to check for the expression of known effectors of Rab27a. It may even be helpful to do this for several sources of lysate, as only a small number of Rab27a effectors tend to be expressed in any one cell type. Melanocytes may be considered as a control lysate for future experiments as the effector melanophilin is known to be robustly expressed. Fractionation may be required to mitigate dynamic range.

It would also be of interest to compare the results from crosslinking with that of a classic co-immunoprecipitation experiment, where Rab27a is pulled down by a solid-supported antibody rather than *via* an introduced protein tag (without cross-linking). More than one antibody may need to be tested; however, it serves as a benchmark against which crosslinking methods are compared.

5.6.3 Controls

It may also be easier to test this methodology first on proteins with well-characterised effectors before applying to more elusive proteins like Rab27a. Alternatively, known effectors of Rab27a could be co-transfected. Already available to the group are plasmids of TS-tagged KRas and PDE6δ. These could be used to validate changes to the proteomic protocol as well as new crosslinker designs.

The behaviour of crosslinked proteins in MS can also be conducted with recombinant Rab27a-Slp4. In this case, it may be possible to observe the type-2 intercrosslinked peptides.

5.6.4 Cells, Plasmids, Protein Constructs

The transfection of TST-Rab27a into cell cultures means that the protein will be overexpressed. Such superabundance of a protein in such a short space of time (24 h) will inevitably cause problems such as toxicity, but will also saturate the enzymes involved in post-translational modifications resulting not just in incompletely prenylated Rab27a but all other proteins requiring prenylation, which could result in many proteins being incorrected localised in the cell. This means that the proportion of endogenous-like TST-Rab27a, that is prenylated, localised on membranes or stabilised by GDIs and otherwise behaves similarly to the native protein, may be very small. Furthermore, all effectors would be expressed at their endogenous levels, which may also be very low. Neither would not be accounted for by the pull-down, resulting in issues of dynamic range.

Different protein tags could also be considered, or change to biotin instead. Unfortunately, a lot of well-known peptide affinity handles have lysines in them, including TST and FLAG. The results from PEAKS show that the TST on Rab27a is modified by NitroXL at four residues, which include K and S. This obviously does not completely prevent pull-down but it is likely to affect its affinity to StrepTactin. Also, the TST is on the long side (>30 aa), so even though its PD is clean and efficient, it may adversely affect the behaviour and positioning of the protein in the cell. Producing a biotinylated protein prevents the affinity tag from becoming modified, though StreptAvidin pull-downs will also attract endogenously biotinylated proteins.

5.6.5 Set-Up

The experimental scheme described in Figure 40 in Chapter 4 that underpinned the conception of the photocleavable crosslinker approach may be reconsidered. It would require a set-up that would enable effective UV cleavage of a heterogenous mixture, that is, trying to photocleavage molecules that are attached at one end to a solid substrate. This would be accommodated if there was a source of agitation for the beads during UV irradiation, which would incur experiments to optimise the practical aspects. This approach would bypass the issue of dynamic range with Rab27a peptides, though it excludes type 2 inter-crosslinks and may suffer from low signal intensity.

5.6.6 Crosslinker Redesign

Many options exist for improving the design of the photocleavable crosslinker. One of the first issues requiring resolution is possibly the solubility of NitroXL which, like DSS, requires 10% of DMSO to achieve reasonable solubility, and even then, some precipitation was observed at the start of the experiment. One way of achieving water-solubility is to add sulfonated NHS ester groups, as for the BS3, the doubly sulfonated version of DSS.

Alternatively, a crosslinker with improved water solubility but lacking in ionic groups may be suitable for crosslinking *in vivo*; which may allow some considerations on the choice of lysis buffer to be skipped, though permeability and uptake will become important factors.

Further, it would be desirable to have a crosslinker that does not have not have labile ester bonds beside the NHS esters. Although most esters would hydrolyse slowly under physiological pH, it would be safer to eliminate the possibility.

Other photocleavable cores should be considered; firstly, the routes to the coumarin and benzoin designs should be completed. Other photocleavable cores may have better physical and photocleavage properties and leave behind more stable photocleavage products. More thorough studies on the kinetics of photocleavage should be conducted on new iterations of crosslinkers.

5.6.7 Type 2 Inter-crosslinks

Future crosslinker designs could try to target type 2 inter-crosslinks, and can be general enough not to require pre-tagging of proteins of interest. The crosslinker could include a click-taggable group to facilitate their enrichment and mass-cleavable bonds to take advantage of the simplification they can give for data processing.

6 Discussion and Conclusions

6.1 Summary

6.1.1 Structure-guided inhibitor development of Rab27a

The x-ray derived structure of Rab27a-Slp4 by Chavas *et al.* [PDB: 3BC1] was used as the basis of the crystallisable Fusion-Rab27a construct protein made by M. Jamshidiha where the C-terminus of Rab27a was linked to the bottom helix of Slp2-a, leaving the SF4 pocket empty. This construct made it possible to validate the binding sites of hits obtained from a fragment screen using a thermal shift assay. Crystallisation of the top hits into Fusion-Rab27a revealed two binding sites, both of which were in a narrow channel in the interface between two proteins that formed a repeating unit of the crystal structure.

Analogues were developed for SAR studies of the two most synthetically attractive fragments based their crystal structure in Fusion-Rab27a and tested their binding by DSF and waterLOGSY. Unfortunately, the analogues either gave negative results or suffered from poor solubility.

It was thought that their binding sites were likely to be artefactual, made possible only by the proximity of Rab27a units in the solid-state structure. If this was the case, then it would nullify the rationale behind the SAR studies. Indeed, when a new construct was made without the short beta-chains at the bottom of the aforementioned channel, the fragments failed to crystallise in the same location.

Further work is underway by M. Jamshidiha to create new Rab27a constructs which do not require part of an effector to crystallise. This could also free up more of the Rab27a-effector interface for fragments to interact with.

6.1.2 Peptide binders: WF and lactam bridging

A combination of twenty amino acids are used by eukaryotes to synthesise proteins of every function and form in an organism. Synthetic peptides can incorporate unnatural amino acids

in addition, further increasing their potential versatility. SPPS using *N*-Fmoc-protected amino acids is an established methodology capable of making synthetic peptides more than 100 residues long, though more routinely up to around 30.

However, longer peptides are more apt to suffer from poor physical properties such as low solubility but especially low membrane permeabilization, which is a less useful for cytosolic proteins like Rab27a. The goal here was to make a short peptide that maximised ligand efficiency using the structure of Slp2-a as basis.

By downsizing the Slp2-a helix down to the residues that occupied the SF4 pocket the most deeply, the acetylated and amidated dipeptide **WF** was synthesised and found to bind weakly to recombinant GNP-Rab27a with a kd of ~ 8mM by SPR. This was a key result as it was the first positive control found for Rab27a.

Extension of the peptide sequence on either side of the WF was not successful. However, lactam-bridging was successful in increasing the affinity of WF for **K**WFR**D** and there is scope for experimenting with other combinations of amino acids that may affect its solubility and conformation.

Other members of the group have participated in an *in silico* using WF as the model ligand in the hopes of obtaining a peptidomimetic that is more easily customisable than the dipeptide. With a library of compounds based on its results, an SPR assay was used to screen a small library of compounds. Current efforts are underway in validating and developing the current hits.

6.1.3 Photocleavable Crosslinkers

Three homobifunctional photocleavable crosslinkers were designed. Due to Rab27a's limited number of cysteines, it was chosen to target lysines using NHS esters as the warhead. For the preliminary experiments, the workflow as simple as possible to make it easier to identify issues and bottlenecks. As such, we chose not to target type 2 inter-crosslinks at the outset, and thus did not include options for enriching crosslinked peptides.

The synthesis of NitroXL was successful in the timeframe. Its photocleavage was demonstrated by LCMS and its crosslinking and cleavage demonstrated by silver stained gel experiments with recombinant Rab27a-Slp4 heterodimer and lysates containing TST-Rab27a. Pull-down experiments with MagStrep beads showed that TST-Rab27a can by pulled down along with crosslinked proteins.

A novel proteomic workflow was designed involving NitroXL. LFQ of pulled-down peptides was at first envisaged to be performed using unmodified peptides, based on the assumption type 0 adducted peptides are in the minority and would not affect the conclusion of the analysis if omitted. Proteomic data were obtained for three sets of data: NitroXL-typsin, NitroXL-chymotrypsin and DSS-trypsin. Chymotrypsin was used to obtain shorter and more easily ionisable peptides: proposed to increase coverage.

LFQ in MQ was performed and volcano plots were generated for the chymotrypsin experiment. The highly significant enrichment of the known Rab27a interactor Iqgap1 in set **B1** in the chymotrypsin experiment was promising. However, the fact that many proteins found to be enriched in set **A** over **C**, along with the ratios of modified to unmodified residues found by PEAKS, suggested that the initial assumption was wrong and that a new search needed to be set up to take into account the modifications.

After inspecting the predicted behaviour of different types of peptides, it was concluded that LFQ of never-modified peptides would be the simplest way to identify Rab27a-interacting proteins based on their quantification behaviour under different experimental conditions. This search was attempted, but this was very time-consuming and could not be completed in time.

Due to the non-trivial nature of the workflow and particularly the analysis, it would be useful to develop robust positive controls for this methodology, for example by using proteins with well-validated PPIs instead of Rab27a, or with spiked in effector, or a cell line that reliably

expresses known Rab27a effectors. Certainly, this methodology is in its infancy and has the potential to be taken down a myriad of directions.

6.2 Conclusions

Rab27a is a challenging protein to study in our current paradigm in which structure-guided inhibitor development is held up as the gold standard technique in drug discovery. Certainly, one of the tightest bottlenecks for Rab27a appears to be the difficulty in obtaining a crystal structure, not just of itself but with even in co-crystals with other effectors and binders other than Slp2-a. To this day, Chavas's Rab27a-Slp2-a heterodimer [PDB: 3BC1] remains the only crystal structure in the PDB that includes Rab27a. Closely related is the structure of Rab27b with the Slp homology domain of Slac2-a/melanophilin [PDB: 2ZET], but few others offer clues to the binding modes of Rab27a, especially with GAPs, GEFs and molecules that bind to its GDP-loaded form.

Efforts are underway in the group in collaboration with ICR to obtain hits using SPR. An *in silico* screen was performed using WF as the model ligand, and a bespoke library of compounds was tested with a using an SPR assay. The dipeptide WF is also being made into a covalent binder; a judiciously placed acrylamide warhead would enable its tethering to one of the cysteine side chains around the rim of the SF4 pocket. These relatively new techniques hold promise in delivering novel hits that could be turned into a tool or drug molecule. However, the druggability of Rab27a still remains to be seen.

Even if a strong and specific inhibitor were to be found, it is unknown whether its chronic application would cause a net benefit to the patient given the life-limiting symptoms of Griscelli syndrome. However, these questions are likely to remain in future projects. Nonetheless, any technique that delivers a validated inhibitor of Rab27a will likely work on other members of the Ras superfamily and would greatly increase the ease of drug discovery for this whole class of hitherto elusive proteins.

Mapping interactomes is no easy feat, and the tagged protein approach is a method of simplifying the sample protein profile for faster analysis, and photocleavable sites on a crosslinker offer an orthogonal release point to assist with enriching proteins of interest.

It would be sensible to find a photocleavable group that reliably produces stable and easily detectable cleavage products before introducing and optimising other usable components like affinity tags or clickable groups. Further, it may be necessary to find ways of increasing the computational capacity for the more complex LFQ scheme proposed in Section 5.5. Efforts in searching for type 2 crosslinks in the future will likely require assistance in the form of an MS-cleavable bond in the crosslinker to separate the two peptides so they can fragment separately. This may require the use of triple-MS, and increase the number of potential adducts that the software must search for, adding to the technological load.

The methodology is by no means tied to Rab27a, but perhaps its biggest limitation is the requirement of producing a tagged version of every protein whose interaction network is to be studied. Not only would this become labour and cost-intensive as the number of proteins and tags increase, it still does not solve the question of how disruptive the presence of the tag would be to the protein's endogenous PPIs.

Furthermore, each crosslinker will likely be biased towards certain PPIs, and mapping the full range may require synthesising crosslinkers at a variety of lengths. Depending on the nature of the protein of interest's placement of lysines, the homobifunctional crosslinking approach may be unsuitable for some PPIs.

Nevertheless, this is a project with much depth and untold potential still to be explored, not just in crosslinker design but also ways of conducting the proteomic analysis. The preliminary experiments reported in this project have laid out the starting point and provided valuable learning opportunities upon which future studies can build.

7 Experimental

7.1 Chemical Synthesis

7.1.1 General Organic Synthesis

All reagents and solvents were purchased from Sigma-Aldrich, Novabiochem® UK or Fluorochem Ltd. and used without further purification. Ultrapure water was obtained from MilliQ® Millipore water purification system. Moisture sensitive reactions were performed under nitrogen atmosphere using dried glassware and standard syringe/septa techniques. Thin Layer Chromatography (TLC) was performed on Merck pre-coated Silica plates (Aluminum oxide 60 F254, Merck). Spots were visualized by UV light (operating at 254 nm), and using the appropriate stain (iodine, potassium permanganate, ninhydrin or p-anisaldehyde stain). Silica gel column chromatography was carried either by hand-made columns with Merck Silica 60 Å, or using an Isolera (Biotage, UK) automated apparatus with a fraction collector equipped with SNAP cartridges columns (Biotage, UK). NMR spectra were recorded on 400MHz Bruker instruments and were referenced to residual solvent signals. Data are presented as follows: chemical shift, multiplicity (s = singlet, d = doublet, t = triplet, q = quartet, m = multiplet), coupling constant(s) in Hz and integration. NMR spectrometry was carried out at room temperature except were indicated otherwise.

Mass spectrometry characterisation was obtained from the Mass Spectrometry Service of Department of Chemistry, Imperial College London.

Analytical and semi-preparative RP-HPLC were carried out on a Waters 2767 system equipped with a photodiode array, a mass spectrometer and an X-Bridge C18 column (5 µM, 4.6 mM × 100 mM). Except where indicated, all compounds that were analysed or purified by LCMS used the following gradient: 50 % to 98 % MeOH in H_2O over 10 min, 98 % MeOH was held for 2 min, MeOH was reduced from 98 % to 50 % over 1 min, and held at 50 %

until 18 min. A flow rate of 1.2 mL/min was used for the analytical mode and 20 mL/min were used for the preparative mode.

7.1.2 Characterisation of Fragment Analogues

N-(3-(4-chlorophenyl)-1-methyl-1H-pyrazol-5-yl)formamide (58)

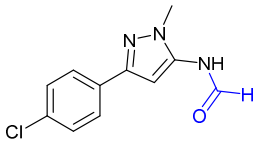

A solution of aminopyrazole **34** (50 mg, 0.24 mmol) in tetrahydrofuran (2 mL) was cooled to 0 °C with stirring. Sodium hydride (12 mg of 60% suspension in mineral oil, 0.29 mmol) was added and the mixture stirred for 20 min. Ethyl formate (40 µL, 0.48 mmol) was added. The reaction was then heated to 50 °C and stirred for 2 h. The reaction was diluted with ethyl acetate. The organic layer was washed with water and brine and dried with sodium sulfate. The solvent was removed in vacuo and the crude residue was purified by column chromatography (5% methanol in dichloromethane) to give a yellowish solid. **^{1}H NMR** rotameric, see Figure 78 below; **HRMS** (ESI, positive mode) found 236.0592 ($[M + H]^+$, requires 236.0585).

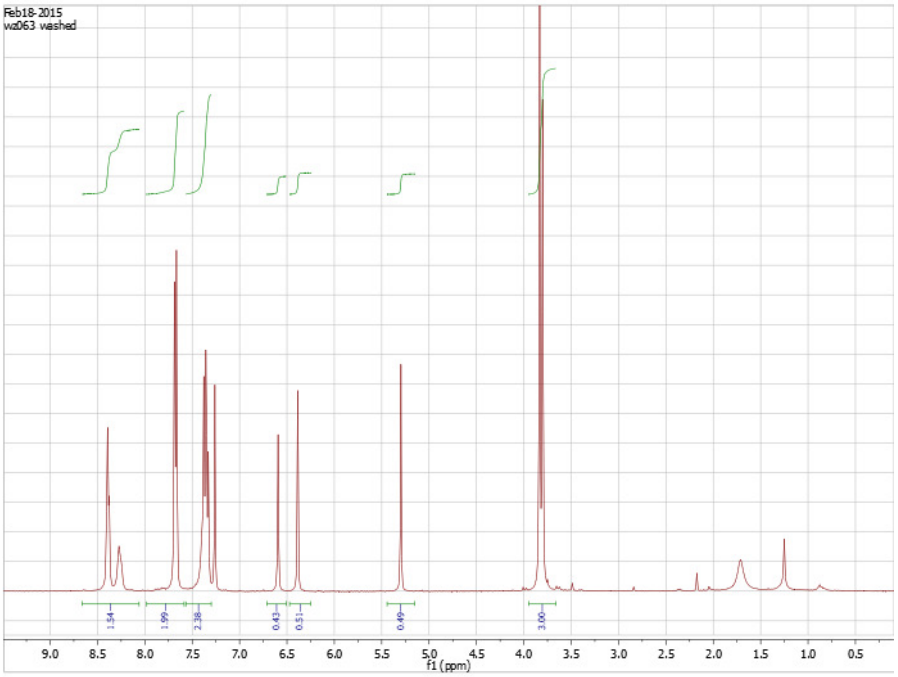

Figure 78 H NMR spectrum of 56 showing existence of rotamers

3-(4-chlorophenyl)-N,1-dimethyl-1H-pyrazol-5-amine (38)

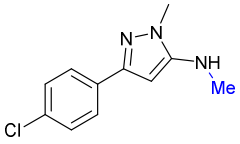

N-(3-(4-chlorophenyl)-1-methyl-1H-pyrazol-5-yl)formamide (**58**, 50 mg, 0.21 mmol) in a solution of dry tetrahydrofuran (2 mL) was cooled to -78 deg. 1.0 M lithium aluminium hydride in THF (1 mL, 1.0 mmol) was added dropwise. The reaction was warmed slowly to room temperature and then stirred for 3 h. The reaction was cooled to 0 °C and diluted with ethyl acetate. A saturated solution of Rochelle's salt was added to the reaction and the mixture was stirred for 1 h or until two separate layers formed. The organic layer was separated, washed with brine and dried with sodium sulfate before removal in vacuo. The residue was purified by column chromatography. **^{1}H NMR** (400 MHz, $CDCl_3$) δ 7.74 – 7.67 (m, 2H), 7.38 – 7.32 (m, 2H), 5.78 (s, 1H), 3.68 (s, 3H), 3.37 (s, 1H), 2.92 (s, 3H).

N-(3-(4-chlorophenyl)-1-methyl-1H-pyrazol-5-yl)acetamide (59)

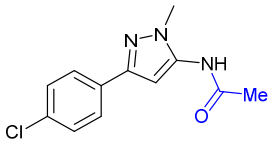

To aminopyrazole **34** (200 mg, 1.0 mmol) was added neat acetic anhydride (2 mL) and the mixture was stirred at 40 °C for 1 h. A white solid was observed to precipitate after 20-30. The mixture was quenched with water and extracted with ethyl acetate. Purification by column chromatography on silica gel with 2.5% methanol in dichloromethane gave the product as a white solid (170 mg, 70%).**^{1}H NMR** (400 MHz, DMSO) δ 10.05 (s, 1H), 7.81 – 7.73 (m, 2H), 7.48 – 7.40 (m, 2H), 6.67 (s, 1H), 3.72 (s, 3H); **HRMS** (ESI, negative mode) found 248.0587 ([M - H]$^-$, requires 248.0596).

3-(4-chlorophenyl)-1,5-dimethyl-1H-pyrazole (40)

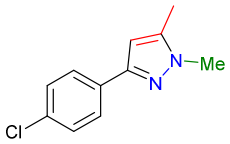

A solution of 3-(4-chlorophenyl)-5-methyl-1H-pyrazole (**62**, 40 mg, 0.26 mmol) was dissolved in of tetrahydrofuran (1.3 mL) and cooled to 0 °C with stirring. Sodium hydride (12 mg of 60% in mineral oil, 0.29 mmol) was added and the reaction was stirred for 30 min. Methyl iodide (18 µL, 0.29 mmol) dissolved in tetrahydrofuran (0.6 mL) was added to the reaction mixture dropwise. The solution was stirred at rt for 17 h. Water was added and the reaction was extracted with ethyl acetate. The organic layer was washed with brine and dried with sodium sulfate before evaporation in vacuo. The residue was purified by column chromatography to give the product as a pale yellow solid (5 mg, 10%). **^{1}H NMR** (400 MHz, CDCl3) δ 7.76 – 7.67 (m, 2H), 7.44 – 7.32 (m, 2H), 6.32 (s, 1H), 3.85 (s, 3H), 2.33 (s, 3H).

4-(4-chlorophenyl)thiazol-2-amine (41)

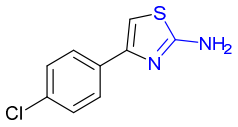

A solution of 2-bromo-1-(4-chlorophenyl)ethan-1-one (**63**, 234 mg, 1.0 mmol) and thiourea (76 mg, 1.0 mmol) in ethanol (4 mL) was stirred at 50 °C for 17 h. The reaction was cooled to room temperature. The mixture then added to water (10 mL) and extracted with dichloromethane (3 x 5 mL). The organic layer was filtered through a short silica column and the solvent removed in vacuo. The resulting product was a white powder and did not require further purification. (180 mg, 85%). **^{1}H NMR** (400 MHz, CDCl3) δ 8.24 (br s, 2H), 7.84 – 7.74 (m, 2H), 7.58 – 7.51 (m, 2H), 7.54 (m, 2H), 7.24 (s, 1H); **HRMS** (ESI, positive mode) found 211.0105 ([M + H]$^+$, requires 211.0091).

3-(4-chlorophenyl)-1-ethyl-1H-pyrazol-5-amine (42)

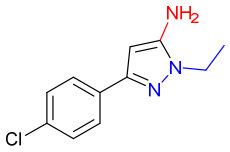

A solution of 3-(4-chlorophenyl)-3-oxopropanenitrile (**64**, 50 mg, 0.28 mmol) and ethylhydrazine oxalate (42 mg, 0.28 mmol) in ethanol (3 mL) was heated under reflux (80 deg) for 17 h. Ethyl acetate was added and the mixture was filtered through a short Celite plug. The organic layer was washed with water and then fried with sodium sulfate. The solvent was removed in vacuo and the residue was purified by column chromatography with 2% methanol in dichloromethane as the eluent to give a pale yellow solid (yield 40%). **^{1}H NMR** (400 MHz, CDCl3) δ 7.72 – 7.64 (m, 2H), 7.38 – 7.31 (m, 2H), 5.84 (s, 1H), 4.05 (q, *J* = 7.3 Hz, 2H),3.56 (br s, 2H), 1.45 (t, *J* = 7.2 Hz, 3H); **HRMS** (ESI, positive mode) found 222.0797 ([M + H]$^+$, requires 222.0793).

2,2-dimethyl-6-phenyl-4H-benzo[d][1,3]dioxine (67)

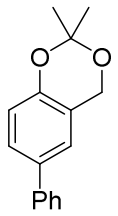

A solution of 3:1 ratio of dimethoxyethane and water (5 mL) was degassed under nitrogen for 30 minutes. 6-bromo-2,2-dimethyl-4H-benzo[d][1,3]dioxine (**66**, 60 mg, 0.25 mmol), phenylboronic acid (33 mg, 0.27 mmol), and tetrakis(triphenylphosphine)palladium(0) (14 mg, 0.013 mmol) to the solution. The mixture was heated under reflux under nitrogen for 4 h. The reaction was quenched by pouring into water. The aqueous mixture was extracted with ethyl acetate. The organic layer was washed with brine, dried with sodium sulfate and evaporated *in vacuo*. The residue was purified by column chromatography on the Biotage Isolera with 5% ethyl acetate in hexane giving the product as white crystals (25 mg, 40%). **^{1}H NMR** (400 MHz, $CDCl_3$) δ 7.55 (d, *J* = 7.6 Hz, 2H), 7.48 – 7.39 (m, 3H), 7.33 (t, *J* = 7.4 Hz, 1H), 7.26 – 7.20 (m, 1H), 6.92 (d, *J* = 8.4 Hz, 1H), 4.94 (s, 2H), 1.61 (s, 6H).

2-(2,2-dimethyl-4H-benzo[d][1,3]dioxin-6-yl)phenol (68)

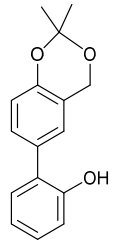

A solution of 3:1 ratio of dimethoxyethane and water (5 mL) was degassed under nitrogen for 30 minutes. 6-bromo-2,2-dimethyl-4H-benzo[d][1,3]dioxine (**66**, 55 mg, 0.23 mmol), (2-hydroxypheny)lboronic acid (48 mg, 0.34 mmol), and tetrakis(triphenylphosphine)palladium(0) (13 mg, 0.012 mmol) to the solution. The mixture was heated under reflux under nitrogen for 4 h. The reaction was quenched by pouring into water. The aqueous mixture was extracted with ethyl acetate. The organic layer was washed

with brine, dried with sodium sulfate and evaporated *in vacuo*. The residue was purified with the Biotage Isolera,with 100% dichloromethane giving the product as white crystals (12 mg, 20%). **^{1}H NMR** (400 MHz, $CO(CD_3)_2$) δ 7.35 – 7.19 (m, 3H), 7.14 – 7.08 (m, 1H), 7.04 – 6.93 (m, 3H), 4.92 (s, 2H), 1.62 (s, 6H).

(2-(2,2-dimethyl-4H-benzo[d][1,3]dioxin-6-yl)phenyl)methanol (69)

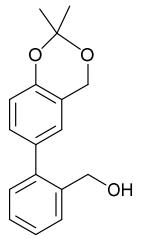

Synthesis as for **67** (17 mg, 25%) **^{1}H NMR** (400 MHz, $CDCl_3$) δ 7.59 – 7.51 (m, 1H), 7.44 – 7.32 (m, 2H), 7.33 – 7.23 (m, 2H), 7.20 (app dd, *J* = 8.3, 2.1 Hz, 1H), 7.13 – 7.00 (m, 1H), 6.99 – 6.86 (m, 1H), 4.96 – 4.89 (m, 2H), 4.68 – 4.61 (m, 2H).

3-(hydroxymethyl)-[1,1'-biphenyl]-4-ol (55)

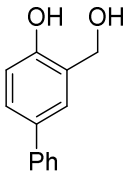

2-(2,2-dimethyl-4H-benzo[d][1,3]dioxin-6-yl)phenol (**67**, 20 mg, 0.08 mmol) was dissolved in methanol (3 mL). Five drops of 5 M hydrochloric acid was added and the solution stirred at room temperature for 2 h. Water was added and the reaction was extracted with ethyl acetate. The organic layer was washed with brine, dried with sodium sulfate and evaporated *in vacuo*. The residue was purified by column chromatography with 25% ethyl acetate in hexane (7 mg, 40%); **^{1}H NMR** (400 MHz, acetone-d_6) δ 8.58 (s, 1H, ArOH), 7.64 – 7.57 (m, 3H), 7.47 – 7.38 (m, 3H), 7.34 – 7.24 (m, 1H), 6.92 (app d, *J* = 8.3 Hz, 1H), 4.83 (d, *J* = 5.4 Hz, 2H), 4.50 (t, *J* = 5.5 Hz, 1H, CH_2OH); **HRMS** (ESI, negative mode) found 199.0763 ([M - H]$^-$, requires 199.0765).

3'-(hydroxymethyl)-[1,1'-biphenyl]-2,4'-diol (56)

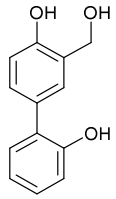

Synthesis as for **55.** The residue was purified by column chromatography with 50% ethyl acetate in hexane. **^{1}H NMR** (400 MHz, acetone-d_6) δ 8.25 (s, 1H), 8.13 (s, 1H), 7.49 (d, J = 2.3 Hz, 1H), 7.38 (dd, J = 8.3, 2.3 Hz, 1H), 7.26 (dd, J = 7.7, 1.8 Hz, 1H), 7.19 – 7.09 (m, 1H), 7.00 – 6.86 (m, 3H), 4.58 (s, 2H),2.93 (s, 1H, OH).

(4'-hydroxy-[1,1'-biphenyl]-2,3'-diyl)dimethanol (57)

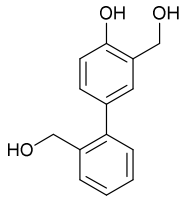

Synthesis as for **55**. **^{1}H NMR** (400 MHz, acetone-d_6) δ 8.58 (br s, 1H), 7.64 – 7.52 (m, 1H),7.36 – 7.06 (m, 5H), 6.89 – 6.80 (m, 1H), 4.89 (s, 1H), 4.79 (s, 1H), 4.57-4.54 (m, 2H), 3.55 (br s, 2H); **HRMS** (ESI, negative mode) found 229.0860 ([M - H]$^-$, requires 229.0870).

7.1.3 Solution-Phase Synthesis of Ac-WF-NH$_2$

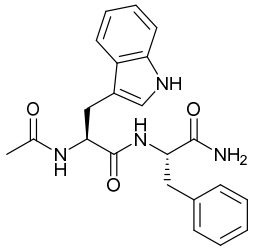

N,N'-Diisopropylcarbodiimide (DIC, 517 µL, 3.3 mmol), hydroxybenzotriazole (HOBt, 445 mg, 3.3 mmol) was added to a solution of N-acetyl-L-tryptophan (815 mg, 3.3 mmol) in chloroform (10 mL). The mixture was stirred at rt for 15 min before it was added to a solution of L-phenylalanine (500 mg, 3.0 mmol) in chloroform (20 mL). The solution was stirred at rt

for 2 h and monitored by TLC. The reaction mixture was filtered and the residue was washed with dichloromethane. The solvent was removed *in vacuo* and the residue was purified by column chromatography with the Biotage Isolera (5% methanol in dichloromethane), yielding the product as a white solid (100 mg, 8%). **^{1}H NMR** (400 MHz, DMSO) δ 10.77 (s, 1H), 8.00 (d, *J* = 7.7 Hz, 1H), 7.93 (d, J = 7.7 Hz, 1H), 7.54 (d, J = 7.7 Hz, 1H), 7.33-7.16 (m, 7H), 7.12-6.93 (m, 4H), 4.60-4.37 (m, 2H),3.07-2.96 (m, 2H), 2.88-2.76 (m, 2H), 1.74 (s, 3H); **^{13}C NMR** (101 MHz, DMSO) δ 172.69, 171.36, 169.29, 137.85, 136.02, 129.19, 127.99, 127.28, 126.20, 123.40, 120.79, 118.31, 118.16, 111.24, 110.21, 53.68, 53.52, 37.37, 27.33, 22.52; **HRMS** (ESI, positive mode) found 393.1926 ($[M + H]^+$, requires 393.1921).

7.1.4 Synthesis of Photocleavable Crosslinkers

4,4'-(((2-nitro-1,4-phenylene)bis(ethane-1,1-diyl))bis(oxy))bis(4-oxobutanoic acid) (109)

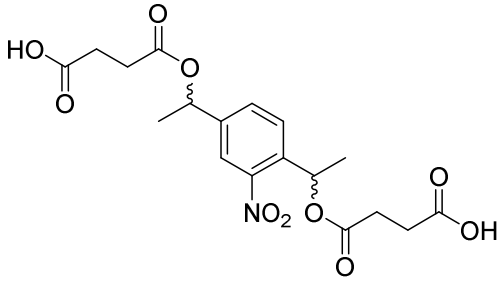

The diol 1,1'-(2-nitro-1,4-phenylene)bis(ethan-1-ol) **103** was synthesised according to the methods described by Piggott *et al.*[273] **103** (50 mg, 0.24 mmol) in dry dichloromethane was added succinyl anhydride (142 mg, 1.42 mmol), followed by triethylamine (234 µL, 1.68 mmol) and 4-dimethylaminopyridine (DMAP, 3 mg, 0.02 mmol). The resulting mixture was stirred in the dark at room temperature for 16 h, or overnight. Water was added to the solution and the organic layer was washed with water at pH 3-4 to protonate the acid. The organic layer was washed with brine and dried with anhydrous sodium sulfate. The solvent was evaporated under reduced pressure at 40°C, leaving a sticky residue that as dissolved in 50 % methanol in water and purified by LCMS using a 50-98 % methanol gradient over 18 min. The solvent was removed from the fractions using a GeneVac. The fractions were combined by dissolving the residue in pure methanol and combining them before being

evaporated off by a stream of air, giving the produce as a clear viscous oil that was used immediately in the next step. Mixture of diasteromers. **^{1}H NMR** (400 MHz, acetone-d_6) δ 8.01-7.87 (1H, m), 7.69-7.60 (2H, m), 6.38-5.74 (2H, m), 2.89-2.38 (8H, m), 1.71-1.45 (6H, m); **LCMS** R_t 4.4 min, m/z 434.1 (ESI^+, $[m + Na]^+$), 410.2 (ESI^-, $[m-1]^-$).

Bis(2,5-dioxopyrrolidin-1-yl) O,O'-((2-nitro-1,4-phenylene)bis(ethane-1,1-diyl)) disuccinate (NitroXL)

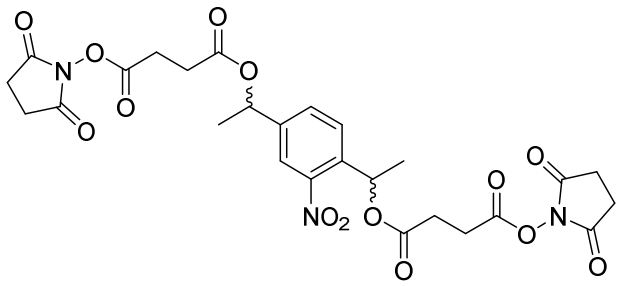

Dry dichloromethane (30 mL) was added to diacid **109** (estimated 100 mg, 0.24 mmol). N-hydroxysuccinimide (134 mg 1.16 mmol) was added to the solution, followed by 1-ethyl-3-(3-dimethylaminopropyl)carbodiimide hydrochloride (EDC.HCl, 234 mg, 1.22 mmol). The solution was stirred at room temperature in the dark for 17 h. The reaction was diluted with more dichloromethane (10 mL) and the organic layer was washed with water and brine and dried with anhydrous sodium sulfate. The solvent was evaporated at 40 °C under reduced pressure. The residue was dissolved in 50% acetonitrile in water and purified by LCMS using a 50-98% acetonitrile gradient over 18 min. The fractions were combined by dissolving the residue in pure methanol and combining them before being evaporated off in the Genevac (66 mg, 58%). **^{1}H NMR** (400 MHz, $CDCl_3$) δ 7.95 (1H, m), 7.62 (2H, m), 6.36 (1H, m), 5.95 (1H, m), 3.05-2.6 (16H, m), 1.67 (3H, m), 1.57 (3H, m); **^{13}C NMR** (101 MHz, $CDCl_3$) δ 170.18, 169.88, 169.05, 168.99, 167.76, 147.90, 142.53, 137.09, 131.67, 131.59, 127.85, 127.77, 122.32, 122.09, 71.93, 69.06, 68.95, 29.06, 28.96, 26.40, 26.32, 25.71, 21.95; **LCMS** R_t 4.4 min, m/z found 628.3 (ESI^+, $[m + Na]^+$); **HRMS** (ESI, positive mode) found 606.1563 ($[M + H]^+$, requires 606.1566).

7.2 Solid Phase Peptide Synthesis

7.2.1 General Peptide Synthesis

All peptide synthesis reagents and solvents were purchased from Sigma-Aldrich, Merck Chemicals or National Diagnostics UK and used without further purification. Synthesis was carried out in peptide synthesis grade *N*-methylpyrrolidine (NMP) and dimethylformamide (DMF). Peptides were synthesised by automated solid phase peptide synthesis with a ResPep SL apparatus (Intavis, Germany).

All peptides were synthesised using Tentagel® S RAM resin (substitution: 0.3 mmol/g).

The resin (20 µmol per well) was swelled in DMF for 30 min before deprotection of the N-terminal Fmoc protecting group with 20% piperidine (v/v) in DMF for 10 min (400 µL; 3 repeats). 4.38 equivalents of the incoming N-Fmoc protected amino acid (as a 0.5 M solution in DMF; 87.5 µmol) was activated in a separate vial with HBTU (0.5 M solution in DMF; 85 µmol, 4.25 eq), N-methyl pyrrolidinone (NMP) (5 µL) and N-methyl-morpholine (4 M; 52 µL; 208 µmol, 10.4 eq). The activated amino acid was added to the resin and allowed to couple for 35 min (repeated twice). The peptide was capped with a solution of 5% (v/v) acetic anhydride in NMP (400 µL). The resin was washed with dichloromethane (2x) and DMF (6x) and the cycle of deprotection, DMF wash, amino acid couplings, capping and DMF wash was repeated for each amino acid in the peptide sequence. After the final amino acid coupling, the N-terminal Fmoc was cleaved using 20% piperidine (v/v) in DMF (400 µL, 3× 10 min).

For any modifications to the resin bound crude peptides after synthesis, resin was transferred to a fritted 5 mL syringe, washed (DMF 3 × 1 mL, DCM 3 × 1 mL, DMF 3 × 1 mL) and swelled in DMF, for a minimum of 1 h with shaking, before subjection to the required conditions.

7.2.1.1 Deprotection, cleavage and purification of peptides

The resin was placed in a 5 mL syringe equipped with a polyethylene frit and a syringe cap. The resin bound peptide was then washed with DMF (3×), dichloromethane (3×), MeOH (3×) and Et_2O (3×) before being dried in a vacuum desiccator overnight. The peptide was deprotected and cleaved from the resin using a mixture of 95% TFA, 2.5% water, 2.5% TIS. 6 mL of this mixture was added to the resin-bound peptide and it was shaken at room temperature for 3 h. The liquid was filtered and the resin washed with 1 mL of deprotection mixture. To the solution was added 10 mL of ice-cold tert-diethyl ether to precipitate the peptide. The mixture was centrifuged (4000 rpm, 4 °C, 10 min) and the solid washed with 10 mL diethyl ether two more times. The peptide was then placed in a vacuum desiccator overnight before being purified by semi-preparative HPLC.

7.2.1.2 Lactam Bridged Peptides

Peptides were synthesized by automated SPPS as in the procedure above up until just before the final Fmoc-deprotection of the N-terminal amino acid. Fmoc-Lys(Mmt) and Fmoc Asp(Opp) in were treated as unnatural amino acids and were preactivated with HATU: HATU (3 eq, 60 umol) and the amino acid (3 eq, 70 umol) and N-methyl-morpholine (6 eq, 120 umol) were mixed in DMF in a separate vial. The activated amino acid was added to the resin and allowed to couple for 35 min (repeated twice). The resin was transferred to a fritted syringe and washed with DMF (3 mL x3) and dichloromethane (3 mL x 3). 1 mL of 3% TFA in dichloromethane was added and the syringe shaken for 1 min. This was repeated five times. The resin was washed with dichloromethane (3 mL x 3) and DMF (3 mL x3). DIC (5 eq, 0.1 mmol) and HOBt (5 eq, 0.1 mmol) were dissolved in 2 mL of DMF and was added to the resin to couple the Lys and Asp side-chains. The resin was incubated at room temperature with shaking for 2 h. The coupling procedure repeated, before washing the resin was washed with DMF (3 mL x 3). Fmoc deprotection and *N*-terminal acetylation were performed using standard procedures. The chloranil test [98] was used to confirm coupling and deprotection, and analytical LCMS was used to monitor side-chain cyclisation.

7.2.1.3 N-terminal coupling to FITC

FITC (100 µmol, 5 eq.) was dissolved in 0.5 mL DMF and DIPEA (100 µmol, 5 eq.). HATU (98 µmol, 4.9 eq.) was added, and the mixture agitated for 5 min. After this time the preactivated FITC mixture was added to a slurry of resin bound peptide in 0.5 mL DMF and DIPEA (20 µmol, 1 eq.) and shaken vigorously for 1.5 h. The solution was removed by suction, the resin washed and the process was repeated.

7.2.2 Peptide Characterisation

Ref	Sequence	MW (mono)	R_t (min)	ES^+	ES^-	Yield (%)
69	FW	392.174	7.2	415.5 (m+23)	391.4	32
70	wF	392.174	5.9	415.5 (m+23)	391.5	32
71	Fluorescein-WF	708.483	5.9, 6.4*	709.6	707.5	8
72	QWF	520.232	4.8	543.5 (m+23)	519.5	26
73	GWF	449.195	8.1	472.6 (m+23)	448.6	37
74	H-WAF	422.184	3.0	422.5	420.4	20
75	H-WFY	513.227	5.9	514.5	512.5	39
76	WFYE	684.280	4.0	707.6 (m+23)	683.5	24
77	GQWFYE	869.36	5.1	892.7 (m+23)	868.6	28
78	WFYK	683.332	6.5	684.7	682.6	22
79	QWFYE	812.338	5.2	835.6 (m+23)	811.6	23
80	WFYEAK	883.412	2.0	884.9	882.8	14
81	WFYQAK	882.428	5.4	883.8 (m+1)	881.7	30
82	WFYQHK	948.450	4.0	949.8	947.7	23
83	WFYEAKA	954.449	5.7	955.9	953.8	8

84	YY	385.153	5.8	408.6 (m+23)	384.4	30
85	KQWFD (lactam)	745.825	8.0	746.5	744.4	27
86	KRWFD (lactam)	773.885	6.2	774.7	772.6	22
87	KWFRD (lactam)	773.885	5.6	774.7	772.6	34

Table 9 LCMS characterization of peptides. Retention times are from preparative runs. All proteins were prepared with a 50-95% MeOH/H_2O gradient. Masses for ES^+ and ES^- are m+1 and m-1 (plus and minus a proton) respectively unless specified.

7.3 Biophysical Assay Methods

7.3.1 Differential Scanning Fluorimetry

All samples for the DSF experiments contained 2 µM protein, 2 mM GNP, 150 mM NaCl, 5 mM $MgCl_2$, 20 mM HEPES at pH 7.4 and 1:1000 dilution of SYPRO™ orange. Compounds were tested at 2 mM and the maximum DMSO concentration was 2% v/v. The well volume was 20 µL.

All DSF experiments were performed on a Mx3005P qPCR System. Experiments were recorded on a stepwise increment of temperature from 25-96°C in 71 cycles. SYPRO™ was used as the preferred fluorescent dye at an excitation and emission wavelength of 492 nm and 610 nm respectively. Results obtained from these experiments were extracted into Excel files using the MxPro software. The melting point of the protein, T_m, in each condition is defined as the 50% point of each curve and obtained by fitting the data using a sigmoidal equation.[257]

7.3.2 WaterLOGSY NMR

All waterLOGSY NMR experiments were recorded at 298K on a 600 MHz or 800 MHz Bruker AVANCE II spectrometer equipped with triple resonance inverse cryoprobes with a single axis z gradient. All experiments were processed and visualized using the Bruker TopSpin3.5 program. All protein-ligand interaction samples were made with a buffer containing 150 mM NaCl, 5 mM $MgCl_2$, 20 mM HEPES at pH 7.4 ,10% D_2O and 4% DMSO.

All samples for WaterLOGSY experiments were prepared in buffer containing 150 mM NaCl, 5 mM MgCl2, 20 mM HEPES at pH 7.4 and 10% v/v D2O at 298K otherwise indicated. The ligand/protein ratio was kept at 100/1, with 1 mM ligand concentration and 10 µM protein concentration. The ePHOGSY pulse sequence with 128 scans was used for WaterLOGSY experiments. Selective water saturation was achieved using a 7.5 ms 180° selective Gaussian pulse. Solvent suppression was accomplished using two 2.5 ms 10% truncated Gaussian pulses. The relaxation and mixing times were 2.5 and 1.2 s, respectively.

7.3.3 Surface Plasmon Resonance (SPR)

SPR experiments were conducted by Mostafa Jamshidina, Charlotte Sutherell and Martin Rowlands (ICR). More information may be obtained from M. Jamshidiha's PhD thesis. All SPR assays were performed on a T100 Biacore instrument with a T200 upgrade from GE Health Care and analyzed using the Biacore T200 evaluation software. All experiments were done using filtered and degassed buffer containing 10 mM HEPES, 150 mM NaCl, 10 mM MgCl2, 1 mM TCEP and 0.05% v/v Surfactant P20. For assays involving chemical molecules, fresh DMSO was used to adjust the organic solvent's content to 5% DMSO. All experiments were carried out by immobilizing biotinylated Rab27a on Neutravidin-coated CM5 chips. All data analysis was carried out by Biacore™ evaluation software.

7.4 Biological and Biochemical Methods

7.4.1 General

Ultrapure water was obtained using a MilliQ® Millipore purification system. Absorbance in 96-well plates was measured using an EnVision 2104 Multilabel Reader (PerkinElmer). Protein concentration was determined using the BioRad DC Protein Assay following the manufacturer's instructions, measuring absorbance at 750 nm, using BSA as a protein standard. All biological and chemical reagents were purchased from Sigma-Aldrich and Invitrogen and used without further purification. All crosslinkers were prepared as DMSO

stocks unless otherwise stated, stored at -20 ˚C and thawed on the day of use. All solutions and reagents for proteomics were freshly prepared on the day of sample preparation.

7.4.2 Cell Culture

MDA-MB-231 cells were grown in low glucose Dulbecco's Modified Eagle's medium (DMEM) with 5% foetal bovine serum (FBS), incubated at 10% CO_2 and 37 °C. HeLa cells were grown in low glucose Dulbecco's Modified Eagle's medium (DMEM) with 10% foetal bovine serum (FBS), incubated at 10% CO2 and 37 °C.

7.4.3 Cell Lysis

Cells were washed with PBS x 3. 700 µL of lysis buffer was added per 10 cm plate. The lysis buffer used for all experiments described in the thesis comprises the following:

1% Triton
10% glycerol
50 mM HEPES
100 mM NaCl
5 mM $MgCl_2$

This solution will be referred to as Lysis Buffer.

The cells were scraped from the plate with a cell scraper and homogenised by pipetting up and down with a 1 mL tip. The lysate mixture was transferred to an Eppendorf and left on ice for 10 minutes before centrifuging at maximum speed for 10 minutes to separate out the pellet.

7.4.4 Plasmids for TST-tagged proteins

A plasmid of N-terminally tagged TST-Rab27a was bought from InVitrogen; please see Appendix D for the plasmid map and nucleotide sequences. The plasmid was dissolved as per the manufacturer’s instructions.

Plasmids were transformed into competent DH5α -alpha cells (Invitrogen, MAX Efficiency™ DH5α™ Competent Cells) following standard protocols. The bacteria were amplified in LB agar (Merck Millipore) inoculated with ampicillin (100 µg/mL).

A single colony was selected for amplification in LB broth (Merk Millipore) and maxiprep was performed with a HiSpeed® Plasmid Maxi Kit (Qiagen) following the manufacturer's instructions. Plasmid concentrations were tested with a NanoDrop 1000 Spectrophotometer (ThermoScientific).

7.4.5 Transfection Protocol

HeLa cells were grown in 10 cm plates to a confluency of 80-90%. The old media was aspirated and replaced with 6 mL of fresh media per plate. 16.8 µL of Lipofectamine 2000 (ThermoFisher) was added to 310 µL of Opti-MEM™ Reduced Serum Media (ThermoFisher) in a plastic tube, labelled A. A specified amount of plasmid was added to 310 µL of OptiMEM in another tube, labelled B. A and B were mixed together and incubated at room temperature for 10 min.

The following quantities of DNA plasmid were used (per 10 cm plate):

TST-Rab27a - 1 ug
TST-KRas - 6 ug
TST-PDE6d - 6 ug

After 10 min, the mixture was then added to the plate dropwise and incubated at 10% CO_2 and 37 ° C for 16 h. The media was aspirated and replaced with 6 mL of fresh media and incubated at 37 ° C for another 6 h. The media was aspirated and the cells washed 3 times with sterile PBS. The cells were lysed with 0.7 mL of Lysis Buffer per plate. The lysed mixture was incubated in ice for 10 min before centrifuging at full speed for 10 min to separate the pellet. The resulting clear lysate was used directly in experiments or aliquotted and stored at -80 °C.

All transfections were tested by Western Blot by blotting with Streptactin-HRP and against the protein itself if a reliable antibody was available.

7.5 Gel and Western Blot experiments

7.5.1 Gel Electrophoresis

Proteins were separated by sodium dodecyl sulfate polyacrylamide gel electrophoresis (SDS-PAGE) using hand-cast gels with the Mini PROTEAN Tetra Cell system by Bio-Rad. Bis-tris gels were cast in 1.0 mm glass plates with 12% and 4% acrylamide for the resolving and stacking gels respectively using the recipes given in Table 10

Component	Volume (mL) for 10 mL resolving gel (12%)	Volume (mL) for 2.5 mL stacking gel (4%)
30 % acrylamide/bis-acrylamide	4.0	0.33
1.25 M Bis-tris (pH 6.7)	2.9	0.71
H_2O (MilliQ)	3.0	1.5
10 % w/v ammonium persulfate	0.1	0.0125
N,N,N'N'-Tetramethylethylenediamine	4 µL	2 µL

Table 10 Components for hand-cast bis-tris gels with 12% resolving and 4% stacking gels. The recipe is enough for two gels.

Samples were mixed in a 3:1 ratio of 4 × NuPAGE® LDS sample loading buffer containing 20% mercaptoethanol and boiled for 10 min at 95 °C before loading onto the gel.

Precision Plus Protein All Blue Standards (Bio-Rad) was used as the molecular weight ladder. Gels were run using the Mini-PROTEAN Tetra Cell system (Bio-Rad) with MOPS buffer (Invitrogen) and a PowerPac™ Basic Power Supply (Bio-Rad). Gels were run at 85 mV for 15 min and 180 mV for 45-50 min.

Silver staining was achieved by following the manufacturer's instructions in the standard non-heating protocol with the Novex™ SilverQuest™ Silver Staining Kit (Invitrogen™ LC6070).

Coomassie staining was achieved with an in-house stain (50 g ammonium sulfate and 59 mL phosphoric acid) were dissolved in 200 mL water. The solution was topped up with more water up to 400 mL. 1.2 g of Brilliant Blue G (50% dye content) was added. Finally, 100 mL of methanol was added and the mixture stirred until all solids were dissolved. The solution was stored in the dark at room temperature). The SDS-PAGE gel was immersed in the Coomassie solution overnight. The Coomassie solution was decanted and the gel destained in water for a further 24 h before imaging with the ImageQuant LAS4000 (GE Healthcare Life Sciences).

7.5.2 Western Blotting

After electrophoresis, proteins were transferred from non-fixed gels to nitrocellulose membranes (GE Healthcare Life Sciences, Amersham™ Protran® Premium 0.45 µM NC) by wet transfer using a Mini Trans-Blot® Cell (Bio-Rad) according to the manufacturer's guidelines. After transfer, membranes were blocked in 5% (w/v) dried skimmed milk or 1% BSA in TBS plus 0.1% (v/v) Tween-20 (TBST) for 2 h at room temperature and incubated with the appropriate primary antibody in blocking solution with gentle agitation overnight at 4 ˚C with anti-Rab27a (Santa Cruz Biotechnology (discontinued), C-20, sc-22990, goat polyclonal, dilution 1:100), anti -PDE6d (Santa Cruz Biotechnology, A-8, sc-376724, mouse monoclonal IgG, dilution 1:100), anti-HSP90 (Santa Cruz Biotechnology, 4F10, sc-69703, mouse monoclonal, dilution 1:2000), or anti-tubulin (Santa Cruz Biotechnology, TU-02, sc-8035, mouse monoclonal, dilution 1:500).

Membranes were then washed 3 × TBST before being incubated with the appropriate secondary antibody in blocking solution with gentle agitation for 2 h at room temperature secondary antibody or horseradish peroxidase (HRP) conjugate: goat anti-rabbit IgG-HRP (Invitrogen, dilution 1:5,000), goat anti-mouse IgG-HRP (BD Pharminigen, dilution 1:10,000), rabbit anti-goat IgG-HRP (Santa Cruz Biotechnology, sc-2922, dilution 1:10,000), NeutrAvidin™-HRP (ThermoFisher Scientific, A2664, dilution 1:500) or StrepTactin-HRP (Bio-Rad Precision Protein™ StrepTactin-HRP Conjugate, #1610381, dilution 1:5000).

Membranes were then washed with 3 × TBST before being developed with Luminata™ Crescendo Western HRP Substrate (Merck Millipore, cat. no. WBLUR0100) according to the supplier's protocol. The chemiluminescent signal on the membrane was visualised using the ImageQuant LAS4000 (GE Healthcare Life Sciences).

7.5.3 Crosslinking Protocol

10 µL of DMSO was added to 100 µL of 1 µL recombinant protein or 1 mg/ml lysate in Lysis Buffer.1 µL of 100 mM of NitroXL or DSS in DMSO or neat DMSO was added and the solution was mixed by inverting the tube several times to homogenise the mixture. The samples were wrapped in foil and incubated at room temperature on a rotator for 1 h. The reaction was quenched by adding 100 mM glycine (final concentration) and left for an additional 20 minutes. Samples to be irradiated were pipetted into a 96 well plate. For the experiments described in Chapter 4, the plate was placed under the UV lamp in a TLC visualisation box for 1 h 30 min. All other experiments used a Spectrolinker™ XL-1500 UV Crosslinker (Spectroline) with 352 nm UV lamps (Sankyo Denki, Blacklight F15T8BL, FL15BL, 352 nm, 15W). Samples were irradiated for 1 h or a specified time before separation by SDS-PAGE. The gel was visualised by silver staining or Western Blot.

7.6 Proteomics

7.6.1 Sample Preparation Protocol (Sets A, B and C)

HeLa cells were cultured until 90% confluent. The cells were transfected with TST-Rab27a plasmid with Lipofectamine 2000 as described above. The cells were lysed and their concentration adjust to 1 mg/mL. The success of the transfection was validated by Western Blot with Streptactin-HRP (Bio-Rad Precision Protein™ StrepTactin-HRP Conjugate, #1610381, dilution 1:5000) and α-Rab27a antibody (Santa Cruz Biotechnology, C-20, sc-22990, goat polyclonal (discontinued), dilution 1:100).

100 µL the 1 mg/mL lysate was aliquotted into a plastic tube for each sample. 10 µL of DMSO was added to each sample, and the tubes were inverted or gently until it became

homogenous.1 µL of 100 mM NitroXL or DSS in DMSO was added to all the samples in sets **B** and **C** and mixed by pumping gently with a pipette. Some NitroXL was seen to precipitate, but the solution became clear with time. The tubes were wrapped with foil and incubated on a rotator for 1 h at room temperature. Then, all samples were quenched with 50 mM glycine (final concentration) and rotated for a further 20 minutes. 5 µL of a bead suspension of MagStrep "type3" XT beads were added to into nine fresh Eppendorf® LoBind microcentrifuge tubes and washed with 3 x 50 µL of Lysis Buffer.

Samples requiring irradiation were transferred into individual wells in a clear 96-well plate. The plate was placed directly on top of ice and positioned 1-3 cm below the bank of UV lights in a Spectrolinker™ XL-1500 UV Crosslinker (Spectroline) with 352 nm UV lamps (Sankyo Denki, Blacklight F15T8BL, FL15BL, 352 nm, 15W). The samples were irradiated at 365 nm for 30 minutes at full power. Samples from set **A** were left in the dark at rt for the same time. Each sample was transferred to a tube the washed MagStrep beads. They were cover with foil and incubated on a rotator at 4 °C for 2 hours or overnight.

The MagStrep beads were pelleted using a magnetic tube rack. The supernatants were transferred into fresh LoBind tubes and kept frozen at -80 deg. The remaining beads were washed with 3 x 100 µL of Lysis Buffer, followed by 3 x 100 µL of AMBIC. (Because the TST/Streptactin interaction is much weaker than the biotin/neutravidin interaction, harsher detergents containing high levels of SDS must be avoided).

All cysteines were reduced and alkylated by simultaneously adding 5 mM TCEP and 15 mM chloroacetamide (final concentrations) and incubating at rt in the dark for 45 min. For trypsin digestion, the beads were washed with 3 x 100 µL HEPES pH 8. For chymotrypsin, the beads were washed with 3 x 100 µL of 100mM Tris-HCl and 10mM $CaCl_2$. After the final wash, add a fresh 50 µL of of fresh enzyme buffer was added. Trypsin (Sequencing Grade Modified Trypsin

(Promega) or chymotrypsin (Promega) was added at a concentration of 0.1 µg of trypsin per 100 µg of protein and the samples were incubated at 37 °C overnight with gentle agitation. Samples were then centrifuged and the supernatant transferred to a new tube.

The beads were washed with 0.1% formic acid in water and centrifuged and this supernatant added to the same tube. The peptide solutions were then stage-tipped according to a published protocol [279]. Briefly, stage tips were prepared by fitting C18 Empore disks (SDC-XC, 3M) into 200 µL pipette tips. The stage tip was initially washed by centrifuging (2000 × g, 2 min) with MeOH (150 µL) followed by water (150 µL). Peptide solutions were then added to the top of the stage tip and centrifuged (2000 × g, 2 min) to load the peptides onto the C18 sorbent followed by desalting by washing with water (150 µL). Peptides were eluted with 79% acetonitrile in water and dried with speed-vac-assisted solvent removal. Dried samples were stored at -80 °C if not required for immediate analysis. Peptides were then re-dissolved in 0.5% TFA, 2% acetonitrile in water and transferred to LC-MS sample vials for LC-MS/MS analysis.

7.6.2 LCMS/MS Runs

7.6.3 The Q-Exactive

The proteomic experiments in this thesis were performed with a Q-Exactive mass spectrometer. Figure 79 depicts its main features. Each sample undergoes a 90-minute HPLC run with a hydrophobic C18 column. The eluted sample enters the mass spectrometer *via* the NanoSpray Source at **A**. The ion stream is directed to the quadrupole mass filter (**B**), which selects precursor ions based on their mass and sends them through to the (HCD) collision cell (**C**) where collision-induced dissociation (CID) occurs. The fragmented ions are gathered in the C-trap (**D**) before they are progress to the Orbitrap mass analyser (**E**) where the signal output undergoes Fourier transform to yield high resolution spectra[280].

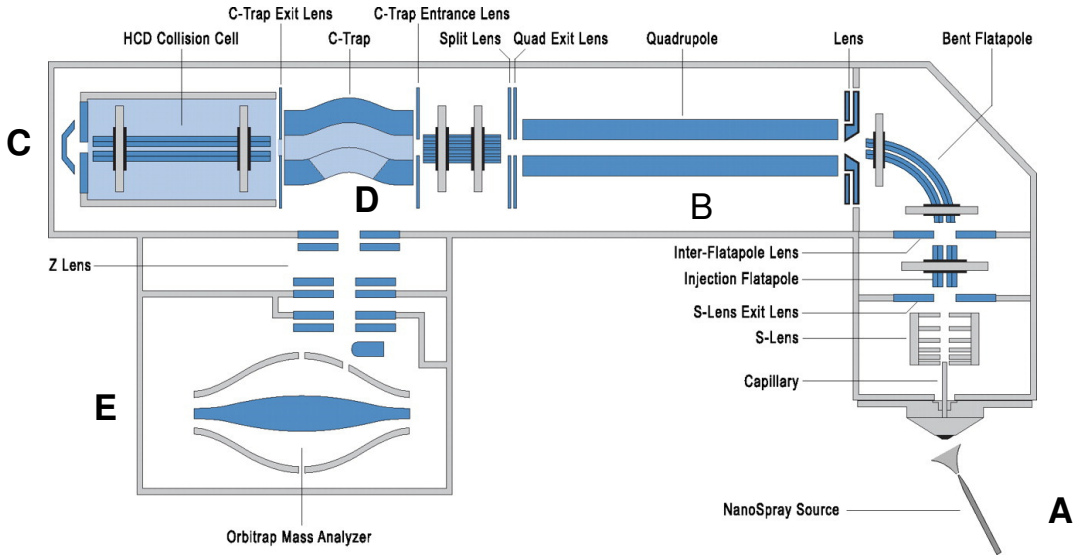

Figure 79 Diagram of the Q-Exactive, a quadrupole orbitrap mass spectrometer. Adapted from a diagram by Michalski et al. [280]. **A**: ionization at NanoSpray Source; **B**: mass selection by quadrupole mass filter; **C**: fragmentation in the HCD cell; **D**: C-Trap; **E**: Orbitrap mass analyser.

7.6.4 Proteomics Facility, Imperial College London

The analysis was performed using reverse phase Acclaim PepMap RSLC column 50 cm × 75 µm inner diameter (Thermo Fisher Scientific) using a 2 h acetonitrile gradient in 0.1 % formic acid at a flow rate of 250 nL/min. Easy nLC-1000 was coupled to Q Exactive™ Hybrid Quadrupole-Orbitrap™ Mass Spectrometer *via* an easy-spray source (all Thermo Fisher Scientific). The Q Exactive was operated in data-dependent mode with survey scans acquired at a resolution of 75 000 at m/z 200 (transient time 256 ms). Up to the top 10 most abundant isotope patterns with charge +2 from the survey scan were selected with an isolation window of 3.0 m/z and fragmented by HCD with normalized collision energies of 25 W. The maximum ion injection times for the survey scan and the MS/MS scans (acquired with a resolution of 17,500 at m/z 200) were 250 and 80 ms, respectively. The ion target value for MS was set to 10^6 and for MS/MS to 10^5.

7.6.5 Data Analysis

7.6.5.1 Peptide Modifications with PEAKS

The search for modified peptides was processed using PEAKS Studio 8.5, which as a default performs *de novo* peptide sequencing prior to database search. The software also

searches for common PTMs (PEAKS PTM) and amino acid mutations (SPIDER). Peptides identified from the MS/MS spectra were searched against the human UniProt database (2015) with the Rab27a sequence replaced with TST-Rab27a as detailed in Appendix C (WZ UniProt + TST-Rab27a). **Digestion**: Trypsin and chymotrypsin-FLWY (specific, up to two missed cleavages allowed) were selected for database searches. The number of non-specific cleavages was set to none. **Modifications**: Cysteine carbamidomethylation (+57.02 Da) was selected as a fixed modification. Variable modifications included Cleaved1: (+275.08 Da), MonoGlycine: (+450.13 Da), MonoOH: (+393.11 Da) and SuccOH (+100.02 Da) and were specified to occur on K, C, S, T and Y. The maximum number of PTMs per peptide was set to three. **Mass error tolerance**: The maximum mass error was set to 5 ppm for precursor (parent) ions and 0.01 Da for product (fragment) ions. **Identification**: The false discovery rate was set to 0.01 for peptides and a minimum of 2 unique peptides per protein was required. Modifications required an A-score of ≥ 20, *de novo* ALC score required ≥ 80%, and peptide- and protein-10lgP required ≥ 38.1 and ≥ 20 respectively. Identified peptides from one gene were grouped together into protein groups. Data were analysed using Microsoft Office Excel 2016.

7.6.5.2 Label Free Quantification

The raw data file obtained from each LC-MS/MS acquisition was directly processed with the software MaxQuant 1.5.8.3, with the peptides being identified from the MS/MS spectra searched against the WZ UniProt + TST-Rab27a database using the Andromeda search engine. Cysteine carbamidomethylation (+57.021 Da) was set as a fixed modification and methionine oxidation (+15.995 Da) as well as the crosslinker-derived adducts (Chapter 5), were set as variable modifications for the search. LFQ with 'match between runs' was selected. The minimum length of a peptide was set to 7 residues, the maximum amount of missed trypsin cleavages was set to 2, the maximum number of modifications per peptide was set to 5 and the maximum charge of a peptide as +7. Peptide and protein FDRs were set to 0.01. Quantification of peptides was allowed for 'razor + unique' peptides carrying no

modifications as well as methionine oxidation or carbamidomethylation (razor peptides are uniquely assigned to protein groups and not to individual proteins). All other parameters were used as pre-set by the software.

Data outputted from MaxQuant was analysed using Perseus 1.6.0.7. Protein identifications by MaxQuant based on 'contaminants', 'only identified by site' and 'reverse' were filtered out. Further filtering only allowed identification of a protein target if it contained at least two 'razor+unique peptides' in both biological duplicates for at least one experimental condition (sample set). Two-sample t-tests (S0 = 1, FDR = 0.01) were carried out between relevant sample sets. LFQ intensities were logarithmised to base 2 (function $\log_2(x)$).

LFQ was performed in MaxQuant 1.5.8.3 using the built-in LFQ algorithm. [208] The output datasets were analyzed with Perseus 1.6.0.7. The label-free approach chosen was based on intensities of proteins calculated by MaxQuant from peak intensities and based on the ion currents carried by several peptides whose sequences match a specific protein to provide an approximation of abundance.

Triplicates were grouped together for each type of treatment (sets **A**, **B**, **C**). For each two-sample test, at least two valid values out of three replicates was required for at least one sample set. For statistical analysis, missing values were imputed by a random number drawn from a normal distribution that mimics low abundance measurements close to the detection limit (imputation criteria: width 0.3 and down shift 1.8). This allows for proteins that were not detected in one of the sample sets to be included in statistical tests. **Statistical tests:** Two-sample, both-sided Student's T-tests were performed between selected sample sets. S0 and was set to 1 to separate outliers from the background distribution. The p-value was set to 0.05 as the significance threshold. The difference between the means of logarithmised LFQ intensities of proteins in the two sets (x axis) was plotted against $-\log_{10}p$ (y axis) values to obtain volcano plots showing the relative distribution of proteins in two experimental conditions.

8 Bibliography

1. Zhen, Y.; Stenmark, H., Cellular functions of Rab GTPases at a glance. *J Cell Sci* **2015**.

2. Wennerberg, K.; Rossman, K. L.; Der, C. J., The Ras superfamily at a glance. *J Cell Sci* **2005,** *118* (5), 843-846.

3. Schwartz, S. L.; Cao, C.; Pylypenko, O.; Rak, A.; Wandinger-Ness, A., Rab GTPases at a glance. *J Cell Sci* **2007,** *120* (22), 3905-3910.

4. Tolmachova, T.; Anders, R.; Stinchcombe, J.; Bossi, G.; Griffiths, G. M.; Huxley, C.; Seabra, M. C., A General Role for Rab27a in Secretory Cells. *Mol Biol Cell* **2004,** *15* (1), 332-344.

5. Ostrowski, M.; Carmo, N. B.; Krumeich, S.; Fanget, I.; Raposo, G.; Savina, A.; Moita, C. F.; Schauer, K.; Hume, A. N.; Freitas, R. P.; Goud, B.; Benaroch, P.; Hacohen, N.; Fukuda, M.; Desnos, C.; Seabra, M. C.; Darchen, F.; Amigorena, S.; Moita, L. F.; Thery, C., Rab27a and Rab27b control different steps of the exosome secretion pathway. *Nat Cell Biol* **2010,** *12* (1), 19-30.

6. Singh, R. K.; Mizuno, K.; Wasmeier, C.; Wavre-Shapton, S. T.; Recchi, C.; Catz, S. D.; Futter, C.; Tolmachova, T.; Hume, A. N.; Seabra, M. C., Distinct and opposing roles for Rab27a/Mlph/MyoVa and Rab27b/Munc13-4 in mast cell secretion. *FEBS J* **2013,** *280* (3), 892-903.

7. Izumi, T., Physiological Roles of Rab27 Effectors in Regulated Exocytosis. *Endocr J* **2007,** *54* (5), 649-657.

8. Kimura, T.; Taniguchi, S.; Niki, I., Actin assembly controlled by GDP-Rab27a is essential for endocytosis of the insulin secretory membrane. *Arch Biochem Biophys* **2010,** *496* (1), 33-37.

9. Pfeffer, S. R., Two Rabs for exosome release. *Nat Cell Biol* **2010,** *12* (1), 3-4.

10. Kimura, T.; Niki, I., Rab27a, actin and beta-cell endocytosis [Review]. *Endocr J* **2011,** *58* (1), 1-6.

11. Seabra, M. C.; Mules, E. H.; Hume, A. N., Rab GTPases, intracellular traffic and disease. *Trends Mol Med* **2002,** *8* (1), 23-30.

12. Stinchcombe, J. C.; Barral, D. C.; Mules, E. H.; Booth, S.; Hume, A. N.; Machesky, L. M.; Seabra, M. C.; Griffiths, G. M., Rab27a Is Required for Regulated Secretion in Cytotoxic T Lymphocytes. *The Journal of Cell Biology* **2001,** *152* (4), 825.

13. Menasche, G.; Pastural, E.; Feldmann, J.; Certain, S.; Ersoy, F.; Dupuis, S.; Wulffraat, N.; Bianchi, D.; Fischer, A.; Le Deist, F.; de Saint Basile, G., Mutations in RAB27A cause Griscelli syndrome associated with haemophagocytic syndrome. *Nat Genet* **2000,** *25* (2), 173-176.

14. Wilson, S. M.; Yip, R.; Swing, D. A.; O'Sullivan, T. N.; Zhang, Y.; Novak, E. K.; Swank, R. T.; Russell, L. B.; Copeland, N. G.; Jenkins, N. A., A mutation in Rab27a causes the vesicle transport defects observed in ashen mice. *Proc Natl Acad Sci U S A* **2000,** *97* (14), 7933-7938.

15. Van Gele, M.; Dynoodt, P.; Lambert, J., Griscelli syndrome: a model system to study vesicular trafficking. *Pigm Cell Melanoma R* **2009,** *22* (3), 268-282.

16. Sahai, E.; Marshall, C. J., Rho-GTPases and cancer. *Nat Rev Cancer* **2002,** *2* (2), 133-142.

17. Aznar, S.; Fernández-Valerón, P.; Espina, C.; Lacal, J. C., Rho GTPases: potential candidates for anticancer therapy. *Cancer Lett* **2004,** *206* (2), 181-191.

18. Hashimoto, S.; Onodera, Y.; Hashimoto, A.; Tanaka, M.; Hamaguchi, M.; Yamada, A.; Sabe, H., Requirement for Arf6 in breast cancer invasive activities. *Proc Natl Acad Sci U S A* **2004,** *101* (17), 6647-6652.

19. Konstantinopoulos, P. A.; Karamouzis, M. V.; Papavassiliou, A. G., Post-translational modifications and regulation of the RAS superfamily of GTPases as anticancer targets. *Nat Rev Drug Discov* **2007,** *6* (7), 541-555.

20. Matchett, K. B.; McFarlane, S.; Hamilton, S. E.; Eltuhamy, Y. S. A.; Davidson, M. A.; Murray, J. T.; Faheem, A. M.; El-Tanani, M., Ran GTPase in Nuclear Envelope Formation and Cancer Metastasis. *Adv Exp Med Biol* **2014,** *773*, 323-351.

21. Barrès, V.; Ouellet, V.; Lafontaine, J.; Tonin, P. N.; Provencher, D. M.; Mes-Masson, A.-M., An essential role for Ran GTPase in epithelial ovarian cancer cell survival. *Mol Cancer* **2010,** *9* (1), 1-11.

22. Goldenring, J. R., A central role for vesicle trafficking in epithelial neoplasia: intracellular highways to carcinogenesis. *Nat Rev Cancer* **2013,** *13* (11), 813-820.

23. Shima, F.; Matsumoto, S.; Yoshikawa, Y.; Kawamura, T.; Isa, M.; Kataoka, T., Current status of the development of Ras inhibitors. *J Biochem* **2015,** *158* (2), 91-99.

24. Wang, W.; Fang, G.; Rudolph, J., Ras inhibition via direct Ras binding—is there a path forward? *Bioorg Med Chem Lett* **2012,** *22* (18), 5766-5776.

25. Cox, A. D.; Fesik, S. W.; Kimmelman, A. C.; Luo, J.; Der, C. J., Drugging the undruggable RAS: Mission Possible? *Nat Rev Drug Discov* **2014,** *13* (11), 828-851.

26. Cromm, P. M.; Spiegel, J.; Grossmann, T. N.; Waldmann, H., Direct Modulation of Small GTPase Activity and Function. *Angew Chem Int Edit* **2015,** *54* (46), 13516-13537.

27. Spiegel, J.; Cromm, P. M.; Zimmermann, G.; Grossmann, T. N.; Waldmann, H., Small-molecule modulation of Ras signaling. *Nat Chem Biol* **2014,** *10* (8), 613-622.

28. Arkin, Michelle R.; Tang, Y.; Wells, James A., Small-Molecule Inhibitors of Protein-Protein Interactions: Progressing toward the Reality. *Chem Biol* **2014,** *21* (9), 1102-1114.

29. Bobrie, A.; Krumeich, S.; Reyal, F.; Recchi, C.; Moita, L. F.; Seabra, M. C.; Ostrowski, M.; Théry, C., Rab27a Supports Exosome-Dependent and -Independent Mechanisms That Modify the Tumor Microenvironment and Can Promote Tumor Progression. *Cancer Res* **2012,** *72* (19), 4920-4930.

30. Feng, F.; Zhang, J.; Fan, X.; Yuan, F.; Jiang, Y.; Lv, R.; Ma, Y., Downregulation of Rab27A contributes to metformin-induced suppression of breast cancer stem cells. *Oncology Lett* **2017**.

31. Feng, F.; Jiang, Y.; Lu, H.; Lu, X.; Wang, S.; Wang, L.; Wei, M.; Lu, W.; Du, Z.; Ye, Z.; Yang, G.; Yuan, F.; Ma, Y.; Lei, X.; Lu, Z., Rab27A mediated by NF-κB promotes the stemness of colon cancer cells via up-regulation of cytokine secretion. *Oncotarget* **2016,** *7* (39), 63342-63351.

32. Shi, C.; Yang, X.; Ni, Y.; Hou, N.; Xu, L.; Zhan, F.; Zhu, H.; Xiong, L.; Chen, P., High Rab27A expression indicates favorable prognosis in CRC. *Diag Pathol* **2015,** *10* (1), 68.

33. Webber, J. P.; Spary, L. K.; Sanders, A. J.; Chowdhury, R.; Jiang, W. G.; Steadman, R.; Wymant, J.; Jones, A. T.; Kynaston, H.; Mason, M. D.; Tabi, Z.; Clayton, A., Differentiation of tumour-promoting stromal myofibroblasts by cancer exosomes. *Oncogene* **2015,** *34* (3), 290-302.

34. Wang, Q.; Ni, Q.; Wang, X.; Zhu, H.; Wang, Z.; Huang, J., High expression of RAB27A and TP53 in pancreatic cancer predicts poor survival. *Med Oncol* **2014,** *32* (1), 372.

35. Ostenfeld, M. S.; Jeppesen, D. K.; Laurberg, J. R.; Boysen, A. T.; Bramsen, J. B.; Primdal-Bengtson, B.; Hendrix, A.; Lamy, P.; Dagnaes-Hansen, F.; Rasmussen, M. H.; Bui, K. H.; Fristrup, N.; Christensen, E. I.; Nordentoft, I.; Morth, J. P.; Jensen, J. B.; Pedersen, J. S.; Beck, M.; Theodorescu, D.; Borre, M.; Howard, K. A.; Dyrskjøt, L.; Ørntoft, T. F., Cellular Disposal of miR23b by RAB27-Dependent Exosome Release Is Linked to Acquisition of Metastatic Properties. *Cancer Res* **2014,** *74* (20), 5758-5771.

36. Wang, H.; Zhao, Y.; Zhang, C.; Li, M.; Jiang, C.; Li, Y., Rab27a Was Identified as a Prognostic Biomarker by mRNA Profiling, Correlated with Malignant Progression and Subtype Preference in Gliomas. *PLOS ONE* **2014,** *9* (2), e89782.

37. Li, W.; Mu, D.; Tian, F.; Hu, Y.; Jiang, T.; Han, Y.; Chen, J.; Han, G.; Li, X., Exosomes derived from Rab27a-overexpressing tumor cells elicit efficient induction of antitumor immunity. *Mol Med Rep* **2013,** *8* (6), 1876-1882.

38. Wu, X.; Hu, A.; Zhang, M.; Chen, Z., Effects of Rab27a on proliferation, invasion, and anti-apoptosis in human glioma cell. *Tumor Biol* **2013,** *34* (4), 2195-2203.

39. Peinado, H.; Aleckovic, M.; Lavotshkin, S.; Matei, I.; Costa-Silva, B.; Moreno-Bueno, G.; Hergueta-Redondo, M.; Williams, C.; Garcia-Santos, G.; Ghajar, C. M.; Nitadori-Hoshino, A.; Hoffman, C.; Badal, K.; Garcia, B. A.; Callahan, M. K.; Yuan, J.; Martins, V. R.; Skog, J.; Kaplan, R. N.; Brady, M. S.; Wolchok, J. D.; Chapman, P. B.; Kang, Y.; Bromberg, J.; Lyden, D., Melanoma

exosomes educate bone marrow progenitor cells toward a pro-metastatic phenotype through MET. *Nat Med* **2012,** *18* (6), 883-891.

40. Akavia, U. D.; Litvin, O.; Kim, J.; Sanchez-Garcia, F.; Kotliar, D.; Causton, H. C.; Pochanard, P.; Mozes, E.; Garraway, L. A.; Pe'er, D., An Integrated Approach to Uncover Drivers of Cancer. *Cell* **2010,** *143* (6), 1005-1017.

41. Wang, J.-S.; Wang, F.-B.; Zhang, Q.-G.; Shen, Z.-Z.; Shao, Z.-M., Enhanced Expression of Rab27A Gene by Breast Cancer Cells Promoting Invasiveness and the Metastasis Potential by Secretion of Insulin-Like Growth Factor-II. *Mol Cancer Res* **2008,** *6* (3), 372-382.

42. Montel, V.; Huang, T.-Y.; Mose, E.; Pestonjamasp, K.; Tarin, D., Expression Profiling of Primary Tumors and Matched Lymphatic and Lung Metastases in a Xenogeneic Breast Cancer Model. *Am J Pathol* **2005,** *166* (5), 1565-1579.

43. Recchi, C.; Seabra, Miguel C., Novel functions for Rab GTPases in multiple aspects of tumour progression. *Biochem Soc T* **2012,** *40* (6), 1398-1403.

44. Dong, W.; Cui, J.-T.; Yang, J.; Li, W.-M.; Lu, Y.-Y.; Xiao, W., Decreased expression of Rab27A and Rab27B correlates with metastasis and poor prognosis in colorectal cancer. *Discov Med* **2015,** *20* (112), 357-367.

45. Worst, T. S.; Meyer, Y.; Gottschalt, M.; Weis, C.-A.; Von Hardenberg, J.; Frank, C.; Steidler, A.; Michel, M. S.; Erben, P., RAB27A, RAB27B and VPS36 are downregulated in advanced prostate cancer and show functional relevance in prostate cancer cells. *Int J Oncol* **2017,** *50* (3), 920-932.

46. Chang, C.; Liu, T.; Huang, Y.; Qin, W.; Yang, H.; Chen, J., MicroRNA-134-3p is a novel potential inhibitor of human ovarian cancer stem cells by targeting RAB27A. *Gene* **2017,** *605*, 99-107.

47. Li, Y.; Chen, S.; Shan, Z.; Bi, L.; Yu, S.; Li, Y.; Xu, S., miR-182-5p improves the viability, mitosis, migration, and invasion ability of human gastric cancer cells by down-regulating RAB27A. *Bioscience Rep* **2017,** *37* (3).

48. Tang, L.; Wei, D.; Yan, F., MicroRNA-145 functions as a tumor suppressor by targeting matrix metalloproteinase 11 and Rab GTPase family 27a in triple-negative breast cancer. *Cancer Gene Ther* **2016,** *23* (8), 258-265.

49. Zhang, X.; Zhang, Y.; Yang, J.; Li, S.; Chen, J., Upregulation of miR-582-5p inhibits cell proliferation, cell cycle progression and invasion by targeting Rab27a in human colorectal carcinoma. *Cancer Gene Ther* **2015,** *22* (10), 475-480.

50. Fukuda, M., Rab27 Effectors, Pleiotropic Regulators in Secretory Pathways. *Traffic* **2013,** *14* (9), 949-963.

51. Li, W.; Hu, Y.; Jiang, T.; Han, Y.; Han, G.; Chen, J.; Li, X., Rab27A regulates exosome secretion from lung adenocarcinoma cells A549: involvement of EPI64. *APMIS* **2014,** *122* (11), 1080-1087.

52. Valencia, A.; Chardin, P.; Wittinghofer, A.; Sander, C., The ras protein family: evolutionary tree and role of conserved amino acids. *Biochemistry* **1991,** *30* (19), 4637-4648.

53. Bourne, H. R.; Sanders, D. A.; McCormick, F., The GTPase superfamily: conserved structure and molecular mechanism. *Nature* **1991,** *349* (6305), 117-127.

54. Shima, F.; Ijiri, Y.; Muraoka, S.; Liao, J.; Ye, M.; Araki, M.; Matsumoto, K.; Yamamoto, N.; Sugimoto, T.; Yoshikawa, Y.; Kumasaka, T.; Yamamoto, M.; Tamura, A.; Kataoka, T., Structural Basis for Conformational Dynamics of GTP-bound Ras Protein. *J Biol Chem* **2010,** *285* (29), 22696-22705.

55. Araki, M.; Shima, F.; Yoshikawa, Y.; Muraoka, S.; Ijiri, Y.; Nagahara, Y.; Shirono, T.; Kataoka, T.; Tamura, A., Solution Structure of the State 1 Conformer of GTP-bound H-Ras Protein and Distinct Dynamic Properties between the State 1 and State 2 Conformers. *J Biol Chem* **2011,** *286* (45), 39644-39653.

56. Kobayashi, C.; Saito, S., Relation between the Conformational Heterogeneity and Reaction Cycle of Ras: Molecular Simulation of Ras. *Biophys J* **2010,** *99* (11), 3726-3734.

57. Geyer, M.; Schweins, T.; Herrmann, C.; Prisner, T.; Wittinghofer, A.; Kalbitzer, H. R., Conformational Transitions in p21ras and in Its Complexes with the Effector Protein Raf-RBD and the GTPase Activating Protein GAP. *Biochemistry* **1996,** *35* (32), 10308-10320.

58. Rajalingam, K.; Schreck, R.; Rapp, U. R.; Albert, Š., Ras oncogenes and their downstream targets. *Biochim Biophys Acta* **2007,** *1773* (8), 1177-1195.

59. Vigil, D.; Cherfils, J.; Rossman, K. L.; Der, C. J., Ras superfamily GEFs and GAPs: validated and tractable targets for cancer therapy? *Nat Rev Cancer* **2010,** *10* (12), 842-857.

60. Hill, B. T.; Perrin, D.; Kruczynski, A., Inhibition of RAS-targeted prenylation: protein farnesyl transferase inhibitors revisited. *Crit Rev Oncol Hematol* **2000,** *33* (1), 7-23.

61. Lazer, G.; Katzav, S., Guanine nucleotide exchange factors for RhoGTPases: Good therapeutic targets for cancer therapy? *Cellular Signalling* **2011,** *23* (6), 969-979.

62. Visscher, M.; Arkin, M. R.; Dansen, T. B., Covalent targeting of acquired cysteines in cancer. *Curr Opin Chem Biol* **2016,** *30*, 61-67.

63. Lim, S. M.; Westover, K. D.; Ficarro, S. B.; Harrison, R. A.; Choi, H. G.; Pacold, M. E.; Carrasco, M.; Hunter, J.; Kim, N. D.; Xie, T.; Sim, T.; Jänne, P. A.; Meyerson, M.; Marto, J. A.; Engen, J. R.; Gray, N. S., Therapeutic Targeting of Oncogenic K-Ras by a Covalent Catalytic Site Inhibitor. *Angew Chem Int Edit* **2014,** *53* (1), 199-204.

64. Hunter, J. C.; Gurbani, D.; Ficarro, S. B.; Carrasco, M. A.; Lim, S. M.; Choi, H. G.; Xie, T.; Marto, J. A.; Chen, Z.; Gray, N. S.; Westover, K. D., In situ selectivity profiling and crystal structure of SML-8-73-1, an active site inhibitor of oncogenic K-Ras G12C. *Proc Natl Acad Sci U S A* **2014,** *111* (24), 8895-8900.

65. Wiegandt, D.; Vieweg, S.; Hofmann, F.; Koch, D.; Li, F.; Wu, Y.-W.; Itzen, A.; Muller, M. P.; Goody, R. S., Locking GTPases covalently in their functional states. *Nat Commun* **2015,** *6*.

66. Ekins, S.; Mestres, J.; Testa, B., In silico pharmacology for drug discovery: methods for virtual ligand screening and profiling. *Brit J Pharmacol* **2007,** *152* (1), 9-20.

67. Gao, Y.; Dickerson, J. B.; Guo, F.; Zheng, J.; Zheng, Y., Rational design and characterization of a Rac GTPase-specific small molecule inhibitor. *Proc Natl Acad Sci U S A* **2004,** *101* (20), 7618-7623.

68. Akbar, H.; Cancelas, J.; Williams, D. A.; Zheng, J.; Zheng, Y., Rational Design and Applications of a Rac GTPase–Specific Small Molecule Inhibitor. *Methods in Enzymology* **2006,** *406*, 554-565.

69. Nassar, N.; Cancelas, J.; Zheng, J.; Williams, D. A.; Zheng, Y., Structure-Function Based Design of Small Molecule Inhibitors Targeting Rho Family GTPases. *Curr Top Med Chem* **2006,** *6* (11), 1109-1116.

70. Montalvo-Ortiz, B. L.; Castillo-Pichardo, L.; Hernández, E.; Humphries-Bickley, T.; De La Mota-Peynado, A.; Cubano, L. A.; Vlaar, C. P.; Dharmawardhane, S., Characterization of EHop-016, Novel Small Molecule Inhibitor of Rac GTPase. *J Biol Chem* **2012,** *287* (16), 13228-13238.

71. Shang, X.; Marchioni, F.; Sipes, N.; Evelyn, Chris R.; Jerabek-Willemsen, M.; Duhr, S.; Seibel, W.; Wortman, M.; Zheng, Y., Rational Design of Small Molecule Inhibitors Targeting RhoA Subfamily Rho GTPases. *Chem Biol* **2012,** *19* (6), 699-710.

72. Shima, F.; Yoshikawa, Y.; Ye, M.; Araki, M.; Matsumoto, S.; Liao, J.; Hu, L.; Sugimoto, T.; Ijiri, Y.; Takeda, A.; Nishiyama, Y.; Sato, C.; Muraoka, S.; Tamura, A.; Osoda, T.; Tsuda, K.-i.; Miyakawa, T.; Fukunishi, H.; Shimada, J.; Kumasaka, T.; Yamamoto, M.; Kataoka, T., In silico discovery of small-molecule Ras inhibitors that display antitumor activity by blocking the Ras–effector interaction. *Proc Natl Acad Sci U S A* **2013,** *110* (20), 8182-8187.

73. Murray, C. W.; Rees, D. C., The rise of fragment-based drug discovery. *Nat Chem* **2009,** *1* (3), 187-192.

74. Rees, D. C.; Congreve, M.; Murray, C. W.; Carr, R., Fragment-based lead discovery. *Nat Rev Drug Discov* **2004,** *3* (8), 660-672.

75. Scott, D. E.; Coyne, A. G.; Hudson, S. A.; Abell, C., Fragment-Based Approaches in Drug Discovery and Chemical Biology. *Biochemistry* **2012,** *51* (25), 4990-5003.

76. Abdelraheem, E. M. M.; Camacho, C. J.; Dömling, A., Focusing on shared subpockets – new developments in fragment-based drug discovery. *Expert Opin Drug Dis* **2015**, 1-9.

77. Davis, B. J.; Erlanson, D. A., Learning from our mistakes: The 'unknown knowns' in fragment screening. *Bioorg Med Chem Lett* **2013,** *23* (10), 2844-2852.

78. Erlanson, D. A.; McDowell, R. S.; O'Brien, T., Fragment-Based Drug Discovery. *J Med Chem* **2004,** *47* (14), 3463-3482.

79. Hajduk, P. J.; Greer, J., A decade of fragment-based drug design: strategic advances and lessons learned. *Nat Rev Drug Discov* **2007,** *6* (3), 211-219.

80. Erlanson, D. A.; Fesik, S. W.; Hubbard, R. E.; Jahnke, W.; Jhoti, H., Twenty years on: the impact of fragments on drug discovery. *Nat Rev Drug Discov* **2016,** *15* (9), 605-619.

81. Sun, Q.; Burke, J. P.; Phan, J.; Burns, M. C.; Olejniczak, E. T.; Waterson, A. G.; Lee, T.; Rossanese, O. W.; Fesik, S. W., Discovery of Small Molecules that Bind to K-Ras and Inhibit Sos-Mediated Activation. *Angew Chem Int Edit* **2012,** *51* (25), 6140-6143.

82. Maurer, T.; Garrenton, L. S.; Oh, A.; Pitts, K.; Anderson, D. J.; Skelton, N. J.; Fauber, B. P.; Pan, B.; Malek, S.; Stokoe, D.; Ludlam, M. J. C.; Bowman, K. K.; Wu, J.; Giannetti, A. M.; Starovasnik, M. A.; Mellman, I.; Jackson, P. K.; Rudolph, J.; Wang, W.; Fang, G., Small-molecule ligands bind to a distinct pocket in Ras and inhibit SOS-mediated nucleotide exchange activity. *Proc Natl Acad Sci U S A* **2012,** *109* (14), 5299-5304.

83. Gao, J.; Ma, R.; Wang, W.; Wang, N.; Sasaki, R.; Snyderman, D.; Wu, J.; Ruan, K., Automated NMR Fragment Based Screening Identified a Novel Interface Blocker to the LARG/RhoA Complex. *PLOS ONE* **2014,** *9* (2), e88098.

84. Winter, J. J. G.; Anderson, M.; Blades, K.; Brassington, C.; Breeze, A. L.; Chresta, C.; Embrey, K.; Fairley, G.; Faulder, P.; Finlay, M. R. V.; Kettle, J. G.; Nowak, T.; Overman, R.; Patel, S. J.; Perkins, P.; Spadola, L.; Tart, J.; Tucker, J. A.; Wrigley, G., Small Molecule Binding Sites on the Ras:SOS Complex Can Be Exploited for Inhibition of Ras Activation. *J Med Chem* **2015,** *58* (5), 2265-2274.

85. Singh, J.; Petter, R. C.; Baillie, T. A.; Whitty, A., The resurgence of covalent drugs. *Nat Rev Drug Discov* **2011,** *10* (4), 307-317.

86. Johnson, D. S.; Weerapana, E.; Cravatt, B. F., Strategies for discovering and derisking covalent, irreversible enzyme inhibitors. *Future Med Chem* **2010,** *2* (6), 949-964.

87. Nussinov, R.; Tsai, C.-J., The Design of Covalent Allosteric Drugs. *Annu Rev Pharmacol Toxicol* **2015,** *55* (1), 249-267.

88. Kumalo, H.; Bhakat, S.; Soliman, M., Theory and Applications of Covalent Docking in Drug Discovery: Merits and Pitfalls. *Molecules* **2015,** *20* (2), 1984.

89. Mah, R.; Thomas, J. R.; Shafer, C. M., Drug discovery considerations in the development of covalent inhibitors. *Bioorg Med Chem Lett* **2014,** *24* (1), 33-39.

90. Ostrem, J. M.; Peters, U.; Sos, M. L.; Wells, J. A.; Shokat, K. M., K-Ras(G12C) inhibitors allosterically control GTP affinity and effector interactions. *Nature* **2013,** *503* (7477), 548-551.

91. Hashimoto, C.; Eichler, J., Turning peptide ligands into small-molecule inhibitors of protein-protein interactions. *ChemBioChem* **2015**, n/a-n/a.

92. Azzarito, V.; Long, K.; Murphy, N. S.; Wilson, A. J., Inhibition of α-helix-mediated protein-protein interactions using designed molecules. *Nat Chem* **2013,** *5* (3), 161-173.

93. Watkins, A. M.; Arora, P. S., Structure-based inhibition of protein–protein interactions. *Eur J Med Chem* **2015,** *94*, 480-488.

94. Chapman, R. N.; Dimartino, G.; Arora, P. S., A Highly Stable Short α-Helix Constrained by a Main-Chain Hydrogen-Bond Surrogate. *J Am Chem Soc* **2004,** *126* (39), 12252-12253.

95. Douse, C. H.; Maas, S. J.; Thomas, J. C.; Garnett, J. A.; Sun, Y.; Cota, E.; Tate, E. W., Crystal Structures of Stapled and Hydrogen Bond Surrogate Peptides Targeting a Fully Buried Protein–Helix Interaction. *ACS Chem Biol* **2014,** *9* (10), 2204-2209.

96. Joy, S. T.; Arora, P. S., An optimal hydrogen-bond surrogate for [small alpha]-helices. *Chem Commun* **2016,** *52* (33), 5738-5741.

97. Patgiri, A.; Jochim, A. L.; Arora, P. S., A Hydrogen Bond Surrogate Approach for Stabilization of Short Peptide Sequences in α-Helical Conformation. *Accounts Chem Res* **2008,** *41* (10), 1289-1300.

98. Patgiri, A.; Menzenski, M. Z.; Mahon, A. B.; Arora, P. S., Solid-phase synthesis of short [alpha]-helices stabilized by the hydrogen bond surrogate approach. *Nat. Protocols* **2010,** *5* (11), 1857-1865.

99. Cromm, P. M.; Spiegel, J.; Grossmann, T. N., Hydrocarbon Stapled Peptides as Modulators of Biological Function. *ACS Chem Biol* **2015,** *10* (6), 1362-1375.

100. Cromm, P. M.; Spiegel, J.; Küchler, P.; Dietrich, L.; Kriegesmann, J.; Wendt, M.; Goody, R. S.; Waldmann, H.; Grossmann, T. N., Protease-Resistant and Cell-Permeable Double-Stapled Peptides Targeting the Rab8a GTPase. *ACS Chem Biol* **2016,** *11* (8), 2375-2382.

101. Spiegel, J.; Cromm, P. M.; Itzen, A.; Goody, R. S.; Grossmann, T. N.; Waldmann, H., Direct Targeting of Rab-GTPase–Effector Interactions. *Angew Chem Int Edit* **2014,** *53* (9), 2498-2503.

102. Patgiri, A.; Yadav, K. K.; Arora, P. S.; Bar-Sagi, D., An orthosteric inhibitor of the Ras-Sos interaction. *Nat Chem Biol* **2011,** *7* (9), 585-587.

103. Leshchiner, E. S.; Parkhitko, A.; Bird, G. H.; Luccarelli, J.; Bellairs, J. A.; Escudero, S.; Opoku-Nsiah, K.; Godes, M.; Perrimon, N.; Walensky, L. D., Direct inhibition of oncogenic KRAS by hydrocarbon-stapled SOS1 helices. *Proc Natl Acad Sci U S A* **2015,** *112* (6), 1761-1766.

104. Kim, B.; Lee, J.-Y.; Lee, H.-Y.; Nam, K.-Y.; Park, J.; Lee, S. M.; Kim, J. E.; Lee, J. D.; Hwang, J. S., Hesperidin Suppresses Melanosome Transport by Blocking the Interaction of Rab27A-Melanophilin. *Biomol Ther* **2013,** *21* (5), 343-348.

105. Joung, J. Y.; Lee, H. Y.; Park, J.; Lee, J.-Y.; Chang, B. H.; No, K. T.; Nam, K.-Y.; Hwang, J. S., Identification of Novel Rab27a/Melanophilin Blockers by Pharmacophore-Based Virtual Screening. *Appl Biochem Biotech* **2014,** *172* (4), 1882-1897.

106. Kang, S.-M.; Nam, K.-Y.; Jung, S.-Y.; Song, K.-H.; Kho, S.; No, K. T.; Choi, H. K.; Song, J.-Y., Inhibition of cancer cell invasion by new ((3,4-dihydroxy benzylidene)hydrazinyl)pyridine-3-sulfonamide analogs. *Bioorg Med Chem Lett* **2016,** *26* (4), 1322-1328.

107. Park, J. i.; Lee, H. Y.; Lee, J. E.; Myung, C. h.; Hwang, J. S., Inhibitory effect of 2-methyl-naphtho[1,2,3-de]quinolin-8-one on melanosome transport and skin pigmentation. *Sci Rep* **2016,** *6*, 29189.

108. Johnson, J. L.; Ramadass, M.; He, J.; Brown, S. J.; Zhang, J.; Abgaryan, L.; Biris, N.; Gavathiotis, E.; Rosen, H.; Catz, S. D., Identification of Nexinhibs, small-molecule inhibitors of neutrophil exocytosis and inflammation - druggability of the small GTPase Rab27a. *J Biol Chem* **2016**.

109. Urs, A. B.; Han Kiat, H.; Shufeng, Z.; Koon Yeow, L., Bioactivation and Hepatotoxicity of Nitroaromatic Drugs. *Curr Drug Metab* **2006,** *7* (7), 715-727.

110. Barral, D. C.; Ramalho, J.; xE; S; Anders, R.; Hume, A. N.; Knapton, H. J.; Tolmachova, T.; Collinson, L. M.; Goulding, D.; Authi, K. S.; Seabra, M. C., Functional redundancy of Rab27 proteins and the pathogenesis of Griscelli syndrome. *J Clin Invest* **2002,** *110* (2), 247-257.

111. Fukuda, M., Versatile Role of Rab27 in Membrane Trafficking: Focus on the Rab27 Effector Families. *J Biochem* **2005,** *137* (1), 9-16.

112. Fukuda, M., Distinct Rab27A binding affinities of Slp2-a and Slac2-a/melanophilin: Hierarchy of Rab27A effectors. *Biochem Biophys Res Commun* **2006,** *343* (2), 666-674.

113. Fukuda, M., *Rab27 and its effectors in secretory granule exocytosis: a novel docking machinery composed of a Rab27·effector complex*. 2006; Vol. 34, p 691-695.

114. Kuroda, T. S.; Fukuda, M.; Ariga, H.; Mikoshiba, K., The Slp homology domain of synaptotagmin-like proteins 1–4 and Slac2 functions as a novel Rab27A binding domain. *J Biol Chem* **2002,** *277* (11), 9212-9218.

115. Booth, A. E. G.; Tarafder, A. K.; Hume, A. N.; Recchi, C.; Seabra, M. C., A Role for Na+,K+-ATPase α1 in Regulating Rab27a Localisation on Melanosomes. *PLOS ONE* **2014,** *9* (7), e102851.

116. Kimura, T.; Yamaoka, M.; Taniguchi, S.; Okamoto, M.; Takei, M.; Ando, T.; Iwamatsu, A.; Watanabe, T.; Kaibuchi, K.; Ishizaki, T.; Niki, I., Activated Cdc42-Bound IQGAP1 Determines the Cellular Endocytic Site. *Mol Cell Biol* **2013,** *33* (24), 4834-4843.

117. Kimura, T.; Kaneko, Y.; Yamada, S.; Ishihara, H.; Senda, T.; Iwamatsu, A.; Niki, I., The GDP-dependent Rab27a effector coronin 3 controls endocytosis of secretory membrane in insulin-secreting cell lines. *J Cell Sci* **2008,** *121* (18), 3092.

118. Brzezinska, A. A.; Johnson, J. L.; Munafo, D. B.; Crozat, K.; Beutler, B.; Kiosses, W. B.; Ellis, B. A.; Catz, S. D., The Rab27a Effectors JFC1/Slp1 and Munc13-4 Regulate Exocytosis of Neutrophil Granules. *Traffic* **2008,** *9* (12), 2151-2164.

119. Johnson, Jennifer L.; Ellis, Beverly A.; Noack, D.; Seabra, Miguel C.; Catz, Sergio D., The Rab27a-binding protein, JFC1, regulates androgen-dependent secretion of prostate-specific antigen and prostatic-specific acid phosphatase. *Biochem J* **2005,** *391* (3), 699-710.

120. Wang, H.; Ishizaki, R.; Xu, J.; Kasai, K.; Kobayashi, E.; Gomi, H.; Izumi, T., The Rab27a effector exophilin7 promotes fusion of secretory granules that have not been docked to the plasma membrane. *Mol Biol Cell* **2013,** *24* (3), 319-330.

121. Chavas, L. M. G.; Ihara, K.; Kawasaki, M.; Torii, S.; Uejima, T.; Kato, R.; Izumi, T.; Wakatsuki, S., Elucidation of Rab27 Recruitment by Its Effectors: Structure of Rab27a Bound to Exophilin4/Slp2-a. *Structure* **2008,** *16* (10), 1468-1477.

122. Kurowska, M.; Goudin, N.; Nehme, N. T.; Garin, J.; Fischer, A.; de Saint Basile, G.; Ménasché, G., Terminal transport of lytic granules to the immune synapse is mediated by the kinesin-1/Slp3/Rab27a complex. *Blood* **2012,** *119* (17), 3879-3889.

123. Fukuda, M., The C2A domain of synaptotagmin-like protein 3 (Slp3) is an atypical calcium-dependent phospholipid-binding machine: comparison with the C2A domain of synaptotagmin I. *Biochem J* **2002,** *366* (2), 681-687.

124. Fukuda, M., Slp4-a/Granuphilin-a Inhibits Dense-core Vesicle Exocytosis through Interaction with the GDP-bound Form of Rab27A in PC12 Cells. *J Biol Chem* **2003,** *278* (17), 15390-15396.

125. van Breevoort, D.; Snijders, A. P.; Hellen, N.; Weckhuysen, S.; van Hooren, K. W. E. M.; Eikenboom, J.; Valentijn, K.; Fernandez-Borja, M.; Ceulemans, B.; De Jonghe, P.; Voorberg, J.; Hannah, M.; Carter, T.; Bierings, R., STXBP1 promotes Weibel-Palade body exocytosis through its interaction with the Rab27A effector Slp4-a. *Blood* **2014,** *123* (20), 3185-3194.

126. Bierings, R.; Hellen, N.; Kiskin, N.; Knipe, L.; Fonseca, A.-V.; Patel, B.; Meli, A.; Rose, M.; Hannah, M. J.; Carter, T., The interplay between the Rab27A effectors Slp4-a and MyRIP controls hormone-evoked Weibel-Palade body exocytosis. *Blood* **2012,** *120* (13), 2757-2767.

127. Kuroda, T. S.; Fukuda, M.; Ariga, H.; Mikoshiba, K., Synaptotagmin-like protein 5: a novel Rab27A effector with C-terminal tandem C2 domains. *Biochemical and biophysical research communications* **2002,** *293* (3), 899-906.

128. Saxena, S. K.; Horiuchi, H.; Fukuda, M., Rab27a regulates epithelial sodium channel (ENaC) activity through synaptotagmin-like protein (SLP-5) and Munc13-4 effector mechanism. *Biochemical and biophysical research communications* **2006,** *344* (2), 651-657.

129. Fukuda, M., Distinct Rab Binding Specificity of Rim1, Rim2, Rabphilin, and Noc2: Identification of a Critical Determinant of Rab3A/Rab27A Recognition by Rim2. *J Biol Chem* **2003,** *278* (17), 15373-15380.

130. Fukuda, M.; Kanno, E.; Yamamoto, A., Rabphilin and Noc2 Are Recruited to Dense-core Vesicles through Specific Interaction with Rab27A in PC12 Cells. *J Biol Chem* **2004,** *279* (13), 13065-13075.

131. Handley, M. T.; Burgoyne, R. D., The Rab27 effector Rabphilin, unlike Granuphilin and Noc2, rapidly exchanges between secretory granules and cytosol in PC12 cells. *Biochemical and biophysical research communications* **2008,** *373* (2), 275-281.

132. Strom, M.; Hume, A. N.; Tarafder, A. K.; Barkagianni, E.; Seabra, M. C., A Family of Rab27-binding Proteins: Melanophilin Link Rab27a and Myosin Va Function in Melanosome Transport. *J Biol Chem* **2002,** *277* (28), 25423-25430.

133. Fukuda, M., Synaptotagmin-like Protein (Slp) Homology Domain 1 of Slac2-a/Melanophilin Is a Critical Determinant of GTP-dependent Specific Binding to Rab27A. *J Biol Chem* **2002,** *277* (42), 40118-40124.

134. Fukuda, M.; Kuroda, T. S., Slac2-c (Synaptotagmin-like Protein HomologueLacking C2 Domains-c), a Novel Linker Protein that Interacts with Rab27, Myosin Va/VIIa, and Actin. *J Biol Chem* **2002,** *277* (45), 43096-43103.

135. Imai, A.; Yoshie, S.; Nashida, T.; Shimomura, H.; Fukuda, M., Functional involvement of Noc2, a Rab27 effector, in rat parotid acinar cells. *Arch Biochem Biophys* **2006,** *455* (2), 127-135.

136. Elstak, E. D.; Neeft, M.; Nehme, N. T.; Voortman, J.; Cheung, M.; Goodarzifard, M.; Gerritsen, H. C.; van Bergen en Henegouwen, P. M. P.; Callebaut, I.; de Saint Basile, G.; van der Sluijs, P., The munc13-4–rab27 complex is specifically required for tethering secretory lysosomes at the plasma membrane. *Blood* **2011,** *118* (6), 1570-1578.

137. Neeft, M.; Wieffer, M.; de Jong, A. S.; Negroiu, G.; Metz, C. H. G.; van Loon, A.; Griffith, J.; Krijgsveld, J.; Wulffraat, N.; Koch, H.; Heck, A. J. R.; Brose, N.; Kleijmeer, M.; van der Sluijs, P., Munc13-4 Is an Effector of Rab27a and Controls Secretion of Lysosomes in Hematopoietic Cells. *Mol Biol Cell* **2005,** *16* (2), 731-741.

138. Shirakawa, R.; Higashi, T.; Tabuchi, A.; Yoshioka, A.; Nishioka, H.; Fukuda, M.; Kita, T.; Horiuchi, H., Munc13-4 Is a GTP-Rab27-binding Protein Regulating Dense Core Granule Secretion in Platelets. *J Biol Chem* **2004,** *279* (11), 10730-10737.

139. Bos, J. L.; Rehmann, H.; Wittinghofer, A., GEFs and GAPs: Critical Elements in the Control of Small G Proteins. *Cell* **2007,** *129* (5), 865-877.

140. Barr, F.; Lambright, D. G., Rab GEFs and GAPs. *Curr Opin Cell Biol* **2010,** *22* (4), 461-470.

141. Cherfils, J.; Zeghouf, M., Regulation of Small GTPases by GEFs, GAPs, and GDIs. *Physiol Rev* **2013,** *93* (1), 269-309.

142. Itoh, T.; Fukuda, M., Identification of EPI64 as a GTPase-activating Protein Specific for Rab27A. *J Biol Chem* **2006,** *281* (42), 31823-31831.

143. Yamaoka, M.; Ishizaki, T.; Kimura, T., GTP- and GDP-Dependent Rab27a Effectors in Pancreatic Beta-Cells. *Biol Pharm Bull* **2015,** *38* (5), 663-668.

144. Imai, A.; Yoshie, S.; Ishibashi, K.; Haga-Tsujimura, M.; Nashida, T.; Shimomura, H.; Fukuda, M., EPI64 Protein Functions as a Physiological GTPase-activating Protein for Rab27 Protein and Regulates Amylase Release in Rat Parotid Acinar Cells. *J Biol Chem* **2011,** *286* (39), 33854-33862.

145. Ishibashi, K.; Kanno, E.; Itoh, T.; Fukuda, M., Identification and characterization of a novel Tre-2/Bub2/Cdc16 (TBC) protein that possesses Rab3A-GAP activity. *Genes to Cells* **2009,** *14* (1), 41-52.

146. Figueiredo, A. C.; Wasmeier, C.; Tarafder, A. K.; Ramalho, J. S.; Baron, R. A.; Seabra, M. C., Rab3GEP Is the Non-redundant Guanine Nucleotide Exchange Factor for Rab27a in Melanocytes. *J Biol Chem* **2008,** *283* (34), 23209-23216.

147. Lee, Y.; Lee, E. K.; Cho, Y. W.; Matsui, T.; Kang, I. C.; Kim, T. S.; Han, M. H., ProteoChip: A highly sensitive protein microarray prepared by a novel method of protein immobilization for application of protein-protein interaction studies. *Proteomics* **2003,** *3* (12), 2289-2304.

148. Keilhauer, E. C.; Hein, M. Y.; Mann, M., Accurate Protein Complex Retrieval by Affinity Enrichment Mass Spectrometry (AE-MS) Rather than Affinity Purification Mass Spectrometry (AP-MS). *Mol Cell Proteomics* **2015,** *14* (1), 120-135.

149. Berggård, T.; Linse, S.; James, P., Methods for the detection and analysis of protein–protein interactions. *Proteomics* **2007,** *7* (16), 2833-2842.

150. Zuiderweg, E. R. P., Mapping Protein−Protein Interactions in Solution by NMR Spectroscopy. *Biochemistry* **2002,** *41* (1), 1-7.

151. Rao, V. S.; Srinivas, K.; Sujini, G. N.; Kumar, G. N. S., Protein-Protein Interaction Detection: Methods and Analysis. *Int J Proteomics* **2014,** *2014*, 12.

152. Zhou, M.; Li, Q.; Wang, R., Current Experimental Methods for Characterizing Protein–Protein Interactions. *ChemMedChem* **2016,** *11* (8), 738-756.

153. Feng, S.; Zhou, L.; Huang, C.; Xie, K.; Nice, E. C., Interactomics: toward protein function and regulation. *Expert Rev Proteomics* **2015,** *12* (1), 37-60.

154. Luck, K.; Sheynkman, G. M.; Zhang, I.; Vidal, M., Proteome-Scale Human Interactomics. *Trends Biochem Sci* **2017,** *42* (5), 342-354.

155. Kuroda, K.; Kato, M.; Mima, J.; Ueda, M., Systems for the detection and analysis of protein–protein interactions. *Appl Microbiol Biot* **2006,** *71* (2), 127-136.

156. Phizicky, E. M.; Fields, S., Protein-protein interactions: methods for detection and analysis. *Microbiol Rev* **1995,** *59* (1), 94-123.

157. Ngounou Wetie, A. G.; Sokolowska, I.; Woods, A. G.; Roy, U.; Deinhardt, K.; Darie, C. C., Protein–protein interactions: switch from classical methods to proteomics and bioinformatics-based approaches. *Cell Mol Life Sci* **2014,** *71* (2), 205-228.

158. Turriziani, B.; von Kriegsheim, A.; Pennington, S. R., Protein-Protein Interaction Detection Via Mass Spectrometry-Based Proteomics. In *Modern Proteomics – Sample Preparation, Analysis and Practical Applications*, Mirzaei, H.; Carrasco, M., Eds. Springer International Publishing: Cham, 2016; pp 383-396.

159. Smits, A. H.; Vermeulen, M., Characterizing Protein–Protein Interactions Using Mass Spectrometry: Challenges and Opportunities. *Trends Biotechnol* **2016,** *34* (10), 825-834.

160. Aebersold, R.; Mann, M., Mass spectrometry-based proteomics. *Nature* **2003,** *422* (6928), 198-207.

161. Aebersold, R.; Mann, M., Mass-spectrometric exploration of proteome structure and function. *Nature* **2016,** *537* (7620), 347-355.

162. Mallick, P.; Kuster, B., Proteomics: a pragmatic perspective. *Nat Biotech* **2010,** *28* (7), 695-709.

163. Bogdanov, B.; Smith, R. D., Proteomics by FTICR mass spectrometry: Top down and bottom up. *Mass Spectrom Rev* **2005,** *24* (2), 168-200.

164. Cox, J.; Hubner, N. C.; Mann, M., How Much Peptide Sequence Information Is Contained in Ion Trap Tandem Mass Spectra? *J Am Soc Mass Spectr* **2008,** *19* (12), 1813-1820.

165. Bateman, N. W.; Goulding, S. P.; Shulman, N. J.; Gadok, A. K.; Szumlinski, K. K.; MacCoss, M. J.; Wu, C. C., Maximizing Peptide Identification Events in Proteomic Workflows Using Data-Dependent Acquisition (DDA). *Mol Cell Proteomics* **2014,** *13* (1), 329-338.

166. Doerr, A., Targeted proteomics. *Nat Meth* **2011,** *8* (1), 43-43.

167. Gillet, L. C.; Navarro, P.; Tate, S.; Röst, H.; Selevsek, N.; Reiter, L.; Bonner, R.; Aebersold, R., Targeted Data Extraction of the MS/MS Spectra Generated by Data-independent Acquisition: A New Concept for Consistent and Accurate Proteome Analysis. *Mol Cell Proteomics* **2012,** *11* (6).

168. Marx, V., Targeted proteomics. *Nat Meth* **2013,** *10* (1), 19-22.

169. Picotti, P.; Aebersold, R., Selected reaction monitoring-based proteomics: workflows, potential, pitfalls and future directions. *Nat Meth* **2012,** *9* (6), 555-566.

170. Doerr, A., DIA mass spectrometry. *Nat Meth* **2015,** *12* (1), 35-35.

171. Hu, A.; Noble, W.; Wolf-Yadlin, A., *Technical advances in proteomics: new developments in data-independent acquisition*. 2016; Vol. 5.

172. Huang, Q.; Yang, L.; Luo, J.; Guo, L.; Wang, Z.; Yang, X.; Jin, W.; Fang, Y.; Ye, J.; Shan, B.; Zhang, Y., SWATH enables precise label-free quantification on proteome scale. *Proteomics* **2015,** *15* (7), 1215-1223.

173. Simbürger, J. M. B.; Dettmer, K.; Oefner, P. J.; Reinders, J., Optimizing the SWATH-MS-workflow for label-free proteomics. *J Proteomics* **2016,** *145*, 137-140.

174. Ong, S.-E.; Mann, M., Mass spectrometry-based proteomics turns quantitative. *Nat Chem Biol* **2005,** *1* (5), 252-262.

175. Mostovenko, E.; Hassan, C.; Rattke, J.; Deelder, A. M.; van Veelen, P. A.; Palmblad, M., Comparison of peptide and protein fractionation methods in proteomics. *EuPA Open Proteomics* **2013,** *1*, 30-37.

176. Ly, L.; Wasinger, V. C., Protein and peptide fractionation, enrichment and depletion: tools for the complex proteome. *Proteomics* **2011,** *11* (4), 513-534.

177. Manadas, B.; Mendes, V. M.; English, J.; Dunn, M. J., Peptide fractionation in proteomics approaches. *Expert Rev Proteomics* **2010,** *7* (5), 655-663.

178. Zhao, X.; Li, G.; Liang, S., Several Affinity Tags Commonly Used in Chromatographic Purification. *J Anal Methods Chem* **2013,** *2013*, 8.

179. Kool, J.; Jonker, N.; Irth, H.; Niessen, W. M. A., Studying protein–protein affinity and immobilized ligand–protein affinity interactions using MS-based methods. *Anal Bioanal Chem* **2011,** *401* (4), 1109.

180. Broncel, M.; Serwa, R. A.; Ciepla, P.; Krause, E.; Dallman, M. J.; Magee, A. I.; Tate, E. W., Myristoylation profiling in human cells and zebrafish. *Data Brief* **2015,** *4*, 379-383.

181. Ciepla, P.; Magee, A. I.; Tate, E. W., Cholesterylation: a tail of hedgehog. *Biochem Soc T* **2015,** *43*, 262-267.

182. Tate, E. W.; Kalesh, K. A.; Lanyon-Hogg, T.; Storck, E. M.; Thinon, E., Global profiling of protein lipidation using chemical proteomic technologies. *Curr Opin Chem Biol* **2015,** *24*, 48-57.

183. Storck, Elisabeth M.; Serwa, Remigiusz A.; Tate, Edward W., Chemical proteomics: a powerful tool for exploring protein lipidation. *Biochem Soc T* **2013,** *41* (1), 56-61.

184. Tate, E. W.; Kalesh, K. A.; Lanyon-Hogg, T.; Storck, E. M.; Thinon, E., Global profiling of protein lipidation using chemical proteomic technologies. *Curr Opin Chem Biol* **2015,** *24* (Supplement C), 48-57.

185. Broncel, M.; Serwa, R. A.; Ciepla, P.; Krause, E.; Dallman, M. J.; Magee, A. I.; Tate, E. W., Multifunctional Reagents for Quantitative Proteome-Wide Analysis of Protein Modification in Human Cells and Dynamic Profiling of Protein Lipidation During Vertebrate Development. *Angew Chem Int Edit* **2015,** *54*, 5948-5951.

186. Zhao, Y.; Jensen, O. N., Modification-specific proteomics: Strategies for characterization of post-translational modifications using enrichment techniques. *Proteomics* **2009,** *9* (20), 4632-4641.

187. Heal, W. P.; Dang, T. H. T.; Tate, E. W., Activity-based probes: discovering new biology and new drug targets. *Chem Soc Rev* **2011,** *40* (1), 246-257.

188. Backus, K. M.; Correia, B. E.; Lum, K. M.; Forli, S.; Horning, B. D.; González-Páez, G. E.; Chatterjee, S.; Lanning, B. R.; Teijaro, J. R.; Olson, A. J.; Wolan, D. W.; Cravatt, B. F., Proteome-wide covalent ligand discovery in native biological systems. *Nature* **2016,** *advance online publication*.

189. Simon, G. M.; Cravatt, B. F., Activity-based Proteomics of Enzyme Superfamilies: Serine Hydrolases as a Case Study. *J Biol Chem* **2010,** *285* (15), 11051-11055.

190. Nomura, D. K.; Dix, M. M.; Cravatt, B. F., Activity-based protein profiling for biochemical pathway discovery in cancer. *Nat Rev Cancer* **2010,** *10* (9), 630-638.

191. Cravatt, B. F.; Wright, A. T.; Kozarich, J. W., Activity-Based Protein Profiling: From Enzyme Chemistry to Proteomic Chemistry. *Annu Rev Biochem* **2008,** *77* (1), 383-414.

192. Chan, E. W. S.; Chattopadhaya, S.; Panicker, R. C.; Huang, X.; Yao, S. Q., Developing Photoactive Affinity Probes for Proteomic Profiling: Hydroxamate-based Probes for Metalloproteases. *J Am Chem Soc* **2004,** *126* (44), 14435-14446.

193. Chahrour, O.; Cobice, D.; Malone, J., Stable isotope labelling methods in mass spectrometry-based quantitative proteomics. *J Pharmaceut Biomed* **2015,** *113*, 2-20.

194. Altelaar, A. F. M.; Frese, C. K.; Preisinger, C.; Hennrich, M. L.; Schram, A. W.; Timmers, H. T. M.; Heck, A. J. R.; Mohammed, S., Benchmarking stable isotope labeling based quantitative proteomics. *J Proteomics* **2013,** *88*, 14-26.

195. Li, Z.; Adams, R. M.; Chourey, K.; Hurst, G. B.; Hettich, R. L.; Pan, C., Systematic Comparison of Label-Free, Metabolic Labeling, and Isobaric Chemical Labeling for Quantitative Proteomics on LTQ Orbitrap Velos. *J Proteome Res* **2012,** *11* (3), 1582-1590.

196. Shiio, Y.; Aebersold, R., Quantitative proteome analysis using isotope-coded affinity tags and mass spectrometry. *Nat. Protocols* **2006,** *1* (1), 139-145.

197. Chen, X.; Wei, S.; Ji, Y.; Guo, X.; Yang, F., Quantitative proteomics using SILAC: Principles, applications, and developments. *Proteomics* **2015,** *15* (18), 3175-3192.

198. Zanivan, S.; Krueger, M.; Mann, M., In Vivo Quantitative Proteomics: The SILAC Mouse. In *Integrin and Cell Adhesion Molecules: Methods and Protocols*, Shimaoka, M., Ed. Humana Press: Totowa, NJ, 2012; pp 435-450.

199. Ong, S.-E.; Mann, M., A practical recipe for stable isotope labeling by amino acids in cell culture (SILAC). *Nat. Protocols* **2007,** *1* (6), 2650-2660.

200. Ong, S.-E.; Blagoev, B.; Kratchmarova, I.; Kristensen, D. B.; Steen, H.; Pandey, A.; Mann, M., Stable Isotope Labeling by Amino Acids in Cell Culture, SILAC, as a Simple and Accurate Approach to Expression Proteomics. *Mol Cell Proteomics* **2002,** *1* (5), 376-386.

201. Boersema, P. J.; Raijmakers, R.; Lemeer, S.; Mohammed, S.; Heck, A. J. R., Multiplex peptide stable isotope dimethyl labeling for quantitative proteomics. *Nat. Protocols* **2009,** *4* (4), 484-494.

202. Gygi, S. P.; Rist, B.; Gerber, S. A.; Turecek, F.; Gelb, M. H.; Aebersold, R., Quantitative analysis of complex protein mixtures using isotope-coded affinity tags. *Nat Biotech* **1999,** *17* (10), 994-999.

203. Evans, C.; Noirel, J.; Ow, S. Y.; Salim, M.; Pereira-Medrano, A. G.; Couto, N.; Pandhal, J.; Smith, D.; Pham, T. K.; Karunakaran, E.; Zou, X.; Biggs, C. A.; Wright, P. C., An insight into iTRAQ: where do we stand now? *Anal Bioanal Chem* **2012,** *404* (4), 1011-1027.

204. Unwin, R. D., Quantification of Proteins by iTRAQ. In *LC-MS/MS in Proteomics: Methods and Applications*, Cutillas, P. R.; Timms, J. F., Eds. Humana Press: Totowa, NJ, 2010; pp 205-215.

205. Wiese, S.; Reidegeld, K. A.; Meyer, H. E.; Warscheid, B., Protein labeling by iTRAQ: A new tool for quantitative mass spectrometry in proteome research. *Proteomics* **2007,** *7* (3), 340-350.

206. Dayon, L.; Sanchez, J.-C., Relative Protein Quantification by MS/MS Using the Tandem Mass Tag Technology. In *Quantitative Methods in Proteomics*, Marcus, K., Ed. Humana Press: Totowa, NJ, 2012; pp 115-127.

207. Thompson, A.; Schäfer, J.; Kuhn, K.; Kienle, S.; Schwarz, J.; Schmidt, G.; Neumann, T.; Hamon, C., Tandem Mass Tags: A Novel Quantification Strategy for Comparative Analysis of Complex Protein Mixtures by MS/MS. *Anal Chem* **2003,** *75* (8), 1895-1904.

208. Cox, J.; Hein, M. Y.; Luber, C. A.; Paron, I.; Nagaraj, N.; Mann, M., Accurate Proteome-wide Label-free Quantification by Delayed Normalization and Maximal Peptide Ratio Extraction, Termed MaxLFQ. *Mol Cell Proteomics* **2014,** *13* (9), 2513-2526.

209. Tate, S.; Larsen, B.; Bonner, R.; Gingras, A.-C., Label-free quantitative proteomics trends for protein–protein interactions. *J Proteomics* **2013,** *81*, 91-101.

210. Bantscheff, M.; Lemeer, S.; Savitski, M. M.; Kuster, B., Quantitative mass spectrometry in proteomics: critical review update from 2007 to the present. *Anal Bioanal Chem* **2012,** *404* (4), 939-965.

211. Neilson, K. A.; Ali, N. A.; Muralidharan, S.; Mirzaei, M.; Mariani, M.; Assadourian, G.; Lee, A.; van Sluyter, S. C.; Haynes, P. A., Less label, more free: Approaches in label-free quantitative mass spectrometry. *Proteomics* **2011,** *11* (4), 535-553.

212. Zhu, W.; Smith, J. W.; Huang, C.-M., Mass Spectrometry-Based Label-Free Quantitative Proteomics. *J Biomed Biotechnol* **2010,** *2010*, 6.

213. Wong, J. W. H.; Cagney, G., An Overview of Label-Free Quantitation Methods in Proteomics by Mass Spectrometry. In *Proteome Bioinformatics*, Hubbard, S. J.; Jones, A. R., Eds. Humana Press: Totowa, NJ, 2010; pp 273-283.

214. Patel, V. J.; Thalassinos, K.; Slade, S. E.; Connolly, J. B.; Crombie, A.; Murrell, J. C.; Scrivens, J. H., A Comparison of Labeling and Label-Free Mass Spectrometry-Based Proteomics Approaches. *J Proteome Res* **2009,** *8* (7), 3752-3759.

215. Sinz, A., Divide and conquer: cleavable cross-linkers to study protein conformation and protein–protein interactions. *Anal Bioanal Chem* **2017,** *409* (1), 33-44.

216. Barysz, H. M.; Malmstroem, J., Development of large-scale cross-linking mass spectrometry. *Mol Cell Proteomics* **2017**.

217. Tran, B. Q.; Goodlett, D. R.; Goo, Y. A., Advances in protein complex analysis by chemical cross-linking coupled with mass spectrometry (CXMS) and bioinformatics. *BBA - Proteins and Proteomics* **2016,** *1864* (1), 123-129.

218. Mehta, V.; Trinkle-Mulcahy, L., *Recent advances in large-scale protein interactome mapping*. 2016; Vol. 5.

219. Liu, F.; Rijkers, D. T. S.; Post, H.; Heck, A. J. R., Proteome-wide profiling of protein assemblies by cross-linking mass spectrometry. *Nat Meth* **2015,** *12* (12), 1179-1184.

220. Holding, A. N., XL-MS: Protein cross-linking coupled with mass spectrometry. *Methods* **2015,** *89*, 54-63.

221. Tinnefeld, V.; Sickmann, A.; Ahrends, R., Catch Me if You Can: Challenges and Applications of Cross-Linking Approaches. *Eur J Mas Spectrom* **2014,** *20* (1), 99-116.

222. Budayeva, H. G.; Cristea, I. M., A Mass Spectrometry View of Stable and Transient Protein Interactions. In *Advancements of Mass Spectrometry in Biomedical Research*, Woods, A. G.; Darie, C. C., Eds. Springer International Publishing: Cham, 2014; pp 263-282.

223. Zybailov, B. L.; Glazko, G. V.; Jaiswal, M.; Raney, K. D., Large Scale Chemical Cross-linking Mass Spectrometry Perspectives. *J Proteomics Bioinform* **2013,** *6* (Suppl 2), 001.

224. Pham, N. D.; Parker, R. B.; Kohler, J. J., Photocrosslinking approaches to interactome mapping. *Curr Opin Chem Biol* **2013,** *17* (1), 90-101.

225. Paramelle, D.; Miralles, G.; Subra, G.; Martinez, J., Chemical cross-linkers for protein structure studies by mass spectrometry. *Proteomics* **2013,** *13* (3-4), 438-456.

226. Xu, G.; Takamoto, K.; Chance, M. R., Radiolytic Modification of Basic Amino Acid Residues in Peptides: Probes for Examining Protein–Protein Interactions. *Anal Chem* **2003,** *75* (24), 6995-7007.

227. Mädler, S.; Bich, C.; Touboul, D.; Zenobi, R., Chemical cross-linking with NHS esters: a systematic study on amino acid reactivities. *J Mass Spectrom* **2009,** *44* (5), 694-706.

228. Kalkhof, S.; Sinz, A., Chances and pitfalls of chemical cross-linking with amine-reactive N-hydroxysuccinimide esters. *Anal Bioanal Chem* **2008,** *392* (1), 305-312.

229. Mattson, G.; Conklin, E.; Desai, S.; Nielander, G.; Savage, M. D.; Morgensen, S., A practical approach to crosslinking. *Mol Biol Rep* **1993,** *17* (3), 167-183.

230. Gutierrez, C. B.; Yu, C.; Novitsky, E. J.; Huszagh, A. S.; Rychnovsky, S. D.; Huang, L., Developing an Acidic Residue Reactive and Sulfoxide-Containing MS-Cleavable Homobifunctional Cross-Linker for Probing Protein–Protein Interactions. *Anal Chem* **2016,** *88* (16), 8315-8322.

231. Leitner, A.; Joachimiak, L. A.; Unverdorben, P.; Walzthoeni, T.; Frydman, J.; Förster, F.; Aebersold, R., Chemical cross-linking/mass spectrometry targeting acidic residues in proteins and protein complexes. *Proc Natl Acad Sci U S A* **2014,** *111* (26), 9455-9460.

232. Murale, D. P.; Hong, S. C.; Haque, M. M.; Lee, J.-S., Photo-affinity labeling (PAL) in chemical proteomics: a handy tool to investigate protein-protein interactions (PPIs). *Proteome Sci* **2017,** *15* (1), 14.

233. Ai, H.-w.; Shen, W.; Sagi, A.; Chen, P. R.; Schultz, P. G., Probing Protein–Protein Interactions with a Genetically Encoded Photo-crosslinking Amino Acid. *ChemBioChem* **2011,** *12* (12), 1854-1857.

234. Nadeau, O. W.; Carlson, G. M., Protein Interactions Captured by Chemical Cross-linking: One-Step Cross-linking with Formaldehyde. *CSH Protocols* **2007,** *2007* (4), pdb.prot4634.

235. Sutherland, B. W.; Toews, J.; Kast, J., Utility of formaldehyde cross-linking and mass spectrometry in the study of protein–protein interactions. *J Mass Spectrom* **2008,** *43* (6), 699-715.

236. Merkley, E. D.; Rysavy, S.; Kahraman, A.; Hafen, R. P.; Daggett, V.; Adkins, J. N., Distance restraints from crosslinking mass spectrometry: Mining a molecular dynamics simulation database to evaluate lysine–lysine distances. *Protein Sci* **2014,** *23* (6), 747-759.

237. Sriswasdi, S.; Harper, S. L.; Tang, H.-Y.; Speicher, D. W., Enhanced Identification of Zero-Length Chemical Cross-Links Using Label-Free Quantitation and High-Resolution Fragment Ion Spectra. *Journal of Proteome Research* **2014,** *13* (2), 898-914.

238. Rinner, O.; Seebacher, J.; Walzthoeni, T.; Mueller, L.; Beck, M.; Schmidt, A.; Mueller, M.; Aebersold, R., Identification of cross-linked peptides from large sequence databases. *Nat Meth* **2008,** *5* (4), 315-318.

239. Arlt, C.; Götze, M.; Ihling, C. H.; Hage, C.; Schäfer, M.; Sinz, A., Integrated Workflow for Structural Proteomics Studies Based on Cross-Linking/Mass Spectrometry with an MS/MS Cleavable Cross-Linker. *Anal Chem* **2016,** *88* (16), 7930-7937.

240. Müller, M. Q.; Dreiocker, F.; Ihling, C. H.; Schäfer, M.; Sinz, A., Fragmentation behavior of a thiourea-based reagent for protein structure analysis by collision-induced dissociative chemical cross-linking. *J Mass Spectrom* **2010,** *45* (8), 880-891.

241. Götze, M.; Pettelkau, J.; Fritzsche, R.; Ihling, C. H.; Schäfer, M.; Sinz, A., Automated Assignment of MS/MS Cleavable Cross-Links in Protein 3D-Structure Analysis. *J Am Soc Mass Spectr* **2015,** *26* (1), 83-97.

242. Zhong, X.; Navare, A. T.; Chavez, J. D.; Eng, J. K.; Schweppe, D. K.; Bruce, J. E., Large-Scale and Targeted Quantitative Cross-Linking MS Using Isotope-Labeled Protein Interaction Reporter (PIR) Cross-Linkers. *Journal of Proteome Research* **2017,** *16* (2), 720-727.

243. Weisbrod, C. R.; Chavez, J. D.; Eng, J. K.; Yang, L.; Zheng, C.; Bruce, J. E., In Vivo Protein Interaction Network Identified with a Novel Real-Time Cross-Linked Peptide Identification Strategy. *J Proteome Res* **2013,** *12* (4), 1569-1579.

244. Tang, X.; Bruce, J. E., A new cross-linking strategy: protein interaction reporter (PIR) technology for protein-protein interaction studies. *Mol BioSyst* **2010,** *6* (6), 939-947.

245. Hoopmann, M. R.; Weisbrod, C. R.; Bruce, J. E., Improved Strategies for Rapid Identification of Chemically Cross-Linked Peptides Using Protein Interaction Reporter Technology. *J Proteome Res* **2010,** *9* (12), 6323-6333.

246. Zhang, H.; Tang, X.; Munske, G. R.; Tolic, N.; Anderson, G. A.; Bruce, J. E., Identification of Protein-Protein Interactions and Topologies in Living Cells with Chemical Cross-linking and Mass Spectrometry. *Mol Cell Proteomics* **2009,** *8* (3), 409-420.

247. Petrotchenko, E. V.; Serpa, J. J.; Borchers, C. H., An Isotopically Coded CID-cleavable Biotinylated Cross-linker for Structural Proteomics. *Mol Cell Proteomics* **2011,** *10* (2).

248. Tan, D.; Li, Q.; Zhang, M.-J.; Liu, C.; Ma, C.; Zhang, P.; Ding, Y.-H.; Fan, S.-B.; Tao, L.; Yang, B.; Li, X.; Ma, S.; Liu, J.; Feng, B.; Liu, X.; Wang, H.-W.; He, S.-M.; Gao, N.; Ye, K.; Dong, M.-Q.; Lei, X., Trifunctional cross-linker for mapping protein-protein interaction networks and comparing protein conformational states. *eLife* **2016,** *5*, e12509.

249. de Souza, N., Chemical biology: A multi-purpose cross-linker. *Nat Meth* **2016,** *13* (5), 392-393.

250. Chowdhury, S. M.; Du, X.; Tolić, N.; Wu, S.; Moore, R. J.; Mayer, M. U.; Smith, R. D.; Adkins, J. N., Identification of Cross-Linked Peptides after Click-Based Enrichment Using Sequential Collision-Induced Dissociation and Electron Transfer Dissociation Tandem Mass Spectrometry. *Anal Chem* **2009,** *81* (13), 5524-5532.

251. Burke, A. M.; Kandur, W.; Novitsky, E. J.; Kaake, R. M.; Yu, C.; Kao, A.; Vellucci, D.; Huang, L.; Rychnovsky, S. D., Synthesis of two new enrichable and MS-cleavable cross-linkers to define protein-protein interactions by mass spectrometry. *Org Biomol Chem* **2015,** *13* (17), 5030-5037.

252. Milanesi, L.; Reid, G. D.; Beddard, G. S.; Hunter, C. A.; Waltho, J. P., Synthesis and Photochemistry of a New Class of Photocleavable Protein Cross-linking Reagents. *Chem-Eur J* **2004,** *10* (7), 1705-1710.

253. Omran, Z.; Specht, A., Synthesis and photochemical properties of photo-cleavable crosslinkers. *Tetrahedron Lett* **2009,** *50* (20), 2434-2436.

254. Yang, L.; Tang, X.; Weisbrod, C. R.; Munske, G. R.; Eng, J. K.; von Haller, P. D.; Kaiser, N. K.; Bruce, J. E., A Photocleavable and Mass Spectrometry Identifiable Cross-Linker for Protein Interaction Studies. *Anal Chem* **2010,** *82* (9), 3556-3566.

255. Yang, L.; Zheng, C.; Weisbrod, C. R.; Tang, X.; Munske, G. R.; Hoopmann, M. R.; Eng, J. K.; Bruce, J. E., In Vivo Application of Photocleavable Protein Interaction Reporter Technology. *Journal of Proteome Research* **2012,** *11* (2), 1027-1041.

256. Leeson, P. D.; Springthorpe, B., The influence of drug-like concepts on decision-making in medicinal chemistry. *Nat Rev Drug Discov* **2007,** *6* (11), 881-890.

257. Niesen, F. H.; Berglund, H.; Vedadi, M., The use of differential scanning fluorimetry to detect ligand interactions that promote protein stability. *Nat. Protocols* **2007,** *2* (9), 2212-2221.

258. Mashalidis, E. H.; Śledź, P.; Lang, S.; Abell, C., A three-stage biophysical screening cascade for fragment-based drug discovery. *Nat. Protocols* **2013,** *8* (11), 2309-2324.

259. Layton, C. J.; Hellinga, H. W., Quantitation of protein–protein interactions by thermal stability shift analysis. *Protein Sci* **2011,** *20* (8), 1439-1450.

260. Dalvit, C.; Fogliatto, G.; Stewart, A.; Veronesi, M.; Stockman, B., WaterLOGSY as a method for primary NMR screening: Practical aspects and range of applicability. *J Biomol NMR* **2001,** *21* (4), 349-359.

261. Antanasijevic, A.; Ramirez, B.; Caffrey, M., Comparison of the sensitivities of WaterLOGSY and saturation transfer difference NMR experiments. *J Biomol NMR* **2014,** *60* (1), 37-44.

262. Baell, J. B.; Holloway, G. A., New Substructure Filters for Removal of Pan Assay Interference Compounds (PAINS) from Screening Libraries and for Their Exclusion in Bioassays. *J Med Chem* **2010,** *53* (7), 2719-2740.

263. Henchey, L. K.; Jochim, A. L.; Arora, P. S., Contemporary strategies for the stabilization of peptides in the α-helical conformation. *Curr Opin Chem Biol* **2008,** *12* (6), 692-697.

264. Bakhtiar, R., Surface Plasmon Resonance Spectroscopy: A Versatile Technique in a Biochemist's Toolbox. *J Chem Educ* **2013,** *90* (2), 203-209.

265. Patching, S. G., Surface plasmon resonance spectroscopy for characterisation of membrane protein–ligand interactions and its potential for drug discovery. *BBA - Biomembranes* **2014,** *1838* (1, Part A), 43-55.

266. Taylor, J. W., The synthesis and study of side-chain lactam-bridged peptides. *Peptide Science* **2002,** *66* (1), 49-75.

267. Harrison, R. S.; Shepherd, N. E.; Hoang, H. N.; Ruiz-Gómez, G.; Hill, T. A.; Driver, R. W.; Desai, V. S.; Young, P. R.; Abbenante, G.; Fairlie, D. P., Downsizing human, bacterial, and viral proteins to short water-stable alpha helices that maintain biological potency. *Proc Natl Acad Sci U S A* **2010,** *107* (26), 11686-11691.

268. Forood, B.; Feliciano, E. J.; Nambiar, K. P., Stabilization of alpha-helical structures in short peptides via end capping. *Proc Natl Acad Sci U S A* **1993,** *90* (3), 838-842.

269. Pelliccioli, A. P.; Wirz, J., Photoremovable protecting groups: reaction mechanisms and applications. *Photoch Photobio Sci* **2002,** *1* (7), 441-458.

270. Klan, P.; Solomek, T.; Bochet, C. G.; Blanc, A.; Givens, R.; Rubina, M.; Popik, V.; Kostikov, A.; Wirz, J., Photoremovable Protecting Groups in Chemistry and Biology: Reaction Mechanisms and Efficacy. *Chem Soc Rev* **2013,** *113* (1), 119-191.

271. Lee, H. B.; Balasubramanian, S., Studies on a Dithiane-Protected Benzoin Photolabile Safety Catch Linker for Solid-Phase Synthesis. *J Org Chem* **1999,** *64* (10), 3454-3460.

272. DeMartino, J. K.; Hwang, I.; Connelly, S.; Wilson, I. A.; Boger, D. L., Asymmetric Synthesis of Inhibitors of Glycinamide Ribonucleotide Transformylase. *J Med Chem* **2008,** *51* (17), 5441-5448.

273. Piggott, A. M.; Karuso, P., Synthesis of a new hydrophilic o-nitrobenzyl photocleavable linker suitable for use in chemical proteomics. *Tetrahedron Lett* **2005,** *46* (47), 8241-8244.

274. Ivanov, K. I.; Ba; Marta; Varjosalo, M.; kinen, K., One-step Purification of Twin-Strep-tagged Proteins and Their Complexes on Strep-Tactin Resin Cross-linked With Bis(sulfosuccinimidyl) Suberate (BS3). **2014,** (86), e51536.

275. Schmidt, T. G. M.; Batz, L.; Bonet, L.; Carl, U.; Holzapfel, G.; Kiem, K.; Matulewicz, K.; Niermeier, D.; Schuchardt, I.; Stanar, K., Development of the Twin-Strep-tag® and its application for purification of recombinant proteins from cell culture supernatants. *Protein Expres Purif* **2013,** *92* (1), 54-61.

276. Yeliseev, A.; Zoubak, L.; Schmidt, T. G. M., Application of Strep-Tactin XT for affinity purification of Twin-Strep-tagged CB2, a G protein-coupled cannabinoid receptor. *Protein Expres Purif* **2017,** *131*, 109-118.

277. Leitner, A.; Reischl, R.; Walzthoeni, T.; Herzog, F.; Bohn, S.; Förster, F.; Aebersold, R., Expanding the Chemical Cross-Linking Toolbox by the Use of Multiple Proteases and Enrichment by Size Exclusion Chromatography. *Mol Cell Proteomics* **2012,** *11* (3).

278. Hakhverdyan, Z.; Domanski, M.; Hough, L. E.; Oroskar, A. A.; Oroskar, A. R.; Keegan, S.; Dilworth, D. J.; Molloy, K. R.; Sherman, V.; Aitchison, J. D.; Fenyo, D.; Chait, B. T.; Jensen, T. H.; Rout, M. P.; LaCava, J., Rapid, optimized interactomic screening. *Nat Meth* **2015,** *12* (6), 553-560.

279. Rappsilber, J.; Ishihama, Y.; Mann, M., Stop and Go Extraction Tips for Matrix-Assisted Laser Desorption/Ionization, Nanoelectrospray, and LC/MS Sample Pretreatment in Proteomics. *Anal Chem* **2003,** *75* (3), 663-670.

280. Michalski, A.; Damoc, E.; Hauschild, J.-P.; Lange, O.; Wieghaus, A.; Makarov, A.; Nagaraj, N.; Cox, J.; Mann, M.; Horning, S., Mass Spectrometry-based Proteomics Using Q Exactive, a High-performance Benchtop Quadrupole Orbitrap Mass Spectrometer. *Mol Cell Proteomics* **2011,** *10* (9).

9 Appendices

Appendix A: DSF Spectra

In quadruplicates unless specified otherwise. Graphs show normalised results except **62**.

Rab27a Only

Buffer only

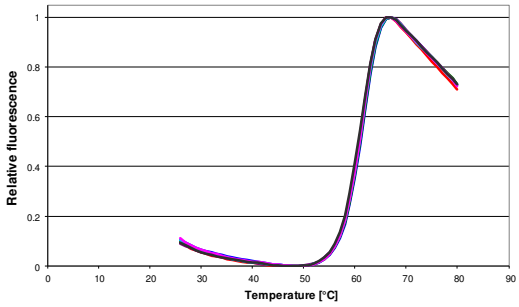

2% DMSO

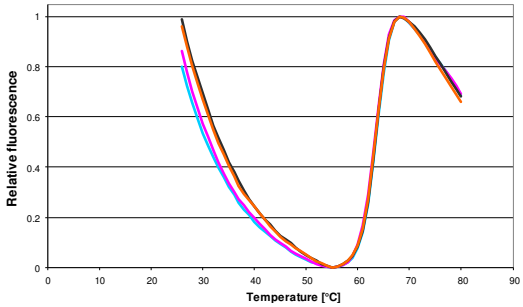

Buffer only has eight replicates.

Top Fragment Hits from DSF Screen

32

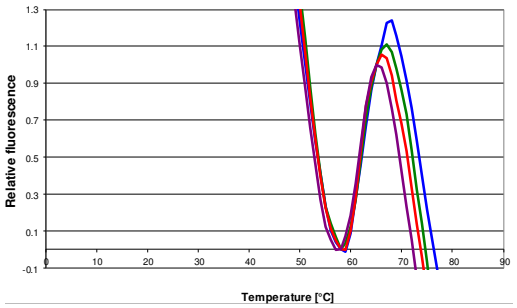

34

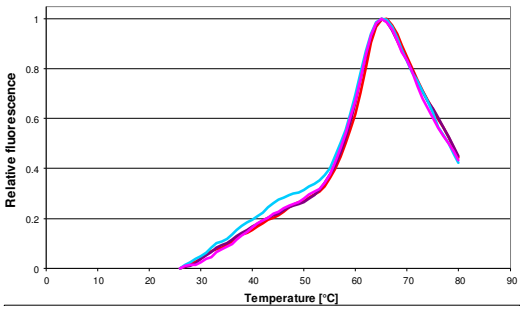

35

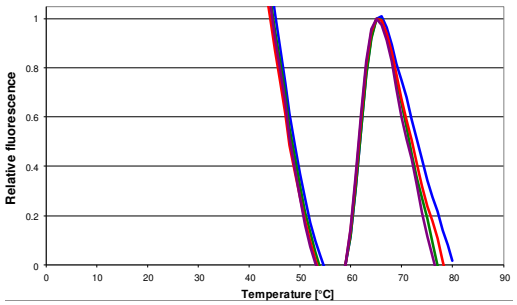

36

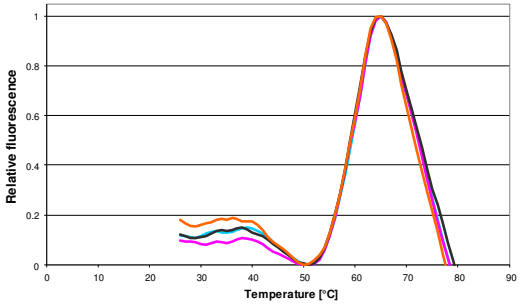

37

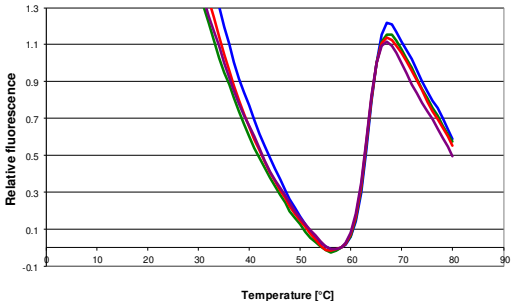

Synthesised Analogues

41

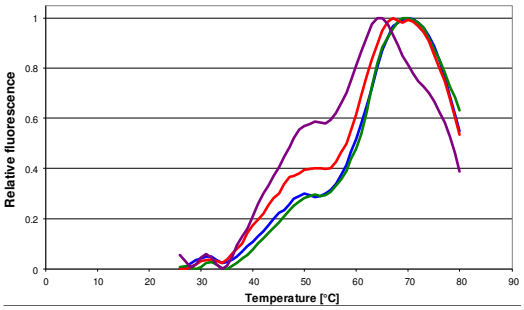

42

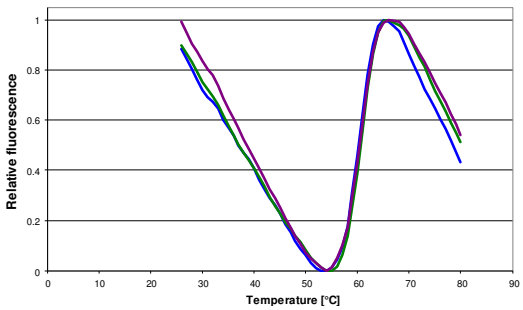

58

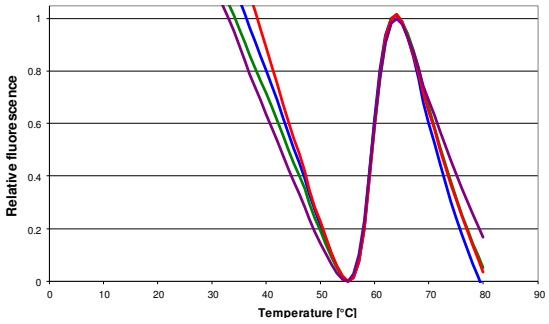

62

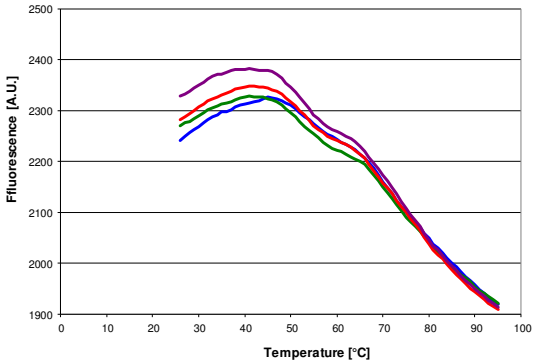

59

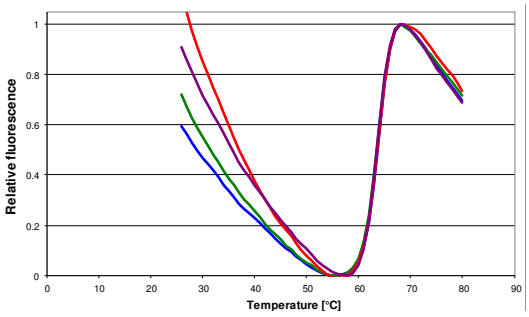

WF

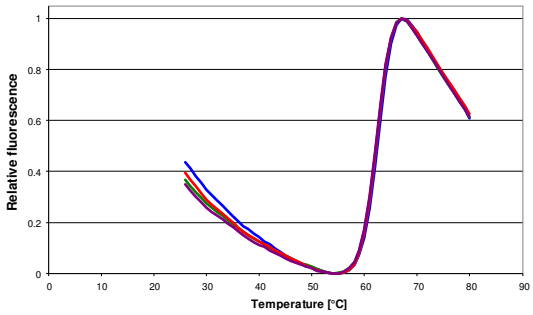

Numerical Data

Compound	T_m 1	T_m 2	T_m 3	T_m 4	Avg T_m	ΔT_m*
Buffer only	60.2 60.8	60.5 60.3	60.3 61.0	60.1 61.1	60.5	**-0.2**
2% DMSO	60.8	60.6	60.9	60.5	60.7	**0.0**
32	60.7	59.7	60.3	60.4	60.3	**-0.4**
34	60.4	60.4	60.4	60.6	60.4	**-0.2**
35	N/A	N/A	60.3	60.4	60.4	**-0.3**
36	N/A	N/A	60.3	60.4	60.4	**-0.3**
37	60.6	59.9	60.4	60.5	60.3	**-0.4**
41	N/A	N/A	N/A	N/A	N/A	**N/A**
42	60.6	60.6	60.1	60.4	60.4	**-0.3**
58	60.5	60.5	**63.0**	60.3	61.1	**0.4**
59	60.5	60.5	60.4	60.3	60.4	**-0.3**
62	N/A	N/A	N/A	N/A	N/A	**N/A**
WF	60.7	60.5	60.7	60.6	60.6	**-0.1**

Melting point values could not be calculated where the melting point curves did not conform to the expected sigmoidal shape.

Appendix B: WaterLOGSY Spectra

Green – 1D (scaled down x 0.1)

Blue – waterLOGSY with 1 mM ligand

Red – waterLOGSY with 1 mM ligand and 10 μM Rab27a

Ref	Sequence	waterLOGSY overlay
-	WF	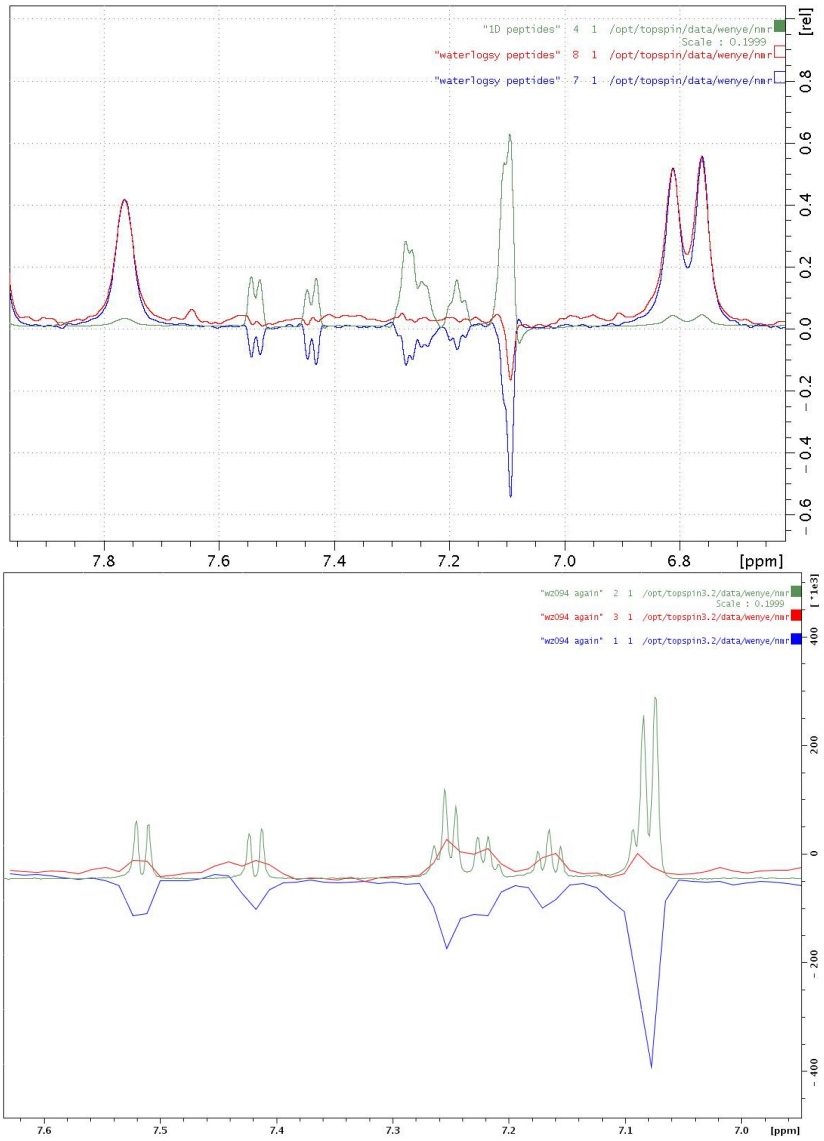

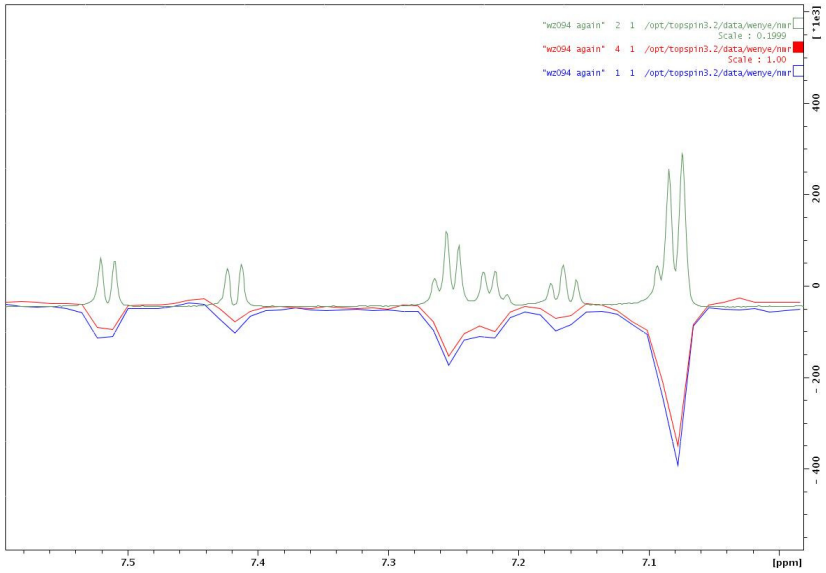

with WT-Rab27a-Slp1 complex, 800 MHz (above)

34 Pyrazole Fragment

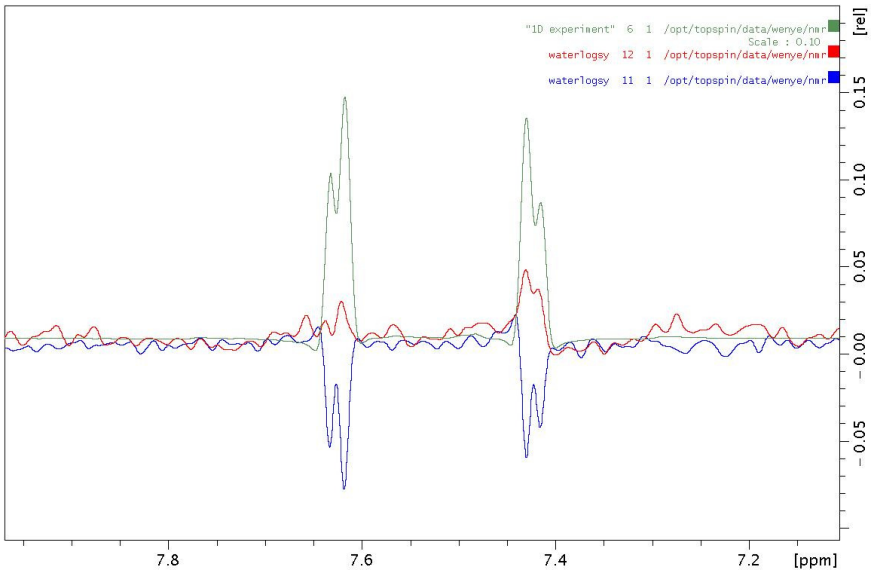

69 FW

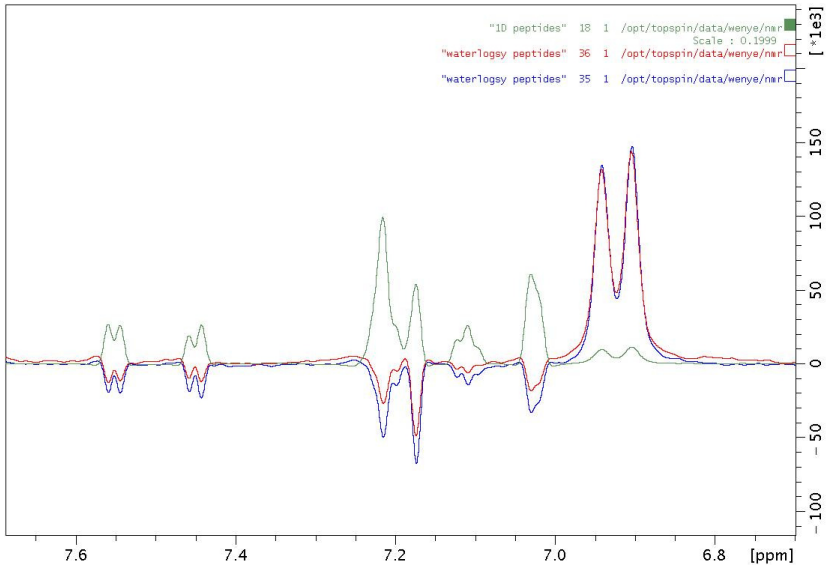
"1D peptides" 18 1 /opt/topspin/data/wenye/nmr
Scale : 0.1999
"waterlogsy peptides" 36 1 /opt/topspin/data/wenye/nmr
"waterlogsy peptides" 35 1 /opt/topspin/data/wenye/nmr
[*1e3]
150
100
50
0
-50
-100
7.6
7.4
7.2
7.0
6.8
[ppm]

70 wF

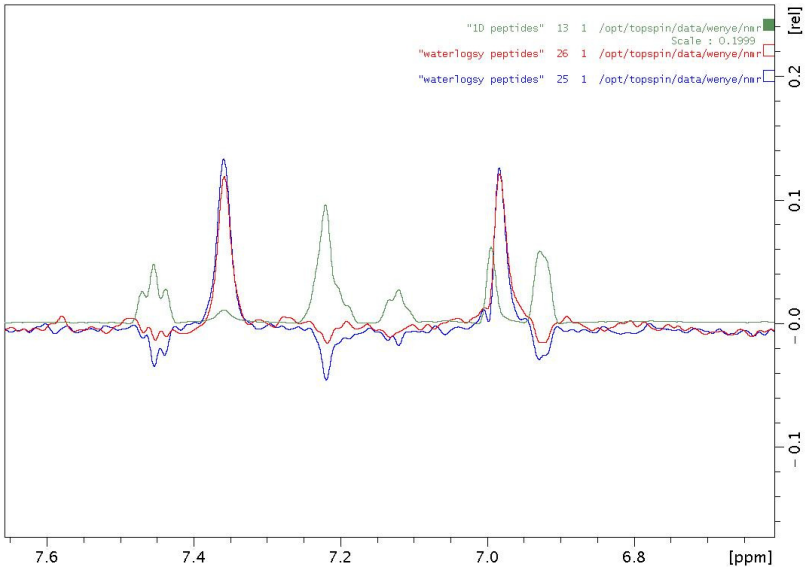
"1D peptides" 13 1 /opt/topspin/data/wenye/nmr
Scale : 0.1999
"waterlogsy peptides" 26 1 /opt/topspin/data/wenye/nmr
"waterlogsy peptides" 25 1 /opt/topspin/data/wenye/nmr
[rel]
0.2
0.1
-0.0
-0.1
7.6
7.4
7.2
7.0
6.8
[ppm]

71 Fluorescein

-WF

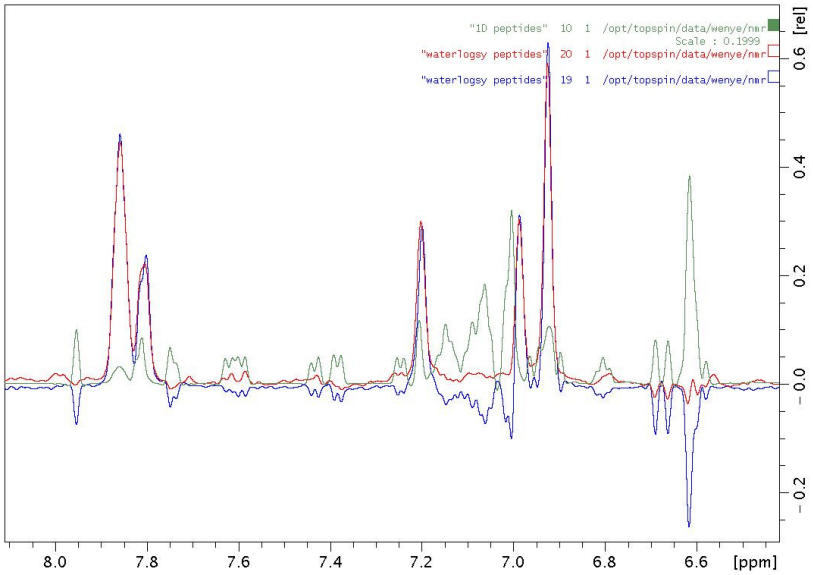

72 QWF

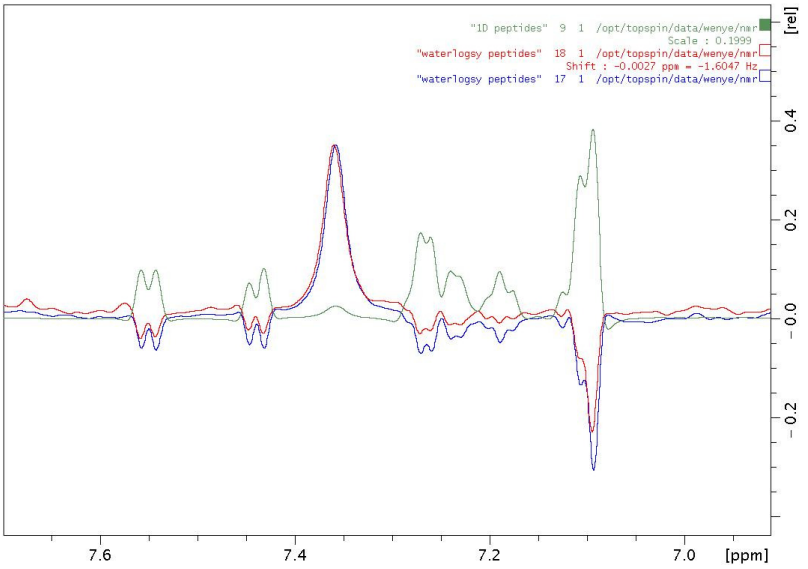

73 GWF

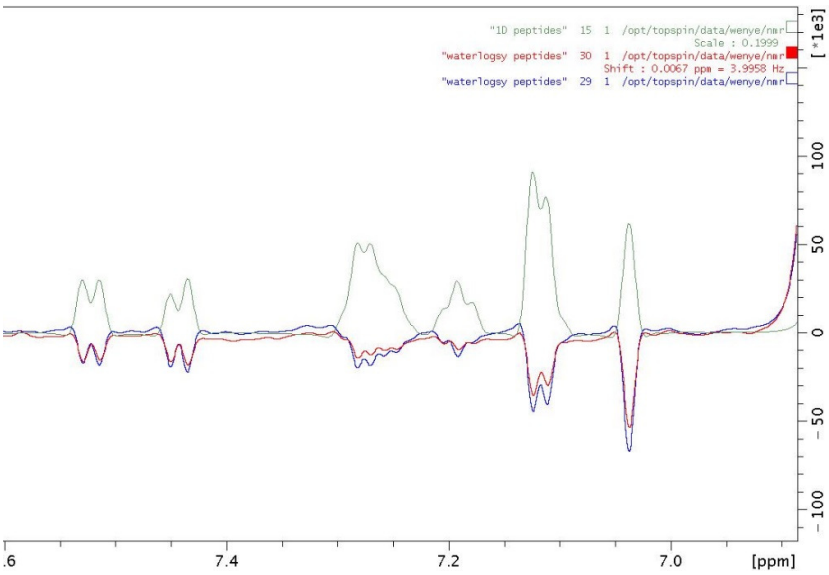

74 WAF

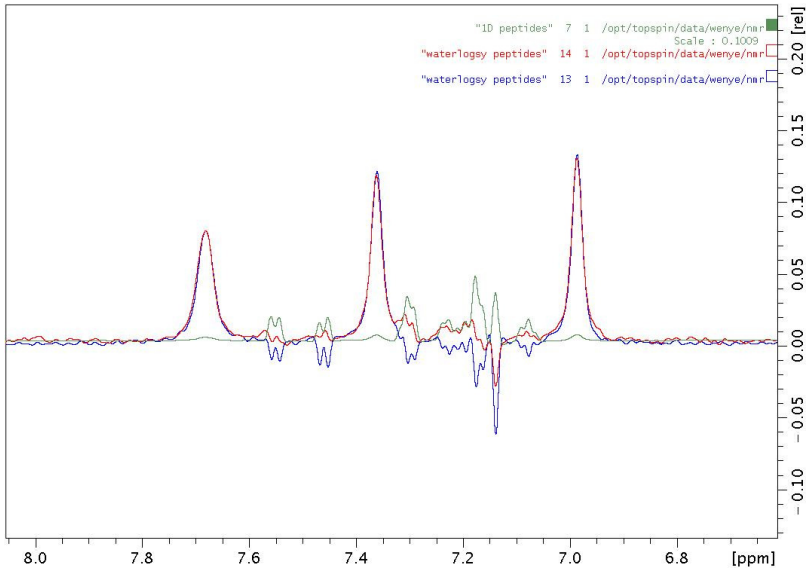

75 H-WFY

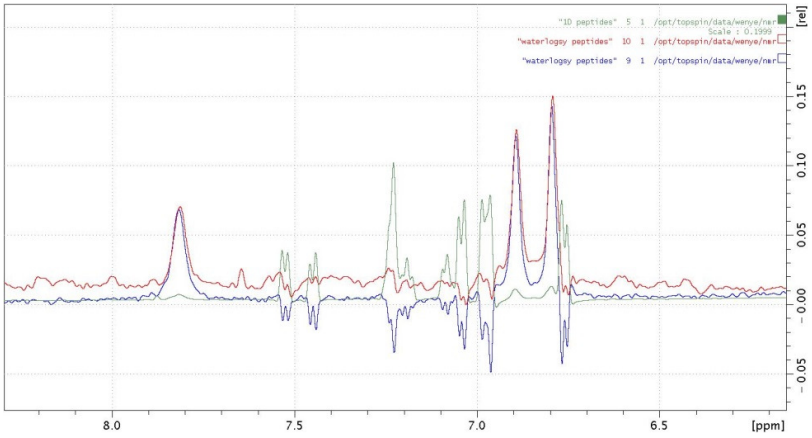

76 WFYE

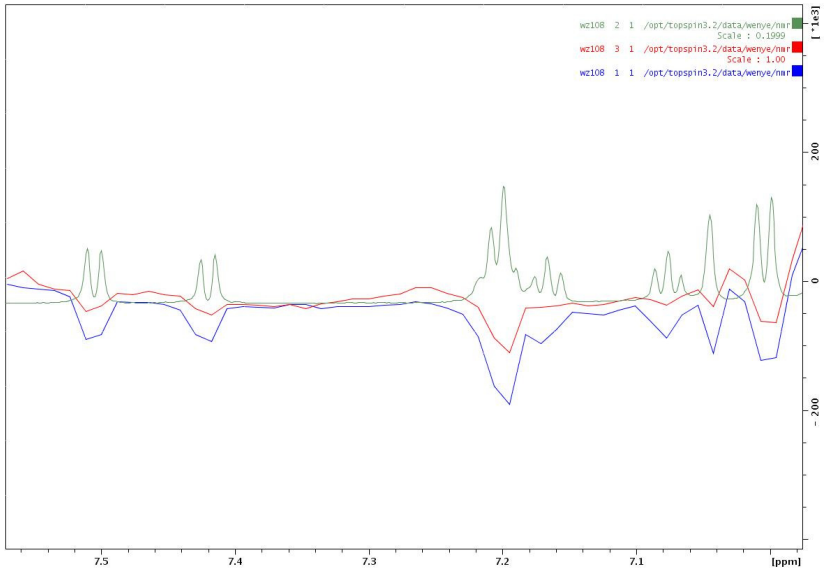

77 WFYK

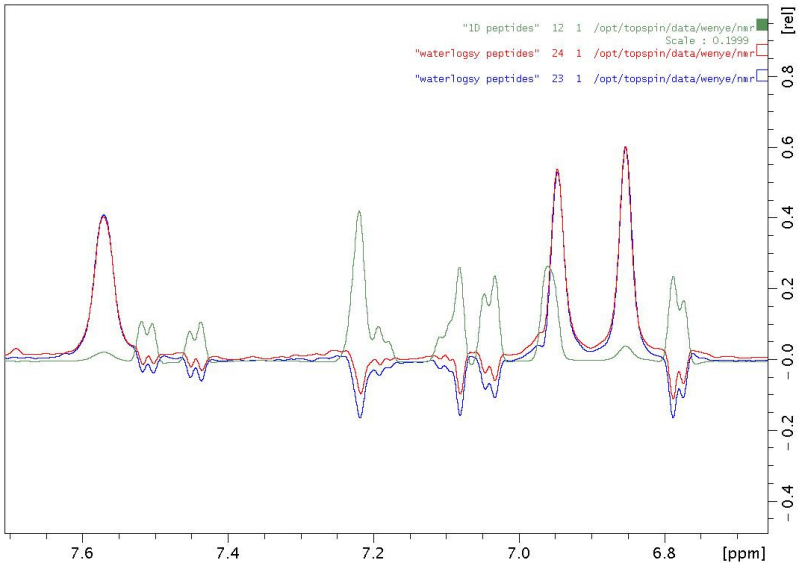

78 QWFYE

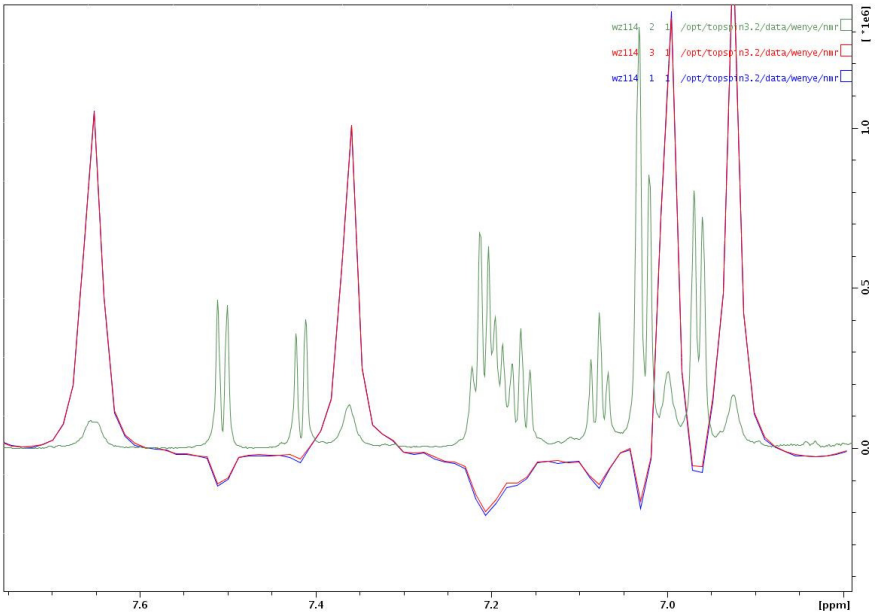

79 GQWFYE

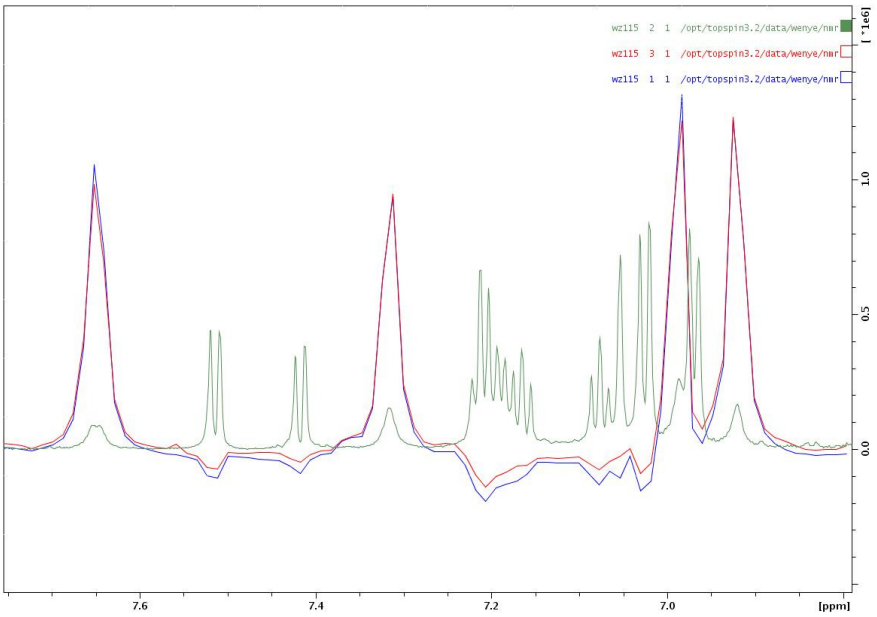

80 WFYEAK

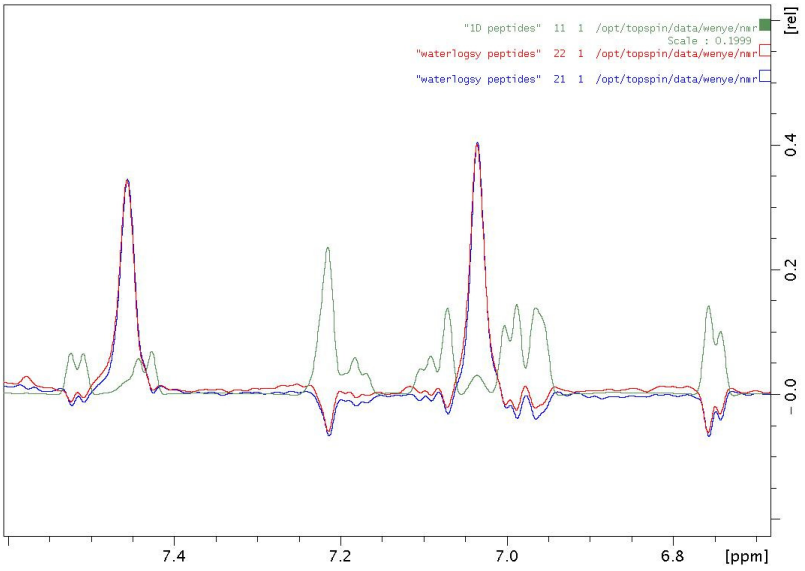

81 WFYQAK

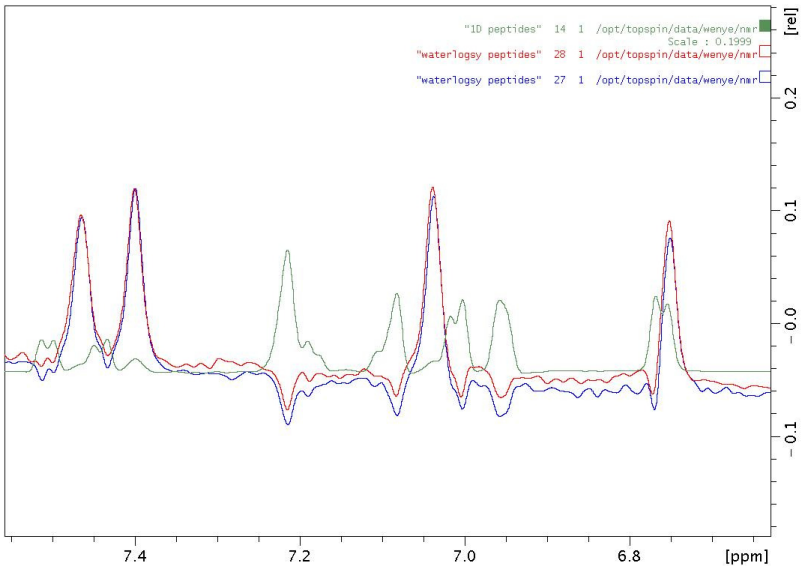

82 WFYQHK

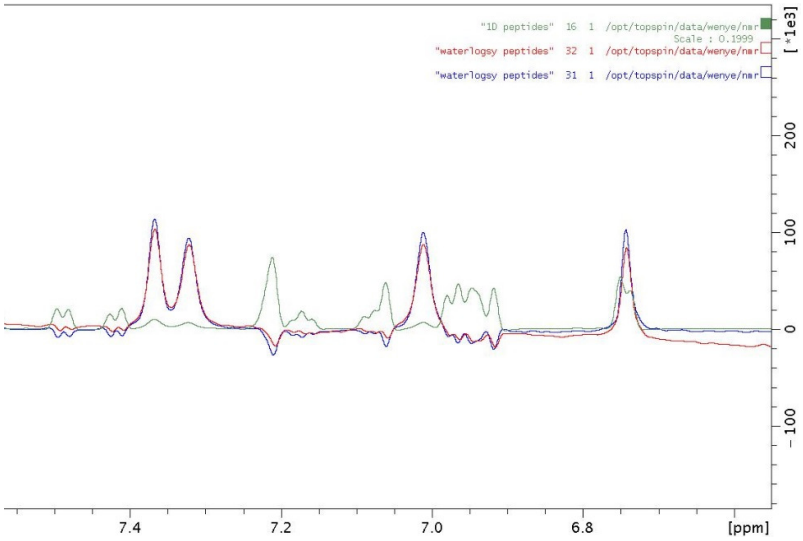

83 WFYEAKA

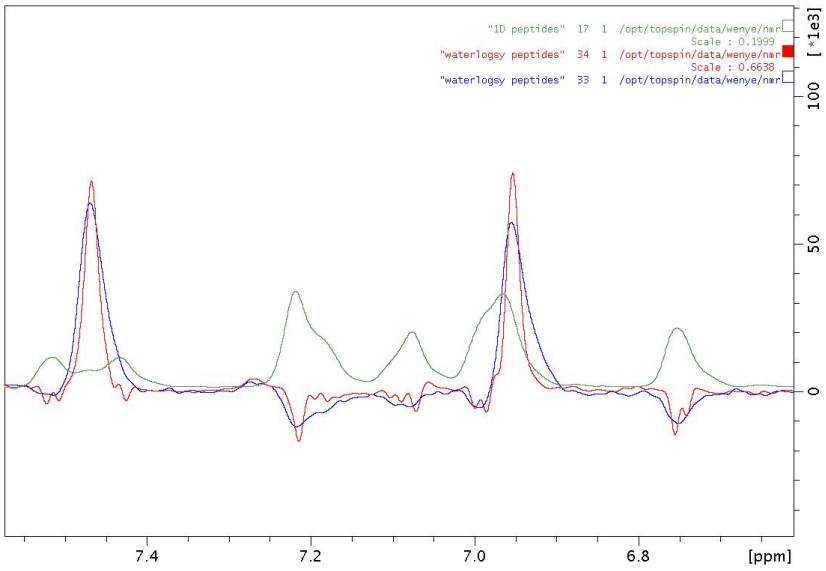

84 YY

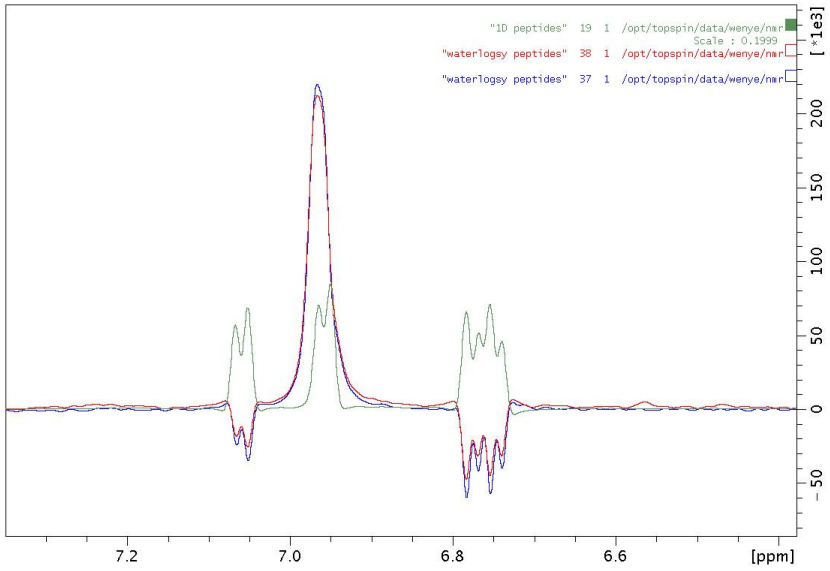
"1D peptides" 19 1 /opt/topspin/data/wenye/nmr
Scale : 0.1999
"waterlogsy peptides" 38 1 /opt/topspin/data/wenye/nmr
"waterlogsy peptides" 37 1 /opt/topspin/data/wenye/nmr
[*1e3]
200
150
100
50
0
-50
7.2
7.0
6.8
6.6
[ppm]

Appendix C: Protein Sequences

Wild Type Rab27a

SDGDYDYLIKFLALGDSGVGKTSVLYQYTDGKFNSKFITTVGIDFREKRVVYRASGPDGATG
RGQRIHLQLWDTAGQERFRSLTTAFFRDAMGFLLLFDLTNEQSFLNVRNWISQLQMHAYC
ENPDIVLCGNKSDLEDQRVVKEEEAIALAEKYGIPYFETSAANGTNISQAIEMLLDLIMKRME
RCVDKSWIPEGVVRSNGHASTDQLSEEKEKGACGC

Recombinant Rab27a

SDGDYDYLIKFLALGDSGVGKTSVLYQYTDGKFNSKFITTVGIDFREKRVVYRASGPDGATG
RGQRIHLQLWDTAGQERFRSLTTAFFRDAMGFLLLFDLTNEQSFLNVRNWISQLQMHAYC
ENPDIVLCGNKSDLEDQRVVKEEEAIALAEKYGIPYFETSAANGTNISQAIEMLLDLIMKRME
RCVDKS

Biotin-Rab27a

GLNDIFEAQKIEWHEGSGSGSGMSDGDYDYLIKFLALGDSGVGKTSVLYQYTDGKFNSKFI
TTVGIDFREKRVVYRASGPDGATGRGQRIHLQLWDTAGQERFRSLTTAFFRDAMGFLLLFD
LTNEQSFLNVRNWISQLQMHAYCENPDIVLCGNKSDLEDQRVVKEEEAIALAEKYGIPYFET
SAANGTNISQAIEMLLDLIMKRMERCVDKS

Fusion-Rab27a

SSGRENLYFQGHMSFLTEEEQEAIMKVLQRDAALKRAEEERGSGSGSGMSDGDYDYLIKF
LALGDSGVGKTSVLYQYTDGKFNSKFITTVGIDFREKRVVYRASGPDGATGRGQRIHLQLW
DTAGLERFRSLTTAFFRDAMGFLLLFDLTNEQSFLNVRNWISQLQMHAYSENPDIVLCGNK
SDLEDQRVVKEEEAIALAEKYGIPYFETSAANGTNISQAIEMLLDLIMKRMERSVDKS

Slp4

SFLSEEEKDLILSVLQRDEEVRKADEKRIRRLKNELLEIKRKGAKRGSQHYSDRTCARCQES
LGRLSPKTNTCRGCNHLVCRDCRIQESNGTWRCKVCAKEIELKKATGDWFYDQ

TST-Rab27a

MWSHPQFEKGGGSGGGSGGSAWSHPQFEKSGLRSRAMSDGDYDYLIKFLALGDSGVGK
TSVLYQYTDGKFNSKFITTVGIDFREKRVVYRASGPDGATGRGQRIHLQLWDTAGQERFRS
LTTAFFRDAMGFLLLFDLTNEQSFLNVRNWISQLQMHAYCENPDIVLCGNKSDLEDQRVVK
EEEAIALAEKYGIPYFETSAANGTNISQAIEMLLDLIMKRMERCVDKSWIPEGVVRSNGHAST
DQLSEEKEKGACGC

Appendix D: TST-Rab27a plasmid

Description

Plasmid DNA Description:

The synthetic gene TST-Rab27a was assembled from synthetic oligonucleotides and/or PCR products. The fragment was inserted into pcDNA3.1(+). The plasmid DNA was purified from transformed bacteria and concentration determined by UV spectroscopy. The final construct was verified by sequencing. The sequence congruence within the insertion sites was 100%. See the accompanying data sheets for sequences and find the original ABI trace files as well as the assembled sequences electronically on disk.
5 µg of the plasmid preparation were lyophilized for shipping.

Plasmid Map:

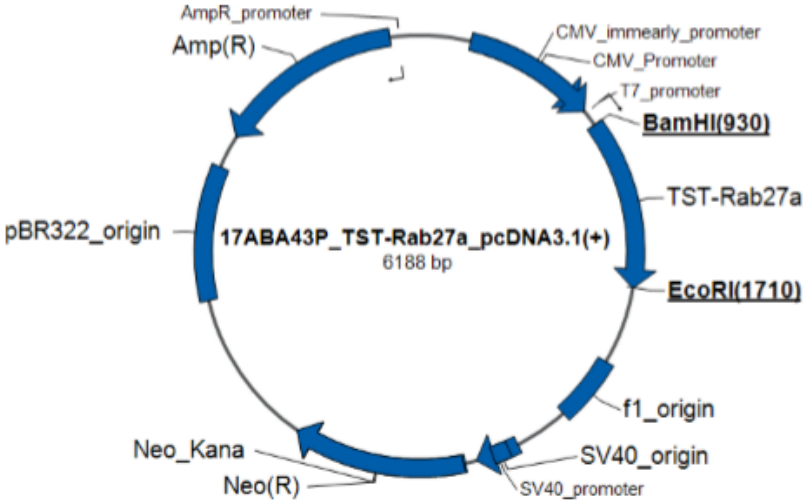

Documentation

invitrogen
by Thermo Fisher Scientific

Quality Assurance Documentation: 17ABA43P

Ref. No.: 2093454

Designation:	E.coli K12 DH10B™ T1R
Gene name:	**TST-Rab27a**
Gene size:	786 bp
Vector backbone:	pcDNA3.1(+)
Cloning sites:	BamHI / EcoRI
Quantity:	~5 µg Plasmid DNA
Note:	Please dissolve lyophilized DNA in 50 µl distilled water or 10 mM Tris-HCl (pH 8.0). We recommend sequence verification after each transformation step.
Date:	16 March 2017

Monique Gärtner
Quality control

www.thermofisher.com **geneartsupport@thermofisher.com**

TST-Rab27a only nucleotide sequence

AAGCTGGCTAGCGTTTAAACTTAAGCTTGGTACCGAGCTCGGATCCATGTGGTCCCATC
CTCAGTTCGAGAAAGGCGGCGGATCTGGCGGTGGAAGCGGAGGATCTGCTTGGAGCC
ATCCACAGTTTGAAAAGTCCGGCCTGCGGAGCAGAGCCATGTCCGATGGCGATTACGA
CTACCTGATCAAGTTTCTGGCCCTGGGCGATAGCGGCGTGGGCAAAACATCTGTGCTG
TACCAGTACACCGACGGCAAGTTCAACAGCAAGTTCATCACCACCGTGGGCATCGACT
TCCGCGAGAAGAGAGTGGTGTACAGAGCCAGCGGACCTGATGGCGCTACTGGCAGAG
GACAGAGAATCCATCTGCAGCTGTGGGACACAGCCGGCCAAGAGAGATTCAGAAGCCT
GACCACCGCCTTTTTCCGGGACGCCATGGGATTTCTGCTGCTGTTCGACCTGACCAAC
GAGCAGAGCTTCCTGAACGTGCGGAACTGGATCAGCCAGCTCCAGATGCACGCCTACT
GCGAGAACCCCGATATCGTGCTGTGCGGCAACAAGAGCGACCTGGAAGATCAGCGGG
TCGTGAAAGAGGAAGAGGCAATCGCCCTGGCCGAGAAGTACGGCATCCCCTACTTTGA
GACAAGCGCCGCCAACGGCACCAACATCTCTCAGGCCATTGAGATGCTGCTGGACCTG
ATCATGAAGCGGATGGAAAGATGCGTGGACAAGAGCTGGATTCCCGAGGGCGTCGTG
CGGTCTAATGGACACGCTAGCACAGACCAGCTGTCCGAGGAAAAAGAGAAGGGCGCC
TGCGGCTGTTGAGAATTCTGCAGATATCCAGCACAGTGGCGGCCGCTCGAGTCTAGAG

Appendix E: MaxQuant Statistical Tests – Tables

The following abbreviations are used:

- #Pep – number of razor and unique peptides
- Cov [%] – sequence coverage of unique and razor peptides
- #MS/MS – number of assigned MS/MS spectra
- -log p – minus $\log_2$ (student t-test significance value)
- Diff – t-test difference between the compared sets

Imputed values are in italic red text. Proteins that are enriched in sets containing crosslinker are labelled in red text in the "Diff" column.

Proteins are ordered in descending value of -log p. Only significant values with -Log p ≥ 2.00 are reported here.

A1 vs B1

			Log2 (LFQ intensity)									Student t-test	
			A1			B1							
	Protein names	Gene	1	2	3	4	5	6	#Pep	Cov [%]	#MS/MS	-Log p	Diff
1	ATP-binding cassette sub-family F member 3	ABCF3	26.18	26.36	26.23	*23.92*	*23.89*	*23.90*	6	13	10	5.76	2.35
2	Transportin-1	TNPO1	28.60	29.05	28.93	*23.99*	*24.22*	*23.63*	21	24	51	4.63	4.91
3	Coatomer subunit beta	COPB1	28.39	29.09	28.88	*23.84*	*23.67*	*24.07*	36	45	150	4.50	4.93
4	Exportin-T	XPOT	26.72	27.32	27.01	*23.44*	*23.08*	*23.28*	16	20	31	4.30	3.75

5	Signal peptidase complex catalytic subunit SEC11A	SEC11A	28.33	29.26	28.83	*23.85*	*23.84*	*23.98*	9	43	43	4.26	4.92
6	Serine/threonine-protein kinase mTOR	MTOR	30.09	30.79	30.81	*23.54*	*23.79*	*24.48*	3	1	5	4.26	6.63
7	Surfeit locus protein 4	SURF4	26.38	26.46	26.56	*23.67*	*23.60*	*23.15*	3	14	10	4.20	2.99
8	Coatomer subunit gamma-1	COPG1	27.83	28.41	28.44	*23.38*	*23.99*	*23.54*	33	39	113	4.15	4.59
9	Eukaryotic initiation factor 4A-III	EIF4A3	*22.93*	*23.20*	*23.41*	26.39	26.39	26.82	4	11	6	4.13	-3.35
10	Vesicle-fusing ATPase	NSF	27.56	27.95	28.52	*23.35*	*23.25*	*23.49*	24	38	50	4.06	4.65
11	Cytochrome b-c1 complex subunit 2, mitochondrial	UQCRC2	29.32	30.55	29.90	*23.35*	*23.95*	*23.52*	22	72	99	4.04	6.32
12	60S ribosomal protein L38	RPL38	28.65	28.81	28.47	24.42	24.87	*24.00*	6	59	24	4.00	4.21
13	Calcium-binding mitochondrial carrier protein SCaMC-1	SLC25A24	28.51	27.52	28.22	*23.75*	*23.66*	*23.35*	8	18	16	3.85	4.50
14	Tubulin alpha-1B chain	TUBA1B	34.99	35.65	35.57	31.94	32.38	32.22	57	80	1029	3.72	3.22
15	Acetyl-CoA carboxylase 1; Biotin carboxylase	ACACA	27.07	27.58	27.57	*23.41*	*23.37*	*24.11*	33	18	71	3.68	3.77
16	Importin-7	IPO7	26.56	27.08	27.05	*23.85*	*23.51*	*23.12*	13	14	33	3.64	3.40
17	Putative tubulin-like	TUBA4B	29.02	29.53	30.52	*23.30*	*23.80*	*23.92*	11	23	10	3.63	6.02

	protein alpha-4B												
18	Tubulin beta-4B chain	TUBB4B	33.78	34.33	34.35	31.20	31.63	31.36	58	84	1246	3.60	2.76
19	Signal peptidase complex subunit 2	SPCS2	27.90	28.76	28.88	*23.74*	*24.12*	*24.47*	13	58	51	3.53	4.40
20	GTP-binding protein Rheb	RHEB	25.71	25.81	26.33	*23.70*	*23.69*	*23.77*	6	30	21	3.48	2.23
21	Actin, alpha cardiac muscle 1; Actin, alpha skeletal muscle	ACTC1; ACTA1	29.76	30.40	30.16	26.85	26.16	25.92	31	72	92	3.46	3.80
22	Acylglycerol kinase, mitochondrial	AGK	26.44	27.11	26.68	*23.64*	*23.88*	*24.19*	6	19	13	3.45	2.84
23	Basic leucine zipper and W2 domain-containing protein 1	BZW1	27.89	28.21	27.95	*22.93*	*24.25*	*23.62*	13	34	33	3.44	4.42
24	ADP/ATP translocase 3	SLC25A6	28.71	29.77	29.42	*23.81*	24.90	*24.02*	22	63	132	3.42	5.05
25	ATPase family AAA domain-containing protein 3A	ATAD3A	27.17	26.63	26.65	*24.01*	*24.07*	*24.51*	10	19	20	3.42	2.62
26	Phosphate carrier protein, mitochondrial	SLC25A3	28.02	28.66	29.05	*24.07*	*23.60*	*22.89*	11	25	51	3.42	5.05
27	Sarcoplasmic/endoplasmic reticulum calcium ATPase 2	ATP2A2	28.51	28.83	29.05	*22.27*	*23.97*	*23.33*	22	24	83	3.38	5.61
28	Protein transport protein Sec61 subunit	SEC61A1; SEC61A2	27.99	29.36	28.46	*23.66*	*24.06*	*24.17*	14	33	30	3.38	4.64

	alpha isoform 1 and 2												
29	Translation machinery-associated protein 7	TMA7	29.05	29.21	30.41	*24.06*	*24.44*	*23.43*	5	64	39	3.36	5.58
30	Voltage-dependent anion-selective channel protein 3	VDAC3	28.58	29.10	28.78	*22.52*	*23.91*	*24.00*	13	49	55	3.35	5.34
31	Pyridoxal-dependent decarboxylase domain-containing protein 1	PDXDC1	25.70	26.31	25.73	*23.73*	*23.52*	*23.32*	9	18	9	3.30	2.39
32	EH domain-containing protein 4	EHD4	27.67	28.38	28.16	*22.52*	*23.98*	*23.63*	18	36	47	3.19	4.69
33	Cyclin-dependent kinase 1	CDK1	26.57	26.78	26.73	*23.36*	*24.12*	*24.27*	17	60	54	3.19	2.78
34	Ataxin-10	ATXN10	26.77	27.43	27.46	*23.56*	*24.00*	*22.91*	9	24	26	3.18	3.73
35	ATP-dependent Clp protease ATP-binding subunit clpX-like, mitochondrial	CLPX	27.41	27.86	27.76	*24.00*	*24.50*	*23.23*	8	13	51	3.18	3.77
36	Translational activator GCN1	GCN1L1	27.94	28.65	28.33	*23.89*	*24.77*	*23.39*	43	21	81	3.16	4.29
37	Dolichyl-diphosphooligo-saccharide--protein glycosyltransferase subunit 1	RPN1	30.06	30.27	29.90	26.89	27.62	26.57	35	60	145	3.13	3.05
38	Tubulin beta-6 chain	TUBB6	25.40	26.06	26.05	*23.57*	*23.74*	*23.82*	45	73	103	3.12	2.13

39	U4/U6.U5 small nuclear ribonucleoprotein 27 kDa protein	SNRNP27	26.69	26.97	27.59	*23.43*	*23.73*	*24.33*	5	32	25	3.02	3.26
40	Uncharacterized protein C2orf47, mitochondrial	C2orf47	25.85	26.63	26.87	*23.69*	*23.29*	*23.77*	6	21	8	2.96	2.87
41	Transmembrane 9 superfamily member 2	TM9SF2	27.18	27.81	27.93	*24.52*	*23.57*	*24.67*	8	13	14	2.91	3.39
42	NADH dehydrogenase [ubiquinone] 1 beta subcomplex subunit 10	NDUFB10	26.27	26.80	26.55	*23.79*	*24.38*	*23.36*	4	22	7	2.90	2.70
43	Vacuole membrane protein 1	VMP1	27.15	28.52	27.12	*23.88*	*23.86*	*23.79*	3	9	7	2.90	3.75
44	Tubulin beta-3 chain	TUBB3	25.78	26.35	26.09	*23.36*	*23.73*	*24.18*	36	60	10	2.90	2.32
45	Cystine/glutamate transporter	SLC7A11	27.17	28.12	27.79	*23.14*	*24.51*	*23.76*	8	15	23	2.88	3.89
46	Glutaminase kidney isoform, mitochondrial	GLS	27.32	28.15	27.94	*22.60*	*23.81*	*24.17*	13	26	27	2.87	4.27
47	Carnitine O-palmitoyltransferase 1, liver isoform	CPT1A	25.98	26.13	26.22	*23.24*	*23.85*	*24.22*	15	26	30	2.87	2.34
48	Solute carrier family 2, facilitated glucose transporter member 1	SLC2A1	27.85	28.96	28.29	*23.33*	*24.91*	*23.82*	12	21	52	2.81	4.35
49	Lysophosphatidylcholine acyltransferase 1	LPCAT1	26.56	27.63	26.83	*23.85*	*23.53*	*24.37*	8	16	18	2.80	3.09

50	Very-long-chain 3-oxoacyl-CoA reductase	HSD17B12	25.19	25.56	26.01	*23.88*	*23.61*	*23.71*	8	35	13	2.77	1.85
51	DNA mismatch repair protein Msh2	MSH2	27.36	28.06	27.99	*22.96*	*24.56*	*24.10*	26	34	62	2.77	3.93
52	NAD(P) transhydrogenase, mitochondrial	NNT	27.91	30.01	28.82	*22.96*	*24.20*	*23.88*	36	34	127	2.74	5.23
53	Tubulin beta chain	TUBB	32.29	32.36	33.17	29.46	30.25	30.04	53	80	344	2.73	2.69
54	Calcium-binding mitochondrial carrier protein Aralar2	SLC25A13	26.56	26.71	27.20	*22.69*	*23.70*	*24.12*	20	41	36	2.69	3.32
55	Proteasome-associated protein ECM29 homolog	ECM29	25.77	26.80	26.53	*23.61*	*23.27*	*24.05*	16	11	29	2.69	2.72
56	ER membrane protein complex subunit 1	EMC1	24.81	25.42	25.49	*23.46*	*22.78*	*23.23*	8	11	8	2.68	2.08
57	Signal recognition particle receptor subunit beta	SRPRB	27.02	27.68	27.49	*23.34*	*23.63*	*24.81*	7	27	31	2.68	3.47
58	Nuclear pore complex protein Nup93	NUP93	25.90	26.40	26.82	*23.73*	*23.47*	*24.29*	13	18	24	2.68	2.54
59	Dual specificity mitogen-activated protein kinase kinase 3	MAP2K3	27.01	27.74	27.72	*21.83*	*23.23*	*23.84*	15	38	45	2.67	4.52
60	Sodium/potassium-transporting ATPase subunit alpha-1	ATP1A1	26.59	27.55	27.34	*24.44*	*24.99*	*24.21*	35	41	188	2.67	2.61

61	60S ribosomal protein L27	RPL27	28.09	26.99	27.52	*22.57*	*24.24*	*23.73*	2	27	6	2.62	4.02
62	Voltage-dependent anion-selective channel protein 2	VDAC2	26.25	26.71	26.08	*23.68*	*24.55*	*24.32*	7	30	17	2.60	2.16
63	Activated RNA polymerase II transcriptional coactivator p15	SUB1	30.61	30.98	31.28	*24.33*	26.79	*24.15*	17	79	230	2.60	5.87
64	Tubulin alpha-1C chain	TUBA1C	26.99	27.67	27.54	*22.60*	*24.31*	*23.97*	54	80	22	2.59	3.77
65	60S ribosomal protein L9	RPL9	26.26	25.87	25.74	27.31	27.58	27.10	5	41	20	2.56	-1.37
66	Prelamin-A/C;Lamin-A/C	LMNA	27.24	26.65	26.64	28.86	28.26	28.98	15	23	44	2.47	-1.86
67	Elongation factor Tu, mitochondrial	TUFM	28.05	27.90	28.19	28.58	28.61	28.55	21	48	108	2.47	-0.53
68	Protein unc-45 homolog A	UNC45A	26.76	27.25	27.05	*23.98*	*23.08*	*24.73*	23	30	46	2.47	3.09
69	Importin-5	IPO5	26.42	27.18	27.05	*23.25*	*24.69*	*23.67*	23	27	61	2.46	3.02
70	FACT complex subunit SSRP1	SSRP1	27.25	27.62	28.27	*22.63*	*24.67*	*23.65*	6	13	10	2.45	4.06
71	Ras-related protein Rab-27A	RAB27A	37.14	37.37	37.45	35.38	34.43	35.56	61	99	4265	2.42	2.19
72	Leucine-rich PPR motif-containing protein, mitochondrial	LRPPRC	28.51	28.97	29.16	*23.35*	25.79	*24.32*	36	33	76	2.41	4.39

73	GTP-binding nuclear protein Ran	RAN	27.46	27.11	27.12	29.31	30.41	29.19	13	49	48	2.40	-2.40
74	Translocon-associated protein subunit delta	SSR4	26.23	27.04	26.91	*22.21*	*23.73*	*23.92*	7	43	30	2.35	3.44
75	Acyl-CoA desaturase	SCD	25.71	26.53	27.04	*23.19*	*22.40*	*23.84*	5	18	9	2.35	3.28
76	Nuclear pore membrane glycoprotein 210	NUP210	*22.56*	*23.47*	*22.54*	26.95	25.24	26.25	2	1	4	2.31	-3.29
77	STE20/SPS1-related proline-alanine-rich protein kinase	STK39	25.26	25.69	25.95	*23.41*	*24.15*	*24.09*	3	10	6	2.30	1.75
78	Structural maintenance of chromosomes protein 4	SMC4	26.37	26.07	26.15	*24.94*	*24.26*	*23.85*	4	4	5	2.29	1.85
79	Tubulin alpha-4A chain	TUBA4A	30.63	31.36	31.07	28.36	28.47	29.45	49	68	118	2.29	2.26
80	Monocarboxylate transporter 4	SLC16A3	28.46	28.54	29.05	*21.83*	24.05	24.85	13	23	45	2.29	5.11
81	Multidrug resistance-associated protein 1	ABCC1	25.84	26.50	26.06	*22.60*	*24.13*	*23.64*	14	14	24	2.26	2.67
82	Glutamate--cysteine ligase regulatory subunit	GCLM	26.46	26.98	26.69	*23.56*	*24.85*	*23.21*	7	30	27	2.26	2.84
83	Epidermal growth factor receptor	EGFR	25.41	25.74	25.80	*23.75*	*24.62*	*24.04*	6	7	12	2.23	1.52
84	Calcium uniporter protein, mitochondrial	MCU	25.63	26.64	25.84	*22.64*	*23.95*	*23.61*	8	26	15	2.22	2.64

85	Reticulocalbin-2	RCN2	26.02	26.25	26.16	*22.70*	*24.29*	*23.83*	5	22	11	2.21	2.53
86	Peptidyl-prolyl cis-trans isomerase FKBP11	FKBP11	*24.03*	*23.63*	*23.27*	26.29	*25.36*	26.82	2	10	3	2.20	-2.52
87	ATP-dependent 6-phosphofructokinase, platelet type	PFKP	27.49	28.72	28.18	*23.69*	25.67	*24.08*	32	40	166	2.19	3.65
88	ADP/ATP translocase 2;ADP/ATP translocase 2, N-terminally processed	SLC25A5	28.03	29.33	28.55	26.07	24.01	*24.74*	22	63	54	2.19	3.70
89	Nucleolin	NCL	26.17	26.35	26.37	26.85	27.24	27.37	11	17	19	2.14	-0.86
90	Exportin-2	CSE1L	29.50	29.81	29.76	27.80	25.83	26.71	43	46	151	2.14	2.91
91	ATP synthase subunit alpha, mitochondrial	ATP5A1	30.44	31.03	30.79	28.56	29.59	28.98	38	62	245	2.11	1.71
92	Importin-4	IPO4	25.40	25.92	25.62	*23.86*	*24.66*	*24.34*	9	12	16	2.11	1.36
93	ATP-dependent 6-phosphofructokinase, muscle type	PFKM	26.69	27.89	28.10	25.43	25.15	*24.38*	23	31	61	2.06	2.57
94	Pachytene checkpoint protein 2 homolog	TRIP13	30.04	29.98	29.94	*23.90*	26.11	26.95	31	69	143	2.05	4.34
95	High mobility group protein B1; Putative high mobility group protein B1-like 1	HMGB1; HMGB1P1	28.09	29.03	28.58	25.53	25.89	*23.55*	17	47	84	2.00	3.58

B1 vs C1

			Log$_2$ (LFQ intensity)									Student t-test	
			B1			C1							
	Protein names	Gene	4	5	6	7	8	9	#Pep	Cov [%]	#MS/ MS	-Log p	Diff
1	Ras GTPase-activating-like protein IQGAP1	IQGAP1	26.65	27.18	27.55	*22.75*	*23.09*	*23.10*	8	4.8	17	3.89	4.15
2	Clathrin heavy chain 1	CLTC	26.66	27.85	26.55	*24.25*	*23.20*	*23.63*	12	11	16	2.52	3.32
3	Activated RNA polymerase II transcriptional coactivator p15	SUB1	*23.40*	26.79	*22.92*	31.67	31.36	30.79	17	78.7	230	2.29	-6.90
4	Nuclear pore membrane glycoprotein 210	NUP210	26.95	25.24	26.25	*23.18*	*22.80*	*23.59*	2	1.3	4	2.25	2.95
5	60S ribosomal protein L30	RPL30	26.21	28.02	26.04	*22.39*	*22.94*	*23.58*	2	26.1	7	2.20	3.78
6	Epiplakin	EPPK1	26.43	26.73	27.31	*23.37*	*24.72*	*22.65*	10	15.5	13	2.10	3.25
7	Importin subunit beta-1	KPNB1	26.27	27.49	26.00	*24.54*	*24.06*	*23.62*	19	23.4	51	2.05	2.51
8	EH domain-containing protein 2	EHD2	*24.05*	24.23	24.25	*22.89*	*23.44*	*23.44*	14	34.4	24	2.03	0.92

A1 vs C1

			Log2 (LFQ intensity)									Student t-test	
			A1			C1							
	Protein names	Gene	1	2	3	7	8	9	#Pep	Cov [%]	#MS/MS	-Log p	Diff
1	ATP-binding cassette sub-family F member 3	ABCF3	26.18	26.36	26.23	*23.28*	*23.34*	*23.46*	6	13	10	5.57	2.90
2	Transportin-1	TNPO1	28.60	29.05	28.93	*22.55*	*22.73*	*22.97*	21	24	51	5.33	6.11
3	Translational activator GCN1	GCN1L1	27.94	28.65	28.33	*23.12*	*23.32*	*23.28*	43	21	81	4.72	5.07
4	ATP-dependent Clp protease ATP-binding subunit clpX-like, mitochondrial	CLPX	27.41	27.86	27.76	*23.48*	*23.54*	*23.84*	8	13	51	4.66	4.06
5	Coatomer subunit gamma-1	COPG1	27.83	28.41	28.44	*23.20*	*23.42*	*23.04*	33	39	113	4.59	5.01
6	T-complex protein 1 subunit alpha	TCP1	26.23	26.06	26.51	*22.67*	*22.99*	*22.89*	7	17	14	4.51	3.42
7	60S ribosomal protein L38	RPL38	28.65	28.81	28.47	*22.68*	*23.53*	*22.87*	6	59	24	4.46	5.62
8	Sarcoplasmic/endoplasmic reticulum calcium ATPase 2	ATP2A2	28.51	28.83	29.05	*22.94*	*23.68*	*23.62*	22	24	83	4.33	5.38
9	Serine/threonine-protein kinase mTOR	MTOR	30.09	30.79	30.81	*22.92*	*23.92*	*22.95*	3	1	5	4.26	7.30
10	Acetyl-CoA carboxylase 1; Biotin carboxylase	ACACA	27.07	27.58	27.57	*23.17*	*23.18*	*23.65*	33	18	71	4.21	4.07
11	Voltage-dependent anion-selective channel protein 3	VDAC3	28.58	29.10	28.78	*24.37*	*23.59*	*24.12*	13	49	55	4.20	4.79
12	Exportin-T	XPOT	26.72	27.32	27.01	*23.12*	*23.53*	*23.20*	16	20	31	4.19	3.73
13	Transmembrane 9 superfamily member 2	TM9SF2	27.18	27.81	27.93	*23.51*	*23.54*	*23.64*	8	13	14	4.17	4.07

14	Importin subunit beta-1	KPNB1	26.54	26.63	26.45	*22.94*	*23.50*	*23.47*	19	23	51	4.15	3.24
15	NAD(P)H dehydrogenase [quinone] 1	NQO1	26.59	26.04	26.44	*23.22*	*23.04*	*23.42*	7	25	12	4.04	3.13
16	UDP-glucose 6-dehydrogenase	UGDH	26.31	26.21	26.31	*23.74*	*23.17*	*23.20*	7	18	8	4.01	2.91
17	Calcium-binding mitochondrial carrier protein Aralar2	SLC25A13	26.56	26.71	27.20	*23.54*	*23.56*	*23.77*	20	41	36	3.99	3.20
18	Phosphate carrier protein, mitochondrial	SLC25A3	28.02	28.66	29.05	*22.28*	*23.10*	*22.62*	11	25	51	3.99	5.91
19	Microsomal glutathione S-transferase 1	MGST1	26.42	26.98	26.67	*23.27*	*23.36*	*23.71*	4	25	8	3.97	3.24
20	Leucine-rich PPR motif-containing protein, mitochondrial	LRPPRC	28.51	28.97	29.16	*22.47*	*22.33*	*23.47*	36	33	76	3.95	6.12
21	Basic leucine zipper and W2 domain-containing protein 1	BZW1	27.89	28.21	27.95	*23.12*	*24.06*	*23.28*	13	34	33	3.91	4.53
22	Pachytene checkpoint protein 2 homolog	TRIP13	30.04	29.98	29.94	*24.38*	*24.43*	*23.16*	31	69	143	3.87	6.00
23	Carnitine O-palmitoyltransferase 1, liver isoform	CPT1A	25.98	26.13	26.22	*22.73*	*23.39*	*23.22*	15	26	30	3.85	2.99
24	DNA mismatch repair protein Msh2	MSH2	27.36	28.06	27.99	*23.94*	*23.66*	*23.22*	26	34	62	3.78	4.19
25	Multidrug resistance-associated protein 1	ABCC1	25.84	26.50	26.06	*22.57*	*23.08*	*22.61*	14	14	24	3.74	3.38
26	Tubulin beta-3 chain	TUBB3	25.78	26.35	26.09	*22.82*	*23.36*	*22.89*	36	60	10	3.69	3.05
27	Vesicle-fusing ATPase	NSF	27.56	27.95	28.52	*22.88*	*23.66*	*22.75*	24	38	50	3.60	4.91
28	Cystine/glutamate transporter	SLC7A11	27.17	28.12	27.79	*23.90*	*24.23*	*24.12*	8	15	23	3.59	3.61

29	Tubulin alpha-1C chain	TUBA1C	26.99	27.67	27.54	*23.06*	*23.86*	*23.08*	54	80	22	3.57	4.07
30	Putative tubulin-like protein alpha-4B	TUBA4B	29.02	29.53	30.52	*23.11*	*24.02*	*23.40*	11	23	10	3.56	6.18
31	D-3-phosphoglycerate dehydrogenase	PHGDH	29.41	29.77	30.22	26.63	26.28	26.75	30	65	154	3.55	3.24
32	60S ribosomal protein L27	RPL27	28.09	26.99	27.52	*23.72*	*23.25*	*23.16*	2	27	6	3.50	4.16
33	DNA-dependent protein kinase catalytic subunit	PRKDC	28.23	29.37	28.19	*23.11*	*22.85*	*23.75*	48	15	99	3.47	5.36
34	Protein unc-45 homolog A	UNC45A	26.76	27.25	27.05	*23.39*	*23.41*	*22.46*	23	30	46	3.47	3.93
35	Solute carrier family 2, facilitated glucose transporter member 1	SLC2A1	27.85	28.96	28.29	*22.95*	*23.54*	*23.97*	12	21	52	3.44	4.88
36	Signal peptidase complex subunit 3	SPCS3	26.03	26.33	25.71	*23.08*	*22.64*	*23.33*	7	39	13	3.44	3.01
37	STE20/SPS1-related proline-alanine-rich protein kinase	STK39	25.26	25.69	25.95	*23.25*	*22.94*	*23.24*	3	10	6	3.42	2.49
38	T-complex protein 1 subunit gamma	CCT3	26.70	26.69	27.05	*23.02*	*23.09*	*23.97*	14	30	40	3.34	3.46
39	Protein transport protein Sec61 subunit alpha isoform 1; Protein transport protein Sec61 subunit alpha isoform 2	SEC61A1 ; SEC61A2	27.99	29.36	28.46	*23.65*	*24.32*	*23.85*	14	33	30	3.32	4.66
40	Epidermal growth factor receptor	EGFR	25.41	25.74	25.80	*22.95*	*23.56*	*23.46*	6	7	12	3.32	2.33
41	Glutaminase kidney isoform, mitochondrial	GLS	27.32	28.15	27.94	*23.46*	*24.13*	*22.99*	13	26	27	3.31	4.27
42	Cyclin-dependent kinase 1	CDK1	26.57	26.78	26.73	*22.95*	*23.90*	*22.88*	17	60	54	3.30	3.45
43	Uncharacterized protein C2orf47, mitochondrial	C2orf47	25.85	26.63	26.87	*22.94*	*22.73*	*23.25*	6	21	8	3.27	3.47

44	Calpain-2 catalytic subunit	CAPN2	26.18	26.69	26.88	*22.40*	*22.07*	*23.23*	6	12	9	3.24	4.02
45	EH domain-containing protein 4	EHD4	27.67	28.38	28.16	*21.84*	*23.08*	*23.51*	18	36	47	3.20	5.25
46	Coatomer subunit beta	COPB1	28.39	29.09	28.88	*23.35*	*23.67*	*24.86*	36	45	150	3.18	4.83
47	Translation machinery-associated protein 7	TMA7	29.05	29.21	30.41	*24.13*	*23.27*	*22.34*	5	64	39	3.14	6.31
48	Importin-7	IPO7	26.56	27.08	27.05	*22.75*	*22.49*	*23.75*	13	14	33	3.13	3.90
49	Translocon-associated protein subunit delta	SSR4	26.23	27.04	26.91	*23.94*	*23.37*	*23.09*	7	43	30	3.11	3.26
50	ATP-dependent 6-phosphofructokinase, platelet type	PFKP	27.49	28.72	28.18	*23.43*	*23.30*	*24.34*	32	40	166	3.11	4.44
51	Surfeit locus protein 4	SURF4	26.38	26.46	26.56	*22.13*	*23.33*	*23.25*	3	14	10	3.11	3.57
52	Transketolase	TKT	26.55	26.16	26.18	28.06	27.85	28.38	18	37	46	3.09	-1.80
53	HLA class I histocompatibility antigen, alpha chains	HLA-A	25.67	26.40	26.32	*23.34*	*23.44*	*23.90*	6	23	15	3.05	2.57
54	Long-chain-fatty-acid--CoA ligase 3	ACSL3	27.79	28.40	27.25	*23.46*	*23.70*	*22.40*	27	46	52	3.05	4.62
55	Kinesin-like protein KIF23	KIF23	26.90	26.08	25.99	*23.70*	*23.65*	*23.84*	5	7	9	3.03	2.59
56	Calcium-binding mitochondrial carrier protein SCaMC-1	SLC25A24	28.51	27.52	28.22	*24.15*	*22.50*	*23.12*	8	18	16	3.00	4.83
57	Tubulin beta-4B chain	TUBB4B	33.78	34.33	34.35	32.14	31.49	32.01	58	84	1246	2.95	2.28
58	FACT complex subunit SSRP1	SSRP1	27.25	27.62	28.27	*23.71*	*24.73*	*23.64*	6	13	10	2.88	3.69
59	Signal recognition particle receptor subunit beta	SRPRB	27.02	27.68	27.49	*22.78*	*23.27*	*24.35*	7	27	31	2.84	3.93
60	Nuclear pore complex protein Nup93	NUP93	25.90	26.40	26.82	*23.33*	*22.85*	*23.83*	13	18	24	2.84	3.04

61	Acylglycerol kinase, mitochondrial	AGK	26.44	27.11	26.68	*22.81*	*24.04*	*23.69*	6	19	13	2.84	3.23
62	Vacuole membrane protein 1	VMP1	27.15	28.52	27.12	*22.06*	*22.87*	*23.46*	3	9	7	2.83	4.80
63	Monocarboxylate transporter 4	SLC16A3	28.46	28.54	29.05	*22.87*	24.61	*24.59*	13	23	45	2.82	4.67
64	Aldehyde dehydrogenase X, mitochondrial	ALDH1B1	26.09	26.72	26.68	*22.32*	*22.54*	*23.71*	6	14	12	2.80	3.64
65	Structural maintenance of chromosomes protein 4	SMC4	26.37	26.07	26.15	*23.91*	*22.99*	*22.60*	4	4	5	2.79	3.03
66	Lysophosphatidylcholine acyltransferase 1	LPCAT1	26.56	27.63	26.83	*22.56*	*23.97*	*22.92*	8	16	18	2.72	3.85
67	Calcium uniporter protein, mitochondrial	MCU	25.63	26.64	25.84	*22.47*	*22.59*	*23.47*	8	26	15	2.72	3.19
68	Proteasome-associated protein ECM29 homolog	ECM29	25.77	26.80	26.53	*22.87*	*23.64*	*23.73*	16	11	29	2.69	2.95
69	Propionyl-CoA carboxylase alpha chain, mitochondrial	PCCA	*23.85*	*23.21*	*24.44*	28.45	27.04	27.56	8	13	19	2.68	-3.85
70	Exportin-2	CSE1L	29.50	29.81	29.76	*23.28*	25.50	25.32	43	46	151	2.65	4.99
71	T-complex protein 1 subunit zeta	CCT6A	27.59	27.13	26.85	*23.58*	*22.03*	*23.75*	11	27	17	2.64	4.07
72	Importin-5	IPO5	26.42	27.18	27.05	*24.33*	*23.88*	*24.86*	23	27	61	2.64	2.53
73	CAD protein; Glutamine-dependent carbamoyl-phosphate synthase; Aspartate carbamoyltransferase; Dihydroorotase	CAD	26.60	26.20	26.11	*23.62*	*22.49*	*21.90*	17	13	24	2.64	3.64
74	Acyl-CoA desaturase	SCD	25.71	26.53	27.04	*23.50*	*23.28*	*23.83*	5	18	9	2.63	2.89
75	Signal peptidase complex subunit 2	SPCS2	27.90	28.76	28.88	*23.99*	*24.30*	*22.14*	13	58	51	2.61	5.04

76	ATPase family AAA domain-containing protein 3A	ATAD3A	27.17	26.63	26.65	*24.30*	*22.71*	*23.53*	10	19	20	2.60	3.30
77	Tubulin alpha-1B chain	TUBA1B	34.99	35.65	35.57	32.62	31.34	32.66	57	80	1029	2.57	3.19
78	Mitochondrial import receptor subunit TOM40 homolog	TOMM40	26.38	27.52	27.21	*24.50*	*23.87*	*24.63*	13	37	32	2.55	2.71
79	Epiplakin	EPPK1	26.86	26.53	27.83	*23.87*	*22.36*	*23.38*	10	16	13	2.55	3.87
80	Putative elongation factor 1-alpha-like 3; Elongation factor 1-alpha 1	EEF1A1P5; EEF1A1	32.38	32.58	32.22	31.51	31.12	30.95	33	63	421	2.46	1.20
81	Serine/arginine-rich splicing factor 1	SRSF1	26.64	27.29	26.89	28.47	28.76	28.19	12	43	73	2.44	-1.53
82	GTP-binding nuclear protein Ran	RAN	27.46	27.11	27.12	30.37	29.03	30.17	13	49	48	2.42	-2.62
83	Cytochrome b-c1 complex subunit 2, mitochondrial	UQCRC2	29.32	30.55	29.90	*23.36*	*22.51*	25.66	22	72	99	2.42	6.08
84	Importin-4	IPO4	25.40	25.92	25.62	*23.96*	*23.87*	*23.01*	9	12	16	2.42	2.03
85	Lamina-associated polypeptide 2	TMPO	25.36	24.91	25.35	*23.76*	*22.92*	*22.72*	4	11	8	2.38	2.07
86	ATP-dependent 6-phosphofructokinase, muscle type	PFKM	26.69	27.89	28.10	*24.68*	*24.60*	*23.61*	23	31	61	2.38	3.26
87	Voltage-dependent anion-selective channel protein 2	VDAC2	26.25	26.71	26.08	*24.39*	*23.01*	*23.82*	7	30	17	2.37	2.60
88	Pyruvate kinase PKM	PKM	29.28	28.63	28.64	30.85	30.52	30.17	38	54	265	2.34	-1.66
89	Elongation factor 1-gamma	EEF1G	27.35	26.87	27.11	26.07	26.25	26.32	12	28	33	2.33	0.89
90	Eukaryotic translation initiation factor 5A-1	EIF5A	*24.26*	26.18	*24.23*	28.27	29.05	29.25	7	48	28	2.30	-3.97
91	Eukaryotic initiation factor 4A-I	EIF4A1	27.97	27.33	27.61	30.49	29.24	30.17	24	55	128	2.29	-2.33
92	Unconventional myosin-Ic	MYO1C	28.64	26.49	26.80	*23.93*	*23.10*	*23.20*	13	16	17	2.25	3.90

93	U4/U6.U5 small nuclear ribonucleoprotein 27 kDa protein	SNRNP27	26.69	26.97	27.59	*23.82*	*23.03*	*24.85*	5	32	25	2.25	3.19
94	Coatomer subunit alpha; Xenin; Proxenin	COPA	27.10	26.45	27.45	*22.69*	*23.23*	*24.66*	19	20	41	2.22	3.48
95	ATP synthase subunit alpha, mitochondrial	ATP5A1	30.44	31.03	30.79	27.22	28.37	28.78	38	62	245	2.21	2.63
96	40S ribosomal protein S7	RPS7	26.99	25.57	26.08	*23.88*	*23.95*	*23.17*	7	51	13	2.20	2.55
97	Ataxin-10	ATXN10	26.77	27.43	27.46	*22.47*	*23.99*	*24.63*	9	24	26	2.18	3.52
98	ATP synthase subunit gamma, mitochondrial	ATP5C1	25.88	26.38	26.94	*22.81*	*24.26*	*23.88*	8	31	16	2.18	2.75
99	Bifunctional purine biosynthesis protein PURH; Phosphoribosylaminoimidazolecarboxamide formyltransferase; IMP cyclohydrolase	ATIC	24.45	24.68	*23.88*	*23.18*	*23.15*	*22.89*	8	18	8	2.10	1.26
100	Sodium/potassium-transporting ATPase subunit alpha-1	ATP1A1	26.59	27.55	27.34	*23.38*	*25.08*	*24.54*	35	41	188	2.09	2.82
101	Glyceraldehyde-3-phosphate dehydrogenase	GAPDH	30.92	29.89	29.96	31.97	31.86	31.82	34	77	212	2.07	-1.63
102	Tubulin beta chain	TUBB	32.29	32.36	33.17	30.81	29.35	30.30	53	80	344	2.06	2.45
103	Methionine--tRNA ligase, cytoplasmic	MARS	26.21	*24.93*	26.71	*23.14*	*23.66*	*23.33*	17	25	43	2.02	2.57
104	T-complex protein 1 subunit epsilon	CCT5	24.83	24.71	24.85	*23.84*	*22.73*	*23.33*	4	11	5	2.01	1.50
105	Geranylgeranyl transferase type-2 subunit beta	RABGGTB	25.53	25.96	25.51	*24.23*	*23.73*	*24.69*	3	14	7	2.01	1.45

D vs E

			Log2 (LFQ intensity)									Student t-test	
			D			E							
	Protein names	Gene	1	2	3	4	5	6	#Pep	Cov [%]	#MS/MS	-Log p	Diff
1	Mitochondrial import inner membrane translocase subunit Tim23	TIMM23	25.27	25.32	25.40	*22.31*	*21.99*	*22.30*	4	37	8	5.03	3.13
2	Multidrug resistance-associated protein 1	ABCC1	27.18	27.19	27.39	*21.76*	*21.62*	*22.23*	14	14	24	4.97	5.38
3	V-type proton ATPase subunit H	ATP6V1H	25.41	25.18	25.21	*22.98*	*23.11*	*22.99*	4	11	8	4.96	2.24
4	Serine/arginine-rich splicing factor 1	SRSF1	24.41	24.13	23.84	28.48	28.36	28.32	12	43	73	4.82	-4.26
5	Serine/arginine-rich splicing factor 6	SRSF6	*22.54*	*22.19*	*22.15*	27.78	27.47	27.17	3	11	6	4.77	-5.18
6	Exportin-T	XPOT	26.21	26.27	26.06	*22.36*	*22.60*	*22.08*	16	20	31	4.72	3.83
7	Mitochondrial import receptor subunit TOM40 homolog	TOMM40	26.60	26.15	26.13	*22.80*	*22.61*	*22.64*	13	37	32	4.60	3.61
8	Ribonucleoside-diphosphate reductase large subunit	RRM1	25.65	25.89	25.52	*23.03*	*22.76*	*22.84*	8	14	10	4.49	2.81
9	ATP synthase subunit f, mitochondrial	ATP5J2	26.46	26.34	26.61	*21.61*	*22.39*	*22.16*	2	26	21	4.24	4.42

10	Signal peptidase complex subunit 3	SPCS3	26.70	26.72	26.36	*22.46*	*21.86*	*22.54*	7	39	13	4.21	4.31
11	Extended synaptotagmin-2	ESYT2	26.22	25.98	26.51	*22.31*	*22.56*	*22.81*	8	12	19	4.20	3.67
12	Cystine/glutamate transporter	SLC7A11	26.21	25.91	25.56	*22.73*	*22.55*	22.61	8	15	23	4.12	3.26
13	Heterogeneous nuclear ribonucleoprotein A1;Heterogeneous nuclear ribonucleoprotein A1, N-terminally processed	HNRNPA1	*22.47*	*22.23*	*22.02*	25.53	25.88	25.33	8	23	19	4.08	-3.34
14	ATP-citrate synthase	ACLY	25.73	25.50	25.63	*23.04*	*22.59*	*22.50*	16	19	28	4.06	2.91
15	Calcium-binding mitochondrial carrier protein SCaMC-1	SLC25A24	25.85	25.91	25.97	*22.67*	*23.29*	*22.97*	8	18	16	4.05	2.93
16	Tricarboxylate transport protein, mitochondrial	SLC25A1	26.06	25.48	25.59	*22.33*	*22.17*	*21.79*	4	14	12	3.94	3.61
17	Serine/arginine-rich splicing factor 10	SRSF10	*21.93*	*21.86*	*22.10*	27.22	26.19	26.48	6	24	13	3.92	-4.67
18	NADH dehydrogenase [ubiquinone] 1 alpha subcomplex subunit 9, mitochondrial	NDUFA9	25.35	25.35	25.93	*22.34*	*22.41*	*22.05*	5	17	5	3.89	3.28
19	Importin-7	IPO7	26.66	26.90	27.39	*22.95*	23.31	23.44	13	14	33	3.88	3.75
20	Proteasome subunit alpha type-7; Proteasome subunit alpha type-7-like	PSMA7; PSMA8	24.11	24.32	24.12	*22.08*	*21.60*	*21.61*	3	19	7	3.84	2.42
21	Serine/arginine-rich splicing factor 3	SRSF3	28.99	28.81	29.03	31.58	31.79	31.21	16	52	192	3.84	-2.58
22	Rab GDP dissociation	GDI2; GDI1	*23.30*	*22.17*	*22.96*	28.51	27.83	28.20	11	32	18	3.80	-5.37

	inhibitor beta;Rab GDP dissociation inhibitor alpha												
23	Translational activator GCN1	GCN1L1	28.41	28.68	28.99	*23.26*	23.33	24.28	43	21	81	3.79	5.07
24	EH domain-containing protein 2	EHD2	26.20	26.15	26.94	*22.71*	*22.63*	*22.91*	14	34	24	3.78	3.68
25	Uridine-cytidine kinase 2	UCK2	25.76	25.53	25.73	*22.30*	*21.60*	*22.40*	5	28	12	3.78	3.57
26	Transportin-1	TNPO1	27.46	27.41	26.43	*22.60*	*22.29*	*22.32*	21	24	51	3.75	4.70
27	RuvB-like 1	RUVBL1	27.00	26.90	27.43	*23.00*	*22.30*	*21.93*	10	28	25	3.73	4.70
28	Proteasome-associated protein ECM29 homolog	ECM29	26.40	27.16	27.33	*22.65*	*22.04*	*22.67*	16	11	29	3.67	4.51
29	Peptidyl-prolyl cis-trans isomerase B	PPIB	28.65	28.22	28.05	*23.28*	*22.44*	*21.85*	19	62	79	3.67	5.78
30	Heterogeneous nuclear ribonucleoprotein A0	HNRNPA0	25.43	26.04	25.35	*22.80*	*22.51*	*22.75*	5	19	10	3.62	2.92
31	Tubulin alpha-1C chain	TUBA1C	26.40	26.33	26.33	*21.90*	*22.99*	*22.47*	54	80	22	3.60	3.90
32	Fanconi anemia group I protein	FANCI	25.50	25.51	26.07	*22.73*	*22.92*	*23.16*	10	10	12	3.59	2.76
33	ADP/ATP translocase 2	SLC25A5	27.64	28.15	28.75	*22.84*	*22.09*	*23.17*	22	63	54	3.58	5.48
34	Dynein assembly factor 5, axonemal	DNAAF5	26.03	25.88	26.82	*22.79*	*22.63*	*22.64*	8	12	14	3.57	3.56
35	Glutathione S-transferase Mu 3	GSTM3	25.74	25.35	25.81	*22.57*	*21.81*	*22.49*	4	24	7	3.55	3.35
36	Cleavage and polyadenylation specificity factor subunit 5	NUDT21	*22.14*	*22.38*	*22.68*	25.11	25.12	24.67	2	13	3	3.55	-2.56
37	Tubulin beta-4B chain	TUBB4B	33.56	33.24	33.29	32.07	32.10	32.21	58	84	1246	3.51	1.23
38	Epidermal growth factor	EGFR	25.15	25.24	25.45	*23.48*	*23.63*	*23.17*	6	7	12	3.47	1.85

	receptor												
39	Serine/arginine-rich splicing factor 2	SRSF2	26.45	26.03	25.90	29.84	29.40	29.02	10	29	81	3.47	-3.29
40	Actin, cytoplasmic 1	ACTB	32.44	32.18	32.38	31.44	31.41	31.37	39	85	683	3.46	0.93
41	Rab proteins geranylgeranyl-transferase component A 1 and 2	CHM; CHML	*22.18*	*21.75*	*21.20*	26.56	25.60	26.19	2	4	6	3.43	-4.41
42	General transcription factor IIF subunit 1	GTF2F1	25.24	24.74	25.30	*22.93*	*23.01*	*22.68*	4	11	5	3.38	2.22
43	Myosin light polypeptide 6	MYL6	25.49	24.83	25.15	*22.15*	*21.52*	*21.25*	9	58	23	3.38	3.52
44	Eukaryotic initiation factor 4A-I	EIF4A1	27.11	26.75	26.87	30.10	29.48	29.32	24	55	128	3.32	-2.73
45	Protein QIL1	QIL1	26.19	26.26	27.11	*23.21*	*22.58*	*23.01*	2	36	7	3.30	3.59
46	ADP/ATP translocase 3	SLC25A6	30.49	30.55	30.80	28.39	27.89	28.59	22	63	132	3.28	2.32
47	Voltage-dependent anion-selective channel protein 3	VDAC3	29.19	28.83	28.68	*22.93*	*23.32*	24.58	13	49	55	3.27	5.30
48	ATP synthase subunit alpha, mitochondrial	ATP5A1	30.57	30.45	30.71	29.70	29.55	29.72	38	62	245	3.26	0.92
49	Cancer-related nucleoside-triphosphatase	NTPCR	26.05	25.44	26.55	*22.55*	*22.81*	*22.42*	5	38	9	3.25	3.42
50	Heat shock 70 kDa protein 1B; Heat shock 70 kDa protein 1A	HSPA1B; HSPA1A	25.81	25.26	25.26	27.41	27.25	27.32	18	35	27	3.24	-1.88
51	NAD(P)H dehydrogenase [quinone] 1	NQO1	24.78	24.74	25.15	*22.11*	*21.06*	*21.63*	7	25	12	3.24	3.29
52	Sodium/potassium-	ATP1A1	30.22	30.11	30.39	27.91	28.34	28.53	35	41	188	3.23	1.99

	transporting ATPase subunit alpha-1												
53	Splicing factor U2AF 35 kDa subunit	U2AF1	25.76	25.25	25.91	27.64	27.94	27.95	5	21	20	3.23	-2.21
54	DnaJ homolog subfamily A member 1	DNAJA1	27.33	27.44	27.49	*22.64*	*22.28*	*23.79*	8	29	24	3.22	4.51
55	Transmembrane protein 165	TMEM165	26.38	26.19	26.25	*23.40*	*22.75*	*22.16*	4	20	22	3.19	3.50
56	Mitofusin-1	MFN1	26.00	26.10	25.79	*22.95*	*22.44*	*21.70*	3	5	12	3.19	3.60
57	Importin-4	IPO4	25.86	26.60	25.53	*22.91*	*22.46*	*22.74*	9	12	16	3.19	3.30
58	Coatomer subunit alpha;Xenin;Proxenin	COPA	27.26	27.02	27.37	*23.70*	*22.26*	*22.50*	19	20	41	3.18	4.39
59	Histone H2A type 1	HIST1H2A	27.49	27.19	26.37	*22.83*	*21.80*	*22.85*	8	61	64	3.14	4.52
60	Succinate dehydrogenase [ubiquinone] flavoprotein subunit, mitochondrial	SDHA	24.70	24.98	24.19	26.75	26.69	26.67	7	13	20	3.07	-2.08
61	60 kDa heat shock protein, mitochondrial	HSPD1	28.24	28.08	28.36	29.37	29.20	29.54	25	49	123	3.07	-1.14
62	Splicing factor, proline- and glutamine-rich	SFPQ	*22.29*	*23.00*	*21.72*	25.71	26.29	26.40	4	6	9	3.05	-3.80
63	Ataxin-10	ATXN10	27.25	27.27	26.57	*22.89*	*22.81*	*21.41*	9	24	26	3.03	4.66
64	Vesicle-fusing ATPase	NSF	28.09	27.66	28.43	*23.59*	23.26	24.68	24	38	50	3.02	4.22
65	Sister chromatid cohesion protein PDS5 homolog A	PDS5A	24.85	24.73	25.17	*22.66*	*21.90*	*21.67*	5	5	11	3.02	2.84
66	Tubulin alpha-4A chain	TUBA4A	30.01	30.42	30.40	28.72	28.12	28.38	49	68	118	2.98	1.87
67	Cytochrome b-c1 complex subunit Rieske, mitochondrial; Cytochrome b-c1	UQCRFS1; UQCRFS1 P1	25.54	24.86	24.77	*22.55*	*21.70*	*22.20*	3	19	6	2.96	2.91

	complex subunit 11												
68	Fatty acid desaturase 2	FADS2	24.67	24.76	25.08	*22.85*	*22.03*	*21.98*	2	7	3	2.93	2.55
69	ATP synthase subunit g, mitochondrial	ATP5L	26.95	26.65	27.12	*23.75*	*22.37*	*23.56*	8	83	20	2.90	3.68
70	DNA-directed RNA polymerases I, II, and III subunit RPABC3	POLR2H	*21.69*	*21.19*	*22.36*	25.58	25.05	26.22	2	19	2	2.89	-3.87
71	Mitochondrial carrier homolog 1	MTCH1	25.38	25.14	25.53	*21.97*	*22.61*	*23.10*	3	11	9	2.89	2.79
72	Tubulin alpha-1B chain	TUBA1B	34.83	34.60	34.90	33.24	32.68	33.28	57	80	1029	2.88	1.71
73	Glutaryl-CoA dehydrogenase, mitochondrial	GCDH	25.77	25.47	26.02	*23.46*	*22.87*	*22.29*	7	26	9	2.82	2.88
74	Large neutral amino acids transporter small subunit 1	SLC7A5	28.16	27.60	27.86	25.58	25.73	26.27	13	21	60	2.80	2.01
75	Importin-9	IPO9	26.59	26.53	27.03	*22.12*	*21.43*	*23.34*	8	12	20	2.79	4.42
76	Phosphatidate cytidylyltransferase, mitochondrial	TAMM41	25.42	25.21	25.09	*23.01*	*21.70*	*22.16*	4	11	9	2.77	2.95
77	Dolichyl-diphosphooligosaccharide--protein glycosyltransferase subunit STT3A	STT3A	24.09	24.53	24.44	*22.42*	*22.14*	*21.46*	5	10	8	2.76	2.35
78	Heterogeneous nuclear ribonucleoprotein K	HNRNPK	27.20	26.81	26.77	28.17	28.13	28.50	17	39	71	2.75	-1.34
79	Monocarboxylate transporter 1	SLC16A1	26.55	26.59	26.98	24.53	24.54	25.23	6	10	18	2.70	1.94
80	Very-long-chain 3-oxoacyl-CoA reductase	HSD17B12	26.09	25.24	26.01	*22.18*	*22.51*	*23.35*	8	35	13	2.67	3.10

81	78 kDa glucose-regulated protein	HSPA5	29.62	29.12	29.79	31.54	31.17	31.04	34	50	156	2.65	-1.74
82	Importin-8	IPO8	25.07	25.35	24.82	*23.13*	*22.10*	*22.05*	4	5	8	2.65	2.65
83	Cleft lip and palate transmembrane protein 1-like protein	CLPTM1L	23.56	23.71	24.24	*22.27*	*22.47*	*22.29*	2	6	5	2.64	1.49
84	Exportin-1	XPO1	29.11	29.28	29.49	*22.94*	22.59	25.21	29	33	118	2.64	5.72
85	ATP synthase subunit O, mitochondrial	ATP5O	24.47	24.14	24.42	*22.68*	*21.92*	*22.69*	5	27	7	2.63	1.91
86	Tubulin alpha-1A chain;Tubulin alpha-3C/D chain; Tubulin alpha-3E chain	TUBA1A; TUBA3C; TUBA3E	26.04	25.54	26.61	*22.86*	*22.49*	*21.29*	55	80	37	2.61	3.85
87	Translation machinery-associated protein 7	TMA7	27.30	26.99	27.07	*23.49*	*21.82*	23.72	5	64	39	2.61	4.10
88	Mitochondrial import inner membrane translocase subunit TIM50	TIMM50	26.35	25.73	25.89	*23.32*	*21.63*	*22.40*	8	28	14	2.60	3.54
89	Protein transport protein Sec61 subunit alpha isoform 1; Protein transport protein Sec61 subunit alpha isoform 2	SEC61A1; SEC61A2	27.03	27.01	27.16	24.29	24.75	25.43	14	33	30	2.59	2.24
90	Armadillo repeat-containing protein 6	ARMC6	25.09	24.55	24.29	*22.50*	*21.79*	*22.61*	3	9	8	2.59	2.34
91	Elongation factor 2	EEF2	26.85	26.86	26.99	28.21	27.96	27.68	27	37	71	2.58	-1.05
92	Transketolase	TKT	25.15	24.96	24.68	27.19	26.73	26.36	18	37	46	2.57	-1.83
93	Transmembrane 9 superfamily member 2	TM9SF2	26.95	26.32	26.15	*22.89*	*24.14*	*23.67*	8	13	14	2.57	2.91
94	Replication factor C	RFC3	25.15	24.50	24.55	*23.18*	*23.07*	*22.61*	4	17	5	2.55	1.78

	subunit 3												
95	Coiled-coil domain-containing protein 47	CCDC47	25.25	24.99	25.55	*23.12*	*22.21*	*23.27*	5	17	8	2.55	2.40
96	Manganese-transporting ATPase 13A1	ATP13A1	24.43	24.88	25.00	*23.26*	*22.81*	*23.42*	4	4	6	2.50	1.61
97	Exportin-2	CSE1L	30.05	29.62	29.95	23.73	25.50	26.21	43	46	151	2.49	4.73
98	Dolichol-phosphate mannosyltransferase subunit 1	DPM1	25.52	26.02	26.52	*23.33*	*22.29*	*23.49*	5	21	12	2.48	2.98
99	Desmoglein-1	DSG1	23.97	24.49	24.77	26.06	26.16	25.80	11	12	32	2.46	-1.60
100	SRA stem-loop-interacting RNA-binding protein, mitochondrial	SLIRP	24.48	25.96	25.36	*21.75*	*22.68*	*21.79*	3	35	11	2.43	3.20
101	Acylglycerol kinase, mitochondrial	AGK	25.21	24.73	25.08	*23.26*	*22.45*	*23.39*	6	19	13	2.42	1.97
102	Methylcrotonoyl-CoA carboxylase subunit alpha, mitochondrial	MCCC1	26.10	25.75	26.05	27.08	26.85	27.38	9	17	23	2.41	-1.14
103	Heterogeneous nuclear ribonucleoproteins A2/B1	HNRNPA2 B1	*22.76*	*22.20*	*23.23*	25.51	24.82	24.75	8	26	28	2.40	-2.30
104	ATP-dependent RNA helicase DDX39A	DDX39A	30.02	29.69	29.84	29.23	29.29	29.28	26	52	115	2.40	0.59
105	Protein unc-45 homolog A	UNC45A	27.98	27.67	26.56	*23.23*	24.29	24.43	23	30	46	2.40	3.42
106	MICOS complex subunit MIC60	IMMT	23.60	23.82	23.53	*22.38*	*21.54*	*21.41*	3	6	4	2.39	1.87
107	DNA mismatch repair protein Msh2	MSH2	28.04	28.71	28.62	25.56	24.10	25.76	26	34	62	2.38	3.31
108	Glutaminase kidney isoform, mitochondrial	GLS	27.06	26.92	26.75	*24.00*	*21.51*	*22.28*	13	26	27	2.36	4.31

109	Microtubule-associated protein RP/EB family member 2	MAPRE2	25.30	24.62	25.09	*22.65*	*21.07*	*22.28*	2	12	3	2.36	3.00
110	Replication factor C subunit 4	RFC4	24.25	24.29	24.62	*23.10*	*22.48*	*22.09*	3	12	6	2.35	1.83
111	Calcium uniporter protein, mitochondrial	MCU	25.24	25.19	26.21	*23.35*	*22.97*	*22.22*	8	26	15	2.34	2.70
112	Dolichyl-diphosphooligosaccharide--protein glycosyltransferase subunit 1	RPN1	29.88	29.70	29.73	27.07	27.13	28.28	35	60	145	2.34	2.28
113	ATP-dependent 6-phosphofructokinase, platelet type	PFKP	29.76	29.75	30.07	29.04	28.71	29.10	32	40	166	2.32	0.91
114	Elongation factor 1-gamma	EEF1G	26.30	26.19	26.45	25.41	25.62	25.10	12	28	33	2.31	0.93
115	Plasma membrane calcium-transporting ATPase 1 and 4	ATP2B1; ATP2B4	23.98	23.88	23.83	*23.03*	*22.39*	*22.89*	3	4	5	2.30	1.13
116	Heterogeneous nuclear ribonucleoprotein H	HNRNPH1	26.62	26.25	26.44	27.31	27.88	27.96	10	27	46	2.29	-1.28
117	High mobility group protein HMG-I/HMG-Y	HMGA1	25.40	24.95	25.71	26.80	27.67	27.67	6	51	31	2.28	-2.02
118	Long-chain-fatty-acid--CoA ligase 3	ACSL3	28.27	26.72	27.49	*23.14*	*21.83*	24.20	27	46	52	2.25	4.44
119	Exportin-7	XPO7	24.11	23.52	23.40	*22.54*	*22.48*	*22.48*	5	5	7	2.24	1.18
120	Importin subunit beta-1	KPNB1	28.02	27.90	28.45	26.37	25.82	26.81	19	23	51	2.24	1.79
121	Serpin H1	SERPINH1	25.55	25.43	25.30	26.88	26.57	27.53	15	45	32	2.23	-1.56
122	Up-regulated during skeletal muscle growth	USMG5	25.15	24.80	24.07	*22.53*	*22.11*	*22.94*	3	45	5	2.23	2.14

	protein 5												
123	Importin-5	IPO5	29.01	29.12	29.07	*21.20*	*22.67*	25.10	23	27	61	2.22	6.08
124	NADH-ubiquinone oxidoreductase 75 kDa subunit, mitochondrial	NDUFS1	24.79	24.55	24.29	*22.84*	*22.02*	*23.11*	2	5	3	2.22	1.89
125	Signal transducer and activator of transcription 1-alpha/beta	STAT1	27.21	27.88	27.83	24.51	24.81	25.93	17	27	42	2.22	2.56
126	Basic leucine zipper and W2 domain-containing protein 2	BZW2	24.90	24.83	25.52	*23.04*	*21.21*	*21.96*	6	15	16	2.20	3.01
127	Voltage-dependent anion-selective channel protein 1	VDAC1	24.41	23.78	23.40	25.31	25.59	25.56	8	40	42	2.20	-1.62
128	Tubulin beta chain	TUBB	32.84	32.89	32.56	31.10	30.36	31.47	53	80	344	2.19	1.79
129	Coatomer subunit gamma-1	COPG1	29.24	29.08	29.15	27.07	27.62	28.10	33	39	113	2.19	1.56
130	Cytochrome b-c1 complex subunit 2, mitochondrial	UQCRC2	29.97	29.98	29.70	27.54	26.71	28.26	22	72	99	2.19	2.38
131	Stress-70 protein, mitochondrial	HSPA9	26.64	25.80	25.90	27.94	27.38	27.86	20	31	65	2.16	-1.61
132	Eukaryotic translation initiation factor 4 gamma 1	EIF4G1	24.23	23.80	24.15	*22.87*	*23.22*	*23.28*	7	7	12	2.15	0.94
133	Minor histocompatibility antigen H13	HM13	25.15	24.87	25.04	*23.35*	*21.70*	*21.78*	3	15	17	2.14	2.74
134	Tubulin-specific chaperone D	TBCD	27.16	26.63	27.29	*23.62*	24.00	25.29	12	13	32	2.13	2.73
135	Replication factor C subunit 5	RFC5	25.39	24.95	25.01	*21.49*	*22.92*	*23.09*	7	28	9	2.12	2.61

136	T-complex protein 1 subunit alpha	TCP1	25.26	24.75	24.19	*22.73*	*21.80*	*22.88*	7	17	14	2.11	2.26
137	Elongation factor Tu, mitochondrial	TUFM	26.73	27.15	27.21	28.84	28.43	28.01	21	48	108	2.11	-1.40
138	40S ribosomal protein S2	RPS2	23.95	24.59	24.17	*22.68*	*21.24*	*22.06*	6	17	17	2.10	2.25
139	Acetyl-CoA carboxylase 1; Biotin carboxylase	ACACA	28.47	28.49	28.66	24.36	25.43	26.55	33	18	71	2.09	3.09
140	Protein TBRG4	TBRG4	26.46	26.12	25.83	*23.12*	*23.53*	24.65	12	27	17	2.07	2.37
141	Sideroflexin-1	SFXN1	29.14	29.04	29.16	28.29	28.63	28.09	19	60	90	2.07	0.78
142	Actin, alpha cardiac muscle 1; Actin, alpha skeletal muscle	ACTC1; ACTA1	29.98	29.59	29.64	27.55	27.85	28.68	31	72	92	2.06	1.71
143	Heat shock cognate 71 kDa protein	HSPA8	28.42	27.76	27.60	29.51	29.22	29.09	30	46	141	2.06	-1.35
144	Dimethyladenosine transferase 2, mitochondrial	TFB2M	24.38	24.46	24.94	*22.05*	*23.21*	*22.93*	4	11	5	2.05	1.86
145	Dermcidin; Survival-promoting peptide; DCD-1	DCD	26.63	26.82	26.50	28.71	27.92	29.34	5	35	28	2.05	-2.00
146	Non-histone chromosomal protein HMG-17	HMGN2	27.20	26.96	26.33	22.65	23.72	24.75	3	37	10	2.05	3.12
147	ATP-dependent 6-phosphofructokinase, muscle type	PFKM	27.83	28.79	28.32	26.55	25.09	26.06	23	31	61	2.04	2.41
148	Transmembrane 9 superfamily member 3	TM9SF3	24.42	24.83	24.98	*22.70*	*23.65*	*22.64*	4	8	7	2.04	1.74
149	Coatomer subunit beta	COPB1	29.53	29.23	29.91	25.81	26.43	27.77	36	45	150	2.04	2.89
150	Surfeit locus protein 4	SURF4	25.06	26.56	26.15	*22.50*	*21.41*	*23.44*	3	14	10	2.03	3.47

151	Leucine-rich PPR motif-containing protein, mitochondrial	LRPPRC	28.70	28.11	28.65	*22.06*	*21.56*	25.29	36	33	76	2.02	5.52
152	Fatty acid synthase	FASN	24.76	24.73	25.23	26.23	25.69	26.26	19	10	32	2.02	-1.15
153	Signal peptidase complex subunit 2	SPCS2	27.52	27.12	27.55	24.50	25.71	25.81	13	58	51	2.01	2.06
154	Mitochondrial 2-oxoglutarate/malate carrier protein	SLC25A11	26.67	26.78	27.08	25.45	25.35	26.09	9	39	28	2.00	1.21

Appendix F: PEAKS Modified Peptides

The following abbreviations for common PTMs are used in the table:

- Ac -Acetylation (Protein N-term)
- Cbm - Carbamidomethylation
- Ox – Oxidation
- Phos – Phosphorylation
- Deam – Deamidation
- Dehyd – Dehydration
- #Spec – number of spectral counts

The tables are ordered by gene in alphabetical order. Full stops indicate sites of enzyme cleavage.

NitroXL (Sets A, A1, B, B1, C, C1)

	Gene	Peptide	#Spec	PTM & A-Score
1	ADT2	F.AK(+100.02)DFLAGGVAAAIS(+100.02)KTAVAPIERVK(+100.02)L.L	1	K2: SuccOH: 0.00 S14: SuccOH: 0.00 K25: SuccOH: 41.41
2	ADT2	L.AADVGK(+100.02)AGAEREF.R	2	K6: SuccOH: 80.35
3	ALDOA	L.AADESTGSIAK(+393.11)RL.Q	1	K11: MonoOH: 32.97
4	ALDOA	L.AADESTGSIAK(+100.02)RL.Q	4	K11: SuccOH: 29.32
5	ANXA2	Y.KT(+100.02)DLEK(+100.02)DIISDTSGDF.R	2	T2: SuccOH: 9.34 K6: SuccOH: 29.96
6	ARF5	W.DVGGQDK(+100.02)IRPL.W	1	K7: SuccOH: 50.87
7	ATPB	Y.MVGPIEEAVAK(+393.11)ADKLAEEHSS	1	K11: MonoOH: 28.36
8	COF1	M.A(+42.01)SGVAVSDGVIK(+100.02)VF.N	2	A1: Ac: 1000.00

				K12: SuccOH: 46.62
9	DEST	L.VGDVGVTITDPFK(+100.02)HF.V	2	K13: SuccOH: 25.11
10	DX39A	R.DFLLK(+100.02)PELLR.A	1	K5: SuccOH: 61.69
11	DX39B	R.DFLLK(+100.02)PELLR.A	1	K5: SuccOH: 61.69
12	G3P	R.GALQNIIPASTGAAK(+100.02)AVGK(+100.02)VIPELNGK.L	2	K15: SuccOH: 3.97 K19: SuccOH: 47.82
13	G3P	F.HGTVK(+100.02)AENGKL.V	1	K5: SuccOH: 22.85
14	G3P	Y.DDIKKVVK(+100.02)QASEGPL.K	1	K8: SuccOH: 28.36
15	G3P	M.G(+100.02)KVKVGVN(+.98)GF.G	1	G1: SuccOH: 8.14 N8: Deam (NQ): 1000.00
16	GRP78	L.VGGSTRIPK(+100.02)IQQL.V	1	K9: SuccOH: 32.94
17	HNRH1	F.VVK(+100.02)VRGLPW.S	2	K3: SuccOH: 26.31
18	HS90B	M.P(+100.02)EEVHHGEEEVETF.A	1	P1: SuccOH: 64.80
19	HSP7C	Y.GLDK(+100.02)KVGAERNVL.I	1	K4: SuccOH: 37.81
20	HSPB1	F.ESRAQLGGPEAAKSDETAAK(+100.02)	2	K20: SuccOH: 21.15
21	K1C17	R.TIVEEVQDGK(+100.02)VISSR.E	1	K10: SuccOH: 47.09
22	K22E	F.ASFIDK(+100.02)VRF.L	4	K6: SuccOH: 39.44
23	K2C1	F.ASFIDK(+100.02)VRF.L	4	K6: SuccOH: 39.44
24	K2C1B	F.ASFIDK(+100.02)VRF.L	4	K6: SuccOH: 39.44
25	K2C3	F.ASFIDK(+100.02)VRF.L	4	K6: SuccOH: 39.44
26	K2C5	F.ASFIDK(+100.02)VRF.L	4	K6: SuccOH: 39.44
27	K2C7	F.ASFIDK(+100.02)VRF.L	4	K6: SuccOH: 39.44
28	K2C8	F.ASFIDK(+100.02)VRF.L	4	K6: SuccOH: 39.44
29	KPYM	R.SVETLK(+100.02)EMIK.S	1	K6: SuccOH: 26.31
30	LDHB	L.TSVINQK(+100.02)LKDDEVAQL.K	1	K7: SuccOH: 41.83
31	MPCP	F.SVTLK(+100.02)EDGVRGL.A	3	K5: SuccOH: 39.97

32	NDKB	F.IAIK(+393.11)PDGVQRGL.V	1	K4: MonoOH: 32.97
33	NDKB	F.IAIK(+100.02)PDGVQRGL.V	2	K4: SuccOH: 38.16
34	PPIA	F.ELFADK(+393.11)VPKTAENF.R	1	K6: MonoOH: 44.84
35	PPIA	F.ELFADK(+100.02)VPKTAENF.R	1	K6: SuccOH: 53.53
36	PROF1	K.TFVNITPAEVGVLVGK(+100.02)DR.S	4	K16: SuccOH: 67.24
37	PROF1	L.VGK(+100.02)DRSSF.Y	1	K3: SuccOH: 24.24
38	QCR2	L.IGLGVSHPVLK(+100.02)QVAEQF.L	1	K11: SuccOH: 22.07
39	RACK1	W.DLEGK(+100.02)IIVDEL.K	1	K5: SuccOH: 22.37
40	RAN	F.HTNRGPIK(+100.02)F.N	1	K8: SuccOH: 59.64
41	RB27B	F.ITTVGIDFREK(+100.02)RVVY.N	4	K11: SuccOH: 38.03
42	RL27	Y.SVDIPLDK(+100.02)TVVNKDVF.R	1	K8: SuccOH: 23.10
43	RPN2	W.NVADVVIK(+393.11)FPEEEAPSTVL.S	2	K8: MonoOH: 38.64
44	RPN2	F.TPK(+393.11)QEIQHLF.R	1	K3: MonoOH: 25.66
45	RPN2	W.NVADVVIK(+100.02)FPEEEAPSTVL.S	2	K8: SuccOH: 38.64
46	RPN2	F.TPK(+100.02)QEIQHLF.R	1	K3: SuccOH: 28.86
47	RS27A	L.IFAGK(+100.02)QLEDGRTL.S	1	K5: SuccOH: 67.69
48	SFPQ	L.TTTPRPVIVEPLEQLDDEDGLPEK(+100.02)L.A	1	K24: SuccOH: 40.11
49	SRP14	M.V(+100.02)LLESEQFLTELTR.L	1	V1: SuccOH: 87.62
50	SRSF3	Y.VGNLGNN(+.98)GNK(+393.11)TELERAF.G	1	N7: Deam (NQ): 26.02 K10: MonoOH: 17.01
51	SRSF3	Y.VGNLGNN(+.98)GNK(+100.02)TELERAF.G	1	N7: Deam (NQ): 30.46 K10: SuccOH: 10.11
52	SRSF3	Y.VGNLGNNGNK(+100.02)TELERAF.G	1	K10: SuccOH: 24.44
53	SRSF3	R.VRVELSNGEK(+100.02)R.S	1	K10: SuccOH: 42.89
54	SRSF3	Y.VGNLGNNGNK(+100.02)T(-18.01)ELERAF.G	7	K10: SuccOH: 128.00 T11: Dehyd: 1000.00

55	SRSF7	Y.VGNLGTGAGK(+100.02)GELERAF.S	1	K10: SuccOH: 49.79
56	TBA1C	F.HPEQLITGK(+393.11)EDAANNY.A	2	K9: MonoOH: 22.85
57	TBA1C	Y.APVISAEK(+393.11)AYHEQL.T	2	K8: MonoOH: 33.18
58	TBA1C	R.QLFHPEQLITGK(+100.02)EDAANNYAR.G	1	K12: SuccOH: 26.31
59	TBA1C	R.GHYTIGK(+100.02)EIIDLVLDR.I	1	K7: SuccOH: 32.97
60	TBA1C	Y.APVISAEK(+100.02)AYHEQL.T	6	K8: SuccOH: 40.00
61	TBA1C	F.FSETGAGK(+100.02)HVPRAVF.V	6	K8: SuccOH: 25.11
62	TBA1C	F.SETGAGK(+100.02)HVPRAVF.V	1	K7: SuccOH: 25.70
63	TBA1C	L.FHPEQLITGK(+100.02)EDAANNY.A	1	K10: SuccOH: 22.85
64	TBA1C	Y.APVISAEK(+100.02)AY.H	2	K8: SuccOH: 32.97
65	TBA4A	F.HPEQLITGK(+393.11)EDAANNY.A	2	K9: MonoOH: 22.85
66	TBA4A	Y.APVISAEK(+393.11)AYHEQL.S	2	K8: MonoOH: 33.18
67	TBA4A	R.QLFHPEQLITGK(+100.02)EDAANNYAR.G	1	K12: SuccOH: 26.31
68	TBA4A	Y.APVISAEK(+100.02)AYHEQL.S	6	K8: SuccOH: 40.00
69	TBA4A	L.FHPEQLITGK(+100.02)EDAANNY.A	1	K10: SuccOH: 22.85
70	TBA4A	Y.APVISAEK(+100.02)AY.H	2	K8: SuccOH: 32.97
71	TBB3	L.RFPGQLNADLRK(+100.02)L.A	5	K12: SuccOH: 88.25
72	TBB4B	L.RFPGQLNADLRK(+100.02)L.A	5	K12: SuccOH: 88.25
73	TBB5	L.RFPGQLNADLRK(+100.02)L.A	5	K12: SuccOH: 88.25
74	TBB6	L.RFPGQLNADLRK(+100.02)L.A	5	K12: SuccOH: 88.25
75	TCP4	W.SQLKEQISDIDDAVRK(+100.02)L	1	K16: SuccOH: 49.35
76	TSTRB27A	M(+42.01)(+15.99)WSHPQFEK(+450.13)GGGSGGGSGGSAW.S	1	M1: Ac: 1000.00 M1: Ox (M): 1000.00 K9: MonoGly: 34.30
77	TSTRB27A	M(+42.01)(+15.99)WSHPQFEK(+393.11)GGGSGGGSGGSAW.S	4	M1: Ac: 1000.00 M1: Ox (M): 1000.00

				K9: MonoOH: 37.35
78	TSTRB27A	M(+42.01)(+15.99)WSHPQFEK(+100.02)GGGSGGGSGGSAW.S	9	M1: Ac: 1000.00 M1: Ox (M): 1000.0 K9: SuccOH: 28.70
79	TSTRB27A	M(+42.01)(+15.99)WSHPQFEK(+100.02)GGGSGGGSGGSAWSHPQFEKSGLR.S	1	M1: Ac: 1000.00 M1: Ox (M): 1000.00 K9: SuccOH: 25.70
80	TSTRB27A	M(+42.01)WSHPQFEK(+393.11)GGGSGGGSGGSAW.S	4	M1: Ac: 1000.00 K9: MonoOH: 34.81
81	TSTRB27A	M(+42.01)WSHPQFEK(+100.02)GGGSGGGSGGSAWS(+100.02)HPQFEKSGLR.S	6	M1: Ac: 1000.00 K9: SuccOH: 77.13 S23: SuccOH: 0.00
82	TSTRB27A	M(+42.01)WSHPQFEK(+100.02)GGGSGGGSGGSAW.S	8	M1: Ac: 1000.00 K9: SuccOH: 58.99
83	TSTRB27A	M(+42.01)WSHPQFEKGGGS(+100.02)GGGSGGSAW.S	1	M1: Ac: 1000.00 S13: SuccOH: 0.00
84	TSTRB27A	M(+42.01)WSHPQFEK(+100.02)GGGS(+275.08)GGGSGGSAW.S	2	M1: Ac: 1000.00; K9: SuccOH: 25.70 S13: Cleaved1: 25.70
85	TSTRB27A	R.C(+57.02)VDK(+100.02)SWIPEGVVR.S	14	C1: Cbm: 1000.00; K4: SuccOH: 26.02
86	TSTRB27A	L.C(+57.02)GNKSDLEDQRVVKEEEAIALAEK(+100.02)Y.G	6	C1: Cbm: 1000.00 K24: SuccOH: 9.34
87	TSTRB27A	L.C(+57.02)GNKSDLEDQRVVK(+100.02)EEEAIAL.A	6	C1: Cbm: 1000.00 K14: SuccOH: 30.19
88	TSTRB27A	L.C(+57.02)GNK(+100.02)SDLEDQRVVK(+100.02)EEEAIAL.A	3	C1: Cbm: 1000.00 K4: SuccOH: 17.01 K14: SuccOH: 38.24
89	TSTRB27A	R.C(+57.02)VDK(+100.02)S(+100.02)WIPEGVVR.S	2	C1: Cbm: 1000.00 K4: SuccOH: 1000.00 S5: SuccOH: 1000.00

90	TSTRB27A	L.C(+57.02)GNK(+100.02)SDLEDQRVVKEEEAIAL.A	1	C1: Cbm: 1000.00 K4: SuccOH: 40.00
91	TSTRB27A	R.AMSDGDYDY(+275.08)LIK(+100.02)FLALGDSGVGK.T	1	Y9: Cleaved1: 11.10 K12: SuccOH: 32.97
92	TSTRB27A	R.AMSDGDYDYLIK(+450.13)FLALGDSGVGK.T	4	K12: MonoGly: 68.47
93	TSTRB27A	W.SHPQFEK(+450.13)SGL.R	2	K7: MonoGly: 33.98
94	TSTRB27A	F.LALGDSGVGK(+450.13)TSVL.Y	1	K10: MonoGly: 20.92
95	TSTRB27A	R.AMSDGDYDYLIK(+393.11)FLALGDSGVGK.T	5	K12: MonoOH: 77.24
96	TSTRB27A	K.TSVLYQYTDGK(+393.11)FNSK.F	3	K11: MonoOH: 26.52
97	TSTRB27A	W.SHPQFEK(+393.11)GGGSGGGSGGSAW.S	7	K7: MonoOH: 30.10
98	TSTRB27A	K.FNSK(+393.11)FITTVGIDFR.E	1	K4: MonoOH: 27.96
99	TSTRB27A	W.SHPQFEK(+393.11)SGL.R	4	K7: MonoOH: 30.46
100	TSTRB27A	K.YGIPYFETSAANGTNISQAIEMLLDLIMK(+100.02)R.M	4	K29: SuccOH: 123.16
101	TSTRB27A	K.TSVLYQYTDGK(+100.02)FNSK(+100.02)FITTVGIDFR.E	1	K11: SuccOH: 26.52 K15: SuccOH: 11.06
102	TSTRB27A	R.AMSDGDYDYLIK(+100.02)FLALGDSGVGK.T	3	K12: SuccOH: 68.47
103	TSTRB27A	K.SDLEDQRVVK(+100.02)EEEAIALAEK.Y	3	K10: SuccOH: 66.45
104	TSTRB27A	K.TSVLYQYTDGK(+100.02)FNSK.F	31	K11: SuccOH: 32.97
105	TSTRB27A	K.FNSK(+100.02)FITTVGIDFR.E	13	K4: SuccOH: 30.46
106	TSTRB27A	W.SHPQFEK(+100.02)GGGSGGGSGGSAW.S	6	K7: SuccOH: 37.35
107	TSTRB27A	R.SNGHAS(+100.02)TDQLSEEK(+100.02)EK.G	3	S6: SuccOH: 0.00 K14: SuccOH: 22.85
108	TSTRB27A	W.SHPQFEK(+100.02)GGGS(+100.02)GGGSGGSAW.S	1	K7: SuccOH: 53.33 S11: SuccOH: 11.12
109	TSTRB27A	R.AMSDGDYDYLIK(+100.02)FLALGDS(+100.02)GVGK.T	1	K12: SuccOH: 29.32 S19: SuccOH: 16.76
110	TSTRB27A	F.LALGDSGVGK(+100.02)TSVL.Y	7	K10: SuccOH: 33.98

111	TSTRB27A	W.SHPQFEK(+100.02)SGL.R	12	K7: SuccOH: 26.02
112	TSTRB27A	L.ALGDSGVGK(+100.02)TSVL.Y	2	K9: SuccOH: 23.10
113	TSTRB27A	R.SNGHASTDQLSEEK(+100.02)EK.G	2	K14: SuccOH: 32.97
114	TSTRB27A	K.FLALGDS(+100.02)GVGK.T	1	S7: SuccOH: 26.57
115	TSTRB27A	F.ITTVGIDFREK(+100.02)RVVY.R	4	K11: SuccOH: 38.03
116	TSTRB27A	W.SHPQFEK(+100.02)S(+100.02)GL.R	3	K7: SuccOH: 45.03 S8: SuccOH: 58.52
117	TSTRB27A	L.EDQRVVK(+100.02)EEEAIAL.A	1	K7: SuccOH: 22.09
118	TSTRB27A	Y.TDGKFNSK(+100.02)F.I	1	K8: SuccOH: 26.02
119	TSTRB27A	Y.QYTDGK(+100.02)FNSK(+100.02)F.I	2	K6: SuccOH: 11.12 K10: SuccOH: 21.94
120	TSTRB27A	W.SHPQFEK(+100.02)GGGS(-18.01)GGGSGGSAW.S	2	K7: SuccOH: 13.99 S11: Dehyd: 22.59
121	TSTRB27A	W.SHPQFEK(+100.02)GGGSGGGSGGSAW(+15.99).S	1	K7: SuccOH: 26.50 W20: Ox(HW): 74.98
122	VDAC1	Y.TQTLK(+450.13)PGIKL.T	1	K5: MonoGly: 25.11
123	VDAC1	Y.TQTLK(+100.02)PGIKL.T	2	K5: SuccOH: 32.28
124	VDAC2	L.SALVDGK(+100.02)SINAGGHK(+100.02)VGL.A	1	K7: SuccOH: 30.46 K15: SuccOH: 52.22

DSS (Sets E, D)

	Gene	Peptide	#Spec	PTM & A-Score
1	ADT2	F.AK(+100.02)DFLAGGVAAAIS(+100.02)KTAVAPIERVK(+100.02)L.L	1	K2: SuccOH: 0.00 S14: SuccOH: 0.00 K25: SuccOH: 41.41
2	ADT2	L.AADVGK(+100.02)AGAEREF.R	2	K6: SuccOH: 80.35
3	ALDOA	L.AADESTGSIAK(+393.11)RL.Q	1	K11: MonoOH: 32.97
4	ALDOA	L.AADESTGSIAK(+100.02)RL.Q	4	K11: SuccOH: 29.32
5	ANXA2	Y.KT(+100.02)DLEK(+100.02)DIISDTSGDF.R	2	T2: SuccOH: 9.34 K6: SuccOH: 29.96
6	ARF5	W.DVGGQDK(+100.02)IRPL.W	1	K7: SuccOH: 50.87
7	ATPB	Y.MVGPIEEAVAK(+393.11)ADKLAEEHSS	1	K11: MonoOH: 28.36
8	COF1	M.A(+42.01)SGVAVSDGVIK(+100.02)VF.N	2	A1: Ac: 1000.00 K12: SuccOH: 46.62
9	DEST	L.VGDVGVTITDPFK(+100.02)HF.V	2	K13: SuccOH: 25.11
10	DX39A	R.DFLLK(+100.02)PELLR.A	1	K5: SuccOH: 61.69
11	DX39B	R.DFLLK(+100.02)PELLR.A	1	K5: SuccOH: 61.69
12	G3P	R.GALQNIIPASTGAAK(+100.02)AVGK(+100.02)VIPELNGK.L	2	K15: SuccOH: 3.97 K19: SuccOH: 47.82
13	G3P	F.HGTVK(+100.02)AENGKL.V	1	K5: SuccOH: 22.85
14	G3P	Y.DDIKKVVK(+100.02)QASEGPL.K	1	K8: SuccOH: 28.36
15	G3P	M.G(+100.02)KVKVGVN(+.98)GF.G	1	G1: SuccOH: 8.14 N8: Deam (NQ): 1000.00
16	GRP78	L.VGGSTRIPK(+100.02)IQQL.V	1	K9: SuccOH: 32.94
17	HNRH1	F.VVK(+100.02)VRGLPW.S	2	K3: SuccOH: 26.31

18	HS90B	M.P(+100.02)EEVHHGEEEVETF.A	1	P1: SuccOH: 64.80
19	HSP7C	Y.GLDK(+100.02)KVGAERNVL.I	1	K4: SuccOH: 37.81
20	HSPB1	F.ESRAQLGGPEAAKSDETAAK(+100.02)	2	K20: SuccOH: 21.15
21	K1C17	R.TIVEEVQDGK(+100.02)VISSR.E	1	K10: SuccOH: 47.09
22	K22E	F.ASFIDK(+100.02)VRF.L	4	K6: SuccOH: 39.44
23	K2C1	F.ASFIDK(+100.02)VRF.L	4	K6: SuccOH: 39.44
24	K2C1B	F.ASFIDK(+100.02)VRF.L	4	K6: SuccOH: 39.44
25	K2C3	F.ASFIDK(+100.02)VRF.L	4	K6: SuccOH: 39.44
26	K2C5	F.ASFIDK(+100.02)VRF.L	4	K6: SuccOH: 39.44
27	K2C7	F.ASFIDK(+100.02)VRF.L	4	K6: SuccOH: 39.44
28	K2C8	F.ASFIDK(+100.02)VRF.L	4	K6: SuccOH: 39.44
29	KPYM	R.SVETLK(+100.02)EMIK.S	1	K6: SuccOH: 26.31
30	LDHB	L.TSVINQK(+100.02)LKDDEVAQL.K	1	K7: SuccOH: 41.83
31	MPCP	F.SVTLK(+100.02)EDGVRGL.A	3	K5: SuccOH: 39.97
32	NDKB	F.IAIK(+393.11)PDGVQRGL.V	1	K4: MonoOH: 32.97
33	NDKB	F.IAIK(+100.02)PDGVQRGL.V	2	K4: SuccOH: 38.16
34	PPIA	F.ELFADK(+393.11)VPKTAENF.R	1	K6: MonoOH: 44.84
35	PPIA	F.ELFADK(+100.02)VPKTAENF.R	1	K6: SuccOH: 53.53
36	PROF1	K.TFVNITPAEVGVLVGK(+100.02)DR.S	4	K16: SuccOH: 67.24
37	PROF1	L.VGK(+100.02)DRSSF.Y	1	K3: SuccOH: 24.24
38	QCR2	L.IGLGVSHPVLK(+100.02)QVAEQF.L	1	K11: SuccOH: 22.07
39	RACK1	W.DLEGK(+100.02)IIVDEL.K	1	K5: SuccOH: 22.37
40	RAN	F.HTNRGPIK(+100.02)F.N	1	K8: SuccOH: 59.64
41	RB27B	F.ITTVGIDFREK(+100.02)RVVY.N	4	K11: SuccOH: 38.03
42	RL27	Y.SVDIPLDK(+100.02)TVVNKDVF.R	1	K8: SuccOH: 23.10

43	RPN2	W.NVADVVIK(+393.11)FPEEEAPSTVL.S	2	K8: MonoOH: 38.64
44	RPN2	F.TPK(+393.11)QEIQHLF.R	1	K3: MonoOH: 25.66
45	RPN2	W.NVADVVIK(+100.02)FPEEEAPSTVL.S	2	K8: SuccOH: 38.64
46	RPN2	F.TPK(+100.02)QEIQHLF.R	1	K3: SuccOH: 28.86
47	RS27A	L.IFAGK(+100.02)QLEDGRTL.S	1	K5: SuccOH: 67.69
48	SFPQ	L.TTTPRPVIVEPLEQLDDEDGLPEK(+100.02)L.A	1	K24: SuccOH: 40.11
49	SRP14	M.V(+100.02)LLESEQFLTELTR.L	1	V1: SuccOH: 87.62
50	SRSF3	Y.VGNLGNN(+.98)GNK(+393.11)TELERAF.G	1	N7: Deam (NQ): 26.02 K10: MonoOH: 17.01
51	SRSF3	Y.VGNLGNN(+.98)GNK(+100.02)TELERAF.G	1	N7: Deam (NQ): 30.46 K10: SuccOH: 10.11
52	SRSF3	Y.VGNLGNNGNK(+100.02)TELERAF.G	1	K10: SuccOH: 24.44
53	SRSF3	R.VRVELSNGEK(+100.02)R.S	1	K10: SuccOH: 42.89
54	SRSF3	Y.VGNLGNNGNK(+100.02)T(-18.01)ELERAF.G	7	K10: SuccOH: 128.00 T11: Dehyd: 1000.00
55	SRSF7	Y.VGNLGTGAGK(+100.02)GELERAF.S	1	K10: SuccOH: 49.79
56	TBA1C	F.HPEQLITGK(+393.11)EDAANNY.A	2	K9: MonoOH: 22.85
57	TBA1C	Y.APVISAEK(+393.11)AYHEQL.T	2	K8: MonoOH: 33.18
58	TBA1C	R.QLFHPEQLITGK(+100.02)EDAANNYAR.G	1	K12: SuccOH: 26.31
59	TBA1C	R.GHYTIGK(+100.02)EIIDLVLDR.I	1	K7: SuccOH: 32.97
60	TBA1C	Y.APVISAEK(+100.02)AYHEQL.T	6	K8: SuccOH: 40.00
61	TBA1C	F.FSETGAGK(+100.02)HVPRAVF.V	6	K8: SuccOH: 25.11
62	TBA1C	F.SETGAGK(+100.02)HVPRAVF.V	1	K7: SuccOH: 25.70
63	TBA1C	L.FHPEQLITGK(+100.02)EDAANNY.A	1	K10: SuccOH: 22.85
64	TBA1C	Y.APVISAEK(+100.02)AY.H	2	K8: SuccOH: 32.97
65	TBA4A	F.HPEQLITGK(+393.11)EDAANNY.A	2	K9: MonoOH: 22.85

66	TBA4A	Y.APVISAEK(+393.11)AYHEQL.S	2	K8: MonoOH: 33.18
67	TBA4A	R.QLFHPEQLITGK(+100.02)EDAANNYAR.G	1	K12: SuccOH: 26.31
68	TBA4A	Y.APVISAEK(+100.02)AYHEQL.S	6	K8: SuccOH: 40.00
69	TBA4A	L.FHPEQLITGK(+100.02)EDAANNY.A	1	K10: SuccOH: 22.85
70	TBA4A	Y.APVISAEK(+100.02)AY.H	2	K8: SuccOH: 32.97
71	TBB3	L.RFPGQLNADLRK(+100.02)L.A	5	K12: SuccOH: 88.25
72	TBB4B	L.RFPGQLNADLRK(+100.02)L.A	5	K12: SuccOH: 88.25
73	TBB5	L.RFPGQLNADLRK(+100.02)L.A	5	K12: SuccOH: 88.25
74	TBB6	L.RFPGQLNADLRK(+100.02)L.A	5	K12: SuccOH: 88.25
75	TCP4	W.SQLKEQISDIDDAVRK(+100.02)L	1	K16: SuccOH: 49.35
76	TSTRB27A	M(+42.01)(+15.99)WSHPQFEK(+450.13)GGGSGGGSGGSAW.S	1	M1: Ac: 1000.00 M1: Ox (M): 1000.00 K9: MonoGly: 34.30
77	TSTRB27A	M(+42.01)(+15.99)WSHPQFEK(+393.11)GGGSGGGSGGSAW.S	4	M1: Ac: 1000.00 M1: Ox (M): 1000.00 K9: MonoOH: 37.35
78	TSTRB27A	M(+42.01)(+15.99)WSHPQFEK(+100.02)GGGSGGGSGGSAW.S	9	M1: Ac: 1000.00 M1: Ox (M): 1000.00 K9: SuccOH: 28.70
79	TSTRB27A	M(+42.01)(+15.99)WSHPQFEK(+100.02)GGGSGGGSGGSAWSHPQFEKSGLR.S	1	M1: Ac: 1000.00 M1: Ox (M): 1000.00 K9: SuccOH: 25.70
80	TSTRB27A	M(+42.01)WSHPQFEK(+393.11)GGGSGGGSGGSAW.S	4	M1: Ac: 1000.00 K9: MonoOH: 34.81
81	TSTRB27A	M(+42.01)WSHPQFEK(+100.02)GGGSGGGSGGSAWS(+100.02)HPQFEKSGLR.S	6	M1: Ac: 1000.00 K9: SuccOH: 77.13 S23: SuccOH: 0.00
82	TSTRB27A	M(+42.01)WSHPQFEK(+100.02)GGGSGGGSGGSAW.S	8	M1: Ac: 1000.00 K9: SuccOH: 58.99

83	TSTRB27A	M(+42.01)WSHPQFEKGGGS(+100.02)GGGSGGSAW.S	1	M1: Ac: 1000.00 S13: SuccOH: 0.00
84	TSTRB27A	M(+42.01)WSHPQFEK(+100.02)GGGS(+275.08)GGGSGGSAW.S	2	M1: Ac: 1000.00 K9: SuccOH: 25.70 S13: Cleaved1: 25.70
85	TSTRB27A	R.C(+57.02)VDK(+100.02)SWIPEGVVR.S	14	C1: Cbm: 1000.00 K4: SuccOH: 26.02
86	TSTRB27A	L.C(+57.02)GNKSDLEDQRVVKEEEAIALAEK(+100.02)Y.G	6	C1: Cbm: 1000.00 K24: SuccOH: 9.34
87	TSTRB27A	L.C(+57.02)GNKSDLEDQRVVK(+100.02)EEEAIAL.A	6	C1: Cbm: 1000.00 K14: SuccOH: 30.19
88	TSTRB27A	L.C(+57.02)GNK(+100.02)SDLEDQRVVK(+100.02)EEEAIAL.A	3	C1: Cbm: 1000.00 K4: SuccOH: 17.01 K14: SuccOH: 38.24
89	TSTRB27A	R.C(+57.02)VDK(+100.02)S(+100.02)WIPEGVVR.S	2	C1: Cbm: 1000.00 K4: SuccOH: 1000.00 S5: SuccOH: 1000.00
90	TSTRB27A	L.C(+57.02)GNK(+100.02)SDLEDQRVVKEEEAIAL.A	1	C1: Cbm: 1000.00 K4: SuccOH: 40.00
91	TSTRB27A	R.AMSDGDYDY(+275.08)LIK(+100.02)FLALGDSGVGK.T	1	Y9: Cleaved1: 11.10 K12: SuccOH: 32.97
92	TSTRB27A	R.AMSDGDYDYLIK(+450.13)FLALGDSGVGK.T	4	K12: MonoGly: 68.47
93	TSTRB27A	W.SHPQFEK(+450.13)SGL.R	2	K7: MonoGly: 33.98
94	TSTRB27A	F.LALGDSGVGK(+450.13)TSVL.Y	1	K10: MonoGly: 20.92
95	TSTRB27A	R.AMSDGDYDYLIK(+393.11)FLALGDSGVGK.T	5	K12: MonoOH: 77.24
96	TSTRB27A	K.TSVLYQYTDGK(+393.11)FNSK.F	3	K11: MonoOH: 26.52
97	TSTRB27A	W.SHPQFEK(+393.11)GGGSGGGSGGSAW.S	7	K7: MonoOH: 30.10
98	TSTRB27A	K.FNSK(+393.11)FITTVGIDFR.E	1	K4: MonoOH: 27.96
99	TSTRB27A	W.SHPQFEK(+393.11)SGL.R	4	K7: MonoOH: 30.46

100	TSTRB27A	K.YGIPYFETSAANGTNISQAIEMLLDLIMK(+100.02)R.M	4	K29: SuccOH: 123.16
101	TSTRB27A	K.TSVLYQYTDGK(+100.02)FNSK(+100.02)FITTVGIDFR.E	1	K11: SuccOH: 26.52 K15: SuccOH: 11.06
102	TSTRB27A	R.AMSDGDYDYLIK(+100.02)FLALGDSGVGK.T	3	K12: SuccOH: 68.47
103	TSTRB27A	K.SDLEDQRVVK(+100.02)EEEAIALAEK.Y	3	K10: SuccOH: 66.45
104	TSTRB27A	K.TSVLYQYTDGK(+100.02)FNSK.F	31	K11: SuccOH: 32.97
105	TSTRB27A	K.FNSK(+100.02)FITTVGIDFR.E	13	K4: SuccOH: 30.46
106	TSTRB27A	W.SHPQFEK(+100.02)GGGSGGGSGGSAW.S	6	K7: SuccOH: 37.35
107	TSTRB27A	R.SNGHAS(+100.02)TDQLSEEK(+100.02)EK.G	3	S6: SuccOH: 0.00 K14: SuccOH: 22.85
108	TSTRB27A	W.SHPQFEK(+100.02)GGGS(+100.02)GGGSGGSAW.S	1	K7: SuccOH: 53.33; S11: SuccOH: 11.12
109	TSTRB27A	R.AMSDGDYDYLIK(+100.02)FLALGDS(+100.02)GVGK.T	1	K12: SuccOH: 29.32 S19: SuccOH: 16.76
110	TSTRB27A	F.LALGDSGVGK(+100.02)TSVL.Y	7	K10: SuccOH: 33.98
111	TSTRB27A	W.SHPQFEK(+100.02)SGL.R	12	K7: SuccOH: 26.02
112	TSTRB27A	L.ALGDSGVGK(+100.02)TSVL.Y	2	K9: SuccOH: 23.10
113	TSTRB27A	R.SNGHASTDQLSEEK(+100.02)EK.G	2	K14: SuccOH: 32.97
114	TSTRB27A	K.FLALGDS(+100.02)GVGK.T	1	S7: SuccOH: 26.57
115	TSTRB27A	F.ITTVGIDFREK(+100.02)RVVY.R	4	K11: SuccOH: 38.03
116	TSTRB27A	W.SHPQFEK(+100.02)S(+100.02)GL.R	3	K7: SuccOH: 45.03 S8: SuccOH: 58.52
117	TSTRB27A	L.EDQRVVK(+100.02)EEEAIAL.A	1	K7: SuccOH: 22.09
118	TSTRB27A	Y.TDGKFNSK(+100.02)F.I	1	K8: SuccOH: 26.02
119	TSTRB27A	Y.QYTDGK(+100.02)FNSK(+100.02)F.I	2	K6: SuccOH: 11.12 K10: SuccOH: 21.94
120	TSTRB27A	W.SHPQFEK(+100.02)GGGS(-18.01)GGGSGGSAW.S	2	K7: SuccOH: 13.99

				S11: Dehyd: 22.59
121	TSTRB27A	W.SHPQFEK(+100.02)GGGSGGGSGGSAW(+15.99).S	1	K7: SuccOH: 26.50 W20: Ox(HW): 74.98
122	VDAC1	Y.TQTLK(+450.13)PGIKL.T	1	K5: MonoGly: 25.11
123	VDAC1	Y.TQTLK(+100.02)PGIKL.T	2	K5: SuccOH: 32.28
124	VDAC2	L.SALVDGK(+100.02)SINAGGHK(+100.02)VGL.A	1	K7: SuccOH: 30.4 K15: SuccOH: 52.22